

**OPTICALLY RECORDING THE CARDIAC ACTION POTENTIAL FROM
ISOLATED VENTRICULAR MYOCYTES.**

By Matthew E. L. Hardy

**A thesis submitted for the degree of Doctor of Philosophy
Department of Cell Physiology and Pharmacology
The University of Leicester.**

2007

UMI Number: U495618

All rights reserved

INFORMATION TO ALL USERS

The quality of this reproduction is dependent upon the quality of the copy submitted.

In the unlikely event that the author did not send a complete manuscript and there are missing pages, these will be noted. Also, if material had to be removed, a note will indicate the deletion.



UMI U495618

Published by ProQuest LLC 2013. Copyright in the Dissertation held by the Author.
Microform Edition © ProQuest LLC.

All rights reserved. This work is protected against
unauthorized copying under Title 17, United States Code.



ProQuest LLC
789 East Eisenhower Parkway
P.O. Box 1346
Ann Arbor, MI 48106-1346

Optically Recording the Cardiac Action Potential From Isolated Ventricular Myocytes.

By Matthew E. L. Hardy

1. Use of fast voltage-sensitive dyes in cardiac tissue has primarily been used to measure excitation in whole hearts or ventricular wedges. The application of potentiometric dyes to isolated ventricular myocytes may provide the opportunity to record changes in drug-induced action potential (AP) morphology without the use of more difficult electrophysiological techniques.
2. Conditions were optimised for recording cardiac APs from isolated guinea pig ventricular myocytes stimulated at 1Hz using the ratiometric fluorescence emission of the dyes, di-4-ANEPPS and di-8-ANEPPS. Limiting exposure of cells to excitation light to discrete periods of time minimised phototoxic effects; using di-8-ANEPPS, APs of steady duration were recorded for up to 28 min, when exposed to excitation light for 30 s in every 3 min, and using di-4-ANEPPS up to 24 min when exposed for 5 s in every 4 min. Using voltage-clamp protocols simultaneously with fluorescent recordings demonstrated a linear relationship between membrane potential and the fluorescence emission of both di-4-ANEPPS and di-8-ANEPPS. Additionally, using the ratiometric emission of these dyes removed motion artefacts.
3. Changes in action potential duration in response to increasing concentrations of cisapride were measured using a patch electrode or the emission of di-8-ANEPPS. Values for IC_{50} apparent for action potential prolongation were similar between the two assays (92.4 nm for di-8-ANEPPS, vs. 80.5 nm), however, cells loaded with dye had an increased basal APD_{90} and a decreased sensitivity compared to patch electrode recordings, suggesting additional actions of the dye.
4. Screening a number of structurally similar dyes (di-4-ANEPPS, di-8-ANEPPS, di-12-ANEPPS, di-3-ANEPPDHQ and di-4-ANEPPDHQ) demonstrated a variety of different pharmacological effects. Acute perfusion of 5 μ M di-8-ANEPPS on guinea pig myocytes caused an increase in APD, whereas di-4-ANEPPDHQ caused a significant decrease and di-4-ANEPPS had no significant effects. In canine M cells, voltage clamp experiments provided evidence for multiple effects of di-8-ANEPPS upon L-type calcium channels including a reduced peak current, modification of the voltage dependence of inactivation and activation to more negative potentials and delayed recovery from inactivation. In contrast, di-4-ANEPPS did not significantly effect inactivation or peak current, but decreased the time for recovery from inactivation.
5. A double-blinded validation using the fluorescence emission of di-4-ANEPPS (loaded in guinea pig myocytes) was compared to results from standard proarrhythmia screening techniques: sharp electrode recordings from canine Purkinje fibres and M cells. D-sotalol caused increases in APD and triangulation in all three tissue types. Responses to pinacidil were diminished in canine M cells and guinea pig myocytes compared to decreases in APD observed in Purkinje fibres. Increases in terfenadine concentration resulted in a biphasic response in both types of myocytes, although little effect was observed in Purkinje fibres. These data suggest that guinea pig myocytes respond to drug-induced changes in AP morphology in a more similar manner to canine M cells than Purkinje fibres and show that di-4-ANEPPS can be used to monitor changes in AP duration and triangulation in isolated ventricular cells.
6. This study demonstrates the feasibility of recording drug-induced changes in AP morphology from cardiac cells using a voltage sensitive dye. This provides a higher throughput method for safety-pharmacology screens than standard microelectrode techniques, whilst still providing an indication of the effects of test compounds in native tissue.

Acknowledgements.

Throughout the duration of this project there have been a number of people who have been instrumental in seeing it to completion.

To begin with, I would like to thank my supervisors, Professor Nick Standen and Dr. Glenn Rodrigo, from the University of Leicester, and Dr. Chris Lawrence from AstraZeneca. I can never thank you enough for giving me the chance to study for a PhD and you have all been exceptional mentors. Glenn, without your help I would never have had the confidence to start dismantling and assembling rigs (and attaching a cable to anything that wasn't being used!). Nick, I want to thank you especially for explaining those concepts to me that were otherwise just too difficult for me to grasp and for doing it in a way that was never too complicated. Chris, thanks for looking after me when I was at AZ and always getting me the things that you thought that I should have. I also want to thank all of you for trusting in me and being patient with me at times when I could have been a better student.

I also want to thank everyone who I worked with, both in the labs at the University of Leicester and in the Department of Safety Pharmacology in AstraZeneca. Whilst everyone I came into contact with in those labs has been a help to me in some way or other there are a few who deserve a special mention. At AstraZeneca: Matt Bridgeland-Taylor and Ann Woods, who spent a large amount of time training me on the Ionworks HT™, Phil Jarvis, who wrote the original AP analysis spreadsheet, Duncan Armstrong, who explained Cheng & Prusoff to me, as well as Andy Heuze and Lucy Ashman, whom I have never met but performed the binding experiments. In particular, I would also like to send out a special “thank you” to Najah Abi-Gerges, with whom I have spent a lot of time and whose contribution was above and beyond the call of duty.

At Leicester: everyone in the lab assisted me in some way or another but of particular note is the assistance of Dr. Rich Rainbow, not only a great scientist but one of the people who kept me sane in times of crisis and a bloody good friend as well. Additionally I would like to thank Diane Everitt. Also, Marianne Caine (although technically not in the lab), but without whom CPP would cease to function and also a great friend.

Thanks also to Mum and Dad for always believing in me and being proud of me. Also, thanks to the love of my life, Becky, who is also the most patient and kindest person you could ever meet (and she had to be for putting up with me whilst I was writing this!).

Finally, I would like to thank the BBSRC and the Department of Safety Pharmacology at AstraZeneca for supplying the funds with which I could pursue my studies.

Some of the work presented in this thesis had been published in the following articles:

Journal Publications:

Hardy, M.E., Lawrence C.L., Standen N.B., Rodrigo G.C. (2006) Can optical recordings of membrane potential be used to screen for drug-induced action potential prolongation in single cardiac myocytes? *J Pharmacol Toxicol Methods*. **54(2)**,173-82.

Abstracts:

Hardy, M.E., Lawrence C.L., Standen N.B., Rodrigo G.C. Drug-induced action potential prolongation in isolated cardiac myocytes recorded using a voltage-sensitive dye. The Annual Biophysical Society Meeting, February 2005. Poster presentation.

Hardy, M.E., Lawrence C.L., Standen N.B., Rodrigo G.C. Optical recording of drug-induced action potential prolongation in isolated cardiac myocytes using a voltage-sensitive dye. The Annual Physiological Society Meeting, July 2005. Oral presentation.

Recent work that did not form part of this study but is discussed briefly in Appendix B has recently been published as an abstract:

Hardy, M.E.L., Small, B.G., Valentin, J-P., Pollard, C.E., Abi-Gerges, N. Validation of a voltage-sensitive dye-based method for assessing dog myocyte action potential duration. The Annual Safety Pharmacology Society Meeting, September 2007. Poster presentation.

Contents.

Chapter 1: Introduction	1
1.1. Structure and Function of the Heart.....	5
1.1.1. The cardiac cycle: the mechanical sequence of events which occur during a heartbeat.....	5
1.1.2. Electrical conduction in the heart.	6
1.1.3. The electrocardiogram.	6
1.2. The Cardiac Action Potential.....	8
1.2.1. Ionic theory for determining membrane potential in a single cell.....	8
1.2.2. Structure and function of ion channels.	10
1.2.3. Ionic currents and their role in the cardiac action potential.....	14
1.2.4. Cardiac calcium cycling.....	20
1.3. Generation of LQTS-based arrhythmia.	22
1.3.1. Conditions leading to the generation of Torsade de Pointes (TdP).	23
1.3.2. The M cell.....	27
1.3.3. Afterdepolarizations.....	29
1.3.4. The importance of the hERG gene in acquired LQTS.....	31
1.3.5. <i>In silico</i> hERG binding models.....	32
1.4. Screening for proarrhythmic compounds.	33
1.4.1. Early preclinical screens.	33
1.4.2. <i>In vitro</i> proarrhythmia models.	35
1.4.3. <i>In vivo</i> proarrhythmia models.....	38
1.5. Voltage-sensitive dyes and fluorescent monitoring of membrane potential.....	40
1.5.1. Theory of voltage-sensitive dyes.	40
1.5.2. Noise in epifluorescent recordings.	46
1.5.3. The importance of the light transmitting properties of the objective lens.	47
1.5.4. Light detection.	49
1.6. Aims:.....	50
Chapter 2: Methods	52
2.1 Tissue preparation.....	53
2.1.1. Preparation of rodent isolated ventricular myocytes.	53
2.1.2. Preparation of canine midmyocardial myocytes.....	56
2.1.3. Preparation of canine Purkinje fibres.....	58
2.1.4. Preparation of cloned cells for use in Ionworks™ HT protocols.	58

2.1.5. Preparation of cloned cell membranes for use in radioligand binding protocols.....	59
2.2. Electrophysiological measurements.	60
2.2.1. Obtaining gigaohm seals and whole-cell patch clamp configurations.	60
2.2.2. Measurements of action potentials.	63
2.2.3. Patch-clamp measurements in voltage-clamp.....	65
2.2.4. Recording calcium currents in classical voltage clamp.	66
2.2.5. Ionworks™ HT protocols.	68
2.3. hERG binding protocols.	70
2.4. Optical recording methods.....	71
2.5. Drugs and Solutions.....	75
2.6. Data analysis and statistics.	77

Chapter 3: Considerations in recording action potentials optically from isolated ventricular myocytes. 78

3.1. Results I: Recording cardiac action potentials.....	80
3.1.1. Optically recording cardiac action potentials.	80
3.1.3. Recording cardiac action potentials with sharp electrodes and patch pipettes.	96
3.1.4. The effects of Penicillin/Streptomycin solution on cardiac action potential durations.....	101
3.1.5. Drug-induced changes in APD prolongation monitored with di-8-ANEPPS and a patch electrode.....	103
3.1.6. Can di-8-ANEPPS be used to monitor overshoot potential in isolated cardiac myocytes?.....	113
3.2. Discussion I: Recording cardiac action potentials.....	118
3.2.1. Underlying physiology for species differences in ventricular action potential morphology.....	118
3.2.2. Changes in action potential morphology in response to different pacing frequencies.	120
3.2.3. The effects of antibiotic solutions upon cardiac AP morphology.	122
3.2.4. Optical recordings of action potentials from isolated myocytes.....	123
3.2.5. Alterations in action potential duration in response to cisapride.....	123
3.2.6. Application of optical dyes in the pharmaceutical industry.	125

Chapter 4: Testing the suitability of different “styryl” dyes for use with cardiac myocytes.....	126
4.1.1. The effects of acute application of “styryl” dyes upon guinea pig cardiac action potential duration.	130
4.1.2. The effects of different “styryl” dyes upon canine cardiac L-type calcium currents.....	133
4.1.3. The effects of different “styryl” dyes upon hERG current and binding. ...	150
4.1.4. The effect of different vehicle solutions upon hERG.	157
4.1. Discussion.....	159
4.2.1. The effects of the different dyes upon the L-type calcium current.....	159
4.2.2. The reliability of hERG binding versus hERG current data as measured in the Ionworks HT™.	162
4.2.3. Possible causes for the effects of styryl dyes on cardiac ion channels.	164
4.2.4. Choosing a suitable carrier solution for the dyes.....	165
4.2.5. Summary.....	165
 Chapter 5: Using di-4-ANEPPS to monitor cardiac action potential duration.	167
5.1. Optically detecting drug-induced alterations in APD and comparing them to results from sharp electrode techniques.	169
5.1.1. The effects on APD of d-sotalol	172
5.1.2. The effects on APD of terfenadine.	177
5.1.3. The effects on APD of pinacidil.	182
5.1.4. Negative and positive controls.....	186
5.1.5. Practical considerations in recording APs from myocytes using optical techniques.	186
5.2.1. Discussion.....	190
5.2.2. The underlying cause of the effects of d-sotalol, terfenadine and pinacidil on cardiac repolarisation.	190
5.2.3. Comparison of drug effects upon different preparations.	192
5.2.4. Summarising the effects of different compounds upon repolarisation in canine Purkinje and M cells and guinea pig ventricular myocytes.....	194

Chapter 6: Conclusions and Future Work.....	195
6.1. Final discussion.....	196
6.1.1. What are the advantages and disadvantages of using optical means to acquire cardiac action potentials?	198
6.1.2. Can optical recordings of APD be used as a predictor of proarrhythmic potential?.....	199
6.1.3. Implications for safety-pharmacology.	202
6.1.4. Is di-4-ANEPPS the optimum dye for use in screening for drug-induced alterations in cardiac action potential morphology?	203
6.1.5. The immediate future for an optical assay determining cardiac action potential duration in safety pharmacology screening.	205
6.1.6. Possible long-term developments for an optical assay determining cardiac action potential duration in safety pharmacology screening.	206
6.1.7. Summary.....	208
 APPENDIX A.	 209
 APPENDIX B.	 213
 Bibliography.....	 215

List of Figures.

Figure 1.1. Cross-sectional diagram showing structural features of the heart.....	7
Figure 1.2. Electrical conduction through the heart.....	7
Figure 1.3. The structure of voltage-gated sodium and calcium channels.	12
Figure 1.4. The structure of voltage-gated potassium channels and voltage-gated channel topography.	12
Figure 1.5. N- and C-type inactivation gating in potassium channels.....	13
Figure 1.6. The structure of inwardly rectifying potassium channels and ion channel topography when combined with a β -subunit.....	13
Figure 1.7. Illustration of the major ionic currents during a cardiac action potential.	14
Figure 1.8. Ventricular action potential prolongation and Long QT syndrome.	26
Figure 1.9. Endocardial, Midmyocardial and Epicardial ventricular layers.	28
Figure 1. 10. Extrasystoles: EADs and DADs.....	30
Figure 1.11. Unique structural features of hERG.	30
Figure 1.12. Flow chart displaying the possible mechanisms which can result in Torsade de Pointes generation.....	39
Figure 1.13. Mechanisms of voltage sensitivity exhibited by voltage-sensitive dyes.....	44
Figure 1.14. Electrochromism in di-n-ANEPPS.....	45
Figure 1.15. Changes in spectra of a styryl dye during depolarisation of the membrane.....	45
Figure 1.16. Schematic representation demonstrating increased light transmission through high NA objectives.	48
Figure 1.17. A simplified schematic of a photomultiplier tube.	48
Figure 2.1. The Langendorff apparatus used to enzymatically isolate cells from an intact rodent heart.	55
Figure 2.2. Illustration showing the position of the major cardiac arteries and veins.	57
Figure 2.3. Obtaining whole-cell configuration in Bridge mode.....	61
Figure 2.4. Obtaining whole-cell configuration using a patch-clamp amplifier.....	62
Figure 2.5. Diagram showing the set-up for making sharp electrode recordings from Purkinje fibres.	63
Figure 2.6. Electrical circuits for a patch clamped cell and classical and switch voltage clamp methods.....	67
Figure 2.7. Illustration of the basic principles of recording hERG current from cloned cell lines in the ionworks™ HT.....	70
Figure 2.8. Picture of the heated tissue bath used for optical recordings.	71

Figure 2.9. Schematic showing the set-up of the optical apparatus used for recording cardiac action potentials from isolated myocytes.....	74
Figure 2.10. Illustration displaying the calculation of different action potential durations.....	77
Figure 3.1. A confocal image through a single plane of an isolated myocyte.....	83
Figure 3.2. A ventricular cardiac action potential recorded with di-8-ANEPPS.....	84
Figure 3.3. Cardiac action potentials recorded from cells with different incubation periods in di-8-ANEPPS.....	85
Figure 3.4. Stability of action potential durations recorded with di-4-ANEPPS.....	86
Figure 3.5. Phototoxic effects upon canine cardiac action potentials.....	87
Figure 3.6. Averaging multiple cardiac action potentials to reduce noise.....	88
Figure 3.7. The removal of a motion artefact by ratio emission fluorescence.	89
Figure 3. 8. Changes in fluorescence of di-4-ANEPPS during the upstroke of a rat action potential.	90
Figure 3.9. The relationships between membrane potential and the emitted fluorescence of di-8-ANEPPS and di-4-ANEPPS.....	93
Figure 3.10. Calibrating the ratiometric emission of di-8-ANEPPS using dSEVC.	94
Figure 3.11. A single action potential recorded from an isolated guinea pig cardiac myocyte with a patch electrode.	98
Figure 3.12. The effects of increased pacing rate upon ventricular guinea pig action potentials.	99
Figure 3.13. Figure displaying single action potentials from isolated ventricular myocytes.	100
Figure 3.14. The effects of Pen-Strep solution upon the action potential morphology of guinea pig ventricular myocytes.....	102
Figure 3.15. Changes in cardiac action potential duration recorded using a patch electrode or optically with di-8-ANEPPS.....	107
Figure 3.16. Relative changes in action potential durations as measured by using different values of repolarisation.....	108
Figure 3.17. Measurements of action potential durations recorded simultaneously with di-8-ANEPPS and a patch electrode.....	109
Figure 3.18. Comparing measurements of action potential durations recorded simultaneously with di-8-ANEPPS and a patch electrode.....	110
Figure 3.19. Measurements of action potential durations at 40% repolarisation recorded simultaneously with di-8-ANEPPS and a patch electrode.....	111
Figure 3.20. An early afterdepolarisation.	112
Figure 3.21. Beat-to-beat variability in isolated guinea pig ventricular myocytes.....	112

Figure 3.22. Values of the resting membrane potential and overshoot measured with a patch electrode.....	115
Figure 3.23. Estimates of overshoot potentials using di-8-ANEPPS compared to patch electrode values.....	116
Figure 3.24. The baseline levels and peak change in fluorescence emitted by di-8-ANEPPS during a dose response to cisapride.	117
Figure 4.1. The chemical structures of ANEPPS and ANEPPDHQ fast voltage-sensitive dyes.	129
Figure 4.2. The effects upon APD of acute perfusion of different styryl dyes upon action potential duration.	131
Figure 4.3. The effects upon APD of acute perfusion of different solutes for styryl dyes.	132
Figure 4.4. The voltage protocol and associated current obtained from patch clamp recordings of the L-type calcium current from an isolated midmyocardial canine cell.	135
Figure 4.5. The effects of di-4-ANEPPS and di-8-ANEPPS on peak L-type calcium current in isolated canine M cells.....	136
Figure 4.6. Application of diltiazem during measurements of peak L-type calcium current in isolated canine M cells.....	137
Figure 4.7. The effects of di-4-ANEPPDHQ on peak L-type calcium current in isolated canine M cells.....	138
Figure 4.8. The IV relationship for cardiac L-type calcium channels.	141
Figure 4.9. The effects of di-8-ANEPPS on the IV relationship of cardiac L-type calcium channels.	142
Figure 4.10. The effects of di-4-ANEPPS on the IV relationship of cardiac L-type calcium channels.	143
Figure 4.11. The inactivation IV relationship for cardiac L-type calcium channels.	145
Figure 4.12. The effects of different styryl dyes upon the inactivation IV relationship of cardiac L-type calcium channels.....	146
Figure 4.13. Recovery from inactivation for cardiac L-type calcium channels.	148
Figure 4.14. The effects of different styryl dyes upon the recovery from inactivation of cardiac L-type calcium channels.....	149
Figure 4.15. The voltage protocol and associated current recorded from CHO cells expressing hERG protein in the Ionworks®.....	153
Figure 4.16. The inhibitory effects of different “styryl” dyes upon hERG current measured using Ionworks HT™	154

Figure 4.17. The inhibitory effects of different “styryl” dyes upon inhibition of a radioligand binding to hERG protein.....	155
Figure 4.18. The effects of different vehicles for “styryl” dyes on hERG current measured using Ionworks HT™.	158
Figure 4.19. The effects of different vehicles for “styryl” dyes upon hERG binding.	158
Figure 5. 1. Illustrating the measurement of triangulation.	171
Figure 5.2. Increases in APD recorded optically from guinea pig myocytes in response to increasing concentrations of d-sotalol.	174
Figure 5.3. Increases in APD recorded with a sharp electrode from canine M cells and Purkinje fibres in response to increasing concentrations of d-sotalol.	175
Figure 5.4. Changes in APDs and triangulation recorded optically from guinea pig myocytes or with a sharp electrode from canine M cells and Purkinje fibres in response to increasing concentrations of d-sotalol.	176
Figure 5.5. Changes in APD recorded optically from guinea pig myocytes in response to increasing concentrations of terfenadine.	179
Figure 5.6. Changes in APD recorded with a sharp electrode from canine M cells and Purkinje fibres in response to increasing concentrations of terfenadine.	180
Figure 5.7. APDs and triangulation recorded optically from guinea pig myocytes or with a sharp electrode from canine M cells and Purkinje fibres in response to increasing concentrations of terfenadine.....	181
Figure 5.8. APDs recorded optically from guinea pig myocytes in response to increasing concentrations of pinacidil.....	183
Figure 5.9. Changes in APD recorded with a sharp electrode from canine M cells and Purkinje fibres in response to increasing concentrations of terfenadine.	184
Figure 5.10. APDs and triangulation recorded optically from guinea pig myocytes or with a sharp electrode from canine M cells and Purkinje fibres in response to increasing concentrations of pinacidil.....	185
Figure 5.11. APDs recorded optically from guinea pig myocytes in response to increasing concentrations of glucose.....	188
Figure 5.12. Triangulation in the presence of increasing concentrations of glucose (placebo) and in the presence of 300 nM cisapride.	189
Figure A- 1. Computer assisted analysis of action potential durations.	211
Figure A- 2. Comparison between manual and computer spreadsheet based analysis of action potential durations recorded optically.....	212

Figure B-1. Changes in APD in response to cisapride recorded from canine M cells using di-4-ANEPPS.	214
--	-----

List of Tables.

Table 1.1. Drugs reported to cause QT interval prolongation.	22
Table 3.1. Comparing the recorded membrane potential with the command potential.	95
Table 3.2. Comparing the IC50 apparent values as measured using di-8-ANEPPS or a patch electrode in response to changes in action potential duration caused by cisapride.	108
Table 4. 1. Comparing the effects of different “styryl” dyes on hERG binding and hERG current.	156

List of Equations.

Equation 1.1. The free energy equation	9
Equation 1.2. The Nernst equation	9
Equation 1.3. The Goldman–Hodgkin-Katz equation	9
Equation 2.1. Ohm’s Law.	64
Equation 2.2. Recorded, Membrane and Pipette potentials.	64
Equation 2.3. Pipette current and resistance.	65
Equation 4.1. A modified Boltzman relationship.	139
Equation 4.2. The Boltzman relationship	144
Equation 4. 3. Calculation for hERG binding.	151
Equation 5.1. Calculation for triangulation.	171
Equation A-1. Calculation for determining the amplitude at which repolarisation should be measured.	209

Abbreviations and acronyms.

ACh - Acetylcholine	EGTA - ethylene glycol tetraacetic acid
AP – Action Potential	E_k – Equilibrium potential for potassium ions
APD – Action Potential Duration	E-head – Electronics head (in Ionworks™ HT)
ADP – Adenosine Diphosphate	E_m – Membrane potential
[ADP] _i – Intracellular Adenosine Diphosphate concentration	EMEM - Eagle's modified Eagle's medium
ATP – Adenosine Triphosphate	ERG – Ether-a-go-go Related Gene
[ATP] _i - Intracellular Adenosine Triphosphate concentration	F – the Faraday constant
AVN – AtrioVentricular Node	F-head – Fluidics head (in Ionworks™ HT)
AZ - AstraZeneca	FMP dye – FLIPR membrane potential dye
BSA – Bovine Serum Albumin	HEK cell – Human Embryonic Kidney cell
Ca^{2+} - Calcium ion	HEPES - 4-(2-hydroxyethyl)-1-piperazineethanesulfonic acid
$CaCl_2$ – Calcium chloride	hERG – Human Ether-a-go-go Related Gene
CCD – Charge-coupled device	Hz - Herz
CHO cell – Chinese Hamster Ovary Cell	I – current
Cl^- - Chloride ion	I_{Ca} – Calcium current
[Cl^-] _i – Intracellular chloride ion concentration.	I_{CaL} – L-type calcium current
[Cl^-] _o – Extracellular chloride ion concentration.	I_{CaT} – T-type calcium current
CPMP - European Medicines Agency's Committee for Proprietary Medicinal Products	I_K – Potassium current
CsCl – Caesium chloride	I_{Kr} – Rapidly activating potassium current
CsOH – Caesium hydroxide	I_{Ks} – Slowly activating potassium current
DAD – Delayed Afterdepolarisation	I_{Kto} – Transient outward potassium current
DMSO – DimethylsulphOxide	I_{Kur} – Ultra-rapid activating potassium current
DiBAC ₄ (3) - bis-[1,3-dibutylbarbituric acid]trimethine oxonol	I_{to} – transient outward current
E-C coupling – Excitation-Contraction coupling	K^+ - Potassium Ion
EAD – Early Afterdepolarisation	[K^+] _i – intracellular potassium ion concentration.
ECG – Electrocardiogram	[K^+] _o – Extracellular potassium ion concentration.

KCl – Potassium chloride
 LQTS – Long QT Syndrome
 M cell – Midmyocardial cell
 MgATP – Magnesium adenosine triphosphate
 MgCl₂ – Magnesium chloride
 MirP1 – MinK related protein 1
 n – Refractive index
 NA – Numerical Aperture
 Na⁺ - Sodium Ion
 [Na⁺]_i – intracellular sodium ion concentration
 [Na⁺]_o – Extracellular sodium ion concentration
 Na ATP – Sodium adenosine triphosphate
 NaCl – Sodium Chloride
 Na₂HPO₄ - Sodium
 Na Pyruvate – Sodium Pyruvate
 NCX – Sodium-Calcium Exchanger
 NSB – Non-specific binding
 n-3-PUFAs – ω-3 polyunsaturated fatty acids
 PBS – Dulbecco's Phosphate Buffered Saline
 P_{Cl} - Relative permeability to chloride ions
 P_K – Relative permeability to potassium ions
 PMT – PhotoMultiplier Tube
 P_{Na} – Relative permeability to sodium ions
 R – Resistance
 R – Universal Gas Constant (in the free energy equation)
 RMP – Resting Membrane Potential
 SAN – Sinoatrial Node
 SERCA – Sarco-Endoplasmic Reticulum Calcium ATPase
 S/N – Signal-to-Noise ratio
 SR – Sarcoplasmic Reticulum
 Styryl – naphthylstyryl/aminostyrylpyridinium
 T – Temperature (in Kelvin)
 TdP – Torsade de Pointes
 TEACl – Tetraethylammonium chloride
 TMD – Transmembrane Domain
 TTX – Tetrodotoxin
 V – Voltage
 VF – Ventricular Fibrillation
 z – the charge on an ion

Chapter 1:
Introduction.

Chapter 1: Introduction.

Electrical activity in the heart was first discovered in 1856, when a frog sciatic nerve/gastrocnemius preparation fell onto an isolated frog heart. This resulted in both preparations contracting (Kolliker & Muller, 1856). Following this, a number of efforts were made to record electrical activity of the heart using an electrocardiograph. These included the efforts of Augustus Waller, who managed to record a trace from the heartbeat using a Lipmann capillary electrometer attached to a projector (Waller, 1887). Later still, important breakthroughs were made by Willem Einthoven, who used a string galvanometer to record the electrical activity of the heart. This technique had greater sensitivity than a capillary galvanometer and thus Einthoven was able to assign letters to the deflections viewed on the electrocardiogram (P, Q, R S and T; see later and in Figure 1.2), which he used to describe several cardiovascular disorders (Einthoven, 1901).

Mapping rhythmic activity of heart tissue dates back almost 100 years. In 1913, re-entry was described in a turtle heart and in 1920, Lewis and colleagues mapped both sinus rhythm and atrial flutter (Lewis *et al.*, 1920; Mines, 1913). Early studies mapping the spread of electrical activity in the heart primarily utilised single probes moved to different regions of the heart (Durrer *et al.*, 1961). These became superseded by computer mapping techniques (Durrer & Roos, 1967) and the ability to record electrical activity simultaneously from numerous regions of the heart expanded knowledge of cardiac physiology and disease greatly. However, technical difficulties associated with making recordings using electrodes and the inability to measure refractory periods simultaneously with standard extracellular mapping techniques, led to the development and use of voltage-sensitive dyes as a means to map activation and recovery of cardiac muscle. The development of voltage-sensitive dyes has generated numerous publications on multicellular and whole-heart preparations, owing to their insensitivity to artefacts from high voltage shocks, which allows for the study of defibrillation (Holley & Knisley, 1997), and the ability to simultaneously observe both impulse propagation and the heterogeneity of recovery (Josephson, 2001).

Scientific progress has now also provided a number of techniques to allow for study of electrical activity in individual heart cells. This began with increases in the understanding of electrical activity in excitable tissue; the first demonstrations that action potentials in giant squid axons consist of movements of ions across cell membranes provided a foundation for modern electrophysiology (Hodgkin & Huxley, 1952). Additionally, the development of intracellular electrodes allowed for electrical activity to be monitored in a variety of tissues, including cardiac Purkinje and ventricular fibres (see Hutter & Noble, 1961; Johnson & Tille, 1961; McAllister & Noble, 1967 for examples). Later, acquisition of individual ionic currents

was greatly enhanced by the development of patch electrodes and the patch-clamping technique (Neher & Sakmann, 1976; Neher *et al.*, 1978; Sakmann & Neher, 1984). These advancements, combined with the development of methods to isolate cardiac myocytes from a variety of species (Mitra & Morad, 1985) allowed for cardiac membrane potentials and individual ionic currents to be recorded from isolated cardiac myocytes. Early examples of currents recorded from cardiomyocytes (or membrane patches excised from them) include measurements of sodium currents, sodium-calcium exchange currents and inwardly rectifying potassium currents (Grant *et al.*, 1983; Mechmann & Pott, 1986; Trube & Hescheler, 1984).

Thus, through a combination of studies on isolated heart cells and tissues, combined with clinical use of the ECG, alterations in the electrical activity of the whole heart due to disease can now often be characterised by changes in ionic currents in individual cells. For example, studies have demonstrated that a longer duration of the cardiac action potential in ventricular myocytes is responsible for an increased interval between the Q and T deflections on the electrocardiogram (ECG), which presents in patients with certain types of long QT syndrome (LQTS) (Curran *et al.*, 1995; Keating & Sanguinetti, 2001). This can often be directly associated with inhibition of specific repolarising currents within isolated myocytes from ventricular tissue.

Whilst the advantages of using voltage sensitive dyes in whole heart studies have been frequently employed, the use of these dyes in single myocytes has been less common. This is surprising because of the advantages that may be gained by using voltage-sensitive dyes over the use of an electrode. For example, drug-induced long QT syndrome, which can cause Torsades de Pointes (TdP - a type of ventricular tachycardia), is of substantial concern for the pharmaceutical industry. Currently, medium throughput techniques, such as automated patch-clamp systems, for example Ionworks HT™ (Bridgland-Taylor *et al.*, 2006; Schroeder *et al.*, 2003) are used to monitor individual ionic currents expressed in cloned cells. However, they cannot provide accurate assessment of changes in action potential duration (APD), which arises from multiple ion channels. Current assays include sharp electrode recordings from canine Purkinje fibres (Abi-Gerges *et al.*, 2004; Gintant *et al.*, 2001) to provide measurements of APD and isolated guinea pig and rabbit hearts (Hamlin, 2007; Hondeghem *et al.*, 2003; Hondeghem & Hoffmann, 2003; Lawrence *et al.*, 2006) to evaluate changes in the QT interval and torsadogenic risk. All of these models require a high degree of technical ability as they use conventional electrophysiological techniques. Additionally, they also require large animal numbers and have low throughputs.

However, some studies indicate that it may be possible to monitor cardiac action potentials in isolated myocytes using voltage-sensitive dyes. Sharma and Tung made multiple-site recordings using di-8-ANEPPS along the axis of myocytes to study spatial and

time-dependent changes in transmembrane voltage during field-stimulation, as well as loss of excitation during high intensity pulses (Sharma & Tung, 2002; Sharma *et al.*, 2002; Sharma *et al.*, 2005). Additionally, Windisch *et al.*, (1995) made multisite recordings from regions of myocytes $\geq 14 \mu\text{m}$ in diameter using di-4-ANEPPS. This is promising because it should therefore be possible to record complete action potentials (APs) from a single cardiac cell.

This chapter provides a general description of cardiac physiology, including a general description of the anatomy and function of the whole heart, and emphasis on ionic currents at the single cellular level. Additionally, some aspects of arrhythmia generation are discussed as they pertain to changes in cardiac AP morphology. Finally, the history and characteristics of fast voltage-sensitive dyes are explained, including details of measurement and production of fluorescent signals.

1.1. Structure and Function of the Heart.

The cardiovascular system provides the internal organs with circulation, which helps maintain the distribution of oxygen, nutrients, electrolytes, hormones and water to the various internal organs within the body. In addition, it provides transport for waste products, such as carbon dioxide and urea, to the lungs and excretory organs respectively, as well as contributing to thermoregulation and inflammatory mechanisms. The function of the heart is to be the pump for the vasculature.

1.1.1. The cardiac cycle: the mechanical sequence of events which occur during a heartbeat.

The basic anatomy of the heart can be viewed in Figure 1.1. The heart is divided into four chambers: two atria and two ventricles; the left atrium is connected to the left ventricle via the mitral valve and the right atrium is connected to the right ventricle via the tricuspid valve. These valves are referred to as the atrioventricular valves; both are passive and close as the pressure in the ventricles becomes greater than the pressure in the atria. During diastole, the period during the cardiac cycle when the ventricles are not contracted, blood enters the heart from the body, via the superior and inferior vena cava into the right atrium, and from the lungs via the pulmonary veins. The atrioventricular valves are open and thus the ventricles fill with blood. At the initiation of a beat, the atria contract, thus completing the filling of the ventricles. Then, as the ventricles contract, the ventricular pressure rises quickly (from roughly 0 to 120 mmHg in the left ventricle). When the ventricular pressure exceeds the atrial pressure, this results in the closure of the atrioventricular valves. As the pressure within the ventricles surpasses that of the pressure in the arteries, the semilunar valves open allowing for blood to be pumped to the rest of the body via the aorta and the aortic outflow (semilunar or aortic) valve and for blood to be propelled to the lungs via the pulmonary (semilunar) outflow valve and the pulmonary arteries. Following this contraction and high-pressure period, systole, the ventricles relax (during diastole) and thus the semilunar valves are closed as the arterial pressure exceeds that in the ventricles.

1.1.2. Electrical conduction in the heart.

Cardiac tissue contains certain conducting regions that show intrinsic electrical activity and hence generate their own pacing frequency. These include the nodal tissues: the sinoatrial node (SAN) and the atrioventricular node (AVN); as well as some other tissue including the Purkinje fibres. When the heart is functioning normally, the SAN has a more rapid firing rate and therefore determines the heart rate. The SAN is positioned at the junction between the superior vena cava and the right atrium and thus, following initiation, the AP then propagates throughout both atria (Figure 1.2A). Electrical conduction to the AVN is facilitated by three pathways consisting of larger cells: referred to as the three internodal tracts of Bachman, Wenckebach and Thorei.

Conducting pathways through the ventricles are slightly more complex. The atria and the ventricles are separated by a non-conducting layer of tissue called the annulus fibrosus. Thus the only conduction pathway is via the AVN, which, as a result of its complex arrangement of small cells with slow upstroke velocities, provides a relatively slow conduction pathway for the AP. The impulse then propagates through the Bundle of His, which provides a conducting medium through the annulus fibrosus to the apex of the ventricular septum. Near the septal cusp of the tricuspid valve, the Bundle of His splits to form two branches. The left bundle branch conducts toward the anterior and posterior fascicles, while the right bundle branch conducts down the septum, beneath the endocardium toward the base of the heart, where AP propagation continues through the Purkinje system, which consists of a number of bundles of fast conducting velocity fibres. The result is that the ventricles contract from the base upwards, thus providing an efficient pump.

1.1.3. The electrocardiogram.

The propagation of the APs throughout the heart which occur during each beat, provide potentials which can be measured at the surface of the body. This forms the basis of the diagnostic tool referred to as an electrocardiogram (ECG).

The ECG consists of a number of positive and negative peaks, labelled P, Q, R, S and T (see Figure 1.2B). As the atria depolarize a small upward deflection can be viewed upon the ECG, which is the P wave. Following the P wave is the QRS complex. The PQ segment is isoelectric; because no net current is flowing. This corresponds with the delay in depolarization between the atria and the ventricles caused by the slow conduction through the

AVN. The QRS complex arises when the ventricles depolarize; the large magnitude of the R wave is a consequence of the relatively large muscle mass of the ventricles. The repolarization of the atria, which normally occurs at the same time as the much larger QRS complex, is too diffuse and diminutive to be viewed in the ECG. The ST segment of the ECG is isoelectric and the T wave corresponds to the repolarisation of the ventricles.

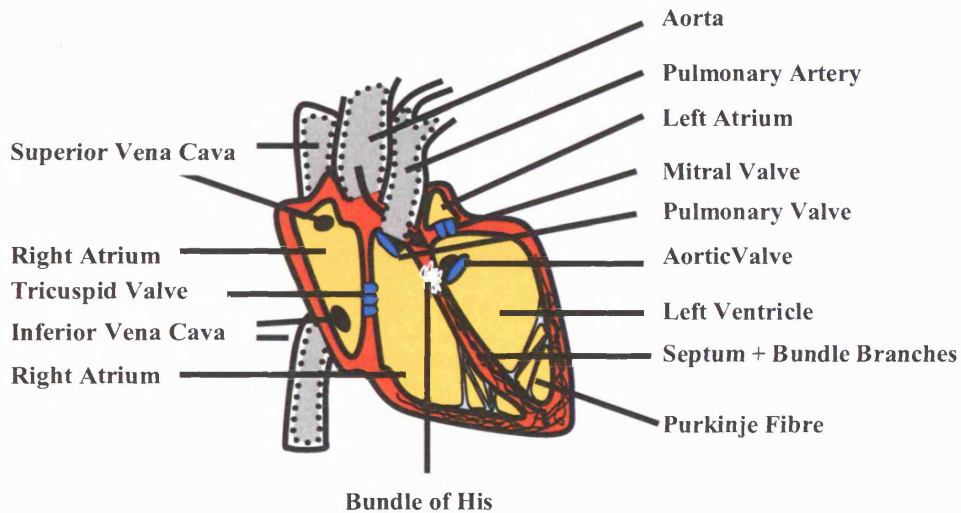


Figure 1.1. Cross-sectional diagram showing structural features of the heart.

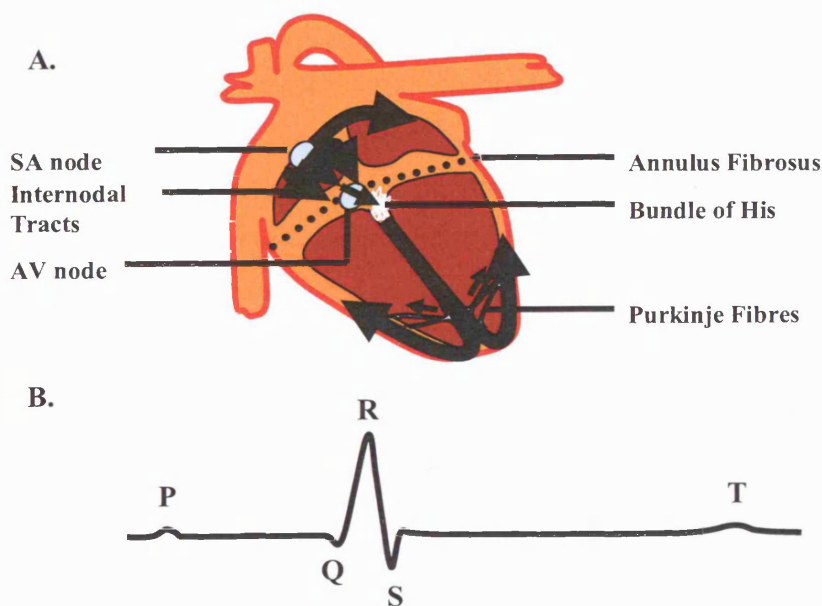


Figure 1.2. Electrical conduction through the heart.

(A) Cross-sectional diagram showing electrical conduction through the heart.

Abbreviations: SA – Sinoatrial; AV – Atrioventricular. (B) An ECG trace. P corresponds with depolarisation of the atria; the QRS complex occurs during depolarisation of the ventricles; and T corresponds with repolarisation of the ventricles.

1.2. The Cardiac Action Potential.

The studies described in this thesis are largely based upon alterations in the cardiac AP resulting from changes in different ionic currents across the sarcolemma. In particular, measurements of APD are made from cells isolated from mammalian ventricles. This section provides a brief summary of the roles of the ionic currents which give rise to the ventricular cardiac AP and the impact of gain or loss of specific ion channel functions on the configuration of the AP.

1.2.1. Ionic theory for determining membrane potential in a single cell.

The cardiac AP is a measurement of changes in membrane potential within a cardiac cell following stimulation. This is the result of opening and closing (or inactivation) of ion specific channels, as well as exchange of certain ions via various exchange systems and the resultant flow of ions across the membrane that generates current. Thus, during an AP, cell membrane permeability for any given ion alters and thus so does the membrane potential.

The effect of ionic permeability on the membrane potential depends on both the chemical driving force and the electrical driving force for each ion. At rest the sarcolemma of a cardiac myocyte is more permeable to potassium ions. Then, as a consequence of I_{K1} channels being open (see later), the resting membrane potential, RMP, is close to the equilibrium potential for potassium ions. If the concentration of potassium ions was equal on either side of the cell membrane, the RMP would therefore be close to 0 mV. However, there is also an ionic concentration gradient for potassium generated by the Na/K-ATPase, thus there is a larger concentration of potassium ions within the cell (≈ 140 mM) than outside (≈ 5 mM). Thus, the chemical driving force leads to potassium ions leaving the cell through open I_{K1} channels, resulting in a build-up of negative charge on the inner surface of the membrane. Consequentially, the RMP is generally between -70 mV and -90 mV, closer to the level at which the chemical driving force and the electrical driving force for potassium ions are opposite and equal, which is termed the “equilibrium potential” for potassium, E_K .

The equilibrium potential can be calculated for any given ion by determining the point at which the chemical and electrical forces being exerted upon the ion are of equal and opposite energy, which can be derived from the free energy equation (Hille, 2001). Equation 1.1 shows the free energy equation for potassium ions:

$$\Delta G = RT \ln \frac{[K]_o}{[K]_i} - zFE_m$$

Equation 1.1. The free energy equation

Where the $RT \ln \frac{[K]_o}{[K]_i}$ is the chemical driving force and zFE_m is the electrical driving force and where R is the Universal Gas Constant, T is the temperature (in Kelvin), z is the charge on the ion and F is the Faraday constant.

From this, when $\Delta G = 0$, the equilibrium potential for potassium ions can be calculated using the Nernst equation (Hille, 2001):

$$E_K = \frac{RT}{zF} \ln \frac{[K]_o}{[K]_i}$$

Equation 1.2. The Nernst equation

Whilst the RMP is much closer to E_K , it is still dependent upon the membrane permeability to a number of other ions. During the AP, as different ionic pathways open and close, the permeability of the membrane to different ions changes and therefore, so does the membrane potential. Whilst the Nernst equation can only derive the equilibrium potential for an individual ion, calculation of the membrane potential requires the calculation of not only the electrochemical potential, but also of the membrane permeability for all of the ions involved. This can be approximated using the Goldman-Hodgkin-Katz voltage equation (Hille, 2001). For example, if one were to consider only sodium, potassium and chloride ions:

$$E_m = \frac{RT}{F} \ln \frac{P_K [K]_o + P_{Na} [Na]_o + P_{Cl} [Cl]_i}{P_K [K]_i + P_{Na} [Na]_i + P_{Cl} [Cl]_o}$$

Equation 1.3. The Goldman–Hodgkin–Katz equation

Where P_K , P_{Na} and P_{Cl} are the relative permeabilities of potassium, sodium and chloride ions respectively. It should be noted that because chloride ions have a negative charge, whereas both sodium and potassium ions have positive charges; it is the intracellular concentration which appears in the numerator of the second part of the equation and the extracellular concentration which appears in the denominator.

1.2.2. Structure and function of ion channels.

In order to carry out their physiological role, ion channels are required to open and close influencing membrane permeability and hence membrane potential. This can be controlled by a number of different factors. Perhaps the most understood and most studied type of ion channels are those which are gated by changes in membrane potential (voltage-sensitive ion channels), but there are also many ion channels which are activated or deactivated by the presence of endogenous ligands. These can be extracellular, for example neurotransmitters such as acetylcholine (ACh), or intracellular such as adenosine triphosphate (ATP) or calcium ions.

The voltage-gated cation channels in cardiac tissue have a number of similarities in structure. The α -subunits of sodium and calcium channels are single proteins made up of 4 homologous components, each of which contains 6 transmembrane domains (TMDs). Both the hydroxyl and the N termini are intracellular (Figure 1.3). Studies using cysteine scanning mutagenesis in sodium channels (Yang *et al.*, 1996) and site-specific fluorescent labelling in potassium channels (Mannuzzu *et al.*, 1996) demonstrated that the fourth TMD, referred to as S4, is the voltage sensor. This is because it has a positively charged amino acid at every 3rd residue; a region that is highly conserved throughout all voltage-gated channels. Thus depolarization shifts these charges outward across the membrane field. In this manner, the voltage sensor moves in response to a change to more positive membrane potentials, channels become activated and then, as the voltage returns to more negative potentials, they become deactivated.

Voltage-gated potassium channels have a similar structure to voltage-gated calcium and sodium channels, except that instead of a single peptide comprised of 4 similar components, the pore-forming region is composed of a tetramer of α -subunits. Each subunit consists of 6 TMDs and TMD 4 acts as the voltage sensor. Figure 1.4 displays a single α -subunit, as well as the topology of most voltage-gated ion channels.

In addition to activation and deactivation, a variety of voltage-dependent channels also undergo inactivation, a distinctly different state, which leads to the inhibition of current passing through them. Generally, this process is dependent upon voltage, although it can also be modulated by other molecules or ions. Inactivation can also be linked to activation, as often a channel is required to be activated prior to inactivation. There are a number of different types of inactivation, of which the two found most commonly in voltage-gated ion channels are C-type and N-type. N-type inactivation occurs when a portion of the protein on the N terminus moves to obstruct the conducting path of the channel. This “ball and chain”

model for N-type inactivation was first suggested in 1977 by Armstrong & Bezanilla (1977) and later this was demonstrated in *shaker* potassium channels* (Hoshi *et al.*, 1990; Zagotta *et al.*, 1990). Further confirmation of the mechanism behind N-type inactivation was presented by mutations in the S4-S5 domains, which resulted in unstable inactivation strongly suggesting that is the site of the N terminal binding (Isacoff *et al.*, 1991; Zagotta *et al.*, 1990). Whilst this “ball and chain” mechanism is normally present on the α -unit of a channel, it is not unknown for it to be located as part of a β -subunit (for example see Morales *et al.*, 1995). C-type inactivation arises when a region of the pore becomes constricted and was again first demonstrated in *shaker* potassium channels (Hoshi *et al.*, 1990; Hoshi *et al.*, 1991; Zagotta *et al.*, 1990). Unlike N-type inactivation, which is relatively rapid, C-type inactivation generally has a long time course (Yellen, 1998), although hERG channels display a fast variant of C-type inactivation.

It is the ability of a channel to inactivate that in a large part determines the impact of any given ionic current upon the cardiac AP. For example, the sodium current, which is very large in ventricular cells (in the order of nA) and determines the upstroke of the AP, has voltage dependent inactivation properties that allow it to inactivate very rapidly. Thus although the sodium current is of great magnitude it is also very brief, not because the channel has deactivated, which would require a return to more negative membrane potentials, but because it has inactivated at more positive potentials.

Similarly to voltage-gated potassium channels, inward rectifying potassium channels in the heart are also expressed as a tetramer, except the α -subunits are much smaller proteins (normally roughly 400 amino acids in length) and have only two TMDs (Figure 1.6). As such, they do not possess the S4 voltage-sensitive domain and instead are often ligand-gated. Figure 1.6 shows an example of an inwardly rectifying potassium channel that also has β -subunits associated with it, such as the ATP-sensitive potassium channel, although some inward rectifiers do not have associated β -subunits, for example, those that underlie I_{K1} .

**Shaker* potassium channels were identified and named because certain mutations of these channels caused a leg-shaking phenotype in *drosophila melogangster* flies when they were exposed to ether (Kaplan & Trout W.E., 1969).

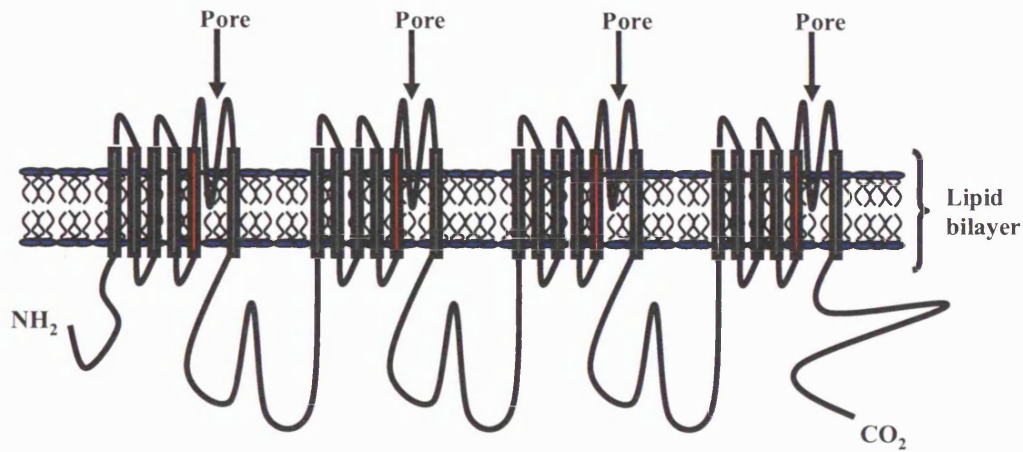


Figure 1.3. The structure of voltage-gated sodium and calcium channels.

Transmembrane domains are depicted as bars of which the voltage sensor (TMD4) is coloured red. Both the amino- and carboxy- termini are located on the intracellular side of the lipid bilayer.

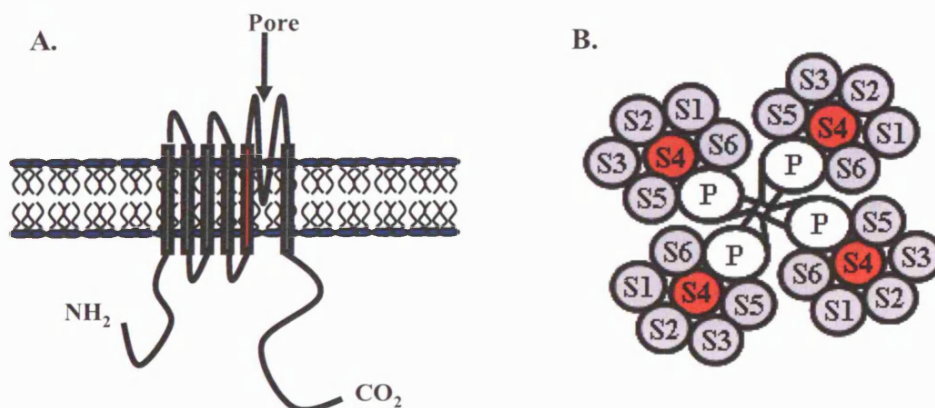


Figure 1.4. The structure of voltage-gated potassium channels and voltage-gated channel topography.

(A) A single α -subunit of a voltage-gated potassium channel. Transmembrane domains are depicted as bars of which the voltage sensor (TMD4) is coloured red. Both the amino- and carboxy- termini are located on the intracellular side of the lipid bilayer. (B) An overhead view of a voltage-gated ion channel showing a likely organisation of transmembrane domains, based upon the diagram shown in Durell *et al.*, 1998.

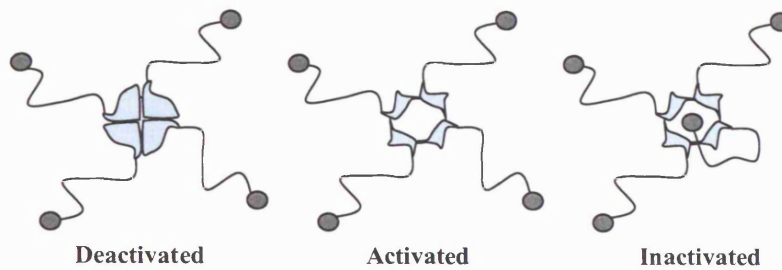
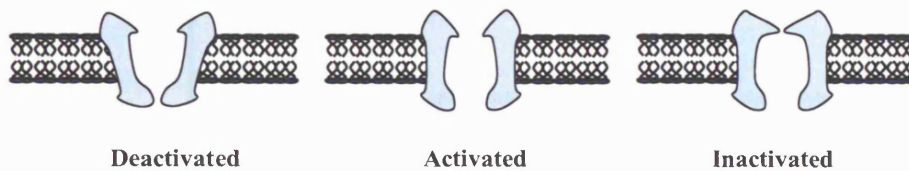
A. N-type inactivation**B. C-type inactivation**

Figure 1.5. N- and C-type inactivation gating in potassium channels.

(A) Top view of a potassium channel in three different conformations: deactivated (closed), activated (open) and inactivated via an N-type mechanism. (B) Cross-section of a potassium channel also shown in three different states except that inactivation has occurred via a C-type mechanism. Figure (A) adapted from Armstrong & Hille, 1998.

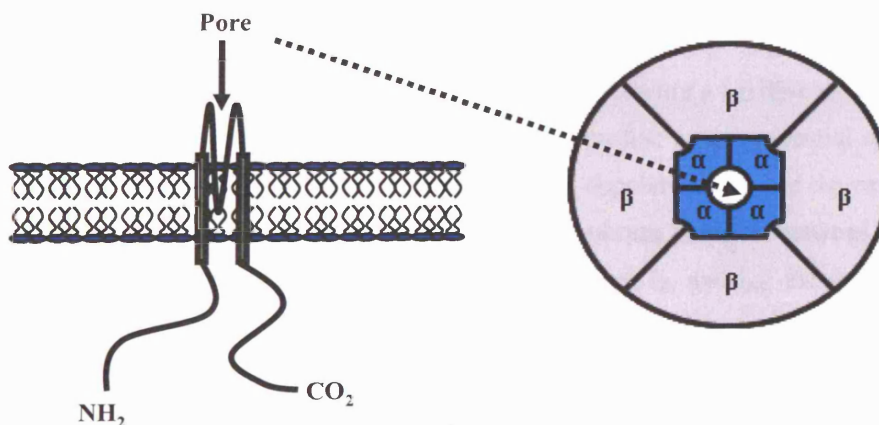


Figure 1.6. The structure of inwardly rectifying potassium channels and ion channel topography when combined with a β -subunit.

(A) A single α -subunit of an inwardly rectifying potassium channel. Both the amino- and carboxy- termini are located on the intracellular side of the lipid bilayer. (B) An overhead view of an inwardly rectifying ion channel showing both α - and also associated β -subunits, as in the example of K_{ATP} channels.

1.2.3. Ionic currents and their role in the cardiac action potential.

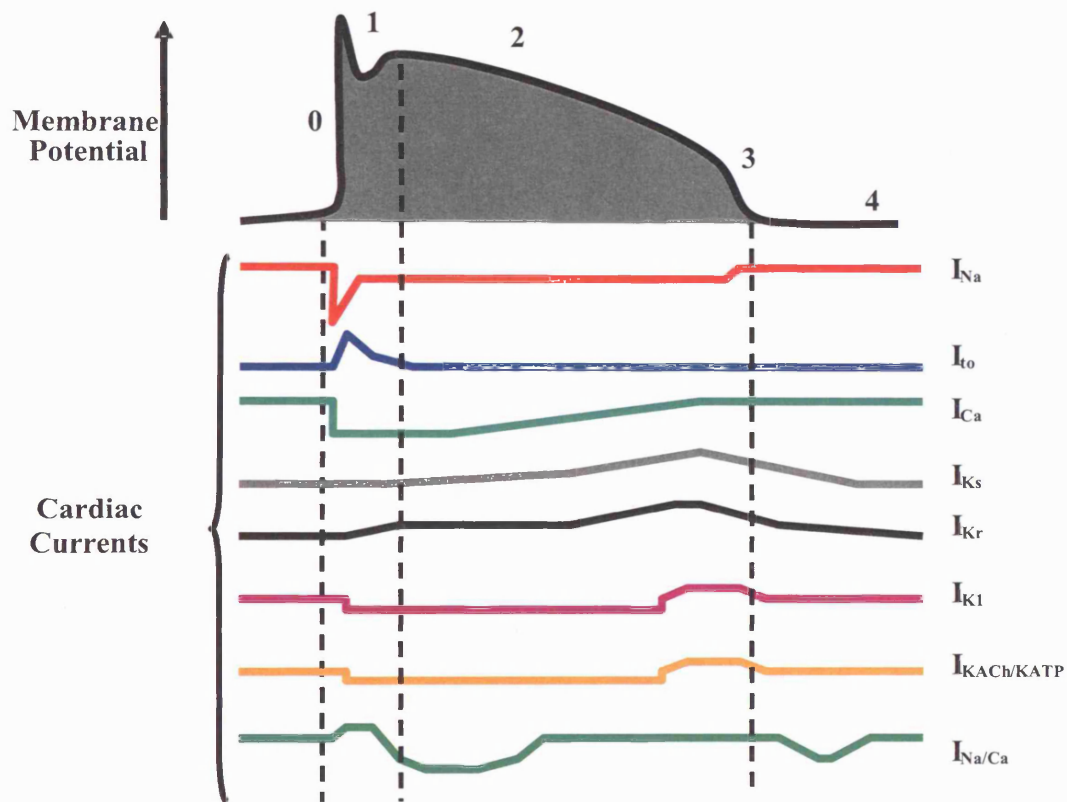


Figure 1.7. Schematic of the major ionic currents during a cardiac action potential.

The variations in membrane potential during a cardiac action potential are shown (top). Different phases of the AP are labelled 0-4. 0 is the initial depolarisation, 1 is the early repolarisation, 2 is the plateau and 3 is the late repolarisation. 4 is the membrane potential between action potentials. Currents shown include: potassium selective delayed rectifiers, I_{Kr} and I_{Ks} ; the inward calcium current which maintains the plateau, I_{Ca} ; I_{K1} , which maintains the membrane current, the sodium calcium exchanger, $I_{Na/Ca}$, sodium current, I_{Na} , which is responsible for the upstroke; the transient outward current, I_{to} , which is responsible for the notch; the inward rectifying currents, I_{KACH} and I_{KATP} . Current amplitudes are not to scale. Adapted from the diagram in Snyders, 1999.

A diagram showing some of the major currents and their temporal relationship with cardiac membrane potential during an AP is shown in Figure 1.7. This also illustrates the 4 different phases of the cardiac AP. Phase 0 is the initial depolarisation, 1 is the early repolarisation, 2 is the plateau and 3 is the late repolarisation. Phase 4 is the membrane potential between action potentials and is normally used to describe pacemaking activity in nodal cells or Purkinje fibres. However, for simplicity, this section shall focus on the ventricular AP, which does not exhibit pacemaker activity.

Sodium channels - Following initiation of an AP by an adjacent cell, the membrane potential rises very rapidly from its resting level between -70 mV and -90 mV, to a positive potential normally between +10 and +55 mV, depending upon cell type and species. This phase of the AP is referred to as phase 0 and is largely due to a rapid and relatively large inward sodium current. There are three different sodium channel α -subunits expressed in the heart: SCN1a, SCN3a and SCN5a (also referred to as Nav1.1, Nav1.3 and Nav1.5, respectively) of which SCN5a contributes the majority of the current and is often termed the cardiac sodium channel (Catterall *et al.*, 2005a). SCN1a and SCN3a are more slowly activating than SCN5a and thus may contribute more to the late sodium current than the early current, which has the primary role of generating the upstroke of the AP. There is also a β -subunit associated with sodium channels (Roden & George, 1997). Sodium channels are modulated by cAMP dependent protein kinases, PKC, (Cukierman, 1996) and thus may be modulated by muscarinic, adrenergic and purinergic innervation.

The sodium current generated is brief because of the very rapid N-type inactivation of these channels, from which most channels will not recover without subsequent repolarisation of sufficient duration. The N-type inactivation in sodium channels is described as a “hinged lid” formed by the intracellular loop between TMDs III and IV. Most likely this is why sodium channels inactivate quickly, as it has been demonstrated in *shaker* potassium channels that shortening “chain” regions in N-type inactivation does speed up the process (MacKinnon *et al.*, 1993). There are also some late openings of sodium channels within cardiac tissue, as demonstrated by voltage-clamp experiments in isolated ventricular myocytes (Saint *et al.*, 1992). These are responsible for late sodium current during an AP and thus contribute to the membrane potential during later stages of the AP.

A very important aspect of the kinetics of the cardiac sodium channel is its recovery from inactivation. Sodium channels require repolarization to recover from inactivation and a finite period in diastole (phase 4), at negative potentials, before another AP can be initiated. The time constant for recovery of sodium channels is 10 ms at -100 mV, 30 ms at -80 mV and 100 ms at -72 mV (Bers, 2001). As a consequence, repolarization must be virtually complete

before these channels can recover. Accordingly, under conditions where APs are greatly prolonged, for example in LQTS, a cell's ability to respond to an extrasystolic stimulus will be weakened. This can contribute to arrhythmogenesis (see later).

Calcium channels - There are two types of calcium channel in cardiac tissue: T-type, which is not detectable in most ventricular myocytes, but is expressed to a variable degree in conductive tissue and also in atrial cells, and L-type, I_{CaL} . In ventricular myocytes I_{CaL} contributes largely toward maintaining the plateau, phase 2. Thus during sustained plateau phases the inward calcium flux is roughly equal to the potassium efflux.

Upon depolarization, I_{CaL} activates rapidly and inactivates in a calcium and voltage-dependent manner. The voltage dependence of inactivation is relatively slow and is therefore largely governed by the size of the calcium transient during an AP. This serves as a negative feedback mechanism; when the calcium transients are larger, inactivation is accelerated, and thus calcium influx during the AP is relatively smaller and vice versa (Puglisi *et al.*, 1999). I_{CaL} plays an important role in regulating calcium transients within ventricular cells and both the influx of calcium through these channels and the resultant release of calcium from intracellular stores provides the calcium essential for excitation-contraction coupling. Although quite rapid, activation is comparably slow compared to sodium channels, so inward calcium flux exerts its predominant effects during the plateau phase of the AP. As such, I_{CaL} is the primary current which is balanced by potassium efflux during this phase. I_{CaL} is described further in Chapter 4.

Potassium channels - The largest and most widely studied family of channels in cardiac tissue is that of the potassium channels. These include the inwardly rectifying channels: I_{K1} , $I_{K(ACh)}$, and $I_{K(ATP)}$. Of these, I_{K1} , which is composed of Kir2.1 subunits (Kubo *et al.*, 1993), is a relatively strong inward rectifier, the purpose of which is to maintain the resting membrane potential near E_K . When the RMP fluctuates further from the equilibrium potential for potassium, the driving force exerted upon potassium ions becomes greater and thus I_{K1} current amplitude increases. However, upon depolarization, the increase in current does not change in a linear fashion with membrane potential due to inward rectification. This is conferred upon the channel by the presence of intracellular magnesium ions (Vandenberg, 1987) and polyamines, such as spermidine and spermine (Ficker *et al.*, 1994; Lopatin *et al.*, 1994). Physiological levels of magnesium and polyamines within a cell are within the range of 0.1 – 1 mM, while magnesium will cause 50 % block of the channel in the μM ranges and polyamines will also do so within the nM ranges. However, in the final phases of an AP, when the membrane potential approaches approximately -50 mV, inward rectification exerts

less of an effect and thus more potassium ions can pass through the channels. Thus, I_{K1} also has a role in the rapid repolarisation, phase 3, of an AP.

Other inwardly rectifying potassium currents which contribute to the ventricular action potential include the potassium channels, $I_{K(ACh)}$, and $I_{K(ATP)}$. $I_{K(ACh)}$ is a tetramer formed from two Kir3.1 subunits and two Kir3.4 subunits (also termed GIRK1 and GIRK4 respectively). These currents are activated by the $G_{i\beta\gamma}$ subunit (Reuveny *et al.*, 1994), which dissociates from the GTP binding protein, G_i , when the muscarinic receptor M_2 is activated. Thus $I_{K(ACh)}$ currents are larger under conditions of parasympathetic stimulation from agonists such as ACh. It is, therefore, unsurprising that there is a larger current density in nodal cells than in ventricular tissue, because the physiological consequence of $I_{K(ACh)}$ activation is to mediate the slowing of the heart rate.

$I_{K(ATP)}$ is present at high density within ventricular myocytes. $I_{K(ATP)}$ channels have a large conductance (Nichols *et al.*, 1991; Weiss *et al.*, 1992), thus it requires <1% of these channels to be open to reduce the AP duration by 50%. Ordinarily however, these currents are inhibited by physiological concentrations of ATP. However, the ability of ATP to inhibit the $I_{K(ATP)}$ is decreased at higher concentrations of intracellular ADP; thus it is most likely the ratio, $[ADP]_i/[ATP]_i$ which determines the activation of these channels; a process which may conserve energy during certain events, such as ischaemia. Expression of $I_{K(ATP)}$ and SUR, ATP binding cassette proteins, in pancreatic islet cells has demonstrated that these channels are modulated by a β -subunit. In fact cardiac $I_{K(ATP)}$ channels are expressed as octomers; the pore-forming region of the channel being composed of four Kir6.2 α -subunits and an outer ring of four β -subunits, SUR2A.

Another class of potassium channels expressed in cardiac tissue are the delayed (or outward) rectifiers: I_{Ks} , I_{Kr} and I_{Kur} . Although these channels are often described as outward rectifiers due to the steeper gradient of current exhibited at more positive membrane potentials, this supposed outward rectification is a result of the voltage-dependent gating of these channels, in contrast to the inward rectifiers which are not voltage-gated. Instead, the current increases as a direct result of more channels being open. They are often referred to as delayed rectifiers because the activation of these channels is relatively slow, thus the potassium efflux resulting from their activation exerts its major physiological role during the latter plateau and repolarization stages of the AP, phases 2 and 3.

The gene (KvLQT1) encoding for the α -subunit of I_{Ks} channels was first identified as the chromosomal location for mutations causing LQT1 (Wang *et al.*, 1996) and is associated with the β -subunit, minK (Sanguinetti *et al.*, 1996b). I_{Ks} is strongly regulated by both PKA

and PKC (Walsh & Kass, 1988; Walsh & Kass, 1991) and β -adrenergic agonists can increase current amplitude two-fold and shift activation to more negative potentials.

The human ether-a-go-go related gene, hERG, encodes for the α -subunit proteins, which form the potassium selective ion channels of I_{Kr} current. Expression in *Xenopus* oocytes has demonstrated mechanistic links between both mutations in hERG, which can cause LQT2, and drug block which can cause acquired LQTS, as well as demonstrating that hERG current is activated by high levels of external potassium (Kiehn *et al.*, 1996; Sanguinetti *et al.*, 1995; Sanguinetti *et al.*, 1996a). hERG is also regulated by a β -subunit. This is most commonly considered to be MinK related protein, MiRP1 (Abbott *et al.*, 1999), although this is still contested due to some discrepancies in voltage-dependent activation and drug affinities between hERG coexpressed with MiRP1 and native I_{Kr} (Weerapura *et al.*, 2002). Similar to other Kv channels, hERG channels are voltage dependent; depolarization results in channel activation at potentials more positive than -60 mV and as the membrane potential is further depolarized, channels also inactivate. Repolarization of the membrane causes the channels to deactivate.

However, the kinetics of hERG channel gating are dissimilar from most other Kv channels. Inactivation is considerably more rapid than activation and recovery from inactivation is significantly quicker than deactivation. Thus, although channels activate in response to depolarization of the membrane during an AP, outward conductance of potassium ions is limited because the channels then inactivate rapidly diminishing the capacity of the channels to contribute to the plateau phase of the AP. However, as the membrane potential begins to repolarize, hERG current increases as the channels recover from inactivation prior to their deactivation. Hence, the majority of current passed through hERG channels during an AP is often termed as tail current.

I_{Kur} is encoded for by Kv1.5. It activates more rapidly than either I_{Kr} or I_{Ks} and thus is likely to contribute to the late plateau or early repolarization (phases 1 and 2) of the cardiac AP. It has been identified in atria (Fedida *et al.*, 1993; Wang *et al.*, 1993) and thus may not influence ventricular repolarization, although it may be the same current as I_{Kp} , which has been identified in ventricular tissue (Backx & Marban, 1993; Nerbonne, 2000).

The transient outward potassium current, I_{to} , contributes to the early repolarisation, phase 1 of the AP. Channels responsible for I_{to} are dependent upon the membrane potential and exhibit relatively rapid activation and inactivation kinetics. There are two main components. The first, which activates more rapidly, is formed of subunits encoded for by Kv4.2 and/or Kv4.3, whilst the slower component is encoded for by Kv1.4 (Nerbonne, 2000; Xu *et al.*, 1999). There is also a difference between the recovery from inactivation for these two

components of I_{to} . Recovery from inactivation of the slower component has a time constant of approximately 1 s, compared to 30-50 ms for the fast component. This limits its contribution to the AP, particularly at higher pacing frequencies.

Thus, a summary of the contribution of different ion channels to the AP in a ventricular myocyte is as follows. Phase 0, the rapid upstroke, is initiated by passive current from a neighbouring cell. This activates sodium channels and as the inward sodium current becomes greater than the outward potassium current the membrane potential rapidly depolarises. As the membrane potential becomes more positive, this also results in reduction of the outward potassium current owing to the inward rectification of I_{K1} channels. Depolarisation ends when the outward current is equal to the inward current. This arises partly because the sodium channels inactivate, but also because potassium efflux increases as I_{to} and I_{Kur} channels open. Early repolarisation, phase 1, arises when the outward currents exceed the inward currents. This is due to further inactivation of sodium channels as well as the current carried by I_{to} and I_{Kur} channels. Following early repolarisation is the plateau, phase 2. This phase is generally relatively flat and consists of a gradual repolarisation. The inward current is largely carried by L type calcium channels. There are also outward currents carried by the delayed rectifier potassium channels (I_{Kr} , I_{Ks} and in some species, I_{Kur}). There is a delicate balance between these inward and outward currents, such that during the initial stages of the plateau they are almost equal in magnitude, hence the shallow slope of this phase. I_{Ks} , which activates more slowly, and I_{Kr} both increase in magnitude as repolarisation progresses. Thus the later stages of the AP have a steeper gradient. Phase 3, late repolarisation occurs when the rate of repolarisation accelerates greatly. As the membrane potential becomes more negative, the magnitude of I_{Kr} and I_{Ks} increases and this results in a progressive increase in the rate of repolarisation. During the initial stage of phase 3, I_{Kr} has a greater impact, however, when the membrane potential reaches more negative potentials (below approximately -30 mV) these channels become largely deactivated. However, the magnitude of I_{K1} is still increasing, again accelerating the rate of repolarisation.

There are also a number of other ion currents which contribute to the ventricular AP. These include a calcium activated chloride current, which is thought to contribute to the notch during Phase 1. These channels do not appear to be regulated by voltage but are instead activated by increases in intracellular calcium during the AP. There are also a number of ion exchangers present in the ventricular cell membrane. The Na/K ATPase is largely responsible for maintaining the ionic gradient for sodium and potassium ions (thus is essential for maintaining the resting membrane potential). A single ATP molecule can cause the Na/K

ATPase to transport two potassium ions into a cell and three sodium ions out of the cell. In healthy cells this is the only direction in which Na/K ATPase will transport ions and hence the current it carries is positive. Another ion exchanger present in cardiac cells is the sodium calcium exchanger (NCX), also discussed in the next section. Unlike the Na/K ATPase, the NCX normally functions in two directions during the AP. The accepted stoichiometry of the NCX is transport of 3 sodium ions in exchange for a single calcium ion. In forward mode the NCX extrudes calcium, whilst causing an inward flux of sodium (during which the resultant current is negative). NCX current is regulated by the intracellular and extracellular concentrations of sodium and calcium ions as well as by membrane potential. During diastole, intracellular calcium concentration is relatively low and therefore, NCX current (in forward mode) is also relatively small. However, during initial stages of the AP, when the membrane potential becomes more positive and passes the reversal potential of the NCX, outward current (calcium influx) becomes favoured. However, as the intracellular calcium concentration increases this moves the reversal potential of the NCX to more positive potentials thus favouring forward mode NCX current.

1.2.4. Cardiac calcium cycling.

The physiological relevance of the cardiac action potential is that it serves as a highly regulated means by which calcium can both enter and leave the intracellular space; the consequence of the rise in intracellular calcium concentration during systole is that the cell contracts. This is due to binding of myosin to actin, which occurs as a result of calcium ions binding to troponin C. Thus regulation of the cardiac AP and intracellular calcium transients governs both the force and frequency of contraction.

Calcium ions enter the intracellular space of ventricular muscle cells as a result of three mechanisms. The first mechanism occurs via opening of L-type calcium channels allowing an influx of calcium ions. The second occurs as a consequence of the calcium current, which causes the open probabilities of ryanodine receptors present on the sarcoplasmic reticulum to increase, thus causing calcium release (termed “calcium induced calcium release”, CICR (Lopez-Lopez *et al.*, 1995)). The third mechanism is via the NCX, which does display a brief positive current at the initial stages of an AP, in reverse mode, but also has a major role in removing calcium during repolarisation in forward mode. Intracellular calcium content is lowered by uptake into the intracellular stores via the energy dependent

sarcoplasmic endoplasmic reticulum calcium ATPase (SERCA) and extrusion via forward mode NCX current.

Calcium transients are governed by a number of feedback mechanisms and by autonomic innervation. For example, if the calcium transient results in a relatively high intracellular concentration, this inhibits the inward calcium flux by causing quicker inactivation of L-type calcium channels, as well as causing a larger efflux of calcium via the NCX. Whereas, at steady state, the calcium influx and efflux via the two pathways are roughly equal (Eisner *et al.*, 2000). β -adrenergic stimulation results in phosphorylation of phospholamban, a protein that would otherwise maintain an inhibitory effect upon SERCA. Thus sympathetic stimulation results in increased SR calcium content and quicker decay of calcium transients (Endoh & Blinks, 1988).

1.3. Generation of LQTS-based arrhythmia.

Drug Class	Examples of compounds associated with LQTS
Antiarrhythmic drugs	Class IA: Quinidine, disopyramide, procainamide Class III: Sotalol, amiodarone, ibutilide, almokalant, dofetilide Antibiotics Macrolides (erythromycin, clarithromycin, clindamycin, etc.) Trimethoprim-sulphamethoxazole Amantadine Pentamidine Imidazoles (ketaconazole, itraconazole, etc.) Chloroquine Quinine
Histamine receptor antagonists	Terfenadine, astemizole, diphenhydramine
Diuretics	Indapamide, thiazide
Antidepressants	Tricyclic antidepressants Fluoxetine, zimeldine (single case reports)
Antipsychotic agents	Thioridazine, chlorpromazine, risperidone, sertindole, trifluoperazine, haloperidol, perphenazine, pimozide
Anticholinergic agents	Cisapride, organophosphates (insecticides)
Inotropic agents	Amrinone, milrinone
Other drugs	Citrate (massive blood transfusions), , carbamazepine

Table 1.1. Drugs reported to cause QT interval prolongation.

Table showing examples of drugs from different classes that are associated with causing increases in the QT interval on an electrocardiogram. Based on the Table shown in Vohra, (2003).

As previously mentioned, mutations in a number of different cardiac ion channels can result in the generation of long QT syndrome (LQTS). These include LQT1, which is the consequence of certain mutations in the alpha subunit encoding for I_{Ks} ion channels (Wang *et al.*, 1996) and LQT2, which is caused by mutations in the hERG gene (Sanguinetti *et al.*, 1996a). Both LQT1 and LQT2 are the consequence of “loss of function” mutations in repolarising potassium currents (with the consequence of an extended AP duration). Some “gain of function” mutations are also associated with LQTS. For example LQT3 is generated by a number of different mutations in SCN5a sodium channels; the first discovered (Bennett *et al.*, 1995) and most widely studied being deletion of a KPQ sequence in the III-IV intracellular loop resulting in bursts of sodium current during later stages of the AP resulting in a prolonged ventricular APD. There are now at least 10 different proteins that may have mutations associated with LQTS, including some mutations of β subunits and anchoring proteins.

Acquired LQTS is a concern for the pharmaceutical industry and is caused by a wide variety of structurally different compounds that can have effects upon cardiac ion channels (Redfern *et al.*, 2003). Table 1.1 shows some examples of different classes of compounds that are associated with an increase in the duration of the QT interval on an ECG. A large proportion of compounds that cause acquired LQTS inhibit I_{Kr} current as a consequence of binding to the protein encoded for by hERG.

This section explains the clinical manifestations of LQTS as seen in ECG recordings and how they relate to changes in APD in ventricular tissue. Additionally, some of the structural characteristics of hERG protein that make it pharmacologically promiscuous are also explained.

1.3.1. Conditions leading to the generation of Torsade de Pointes (TdP).

As the name would suggest, Long QT Syndrome is expressed as a prolongation of the QT interval in the ECG (Figure 1.8.). Broadly speaking, the different waveforms expressed in the ECG correspond to the progression of excitation spreading throughout the different regions of the heart: the P wave relates to the depolarization of the atria, the QRS complex relates to the depolarization of the ventricles (during which the atria also repolarise) and the T wave corresponds to the repolarisation of the ventricles. This indicates that if the ventricular AP prolongs, then the QT interval will increase. If the AP prolongs excessively, a risk arises for the formation of an ectopic or premature beat, which can lead to the generation of

Torsades de Pointes (TdP), which may self-terminate or degenerate into ventricular fibrillation and sudden death.

Discovery of the mechanisms which lead toward the initiation of TdP have been the result of decades of research, firstly into congenital syndromes, which identified changes in ECG characteristics (prolonged QT intervals and abnormal TU waveforms (Jervell & Lange-Nielsen, 1957) and the association of ventricular tachycardias with incidences of sudden death (Ward, 1964). It wasn't until 1966 that the observation of a distinctive undulating formation of QRS complexes and T waves was documented and termed "Torsade de Pointes", which literally means "twisting of the points" (Dessertenne, 1966). The bases for the triggering of TdP, however, remained unknown. Later, early after-depolarizations, EADs, were linked to the production of TdP; under conditions of prolonged AP duration, slowing the stimulation rate of heart muscle cells was shown to generate EADs. This was associated with multiform ventricular tachycardias (Brachmann *et al.*, 1983). Research studies have since demonstrated that despite the apparent rarity of arrhythmogenesis, there are numerous risk factors associated with TdP including genetic predisposition, hypokalemia and the prescription of certain medications (Redfern *et al.*, 2003). It has also been proposed that the onset of TdP most likely requires the association of multiple risk factors at one time (Keating & Sanguinetti, 2001). Prescription medications, whilst they can cause acquired LQTS, can also unmask a genetic predisposition for abnormally increased QT intervals.

Early hypotheses proposed that the onset of TdP required two or more EADs, each behaving as a focus for excitation but firing at slightly different rates. Consequently, the waves of excitation would interact to varying degrees, depending upon the duration between the foci firing, thus resulting in the formation of TdP on the ECG (Bardy *et al.*, 1983). However, this process is unlikely because EADs would be required not only for triggering TdP, but also for sustaining it (Lazzara, 1997).

Currently theories suggest that arrhythmogenesis is the product of enhanced transmural dispersion (TDR): different regions of the ventricle wall repolarize with varying rapidity and a consequence of this is heterogeneous refractoriness across the ventricular wall, an idea that was first suggested in 1989 (Janse & Wit, 1989). The ventricular cell wall consists of three different types of myocytes, which are separable by their location and by differing expressions of a number of ion channels (described in the following section). The epicardial cell layers form the exterior of the ventricle wall, the endocardial cell layers form the inside wall of the ventricle, and midmyocardial cells, M cells, are the regions of myocytes between. In response to slowing of heart rate and to a large number of proarrhythmic conditions, including I_{Ks} block, I_{Kr} block, activation of I_{Na} and activation of I_{Ca} (Antzelevitch, 2005) the APD of M cells prolong disproportionately.

This presents an environment for re-entry; a mechanism first proposed in the jellyfish *Scyphomedusae* (Mayer, 1906) in 1906, although there are now a number of variations which can be described (Antzelevitch, 2001). In cardiac tissue, re-entry occurs when, following the initial depolarisation during a single heartbeat, a region of tissue becomes re-excited as a result of heterogeneous refractory and excitatory periods within that tissue. Cardiac tissue has a number of requirements for re-entry to occur: firstly, the locus of the re-entrant site in the myocardium must be susceptible to excitation by more than one pathway; secondly, one of these pathways must be subject to a conduction block. This can be permanent (eg. the result of physical damage) or dynamic, for example in a refractory state (which is more pertinent to the channelopathies responsible for some conditions of LQTS); and finally, the duration of the circuit must be long enough to allow recovery from the refractory period where required. In principle, if a given region of the myocardium, such as the midmyocardial area, has an abnormally delayed repolarization in response to any proarrhythmic factors, then that region will not have recovered from its refractory period at the same time-point as epicardial and endocardial areas (which do not have as pronounced a delay in repolarisation) will. In a situation where an EAD has occurred, this provides a source of excitation for the epi or endocardial cells, whilst the M cells, which had exceptionally prolonged repolarisation will provide a block to this excitation. Eventually, the wave of excitation will spread around the region in its refractory period until it too has recovered, and is thus excited, but from a different direction than where the EAD originated. This system therefore, provides a unidirectional block and thus fulfils the requirements for re-entry. In the instance of arrhythmia, this pattern can self-propagate and develop into ventricular fibrillation (VF).

On an ECG, the increase in transmural dispersion can often be detected by alterations in the T wave, which occurs due to the repolarization of the ventricles. It may well be this difference in repolarization rates across the ventricular wall that provides the conditions necessary for re-entry to occur. Ultimately, if this were not present, the occurrence of an EAD would probably not be able to propagate into a self-sustaining circuit.

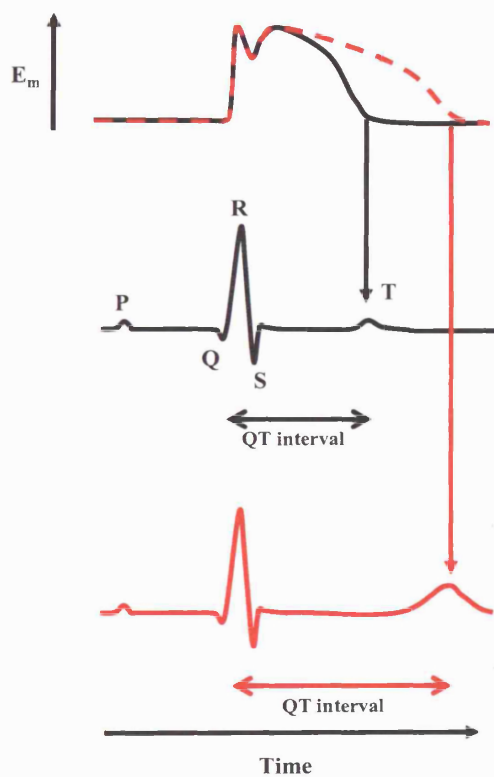


Figure 1.8. Ventricular action potential prolongation and Long QT syndrome.

Upper trace shows an illustration of a ventricular action potential. The middle trace shows an illustration of a corresponding electrocardiogram. The red traces of both the ventricular action potential (top dashed) and an ECG (bottom) show a prolonged ventricular action potential and the corresponding ECG trace.

1.3.2. The M cell.

As discussed, the ventricular wall is composed of three different types of myocyte (see Figure 1.9.): endocardial cells, which form the inner wall; the epicardial cells, which form the outer wall; and the M cells, which are in between. The differences between the different cell types, aside from location within the ventricular wall, are largely based upon differences in ion channel current density and the consequential differences in AP morphology. For example, there is an increased current density of I_{to} toward the outer regions of the canine ventricular wall; thus APs from epicardial and M cells display a characteristic notch and dome appearance (see later in Chapter 3), which is absent in endocardial myocytes (Liu *et al.*, 1993).

M cells display a prominent increase in APD as a result of either drug block of repolarizing currents or in response to bradycardia as a consequence of a lower repolarisation reserve. Specifically, the current density of I_{Ks} is substantially lower in M cells than in either epi or endocardial cells. In contrast M cells display relatively larger late sodium current, which may also contribute to the longer APD, as well as an increased sodium-calcium exchange (Zygmunt *et al.*, 2000). Expression of I_{Kr} and I_{CaL} are similar in both midmyocardial and epicardial cell types (Szabo *et al.*, 2005).

In examples of acquired LQTS, where only I_{Kr} is inhibited, for example during administration of dofetilide, transmural dispersion is increased because both the epi and endocardial regions will repolarise more rapidly due to the presence of I_{Ks} , which is only minimal in M cells. Compounds such as quinidine, which block numerous cardiac ion channels, can therefore have different effects upon TDR depending upon its concentration. At lower concentrations, quinidine causes an increased TDR due to inhibition of I_{Kr} , which causes the APs of M cells to prolong more than either the epi or endocardial cells. However, at higher concentrations, quinidine also inhibits I_{Ks} and I_{Na} , resulting in increases in APD in epi and endocardial cells and a reduction in TDR (Antzelevitch, 2005; Balsler *et al.*, 1991).

The likelihood of an arrhythmogenic event occurring is also increased by the topography of M cells. Whilst the M cells do form a separating layer between the epi and endocardial layers, it is not uniform. Optical mapping techniques across the ventricular wall have revealed that there are islands where the refractory period increases steeply; a situation which, under conditions of LQTS, likely increases the probability of a re-entrant mechanism being able to cycle (Akar *et al.*, 2002).

To summarise, arrhythmic events can arise from conditions during which the TDR across cardiac tissue is increased. Under conditions of proarrhythmia in ventricular tissue, this

can be caused by excessive prolongation of APs in midmyocardial tissue that does not occur in surrounding layers of epi and endocardial tissue.

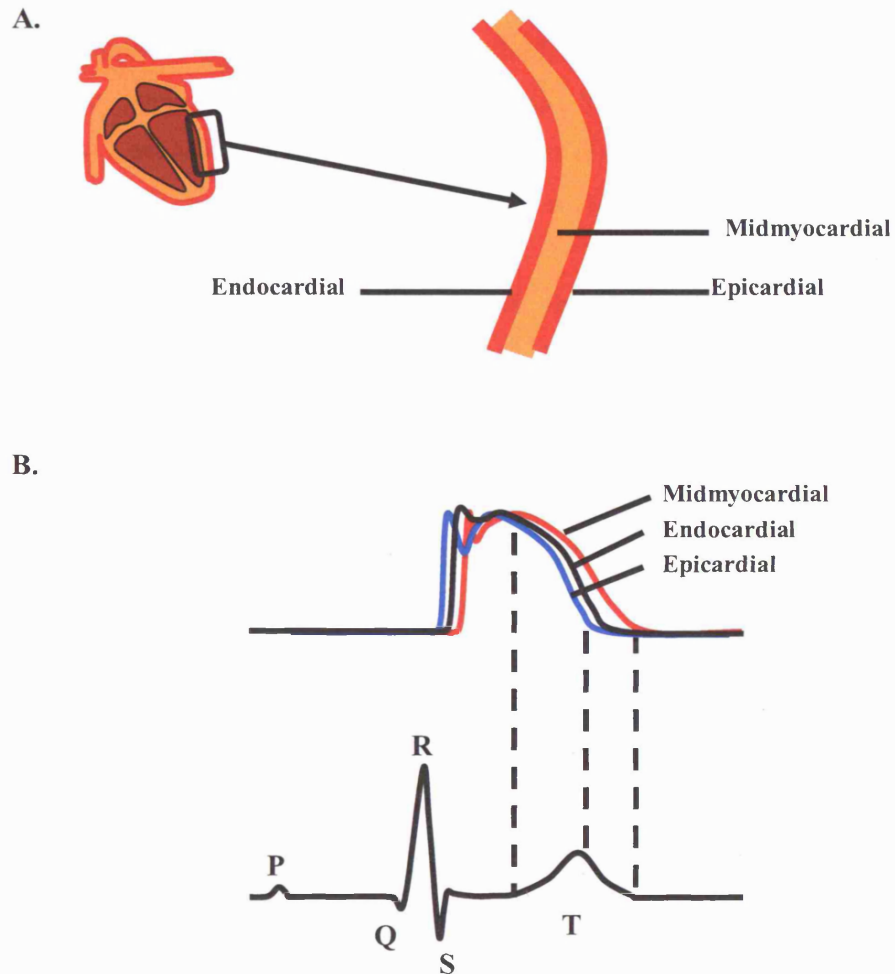


Figure 1.9. Endocardial, Midmyocardial and Epicardial ventricular layers.

(A) Cross-section demonstrating the different layers of the ventricle wall. (B) Representative traces of endocardial (black), epicardial (blue) and midmyocardial (red) action potentials and their temporal relation to an electrocardiogram. Figure (B) adapted from Shimizu & Antzelevitch, 1999.

1.3.3. Afterdepolarizations.

When a region of cardiac tissue is no longer in its refractory period and is therefore susceptible to excitation from neighbouring tissue, a depolarising stimulus is required to trigger re-entry. The presence of an afterdepolarisation is considered likely to trigger such an event. There are two different types of afterdepolarisations that can occur in cardiac cells: early afterdepolarisations (EADs) and delayed afterdepolarisations (DADs) (see Figure 1. 10). Whilst there is some overlap of the actual physiological mechanisms underlying their occurrence, they are defined differently because an EAD can only occur during the late plateau and repolarization stages of the AP, whilst a DAD can only occur after the AP has completely repolarized.

If an EAD occurs at a membrane potential above -40 mV it has been suggested that inward L-type calcium current may be responsible. A cell is vulnerable to this type of event if the AP is prolonged in response to either pharmacological intervention, hypokalemia or bradycardia. As the AP prolongs some calcium channels may recover from inactivation. The likelihood of this increases as the intracellular calcium levels decline, since calcium promotes inactivation of the channels (Luo & Rudy, 1994; Sipido *et al.*, 1995) and if the wave form of the AP becomes triangulated (Guo *et al.*, 2007).

If an EAD occurs during late repolarization, or a DAD occurs, it is not possible for recovery of I_{CaL} to contribute to the extrasystole because at membrane potentials more negative than -40 mV the channels will be deactivated. Thus extrasystoles that occur at more negative potentials are likely to be evoked by currents arising from accumulation of intracellular and SR calcium concentration and consequential SR calcium release events. The prime candidates for calcium activated inward currents under such conditions are reverse-mode NCX and calcium activated chloride current. It appears likely that the NCX is the primary current responsible for DAD occurrence; blocking the chloride currents with niflumate does not prevent DAD occurrence induced by caffeine, whereas inhibition of the NCX current by replacing extracellular sodium and calcium ions with lithium and magnesium ions respectively, results in >90% inhibition of DADs (Schlotthauer & Bers, 2000).

In cases of LQTS, an EAD is considered to be the most likely extrasystolic trigger for re-entry. However, whilst reactivation of L type calcium channels is considered to be the most likely cause, simultaneous optical mapping of membrane potential and intracellular calcium has demonstrated that in rabbit hearts with simulated LQT2, increases in intracellular calcium are also associated with EAD formation (Choi *et al.*, 2002). Similarly, in canine ventricular wedge preparations, the presence of an I_{Ks} inhibitor in conjunction with a β -adrenergic agonist has been shown to produce DADs and not EADs (Burashnikov & Antzelevitch, 2000).

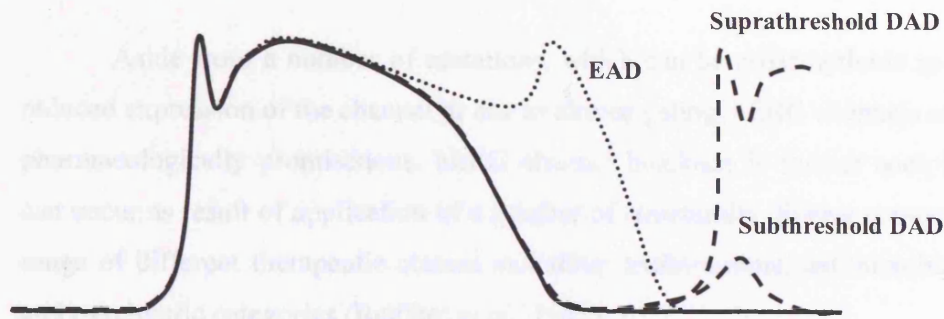


Figure 1.10. Extrasystoles: EADs and DADs.

Traces representing a normal ventricular action potential and those with an extrasystolic depolarization including: an early afterdepolarization (dotted line) and supra and subthreshold delayed afterdepolarizations (dashed lines).

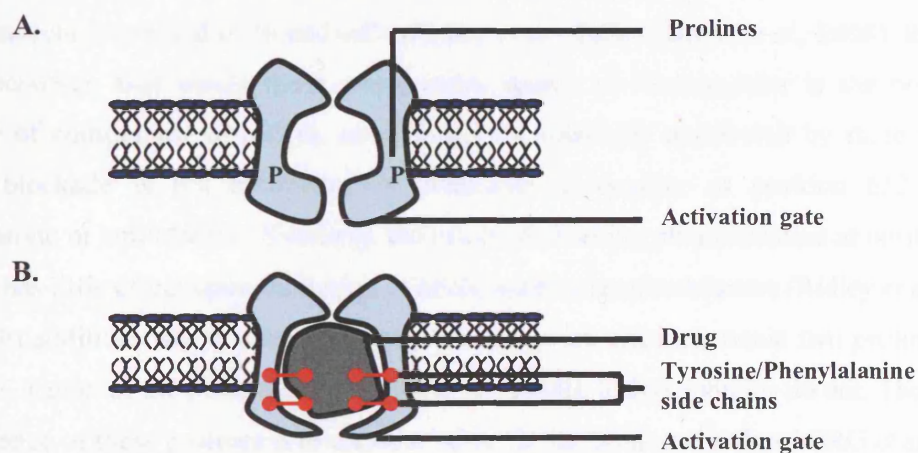


Figure 1.11. Unique structural features of hERG.

A. Cross section showing the structure of a typical Kv type potassium channel. B. Cross-section of a hERG potassium channel showing the increased inner pore space and binding sites within the pore. Based upon the figure in Keating & Sanguinetti, 2001.

1.3.4. The importance of the hERG gene in acquired LQTS.

Aside from a number of mutations, which can be proarrhythmic as a result of either reduced expression of the channel or due to altered gating, hERG channels are also considered pharmacologically promiscuous. hERG channel blockade is further complicated because it can occur as result of application of a number of structurally diverse compounds from a wide range of different therapeutic classes including: antihistamine, antimicrobial, antiarrhythmic and psychiatric categories (Redfern *et al.*, 2003).

A number of studies have since illustrated that hERG ion channels have unique structural characteristics that make them susceptible to pharmacological blockade. One particular study used mutations of individual amino acids to alanine within the pore of hERG. The mutants produced (expressed in oocytes) were then screened with a potent hERG blocker, MK-499 to determine which amino acids were essential for drug binding. Consequently it was discovered that mutating two amino acids: tyrosine at position 652 and phenylalanine at position 656, which are not conserved in other Kv channels, reduced the affinity of not only MK-499, but also other hERG blockers: terfenadine and cisapride (Mitcheson *et al.*, 2000a). These amino acid residues have since been shown to be important in the binding of other compounds to hERG. For example, mutations of tyrosine at position 652 or phenylalanine at position 656 to alanine reduces the inhibitory effects of ketoconazole and thioradizine on hERG current expressed in cloned cells (Ridley *et al.*, 2006; Milnes *et al.*, 2006). It should be noted however, that whilst these amino acids appear to be important in the binding of a number of compounds to hERG, some drugs are relatively unaffected by these mutations. hERG blockade is not eliminated in mutations of tyrosine at position 652 by either dronedarone or amiodarone. Similarly, the effect of mutating phenylalanine at position 656 to alanine has little effect upon inhibition of hERG current by dronedarone (Ridley *et al.*, 2004).

In addition, where other voltage-gated potassium channels retain two proline residues in the S6 region of the protein (del Camino *et al.*, 2000), hERG subunits do not. The structural significance of these prolines is to create a “kink” in the S6 domain, thus hERG channels have a larger pore cavity (del Camino *et al.*, 2000). Thus hERG channels are able to trap larger drugs within the inner cavity where other potassium channels cannot (Mitcheson *et al.*, 2000b). The corollary of the structural differences between hERG and other potassium channels is that hERG has a heightened sensitivity to a more structurally diverse population of drugs.

1.3.5. *In silico* hERG binding models.

The ion channel that is most often implicated for underlying proarrhythmic events is the hERG channel due to its pharmacological promiscuity. For this reason a number of studies have generated pharmacophore models to predict the structures of chemicals that may block hERG. The first attempts to model compounds that increased APD were published prior to the first observations that these compounds may have a detrimental effect. (Morgan & Sullivan, 1992), predicted a pharmacophoric scheme based upon the activity of class III antiarrhythmics, which cause APD prolongation. The suggested structure consisted of a central basic nitrogen atom linked to a *para*-substituted phenyl ring via a 3-4 atom chain; two other substituents are also present, of which one or both must include an aromatic ring within 3 atoms of the basic nitrogen centre. Remarkably, the suggested pharmacophore bears strong similarities to pharmacophores published a decade later; Cavalli *et al.*, (2002) developed a pharmacophore based upon 31 different QT prolonging compounds, whilst Ekins *et al.*, (2002) further tested a pharmacophore model based upon antipsychotic hERG inhibitors. The central basic nitrogen is a feature common to all three models. Seemingly, both the Ekins and Cavalli models describe the presence of either three hydrophobic centres or four aromatic moieties as substituents, respectively, which do not necessarily have to be simultaneously present. Hence, in all cases, the structural format consists of a central ionisable feature bearing a number of hydrophobic groups at similar distances. Unfortunately, whilst pharmacophore models provide a very useful tool in hERG screening assays, they do not yet have the predictive power to replace *in vitro* screens (discussed in detail in the next section). One of the more recent published *in silico* models demonstrates false negative and false positive reports in 29% and 15% of compounds tested respectively (Aronov & Goldman, 2004). However, it is likely that as more compounds are studied the predictive value of these types of test will improve measurably.

1.4. Screening for proarrhythmic compounds.

Screening for proarrhythmic compounds presents a very complex problem. Drug-induced cardiac events are rare enough to make detection difficult, whilst common enough to limit the use of certain compounds, especially where the benefit does not outweigh the risk. For example, cisapride, which has been withdrawn from the U.S. market, only induced TdP in 1 in every 120 000 subjects (Haverkamp *et al.*, 2000), yet its therapeutic value lay in its ability to inhibit acid reflux within the stomach, which is not considered a life threatening event.

Cardiac safety screening is further complicated in that, whilst the majority of drug-induced occurrences of TdP can be associated with hERG blockade, the reverse is not true. In some examples an increase in AP or QT duration may not even be arrhythmic. In addition, due to the complexity of the ionic composition of the cardiac action potential, compounds can cause multi-ion channel blockade. In such instances the severity of cardiac effect may be dependent upon both the ion channels that are inhibited and the affinity of the compound for the ion channels concerned; and in rare circumstances may even constitute an antiarrhythmic effect.

1.4.1. Early preclinical screens.

Due to the high number of potential therapeutic compounds being synthesised using modern techniques, combined with the relatively large number of compounds withdrawn from late stages of drug development, a number of early-stage assays have been developed with the potential for medium-high throughput screening. Largely, these have been developed utilizing hERG transfected mammalian cells and their efficiency for detection of hERG blockers has been measured relative to that of the whole-cell patch clamp.

Binding studies- The most basic of these assays is a binding assay, which uses a tritiated form of the class III antiarrhythmic, dofetilide, as a competitive antagonist against any candidate drug. In a study of 22 known hERG blockers the affinity of compounds compared favourably with their efficacy in patch clamp experiments, both at differing concentrations of external potassium and using membrane preparations or intact cells (Diaz *et al.*, 2004).

Rb efflux- The rubidium efflux assay is performed using hERG transfected human embryonic kidney 293 (HEK 293) cells. Incubation of these cells in a medium in which potassium ions have been replaced with rubidium ions causes the accommodation of an intracellular concentration of rubidium. Thus, subsequent depolarisation with a solution containing a high concentration of potassium ions, 50 mM, results in an efflux of rubidium via hERG channels. Following removal of the supernatant and cell lysis the relative rubidium efflux can then be determined with a spectrometer. If the cells are exposed to a hERG current inhibiting compound prior to the depolarising phase, the rubidium efflux may be diminished, thus providing a valuable assay (Chaudhary *et al.*, 2006).

Optical measurements of membrane potential- The resting membrane potential of cloned mammalian cells transfected with hERG can also be altered by hERG blockade. Thus, whilst until recently (see next paragraph) standard patch clamp techniques do not adequately lend themselves to higher throughput assays, it is still possible to screen large number of compounds using a fluorescence-based system and a voltage-sensitive dye. Use of a multi-well plate and a plate reader has demonstrated that it is possible to record positive shifts in membrane potential in hERG transfected CHO cells in response to a number of hERG inhibiting compounds by using the dye bis-[1,3-dibutylbarbituric acid]trimethine oxonol (DiBAC₄(3)) which partitions itself within cell membranes differentially upon changes in membrane potential (Dorn *et al.*, 2005).

Planar array electrophysiology- A number of planar array-based electrophysiological tools have been developed for medium throughput compound screening. One of the most successful of these is the Ionworks HT™ screen (discussed in more detail in the Methods). The premise is to use a multi-well patchplate™ to separate two fluid layers. Cells are placed into the wells and positioned onto a hole in the base. The cell membrane region covering the hole is then permeabilised using an antibiotic solution, thus forming an equivalent to a whole-cell patch clamp configuration, in multiple wells at one time (Bridgland-Taylor *et al.*, 2006; Schroeder *et al.*, 2003).

The intention of these medium throughput screens is to provide a means to eliminate large numbers of compounds that may cause adverse cardiac events, prior to further testing. This would avoid the excess labour, animal usage and costs involved in drug development. However, whilst they provide a fast and low-cost solution they do have drawbacks. The most widely used comparison in hERG screening is that of the classical whole cell patch clamp using hERG-transfected mammalian cells and a number of these new technically advanced assays do not display the sensitivity of this method. Use of the fluorescence assay has demonstrated a 12% likelihood of a false positive result (Dorn *et al.*, 2005); a problem because this assay may therefore prevent useful compounds from being evaluated further.

The rubidium efflux assay is less responsive to hERG blocking compounds than either the tritiated binding assay or patch clamp recordings (Chaudhary *et al.*, 2006); a result which is due to the use of rubidium as a permeant ion, which lowers the affinity of compounds to hERG by 3-10 fold (Rezazadeh *et al.*, 2004). Most advances appear to have been made in development of the Ionworks HT™ assays. Although in some studies the Ionworks HT™ has been outperformed by both patch clamp studies and the rubidium efflux assay (Guthrie *et al.*, 2005; Sorota *et al.*, 2005), its ongoing development has provided a number of insights into methods, which may increase its productivity. For example, a recent study has demonstrated that the performance of the Ionworks™ is improved by using a minimal cell concentration within the wells (Bridgland-Taylor *et al.*, 2006). Perhaps other reasons for its success include its versatility; unlike the other high throughput assays described, but more akin to the patch clamp, Ionworks HT™ can be used to monitor any cellular current, provided the underlying channel can be transfected into a cell line. As a number of proarrhythmic compounds have been demonstrated to cause multiple ion channel blockade, this advantage outweighs its lack of sensitivity.

However, the predictive values of these screens can be misleading. Use of binding assays assumes that the binding site of the competing antagonist will be the same as that of the compound being tested. Both binding assays and hERG current screening technologies rely upon the efficacies of test compounds being similar in both the cloned and native channels.

1.4.2. *In vitro* proarrhythmia models.

Despite the usefulness of high throughput screens, potential candidate drugs are still required to undergo screens in native cardiac tissue to assess their proarrhythmic potential in a more physiological preparation. *In vitro* preclinical trials are thus required following screening of compounds for their effects upon individual cloned channels. At present there is no single *in vitro* assay that appears to be totally predictive of proarrhythmic potential. Whilst QT prolongation and hERG current inhibition are both associated with TdP, neither can be used alone to predict the proarrhythmic potential of a compound because delay of repolarisation is not necessarily torsadogenic. Furthermore, the degree of QT prolongation cannot be correlated with incidences of TdP (Redfern *et al.*, 2003). A number of studies have demonstrated that QT prolongation alone is not proarrhythmic unless accompanied by another parameter. Antzelevitch and Shimizu (2002) suggest that QT prolongation is only proarrhythmic if accompanied by an increase in transmural dispersion of repolarisation

(TDR). Furthermore, a number of studies also demonstrate that increases in beat-to-beat variability (also referred to as instability) can be used as a predictive marker for proarrhythmia (Thomsen *et al.*, 2004; Thomsen *et al.*, 2006). Therefore, there are a number of different markers used to evaluate proarrhythmic potential including AP prolongation, increases in the QT interval (on a pseudo ECG), reverse use dependence (when the propensity of a compound to prolong the APD decreases with quicker heart rates), instability and triangulation (Hondeghe, 2005). A schematic of the different parameters used for detection of proarrhythmic compounds is shown in Figure 1.12. Thus, the value of an assay is also determined by the parameters it is able to measure. This is further influenced by selection of species and the tissue preparation.

The more basic *in vitro* assays available are based upon electrophysiological recordings of APs from isolated cardiac tissues. These include sharp electrode recordings from Purkinje fibres of either rabbits or dogs (Champeroux *et al.*, 2005; Gintant *et al.*, 2001; Lu *et al.*, 2002). Microelectrode studies on isolated ventricular myocytes have also been shown to be feasible (Liu *et al.*, 1993; Liu & Antzelevitch, 1995). These assays are beneficial because they allow for the use of more than one cell or fibre bundle from a single animal, although, use of Purkinje fibres is significantly time consuming and can often require a single operator per fibre. Although Purkinje fibres are part of the conducting network in the heart, their intrinsic pacemaker activity is very weak, and their ionic conductances bear more similarity to those of an M cell than nodal tissue. Thus, Purkinje fibres, like M cells, will exhibit exaggerated AP prolongation upon either slowed pacing rates or exposure to an AP prolonging drug. When utilizing the AP morphology of myocytes for detecting proarrhythmic potential in test compounds, the M cell is a more suitable cell type to study than either the epi or endocardial cells.

Both of these assays on myocytes and Purkinje fibres are able to monitor AP prolongation, triangulation and reverse-use dependence. Measurements of short-term variability, which may bear similarities to instability, have also been published in myocytes (although not Purkinje fibres) (Thomsen *et al.*, 2004). Thus these assays provide advantages over screens for alterations in cardiac ion currents because they allow for monitoring the interaction of all the different currents as they are expressed in their native cell type. Because compounds may have effects on multiple ion channels at differing concentrations, the net effect upon the cardiac AP may only be seen in assays using native tissue. This is especially important in circumstances when drugs may cause AP prolongation in absence of triangulation or instability, which may be antiarrhythmic (Hondeghe *et al.*, 2001). Whilst it

is not possible to use a single myocyte to demonstrate TDR, it is possible to isolate myocytes from different regions of the ventricles to allow for comparisons to be made.

More technological and animal-intensive assays include a number of different Langendorff whole heart preparations and ventricular wedge preparations. A relatively large number of compounds have been screened using a Langendorff heart model and analysis system called SCREENIT, which relies on a TriaD (Triangulation, Reverse-use dependence, Instability and Dispersion) based system of analysis (Hondeghe *et al.*, 2003; Hondeghe & Hoffmann, 2003). The principle is that AP prolongation alone is not proarrhythmic, so the model therefore uses the parameters described by TRIaD as surrogates for proarrhythmia (Lawrence *et al.*, 2005).

The ventricular wedge preparation has been developed using canine cardiac muscle tissue. This is set up by dissecting an intact wedge of ventricular tissue, perfusing it via an artery and placing floating electrodes in the three different layers of the wedge. Whilst technically difficult to achieve, this preparation allows for the recording of APs from endocardial, midmyocardial and epicardial regions of the heart whilst simultaneously recording a pseudo ECG (Yan *et al.*, 1998). Accordingly, it is possible to obtain a measure of TDR, AP and QT prolongation, reverse-use dependence as well as a visualization of altered ECG characteristics. Thus, this is a data-rich assay, but requires considerably more technical expertise even than electrophysiological experiments on isolated fibres or cells.

In determining the appropriateness of an assay for screening for proarrhythmic potential, an important distinction to be made between different *in vitro* assays is that of the tissue type used. Although Purkinje fibres and M cells do behave similarly in the majority of drug applications there are exceptions. For example, (Gintant *et al.*, 2001) demonstrated a 92% success rate in identifying proarrhythmic compounds using a Purkinje fibre assay; the only known proarrhythmic compound used in this study that did not elicit AP prolongation was terfenadine (discussed in more detail in Chapter 5), whereas, a study utilizing the same maximum terfenadine concentration (10 μ M), was able to induce polymorphic ventricular tachycardia/fibrillation in the ventricular wedge preparation (Fish & Antzelevitch, 2004). Further discrepancies can also arise from species differences. (Lu *et al.*, 2002) demonstrated that, using pharmacological blockers to simulate LQT1, 2 and 3, rabbit hearts displayed QT prolongation only in LQT2 and LQT3. This may arise from lower expression of I_{Ks} in rabbit cardiac cells, for example in comparison to the canine heart (Dumaine & Cordeiro, 2007).

In addition, TdP is a rare event and is considered to occur during the presence of more than one risk factor. Thus, a number of preparations have been designed to increase the

likelihood that a proarrhythmic event may occur. Examples of this include using a relatively low concentration of potassium in the external solution or applying β -agonists to a preparation in addition to test compounds (Burashnikov & Antzelevitch, 2000). One such method that is employed in screening techniques is the use of hearts with remodelled ionic currents. In canine cells, this has been developed by using chronic, complete atrioventricular block, achieved by *in vivo* injection of formaldehyde into the AV node. After 3-4 months this results in an increased ventricular mass, which is suggested to be a compensated form of left ventricular hypertrophy. Of more relevance to proarrhythmia assays however, this preparation also demonstrates a 20-30% increase in monophasic APD in whole hearts, and 10-30% increase in APD in isolated myocytes, which is thought to be attributable to down-regulation of both I_{Kr} and I_{Ks} (Volders *et al.*, 1999). Whilst chronic AV block has demonstrated enhanced susceptibility for TdP in canine cells and rabbit Langendorff models (Eckardt *et al.*, 1998), acute AV block in Langendorff rabbit hearts (Kii & Ito, 2002) has also been used to study drug-induced arrhythmias. Although acute AV block will not allow time for ionic remodelling, the consequence of this technique is a basal bradycardia with greater susceptibility for tachyarrhythmias.

1.4.3. *In vivo* proarrhythmia models.

Ultimately, prior to clinical trial in humans, compounds are required to undergo *in vivo* safety testing. Because the focus of this study is not based upon this type of screening process I shall merely list a couple of illustrations rather than make a detailed analysis. Examples include anaesthetized rabbits concomitantly treated with methoxamine (Carlsson *et al.*, 1990), which predisposes the myocardium to development of TdP-like arrhythmias as a result of mismanaged calcium handling (Lawrence *et al.*, 2005); and the conscious chronic AV block dog model, developed by Vos *et al.*, (1995).

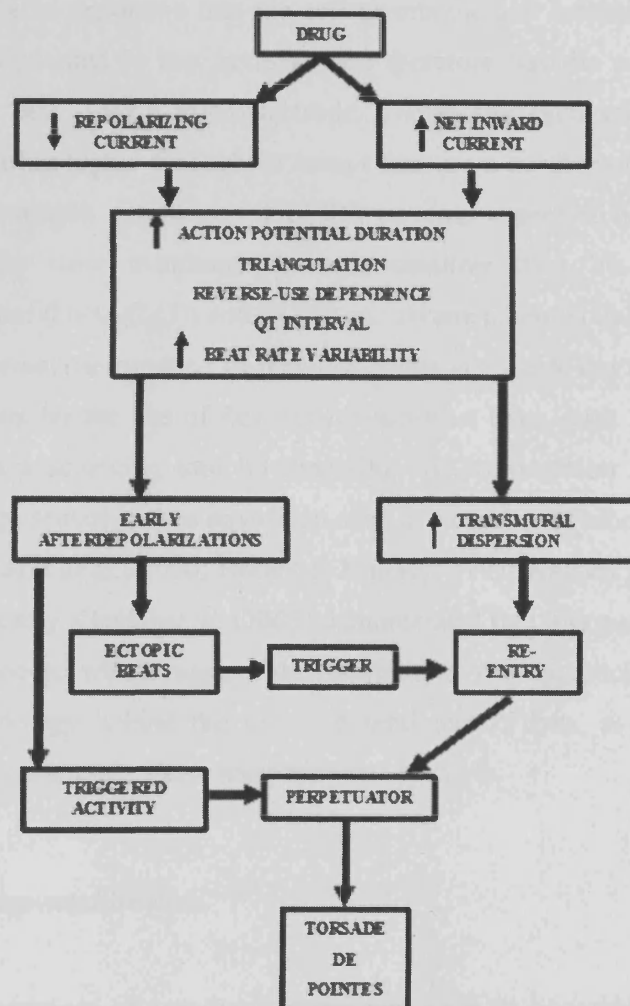


Figure 1.12. Flow chart displaying the possible mechanisms which can result in Torsade de Pointes generation.

Based on figure shown in Lawrence *et al.*, 2005.

1.5. Voltage-sensitive dyes and fluorescent monitoring of membrane potential.

The use of conventional electrophysiological techniques to monitor membrane potential in intact cells can be technically difficult and low throughput. To avoid this voltage sensitive dyes can be incorporated into the cell membrane and emitted fluorescence can be monitored; a technique that is less invasive and therefore has the potential to cause less damage to the cell than does a microelectrode. Techniques such as this also present the possibility of generating higher throughput assays because a number of cells may be studied at one time. For example, inhibition of hERG currents expressed in CHO cells can be monitored using the slow membrane potential-sensitive dyes bis-[1,3-dibutylbarbituric acid]trimethine oxonol (DiBAC₄(3)) and FLIPR membrane potential dye (FMP dye); an assay that in a 384-well format can produce 10 000 data points in a single day (Dorn *et al.*, 2005).

However, thus far the use of fast voltage-sensitive dyes, such as di-4-ANEPPS, has not been applied as a screening tool for assessing AP prolongation in isolated myocytes. However, fast voltage sensitive dyes have been used in a number of other cardiac preparations (for examples see Baker *et al.*, 2000; Holley & Knisley, 1997; Knisley *et al.*, 2000; Rogart *et al.*, 1989). More recently Klauke *et al.*, (2005) demonstrated that it is possible to record an AP from an isolated myocyte, which suggests the feasibility of this approach. This section aims to describe the methodology behind the use of potentiometric dyes, as well as some of the technical innovations that make these measurements possible.

1.5.1. Theory of voltage-sensitive dyes.

The response of any dye is dependent upon its photochemical properties and the properties of light. Any form of matter, including dyes, will absorb and emit light in discrete quanta, photons. When a molecule absorbs a photon, it is termed excitation because the energy of the absorbed photon(s) will raise the energy of that molecule to an excited state. From this excited state, energy can then be lost in 3 possible ways: as heat, by chemical change (i.e. a reaction takes place), or by radiative deactivation which can occur as either phosphorescence or fluorescence. The excitation of molecules occurs as a result of electrons being promoted to higher energy levels (or orbitals). Ordinarily electrons in a ground state molecule are spin paired in both bonding and non-bonding orbitals. However, during excitation, one electron may be promoted to a higher energy level thus allowing for either the spins to be paired, in which case the molecule is in a singlet state, or parallel, which is described as a triplet state. Fluorescence is the result of a transition from states of the same

multiplicity (e.g. singlet to ground state), and has a much briefer lifetime than phosphorescence and is hence used in biological assays requiring monitoring of much quicker biological changes (Sugden, 2004). For any given fluorescent molecule, absorption spectra are of shorter wavelengths (higher energy) than the emission spectra, due to limited energy loss of the molecule prior to emission. The difference between the energy or wavelengths of the absorption and emission spectra is referred to as the Stokes shift.

Design of fluorescent probes for quantitative biological applications requires that a molecule have a fluorescent region or chromophore, of which the optical characteristics will change in response to the measured stimulus. For example, a number of calcium indicators, such as Calcium Green-1 and calcium Green-5N, utilise the fluorescent dye 5-carboxy-2',7',-dichlorofluorescein and couple it to the calcium chelator BAPTA (Haughland & Johnson, 1999). In the development of dyes for detection of changes in membrane potential, fluorescent probes were selected based upon their ability either to have altered fluorescent characteristics in response to changes in the electrical field around them, or to move in response to changes in electric field.

The mechanisms that a dye molecule may undergo to achieve this change in fluorescence include: ON-OFF, redistribution, reorientation and electrochromism (Loew, 2001). It is important to state that these mechanisms are idealised and that dye responses to changes in membrane potential are the result of complex combinations of these and other processes. A simplified diagram of ON-OFF, redistribution and reorientation mechanisms is shown in Figure 1.13. Additionally, these dyes can be separated into fast and slow voltage-sensitive dyes.

ON-OFF- Dyes which utilise an ON-OFF mechanism include the oxonol-based dyes, such as DiBAC₄(3), as well as cyanines. These rely on potential-dependent partitioning between the extracellular medium and the lipid bilayer. The dyes are charged, so alterations in membrane potential can shift the molecules across this partition; the resultant alteration in surrounding environment providing the basis for the spectral change. Generally, partitioning into the membrane produces an increase in fluorescence intensity.

Redistribution- Cyanine dyes can also undergo redistribution; a mechanism that relies upon fluorescent cationic dyes being distributed between the extracellular medium and the intracellular space according to the Nernst equation (see equation 1.2). The ratio of the fluorescence from inside and outside the cell is directly related to membrane potential. This is also the same mechanism that cationic rhodamine dyes employ, such as TMRE which is used to monitor mitochondrial membrane potential. Unfortunately, these dyes are not suitable for use in monitoring excitation of cardiac cell membrane owing to their slow response time. The kinetics of dyes that use a redistribution mechanism are in the order of seconds and some can

take minutes to equilibrate (Loew, 2001). Similarly, although there is some evidence to suggest that a variant ON-OFF mechanism can allow for these dyes to be faster (Waggoner *et al.*, 1977) and that anionic dyes can enter the membrane more quickly (Flewelling & Hubbell, 1986; Loew, 2001), ON-OFF dyes are still generally considered too slow for monitoring APs.

Reorientation- Voltage-sensitive dyes that encompass the use of very small movements of the molecule between environments, or intramolecular rearrangements, can produce much quicker changes in fluorescence. For example, merocyanine 540, which was one of the first dyes used to monitor APs (Morad & Salama, 1979), reorients itself within the membrane. This is a relatively small molecular movement compared to those exhibited by slower dyes such as oxonols and cyanines. The sensitivity of this mechanism to changes in membrane potential relies upon altered fluorescent characteristics between two states of the molecule. In this example, the states relate to different orientations of the molecules within the membrane. The electric field relative to the dipole of the dye is then shifted resulting in altered fluorescent properties.

Electrochromism- However, recent fluorescent studies of membrane potential in excitable tissues have favoured the use of voltage-sensitive dyes that incorporate a naphthylstyryl or aminostyrylpyridinium (styryl) chromophore, such as di-4-ANEPPS or di-8-ANEPPS (Bullen & Saggau, 1999; Entcheva *et al.*, 2004; Girouard *et al.*, 1996; Holley & Knisley, 1997; Knisley *et al.*, 2000; Sharma & Tung, 2002; Sharma *et al.*, 2002; Sharma *et al.*, 2005). These types of dyes are also used extensively in this thesis and thus are described in more detail. Styryl voltage-sensitive dyes change their characteristics in response to changes in membrane potential as a result of electrochromism; a mechanism that requires no molecular movement, but instead a charge shift within a molecule. For example, dyes that incorporate the ANEP naphthylstyryl chromophore, utilise this mechanism. Figure 1.14 shows a generic di-n-ANEPPS molecule in its ground state and an excited state following a change in membrane potential. The negatively charged electron cloud shifts from a density on the aniline moiety (on the bottom right of the molecule in the diagram) to the pyridinium end of the chromophore. Effectively, in its ground state the molecule has its positive charge localised around the nitrogen on the left, which upon a change in membrane potential shifts to the nitrogen on the right. Additionally, ANEPPS and other styryl dyes are designed such that the chromophore, when bound in the cell membrane, will align itself with the phospholipid molecules. This was achieved by attaching lipophilic carbon chains and a hydrophilic sulphate group to opposite ends of the molecule. This ensures that, when dye molecules are bound within a cell membrane, excitation-induced charge shifts will be parallel to the direction of the electric field in the membrane.

The consequence of this is that depolarisation of the membrane increases the energy difference between the ground and excited states; when the dye is excited, the emission spectra are shifted to shorter (higher energy) wavelengths. Conversely, when the membrane repolarises, the energy difference becomes less, and emitted spectra are shifted to longer wavelengths. The same trends can also be applied to absorption spectra. For these reasons a large number of these dyes are used ratiometrically, which can remove or reduce artefacts arising from motion, which is of particular consideration in contractile tissue, wash-off and photobleaching. Figure 1.15 shows hypothetical traces in the changes in emission spectra for a styryl dye. By sampling the emitted spectra at two different wavelengths, labelled A and B, an increase in fluorescence can be detected at shorter wavelengths (A) during a step to a more positive membrane potentials, while a decrease in fluorescence can be detected at higher wavelengths. This allows for ratiometric recordings of membrane potential to be made with a number of styryl dyes including di-4-ANEPPS and di-8-ANEPPS. This also demonstrates that it is better to sample emission spectra at wavelengths that are not at the peak of the emission spectra. Sampling light intensities around wavelengths where the two spectra converge would elicit little or no change in fluorescent intensity.

In practice, dye selection is based upon a number of criteria. Maximal sensitivity to changes in membrane potential is advantageous, but is limited if the response of the probe is required to be very fast. For example, monitoring APs in excitable tissue require probes that will respond in the order of milliseconds. Generally, fast-voltage sensitive dyes elicit comparatively small changes in fluorescence intensity with voltage, when compared to slower probes such as oxonol-based dyes. Di-4-ANEPPS generally gives a fluorescence change of ~10% per 100 mV in a variety of preparations (Loew, 1999). In contrast, applications using DiBAC₄(3) have demonstrated increases in fluorescence of between 1 and 2% per millivolt (Cornfield *et al.*, 1994; Stevens *et al.*, 1994).

Additionally, the molecular structure of the dye is also important. During the development of voltage-sensitive dyes during the 1970s, a large number of compounds were screened which generated a number of guidelines for development of new dyes (Cohen *et al.*, 1974; Ross *et al.*, 1977). Essentially, dyes were required to incorporate hydrophobic/lipophilic adjuncts, to allow for interaction with the membrane, but the use of alkyl groups longer than 8 carbons in length could impart too much insolubility. Unlike other mechanisms of voltage-dependence exhibited by fluorescent dyes, changing the lipophilicity and charge of molecules does not produce large alterations in sensitivity. For example, the styryl dye, JPW-1063 has a head group containing a positively charged ethyltrimethylammonium group, in place of the negatively charged propylsulfonate present on ANEPPS dyes. The consequence of this added positive charge is that this dye exhibits greater

water solubility, allowing for it to penetrate more deeply into thick tissue (Loew, 2001). In contrast, experiments requiring staining of the outside of a preparation, such as in optical mapping studies, or the staining of isolated cells, requires the use of relatively insoluble dyes. Dyes with marginally longer carbon tail lengths, such as di-8-ANEPPS, have been shown to internalise less readily than similar dyes with shorter alkyl chains such as di-4-ANEPPS (Rohr & Salzberg, 1994). However, the low solubility of such dyes often requires that they be applied to preparations via the use of vehicles, such as the non-ionic detergent, F127.

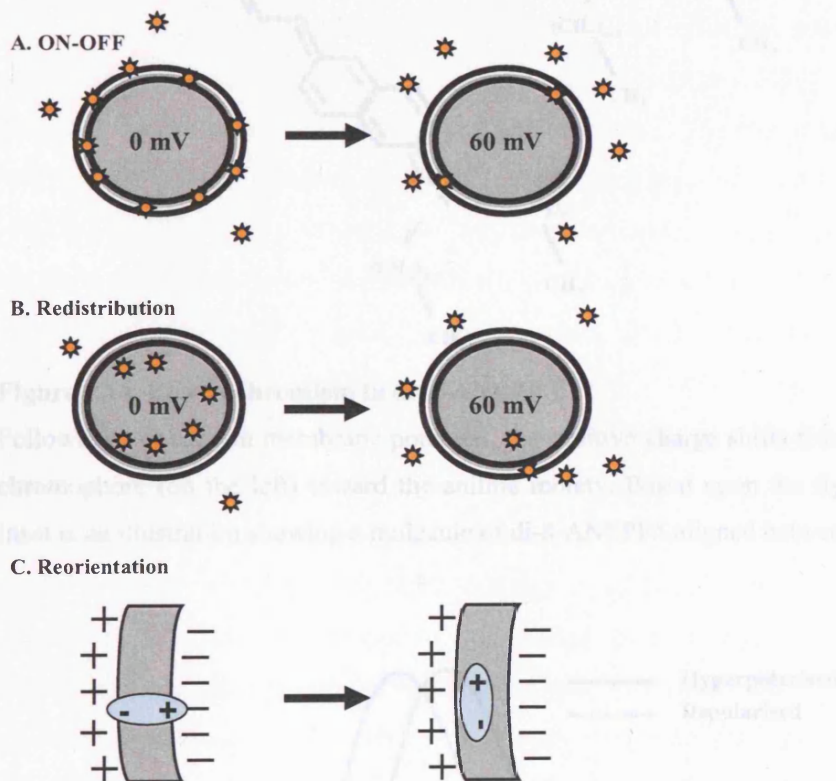


Figure 1.13. Mechanisms of voltage sensitivity exhibited by voltage-sensitive dyes.

(A) ON-OFF; the intensity of the dye changes when it is present in the phospholipid bilayer, which is altered by changes in membrane potential. (B) Redistribution; the dye is distributed on each side of the membrane according to the Nernst equation, thus the ratio of intracellular vs. extracellular fluorescence is directly related to membrane potential. (C) Reorientation; a molecule bound to the membrane reorients itself in response to changes in membrane potential, which alters its fluorescence characteristics. Based upon the figure shown in Loew, 2001.

Figure 1.15. Changes in spectra of a styryl dye during depolarization of the membrane.

Theoretical spectra for a styryl dye in response to a step change in membrane potential. Following depolarization, light of shorter wavelength (sampled at A) will decrease in intensity, while light of longer wavelengths (sampled at B) will increase. Based upon the figure shown in Loew, 2001.

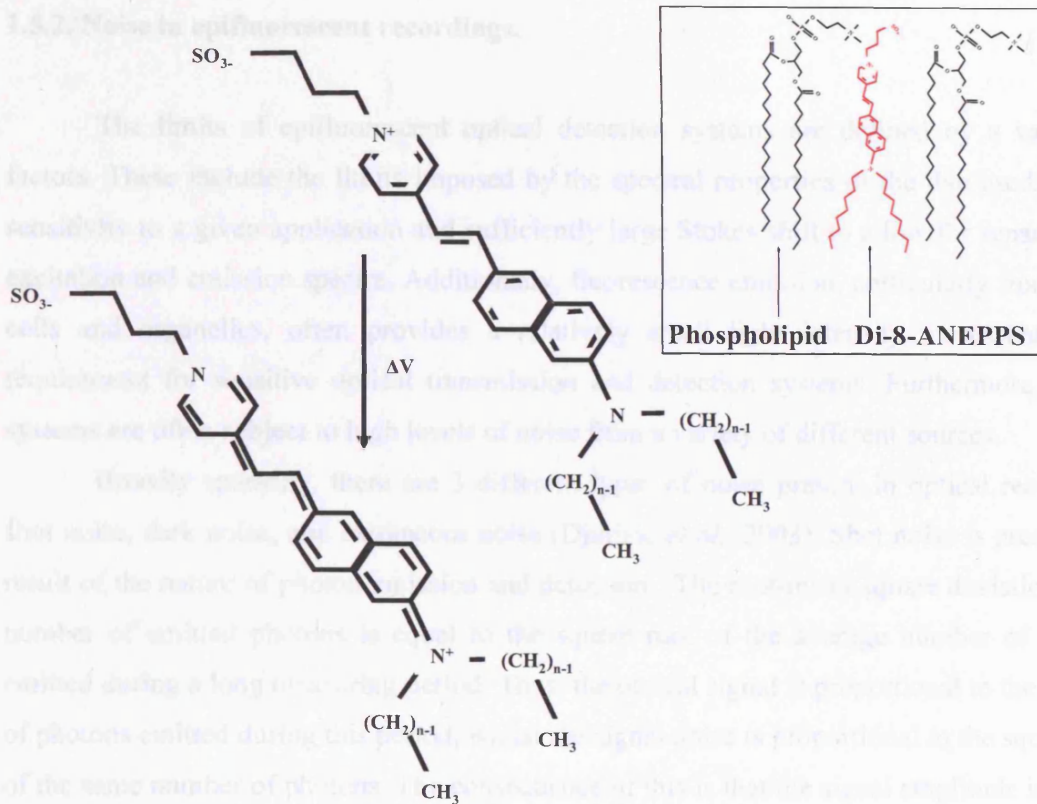


Figure 1.14. Electrochromism in di-n-ANEPPS.

Following a change in membrane potential, the positive charge shifts from the pyridinium end of the chromophore (on the left) toward the aniline moiety. Based upon the figure shown in Loew, 2001. Inset is an illustration showing a molecule of di-8-ANEPPS aligned between two phospholipids.

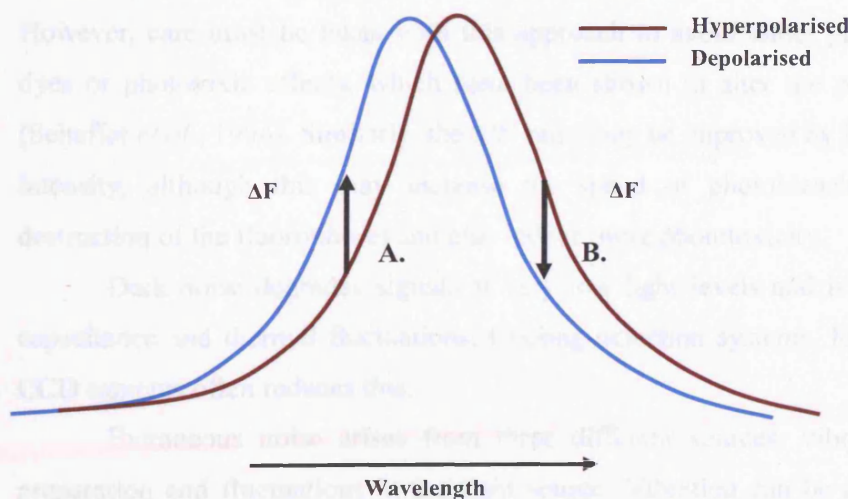


Figure 1.15. Changes in spectra of a styryl dye during depolarisation of the membrane.

Theoretical spectra for a styryl dye in response to a change in membrane potential. Following depolarisation, light of shorter wavelengths, sampled at A, will decrease in intensity, whilst light of longer wavelengths, sampled at B, will increase. Based upon the figure shown in Loew, 2001.

1.5.2. Noise in epifluorescent recordings.

The limits of epifluorescent optical detection systems are defined by a variety of factors. These include the limits imposed by the spectral properties of the dye used, i.e. the sensitivity to a given application and sufficiently large Stokes shift to allow for separation of excitation and emission spectra. Additionally, fluorescence emission, particularly from single cells and organelles, often provides a relatively small light intensity, necessitating the requirement for sensitive optical transmission and detection systems. Furthermore, optical systems are often subject to high levels of noise from a variety of different sources.

Broadly speaking, there are 3 different types of noise present in optical recordings: shot noise, dark noise, and extraneous noise (Djurisic *et al.*, 2003). Shot noise is present as a result of the nature of photon emission and detection. The root-mean-square deviation in the number of emitted photons is equal to the square root of the average number of photons emitted during a long measuring period. Thus, the optical signal is proportional to the number of photons emitted during this period, whilst the signal noise is proportional to the square root of the same number of photons. The consequence of this is that the signal amplitude increases more rapidly with the number of photons emitted, relative to the signal noise. Furthermore, the signal-to-noise ratio (S/N ratio) is also inversely proportional to the bandwidth of the detection system. Provided the optical signal being detected is dependent only on changes in fluorescent characteristics of the dye, as is the case with styryl dyes, and not upon differences in concentrations of the dye in different regions of the specimen (for example when using an oxonol dye), a simple approach to overcoming shot noise is to increase dye concentration. However, care must be taken with this approach to avoid either pharmacological effects of dyes or phototoxic effects, which have been shown to alter the properties of cardiac APs (Schaffer *et al.*, 1994). Similarly, the S/N ratio may be improved by increasing excitation light intensity, although this may increase the speed of photobleaching (the photochemical destruction of the fluorophore) and also induce more phototoxicity.

Dark noise degrades signals at very low light levels and is often the result of stray capacitance and thermal fluctuations. Cooling detection systems, for example, using cooled CCD cameras often reduces this.

Extraneous noise arises from three different sources: vibration, movement of the preparation and fluctuations in the light source. Vibration can be reduced by use of an air table upon which the equipment is mounted. Lasers, whilst providing a collimated emission to allow for illumination of finite areas, produce a relatively large amount of source noise when compared to other light sources such as Tungsten filament lamps or Xenon arc lamps (Dainty, 1984; Djurisic *et al.*, 2003). Additionally, certain aspects of extraneous noise can be limited

by using a ratiometric dye; because noise arising from vibration or the light source will be present in the signal detected from both wavelengths, the ratio of them can remove the noise. This technique has also been used to reduce motion artefacts arising from contraction in cardiac muscle (Knisley *et al.*, 2000).

1.5.3. The importance of the light transmitting properties of the objective lens.

In epifluorescence, both the excitation light and the emitted fluorescence pass through the objective lens. The numerical aperture (NA) of a lens is a critical factor in determining the properties of a lens. The NA is equal to $n(\sin \theta)$ (Figure 1.16), where n is equal to the refractive index of the lens and the conducting medium and θ is equal to the half angle of the cone of light that may enter or exit the lens. Therefore, the NA represents an index of the amount of light, which can travel through a lens. The amount of light collected by an objective lens is proportional to the NA. In experiments using epifluorescence, the intensity of light that reaches the detector is proportional to the 4th power of the NA (Inoue, 1986). Conversely, the brightness of an image is inversely related to the magnification of the lens. For these reasons, ideal quantitative light collection utilizes a small magnification lens combined with a high NA. Studies recording optical APs from whole hearts have demonstrated this principle by using a microscope lens of x4 magnification, for which there are no high NA lenses available, versus a high NA camera lens. The results demonstrated a hundredfold increase in fluorescence intensity when using the higher NA camera lens (Ben-Oren *et al.*, 1996).

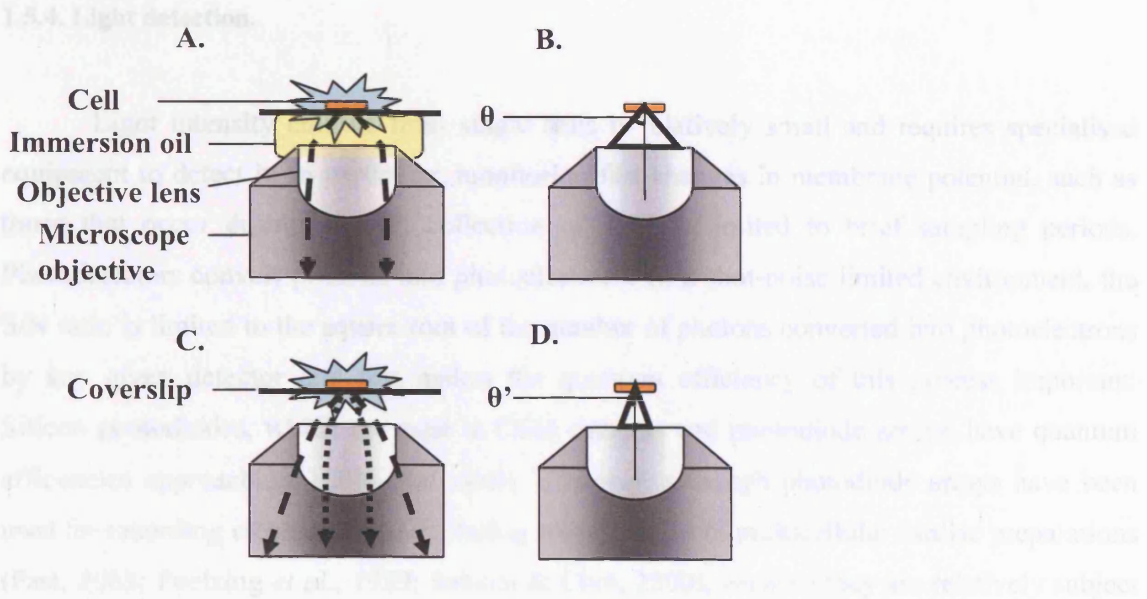


Figure 1.16. Schematic representation demonstrating increased light transmission through high NA objectives.

(A) An oil immersion objective with a relatively high NA allows a larger diameter cone of light to be refracted parallel to the objective. (B) illustrates the angle θ half cone of light emitted/transmitted to/from the cell being examined. C & D. An objective that is of a relatively low NA cannot refract as much light for transmission.

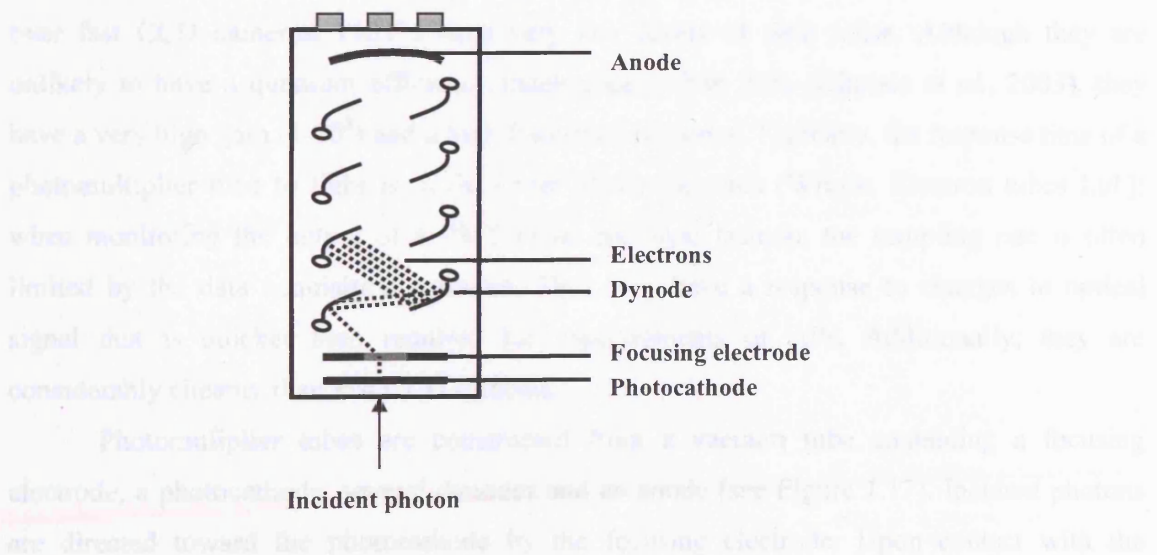


Figure 1.17. A simplified schematic of a photomultiplier tube.

Incident photons form photoelectron when they come into contact with the photocathode. The focusing electrode directs them toward the first dynode. Following each successive dynode a cascade of electrons forms thus amplifying the signal at the anode.

1.5.4. Light detection.

Light intensity emitted from single cells is relatively small and requires specialised equipment to detect it. In particular, monitoring fast changes in membrane potential, such as those that occur during an AP, collection of light is limited to brief sampling periods. Photodetectors convert photons into photoelectrons. In a shot-noise limited environment, the S/N ratio is limited to the square root of the number of photons converted into photoelectrons by any given detector and this makes the quantum efficiency of this process important. Silicon photodiodes, which are used in CCD cameras and photodiode arrays, have quantum efficiencies approaching 100% (the ideal). However, although photodiode arrays have been used for recording electrical activity during recordings from multicellular cardiac preparations (Fast, 2005; Poelzing *et al.*, 1929; Salama & Choi, 2000), because they are relatively subject to dark noise, they are not suitable for use in very low light preparations, for example in the study of a single cell. There are some fast CCD cameras that have the potential for analysis of APs from individual myocytes; these are cooled and the photosensitive area (and hence capacitance) is smaller thus reducing the dark noise. Additionally, even using the full frame (80x80 pixels) it is possible to obtain frame rates of up to 2000 fps (Djurisic *et al.*, 2003).

However, using fluorescent probes to measure AP morphology, requires collection of light intensity in a quantitative manner, hence there is no requirement for pixelated images of the cells being studied. For this type of application, photomultipliers (PMTs) provide benefits over fast CCD cameras. PMT's have very low levels of dark noise. Although they are unlikely to have a quantum efficiency much greater than 20% (Djurisic *et al.*, 2003), they have a very high gain ($1-10^8$) and a high frequency response. Typically, the response time of a photomultiplier tube to light is in the order of nanoseconds (Wright, Electron tubes Ltd.); when monitoring the output of a PMT in an analogue fashion, the sampling rate is often limited by the data acquisition software. Thus they have a response to changes in optical signal that is quicker than required for measurements of APs. Additionally, they are considerably cheaper than fast CCD cameras.

Photomultiplier tubes are constructed from a vacuum tube containing a focusing electrode, a photocathode, several dynodes and an anode (see Figure 1.17). Incident photons are directed toward the photocathode by the focusing electrode. Upon contact with the photocathode, an electron is produced. Each dynode is held at a more positive voltage than the cathode and the previous dynode. Consequentially, electrons are attracted to each dynode in turn and because they are accelerated by the electric field, they arrive with more energy. Thus when an electron strikes a dynode a number of electrons are released, which are attracted to

the next dynode. This results in a cascade effect, whereby a single electron emitted by the photocathode is multiplied through each dynode, until it reaches the cathode.

1.6. Aims:

In this introduction, I have described the basic anatomy and function of the heart, as well as generating a more detailed description of the ionic bases of cardiac AP formation. In addition I have also provided a brief depiction of arrhythmogenesis as it occurs in LQTS with emphasis upon drug-induced LQTS and pharmacological screening for proarrhythmic compounds.

I have also described types of fast voltage-sensitive dyes, which display the kinetics necessary for monitoring changes in membrane potential. Of particular note, di-8-ANEPPS was recently used to record APs from an isolated ventricular cell (Klauke *et al.*, 2005). This demonstrates that it is possible to record entire APs from isolated myocytes in the absence of an electrode; a format that removes some of the technical expertise required for electrophysiological techniques in a cell type that is numerous enough (following isolation from cardiac tissue) to have potential for use in higher throughput assays.

Thus, the aims of my work were:

i) To determine the ability of fast voltage-sensitive dyes to accurately follow the morphology of cardiac APs recorded from isolated ventricular myocytes. - Currently, although there are large numbers of studies in multicellular and whole heart preparations, comparatively little work has used fast voltage-sensitive dyes to record fast changes in membrane potential from isolated cardiac cells. Klauke *et al.* (2005) have demonstrated the feasibility of using this as a technique to record APs using di-8-ANEPPS, however further assessment is still required to determine the optimum conditions for using this as a technique to monitor AP morphology. In particular, the aims of the current study included identification of optimum conditions for recordings APs for maximal time periods whilst attempting to limit phototoxic effects. Furthermore, the use of other dyes including di-4-ANEPPS was also assessed.

ii) To assess the possibility of using optical recordings to record changes in APD from isolated myocytes in response to experimental modulation. – Drug-induced alterations in APD were recorded using standard microelectrode techniques and optically with di-8-ANEPPS. Comparisons between the two techniques were used to assess the accuracy of optical measurements using standard electrophysiological techniques as the gold standard.

iii) To assess of the ability of using optical recordings from isolated ventricular myocytes for identifying alterations in cardiac AP in response to pharmacological intervention. – There are several key aspects of pharmaceutical screens for proarrhythmia which do not present the perfect ideal. Medium throughput assays, for example the Ionworks HT™ (Bridgland-Taylor *et al.*, 2006), whilst providing a screen for a large number of compounds at a cost that is relatively small compared to *in vitro* assays, provide only an indication for drug block of a specific ion channel. In contrast, assays in native tissues, such as the Purkinje fibre (Gintant *et al.*, 2001), which provide parameters governed by multiple ion channels, such as APD and triangulation, are relatively low throughput and both labour and animal intensive. To assess the validity of using optical recordings as an equivalent assay to for preclinical assessment of proarrhythmic assessment, well-characterised compounds were analysed for effects upon APD in a double-blinded manner using a voltage-sensitive dye.

This thesis shows the development of an assay to record drug-induced changes in APD using styryl voltage-sensitive dyes in isolated ventricular myocytes; a format that can provide an increase in throughput, whilst lowering the number of animals and technical skill required.

Chapter 2:

Methods

Chapter 2: Methods

The methods described here are detailed enough to ensure that the experiments described in this thesis may be reproduced. However, owing to the nature of this study, some of the pharmacological data described later in this thesis is provided for comparison to data obtained using optical techniques and the methods used were performed by people other than myself. In particular, experimental data derived from canine Purkinje fibres was obtained by Chris Lawrence, Najah Abi-Gerges, Ben Small and Anne Woods. Similarly, sharp electrode recordings of action potential durations (APDs) from canine M cells were made by Najah Abi-Gerges. I did, however, endeavour to learn the techniques required for both excision of Purkinje fibres and sharp electrode techniques for making recordings from both tissue types. Additionally, I also assisted in writing the computer protocols and finding the conditions for making sharp electrode recordings from M cells.

In addition, transfected cells for use in the Ionworks HT™ assay were provided on site; the methods used in their preparation can be viewed in the article by (Persson *et al.*, 2005). As well as being able to monitor hERG current in a high throughput manner in the Ionworks™, AstraZeneca also provided a hERG binding assay for use. Compounds were sent away for testing using this assay, which was performed by Andrew Heuze and Lucy Ashcroft (although analysis was done by myself). Furthermore, although myocyte isolations were made by myself, excision of canine hearts was performed by staff at AstraZeneca.

The care and killing of the animals conformed to the requirements of the UK Animals (Scientific Procedures) Act 1986.

2.1 Tissue preparation.

2.1.1. Preparation of rodent isolated ventricular myocytes.

Methods for the preparation of isolated ventricular myocytes from guinea pigs and rats have been published previously (Lawrence & Rodrigo, 1999; Rodrigo & Chapman, 1990). Either male Wistar rats or male Dunkin Hartley Guinea Pigs were killed by cervical dislocation. Following this a midline incision was made and the diaphragm and ribs cut to allow access to the heart. The heart was excised rapidly and placed in cold (4 °C) calcium-free Tyrode's solution (see section 2.5 for solution constituents). The heart was then cannulated via the aorta and retrogradely perfused on a Langendorff apparatus (See Figure 2.1) using a peristaltic pump (Ismatech) at ≈ 10 ml/min. Perfusates were preheated to 37 °C using a circulating heater and custom made jacketed beakers. Initially, the heart was perfused with

calcium-free Tyrode for 4-6 min. Subsequently, the solution was changed to calcium-free Tyrode containing 1.66 mg/ml bovine serum albumin, BSA, (made from factor V albumin, Sigma Aldrich), 0.66 mg/ml protease (type XIV, ≈15% calcium, Sigma Aldrich) and 1 mg/ml collagenase (type I, Sigma Aldrich) After approximately 2 min perfusion, the enzyme solution was recycled and perfused for a further 2-10 min as determined by both the consistency of the heart tissue and the appearance of rod shaped myocytes in solution collected from within the heart. When the heart was first exposed to enzyme mix it would harden and expand before gradually getting softer as digestion continued. This was a more obvious indicator in the guinea pig heart, whereas the rat heart generally required solution to be collected from within the heart (to look for live myocytes) as

a marker for ending the perfusion of the enzyme mix. The protease and collagenase present in the enzyme solution digested the heart, removing connective tissue to allow for dissociation of myocytes; the presence of a small amount of calcium in the protease helped to activate the collagenase. In addition, the presence of 1 mM magnesium in each Tyrode's solution prevented the death of the cells as a result of the calcium paradox (Rodrigo & Chapman, 1991). Following this the heart was perfused with normal Tyrode's solution for 2-4 min to wash out and inactivate the enzymes. Then, after removal of the atria, the heart was cut down and the chambers cut open, before being agitated gently in approximately 9 ml normal Tyrode within a conical flask in a shaking tissue bath at 37 °C to allow for dissociation of individual myocytes. When the solution looked opaque it was decanted off and fresh warmed normal Tyrode's solution was added and agitation continued. This process was repeated to produce between 6 and 8 fractions. Each fraction was filtered, washed in warm normal Tyrode's solution twice and combined to produce one fraction from every two, before being placed in Petri dishes. Penicillin-Streptomycin solution (Sigma Aldrich) was added at 200 µl/6 ml and the cells were used within two days. Generally a guinea pig heart and a rat heart would produce a yield of 70-90% or 60-80% respectively, of quiescent, rod-shaped cells displaying clearly visible striations.

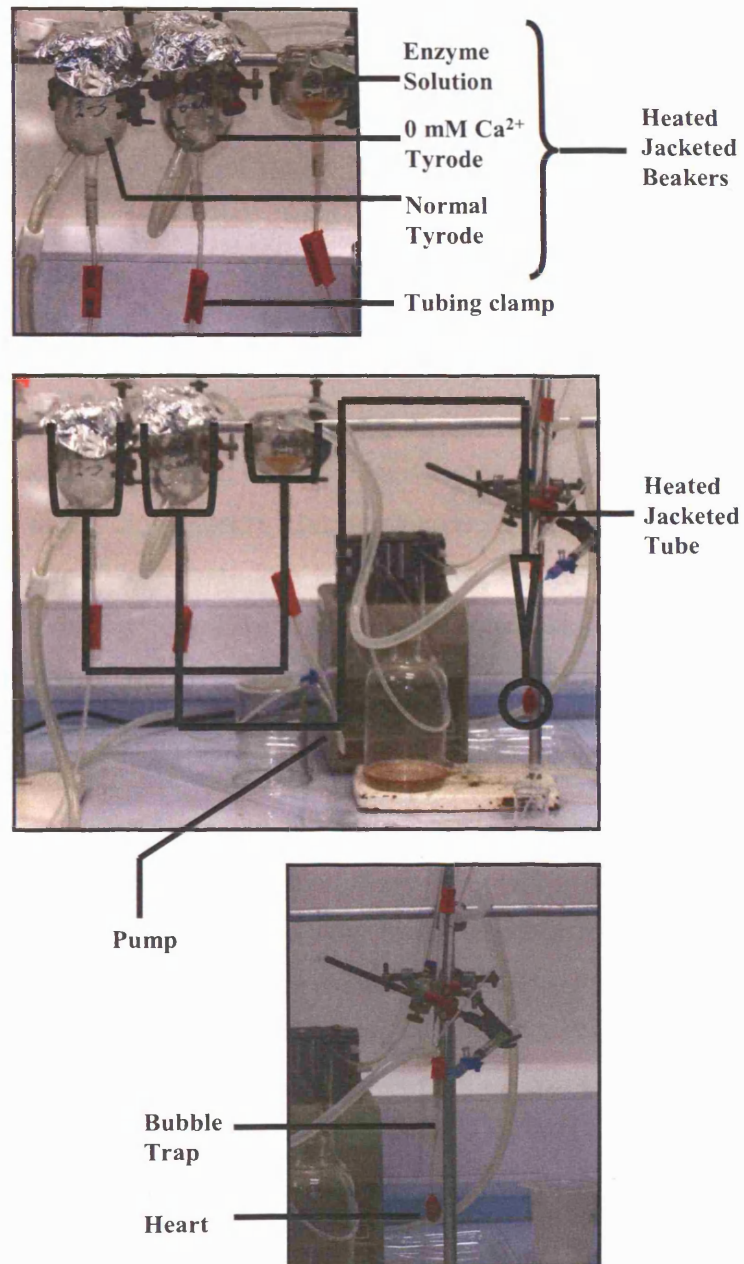


Figure 2.1. The Langendorff apparatus used to enzymatically isolate cells from an intact rodent heart.

Jacketed heated beakers maintain solution temperature at 37 °C (top), the entire isolation apparatus overlaid with a schematic demonstrating the tubing network (middle) and heart suspended on a Langendorff preparation (bottom).

2.1.2. Preparation of canine midmyocardial myocytes.

The preparation of canine M cells differed from the preparation of rodent ventricular cells due to the larger size of the canine heart. Female Beagle dogs had anaesthesia induced with ≈ 45 mg/kg pentobarbitone administered by intravenous injection. If required, additional doses of pentobarbitone were dispensed until there were no pedal or pupil reflexes. Following this, the chest was opened via a left thoracotomy and the heart was excised and rinsed in ice-cold calcium-free Tyrode. The heart was then cannulated for retrograde perfusion. Unlike the rodent heart, which was entirely digested, the canine heart was cannulated only at the left anterior descending artery (LAN) (see Figure 2.2). The vessels were initially cleared using ice-cold calcium-free Tyrode in a 10 ml syringe, before the cannula was connected to a gravity fed perfusion system. The LAN was then perfused with calcium-free Tyrode's solution preheated with a circulating heater to 37 °C at 20 ml/min for a further 5-10 min, before the switching to an enzyme solution containing: 0.5 mg/ml BSA and 1.125 mg/ml collagenase in Tyrode with a concentration of 5 μ M calcium, which was perfused for a further 20 min. The LAN was then perfused with Tyrode's solution with a calcium concentration of 200 μ M for 5-10 min. Subsequently, the cannula was removed from the heart and an incision was made down the ventricle to allow access to the digested region. Fragments of myocardium were dissected out of the heart and manually agitated into beakers containing Tyrode's solution with a calcium concentration of 200 μ M. Care was taken to avoid the tissue within 1.5 mm of the endocardial and epicardial regions of the ventricular wall to ensure that the cells collected were M cells. These were filtered and allowed to settle. Canine M cells were then washed twice in Tyrode's solution containing 200 μ M calcium and BSA at a concentration of 5 mg/ml. Finally the cells were re-suspended in normal Tyrode's solution. In this way the calcium concentration was gradually increased. Unlike the protocol used for isolating myocytes from rodent cardiac tissue, more steps were used to increase the calcium concentration, including a relatively small concentration of calcium (5 μ M) during the enzyme step to help activate the collagenase.

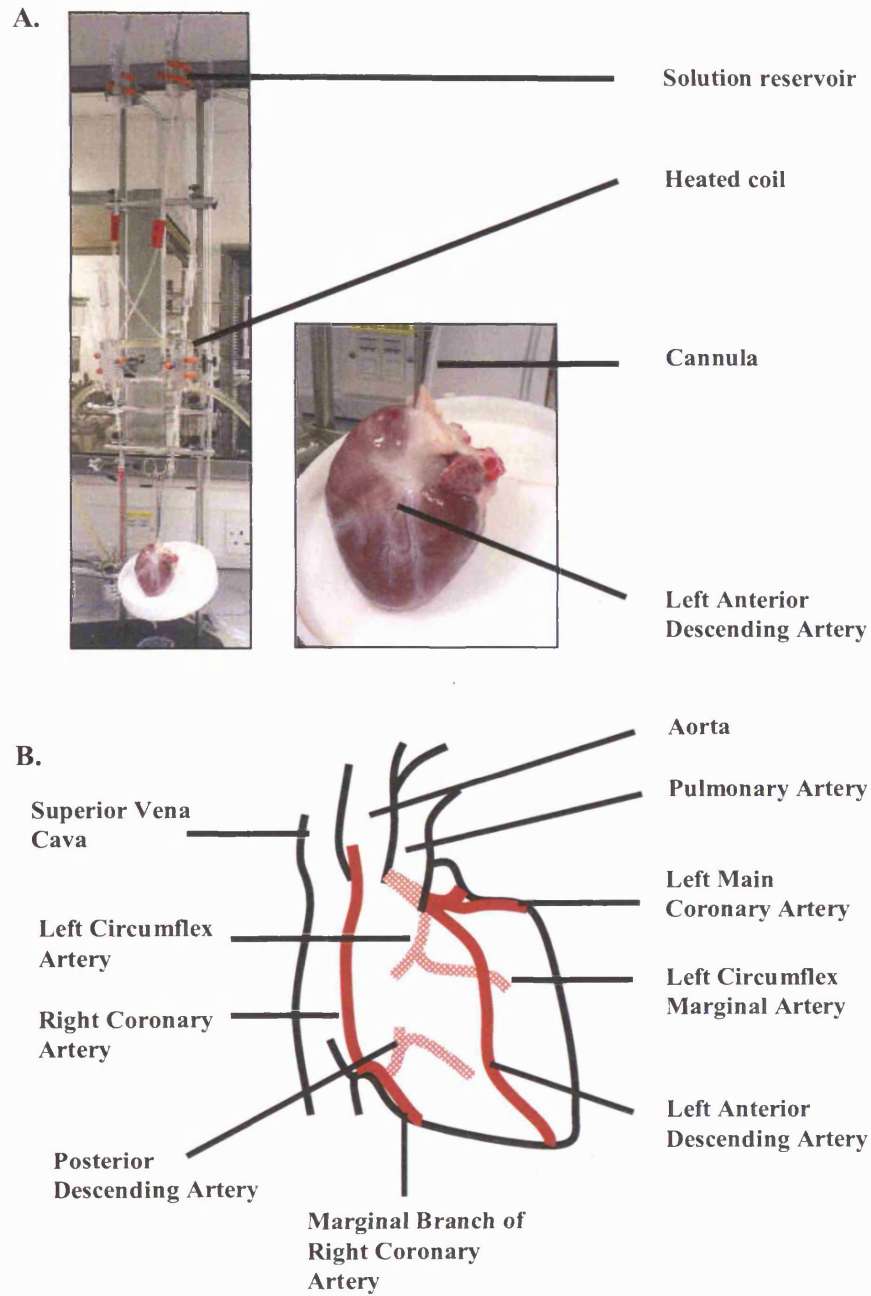


Figure 2.2. Illustration showing the position of the major cardiac arteries and veins.

For isolation of canine myocytes, the heart was cannulated via the aorta and the Left Anterior Descending artery. (A) Photo's showing the apparatus for isolating canine ventricular myocytes and the cannulation of the LAN. (B) Diagram illustrating the position of some of the main blood vessels in the heart.

2.1.3. Preparation of canine Purkinje fibres.

The methods for obtaining canine Purkinje fibres have been previously described in (Abi-Gerges *et al.*, 2004) and the method for excision of the heart was identical to that previously discussed for isolation of canine ventricular myocytes. The ventricular chambers were then cut open and Purkinje fibre bundles were dissected out, ensuring that as little tensile stress as possible was placed upon them and that each end of the fibre bundles retained a sufficient amount of ventricular muscle to facilitate being pinned out in Sylguard at the base of the recording chamber. Each bundle was stored in Krebs buffer and used within 6 hours (Gintant *et al.*, 2001).

2.1.4. Preparation of cloned cells for use in Ionworks™ HT protocols.

The cell line used for assessing effects upon hERG current using Ionworks™ HT was that previously described (Persson *et al.*, 2005). Stably transfected cells were prepared for use in the Ionworks™ HT array as previously described in (Bridgland-Taylor *et al.*, 2006). hERG-expressing CHO K1 cells were grown to semi-confluence at 37 °C in a humidified environment (5% CO₂) in Ham medium containing L-glutamine, 10% foetal calf serum and 0.6 mg/ml Hygromycin (Sigma-Aldrich). Immediately prior to use cells were resuspended into Dulbecco's Phosphate buffered saline (PBS) using the following method: The monolayer in a culture flask was washed using 3 ml Versene 1:5000 (Invitrogen) prewarmed to 37 °C. This was replaced with fresh 2 ml Versene 1:5000 and incubated for a further 6 min at 37 °C. Following this, the flask was tapped gently to detach cells from the base of the flask, prior to the addition of 10 ml PBS. The resultant suspension was aspirated into a 15 ml centrifuge tube and centrifuged for 4 min at 50g. The supernatant was removed and the pellet was gently resuspended in 3 ml PBS, from which 0.5 ml was removed to determine of the number of viable cells, which was calculated using Tryptan blue exclusion (in an automated reader, Cedex, Innovatis). The remaining 2.5 ml cell suspension was further diluted in PBS to yield 250 000 cells/ml.

2.1.5. Preparation of cloned cell membranes for use in radioligand binding protocols.

The stable cell line, from which membranes used for radioligand binding studies were obtained, was made using the hERG potassium channel transfected into HEK 293 cells using the pcDNA3 vector. The hERG-pcDNA3 was linearised with the ampicillin resistance gene and the cells were transfected with lipofectin. These were supplied by AstraZeneca.

Cell membranes were prepared as follows: After the cells were harvested and pelleted, the packed cell volume was measured. The pellet was then resuspended in hypotonic buffer solution (a 3:1 ratio of water: serum free buffer with 1 tablet/50 ml of protease inhibitor (Boehringer, catalogue number 1 697 498)) at a volume of 4x the packed cell volume. The cells were stored on ice for two minutes to allow them to swell, prior to being lysed with a tissue homogeniser (Polytron) at 22, 000 rpm. The cells were kept on ice and the homogeniser was allowed to build up speed before being turned off and allowed to cool for 30s. This was repeated twice and samples were checked macroscopically to ensure complete lysis. The lysed membrane solution was then overlaid on 10 ml of 41% sucrose solution in buffer in 38 ml centrifuge tube (Beckman). Any debris remaining in the homogeniser tube was washed out with buffer. The centrifuge tube was then filled with cold buffer. This was centrifuged at 28, 000 rpm for 1 hour at 4 °C. The membranes could then be viewed as a white band at the interphase between the sucrose and buffer. The top layer of buffer was then discarded and the membrane band was removed and placed in a fresh tube. This was then diluted with at least three times the volume of ice cold buffer containing protease inhibitor (1 tablet/50 ml). This was centrifuged at 23, 000 rpm for 20 minutes at 4 °C. The supernatant was then removed and the remaining pellet was resuspended on ice in buffer containing protease inhibitor. Aliquots of cell membranes were stored at -80 °C.

2.2. Electrophysiological measurements.

Throughout this project calibration and validation of the optical techniques was adhered using conventional electrophysiological methods. This section describes the methods used and describes the advantages of using different techniques for different applications. Although this section does describe some of the more basic stimulation protocols utilized, more complex voltage waveforms and their resultant currents are described in the relevant results chapters.

2.2.1. Obtaining gigaohm seals and whole-cell patch clamp configurations.

Whole-cell patch clamp was used to obtain measurements of AP morphology from isolated rodent myocytes and calcium currents from canine M cells. However, experiments in current clamp utilized an Axoclamp 2A amplifier with an HS-2 head stage (Axon Instruments) in bridge mode, whilst voltage-clamp experiments were made using an Axopatch 200B amplifier (Molecular Devices Corp.). Owing to differences between the two amplifiers, the methods used to obtain the whole-cell configuration also differed.

In order to obtain a gigaohm seal using the Axoclamp 2A, the tip of the electrode was placed in the bath solution and a repetitive 5 ms square current pulse was applied across the tip of the electrode. By monitoring the voltage the bridge was then balanced and the pipette tip resistance was calculated by using a circuit equivalent to a Wheatstone bridge. The pipette tip was moved close to the cell with a micromanipulator (Marzhauser). When the tip of the electrode touched the cell (as detected by monitoring the voltage waveform), gentle suction was applied to obtain a high resistance seal (see Figure 2.3).

Instead of using a constant current pulse, seals were obtained using the Axopatch 200B by applying a repetitive 5 mV square pulse and monitoring the current. When the tip of the patch electrode touched a cell the current wave would decrease (as the resistance increased), until, following gentle suction, a gigaohm seal formed (see Figure 2.4).

Following the formation of a gigaohm seal with either amplifier, capacitance neutralisation (pipette capacitance neutralisation on the axopatch 200B) could be applied to minimise the capacitance transients. The bridge could be further balanced on the Axoclamp 2A to compensate for additional access resistance arising from cell membrane around the tip of the electrode, whereas for measurements on the Axopatch 200B, series resistance compensation and whole cell capacitance compensation would be applied.

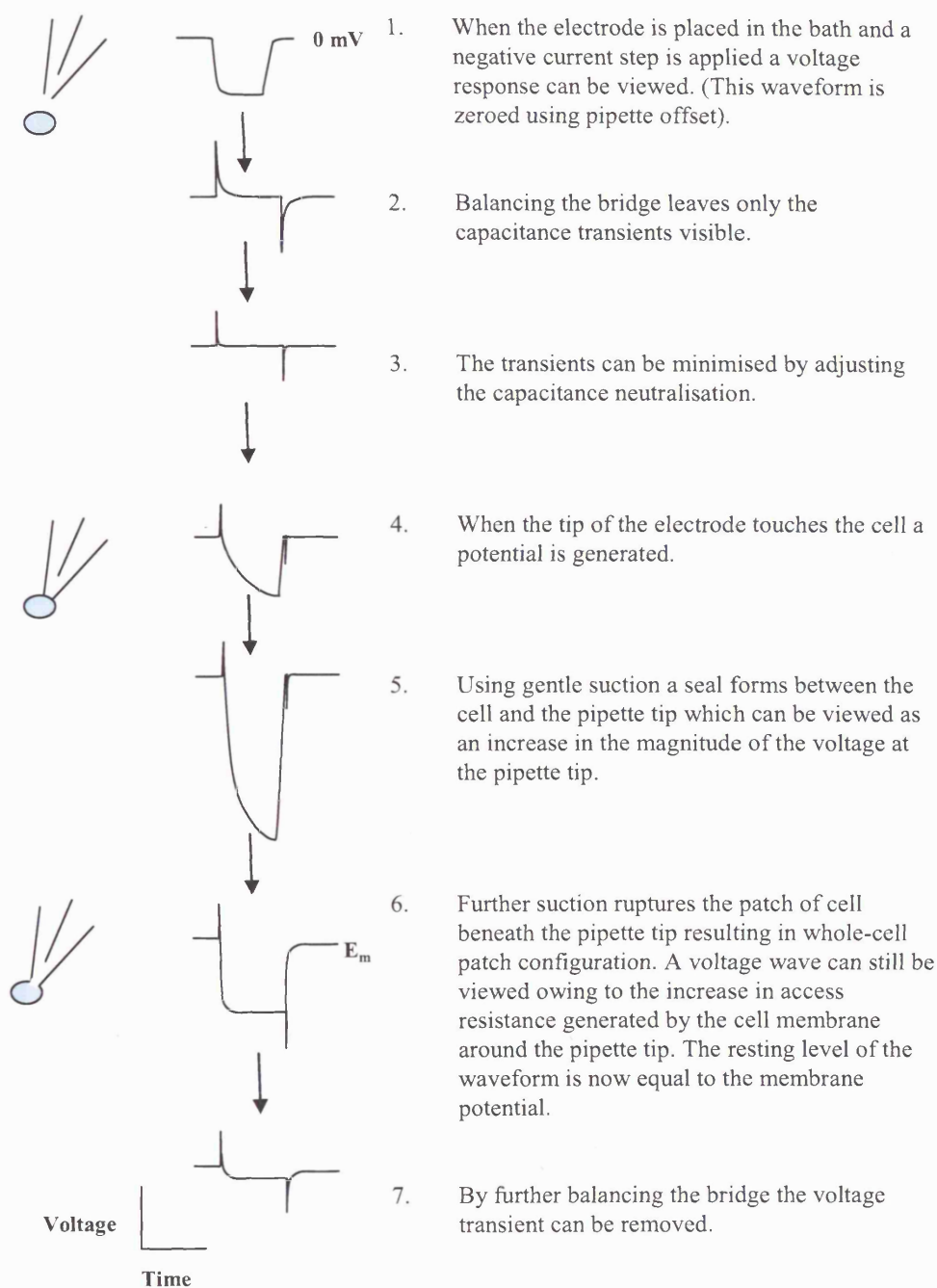


Figure 2.3. Obtaining whole-cell configuration in Bridge mode.

Illustrations showing the steps used to obtain a whole-cell configuration using an Axoclamp 2A amplifier. Diagrams (left) illustrate the presence of a patch-pipette and a single cell. Waveforms illustrate the different effects upon the voltage transient being viewed each step (described in point 1-7) produces.

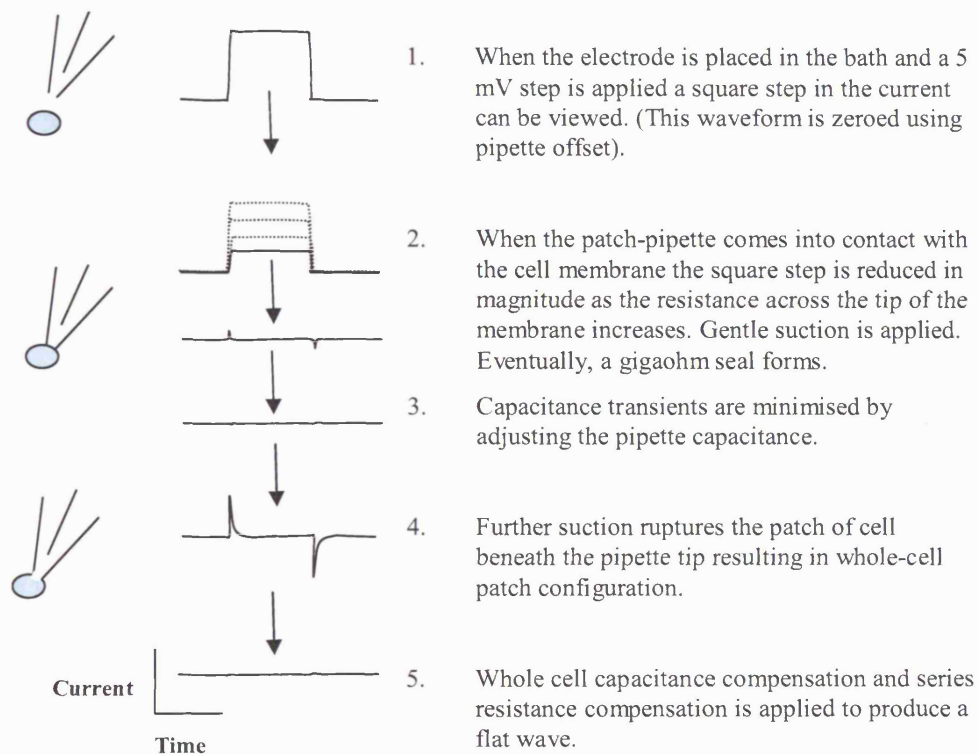


Figure 2.4. Obtaining whole-cell configuration using a patch-clamp amplifier.

Illustrations showing the steps used to obtain a whole-cell configuration using an Axopatch 200B amplifier. Diagrams (left) illustrate the presence of a patch-pipette and a single cell. Waveforms illustrate the different effects upon the current transient being viewed each step (described in point 1-5) produces.

2.2.2. Measurements of action potentials.

Methods for recording APs from Purkinje fibres have previously been published (Abi-Gerges *et al.*, 2004). Purkinje fibre bundles were pinned out in custom made recording chambers (Aztec Scientific Glass Blowing Company) using pins that also served to act as stimulating electrodes (see Figure 2.5), thus avoiding series resistance artefacts. The fibres were superfused by a peristaltic pump (Gilson) at 5 ml/min with Krebs solution preheated to 37.5 ± 0.2 °C by a DC50 heating circulator (Thermohake Instruments). APs were elicited by a pulse of 200% threshold, of duration 2 ms at a frequency of 1 Hz via a DS2A stimulator (Digitimer Ltd.). APs were recorded using pipettes pulled to resistances of 12-19 M Ω on a P97 pipette puller (Sutter Instrument Company) backfilled with 3 M KCl. The resultant output was Bessel filtered at 1 KHz using a Multiclamp 700A (Axon Instruments) and digitized via a DT 3010 interface (Notocord Systems S.A.). Acquisition was achieved using Notocord HEM software version 3.4.

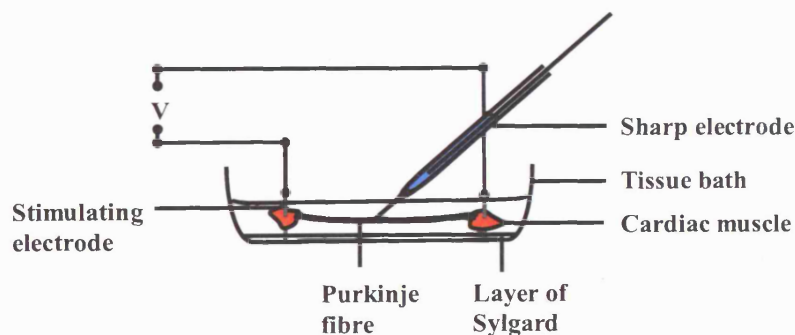


Figure 2.5. Diagram showing the set-up for making sharp electrode recordings from Purkinje fibres.

For experiments monitoring AP morphology from both rodent and canine ventricular cells, myocytes were placed in a 400- μ l heated chamber (HW-30 Temperature Controller, Dagan Corporation) mounted on the stage of an inverted microscope (Eclipse, Nikon) and continuously superfused with normal Tyrode at 3 ml/min at 36 ± 1 °C.

Action potential recordings from rodent myocytes were performed using patch pipettes with a resistance of 10–15 M Ω . Action potentials (APs) were initiated with a suprathreshold stimulus of 4 ms duration maintained at a frequency of 1 Hz, unless stated otherwise. Action potential duration (APD) measurements from canine M cells were performed using sharp electrodes pulled to resistances of 20-40 M Ω on a P97 pipette puller (Sutter Instrument Company) backfilled with 3 M KCl, which had penetrated the membrane following usage of the buzz function on a Multiclamp 700A amplifier (Molecular Devices Corp.). Cells were stimulated until a steady APD had been attained before recordings were started.

Difficulties arise using both techniques as a result of series resistance. During measurements performed on the Axoclamp 2A series resistance was only compensated via the bridge balance circuit, which is only completely effective if the series resistance is fully compensated and remains stable. Generally, series resistance would change throughout an experiment caused by blockage of the pipette tip during recordings. Similarly, during sharp electrode recordings using the Multiclamp 700A it is not possible to compensate 100% of the series resistance without causing large oscillations in voltage across the membrane. This is because the series resistance compensation is produced by a negative feedback circuit. The consequence of inadequate series resistance compensation in both cases was to cause artefacts during current injection through the microelectrode. These can be explained using Ohm's Law, where V is the voltage, I is the current and R is the resistance.

$$V = IR$$

Equation 2.1. Ohm's Law.

If the voltage is divided into the membrane potential, V_m , and the pipette potential, V_p , then the recorded potential, V_r can be calculated thus:

$$V_r = V_m + V_p$$

Equation 2.2. Recorded, Membrane and Pipette potentials.

V_p is also equal to the product of the current across the tip of the electrode, I_p and the resistance across the tip of the electrode, R_p , which is the main contributor to the series resistance. Thus,

$$V_r = V_m + (I_p \times R_p)$$

Equation 2.3. Pipette current and resistance.

Throughout the majority of an AP measurement, I_p is clamped at zero, thus fluctuations in R_p have no effect upon V_r . However, during the stimulus for each AP, current passes through the pipette tip, thus the product of I_p and R_p is no longer zero and an error is produced in the recorded potential that is additive to the membrane potential. For the purposes of our recordings this resulted in a stimulus artefact during phase one of the action potential, during which the command pulse was elicited. To avoid this, recordings utilized to monitor the upstroke of the AP used a much larger suprathreshold pulse of 0.1 ms duration, which generated an artefact brief enough to allow for the upstroke of the AP to be viewed.

2.2.3. Whole-cell measurements in voltage-clamp.

An Axoclamp 2A amplifier with an HS-2 head stage (Axon Instruments) was used in the discontinuous single electrode voltage-clamp mode, dSEVC, to voltage clamp myocytes at a switch frequency of 4 kHz. Initially, balancing the bridge and obtaining the whole cell configuration was performed in Bridge mode as described in section 2.2.1. Following this the amplifier was turned to discontinuous current clamp mode and both the current and voltage waveforms were monitored. A repeating 10 ms square current pulse was applied and the capacitance neutralization was increased until the voltage waveform decayed most rapidly, but without overshoot, to a horizontal line. The amplifier was then returned to Bridge mode and the holding position was adjusted to obtain equal brightness in both LEDs. At this point, there was no current being passed across the tip of the electrode so that when the amplifier was then set into voltage-clamp mode, the holding potential was equal to the resting membrane potential. The amplifier was then turned to dSEVC mode and the gain was increased as much as possible to obtain the optimum step response in voltage waveform. The gain was then turned down slightly, to give greater stability throughout recordings. The anti-alias filter was then increased to decrease the noise in the monitored waveforms. At no point was the phase lag used and thus recordings were not subject to false settings of capacitance or erroneous rise-times during voltage steps.

As shown in chapter 3, the use of a discontinuous voltage clamp allows for greater accuracy to be obtained in monitoring the membrane potential. This is because errors in voltage measurement which arise due to lack of compensation of series resistance (see earlier) are avoided by monitoring the voltage at point where there is no current passing across the tip of the electrode. Figure 2.6 compares the circuit used for recording in discontinuous SEVC mode with that of the classical patch clamp, which is discussed in the next section.

2.2.4. Recording calcium currents in classical voltage clamp.

Recordings of calcium currents in canine M cells were performed using an Axopatch 200B amplifier in voltage clamp mode. Similar to recordings in Bridge mode (or continuous SEVC mode) on an Axoclamp amplifier, determinations of membrane potential can be subject to series resistance error, which in voltage-clamp measurements could cause currents to be recorded at an incorrect voltage. Therefore, series resistance compensation was performed with a compensation circuit, which fed back a proportion of the current signal into the command voltage. Although in practice 100% series resistance compensation cannot be provided, the voltage error remains small or negligible so long as the recorded current remains small and the pipette tip resistance is kept to a minimum. This is because the voltage error is given by the product of these two values (see Ohm's Law).

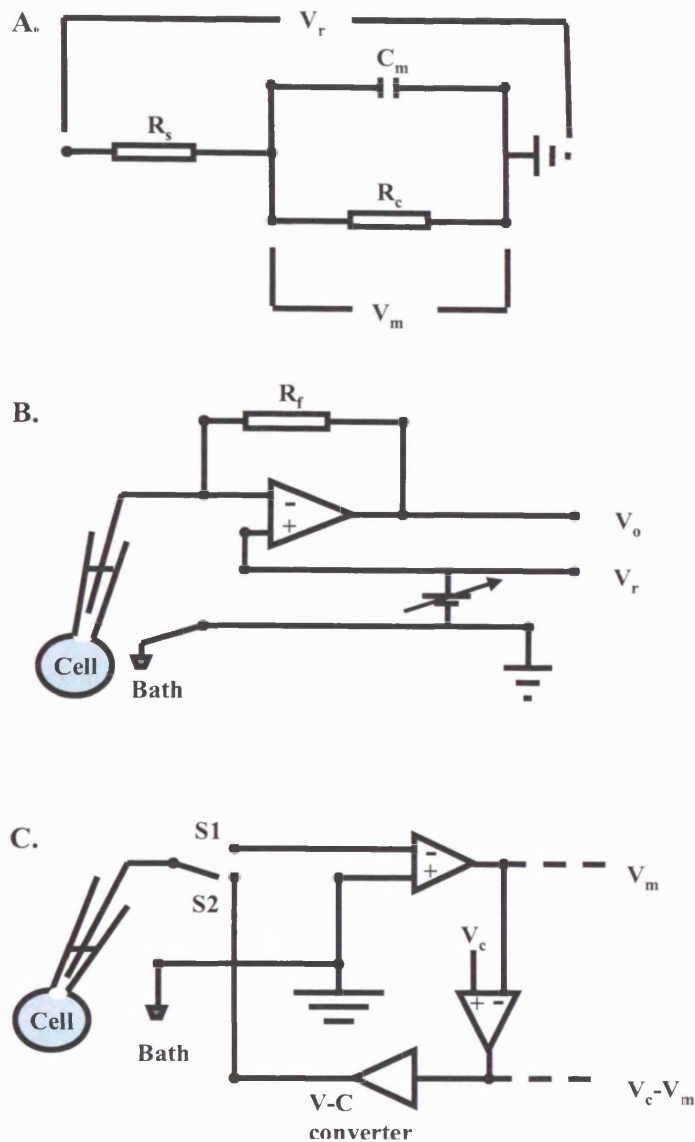


Figure 2.6. Electrical circuits for a patch clamped cell and classical and switch voltage clamp methods.

(A) Schematic showing an equivalent electrical circuit to that of a cellular membrane; the recorded potential V_r , can have errors introduced by the series resistance R_s . R_c and C_m are the resistance and capacitance of the cell, respectively, and V_m is the membrane potential. (B) Simplified schematic of a classical patch clamp circuit; the amplifier maintains the negative input at the same potential as the positive (i.e. V_r) by use of a feedback resistor, R_f (which sets the gain). V_o is the output of the clamping amplifier. Series resistance compensation is achieved by feeding back a proportion of the current signal into the command voltage. Based on diagram shown in Ogden (1994). (C) Simplified schematic of a "switch" voltage clamp circuit. When the switch is in position S1, no current is being injected so IR_s is equal to zero during voltage recording. When the switch is in position S2, current is injected to correct the difference between V_m and the command potential, V_c .

2.2.5. Ionworks™ HT protocols.

The principles of the Ionworks™ HT have been described in much greater detail previously (Schroeder *et al.*, 2003) and in the introduction I have already referred to the advantages and drawbacks of the more classical electrophysiology methods versus the Ionworks™ HT, in terms of both versatility and throughput.

The concept of the Ionworks™ HT is illustrated in Figure 2.7. The principle is based upon positioning a cell onto a small hole separating two fluidic microchambers using an approach that requires little or no manual intervention. In practise this is achieved by utilizing a 384-well PatchPlate™, each of which is designed for a single use only. Beneath the PatchPlate™ is the intracellular fluidics system consisting of: the PatchPlate™ clamp system, the PatchPlate™ plenum (or reservoir), a vacuum regulation system and a number of peristaltic pumps. This allows for generation of a pressure difference across between each of the chambers in the PatchPlate™ and the plenum beneath which serves two purposes. Firstly, the PatchPlate™ is primed and debubbled, as phosphate buffered saline (PBS) is sucked through the microholes and, secondly, the resultant fluid flow attracts cells onto the extracellular side of the microholes where the majority of them will form a high resistance seal. Following this, during maintenance of a precise pressure across the PatchPlate™ and the plenum, the intracellular solution is exchanged with a second solution containing an antibiotic to allow for perforation of the cellular membrane across the microhole to generate a low resistance electrical pathway. Because there is no means for temperature regulation in the Ionworks™ HT, these protocols were performed at room temperature (~21 °C).

Prior to experimentation the Ionworks™ HT apparatus was set up as follows: Reservoirs containing approximately 4 ml PBS and cell suspension (see section 3.1.3.) were placed in the “buffer” position and the “cells” position respectively. The different dyes to be tested were laid out in a 96 well plate placed in the “compounds” position at 3x the final test concentration (because of later dilution in the PatchPlate™). Negative controls consisting of different vehicles for the dyes and a positive control of cisapride (final concentration 10 µM) were also incorporated into the compound plate. The fluidics head (F-head) then deposited 3.5 µL PBS into each well of the PatchPlate™, which was then primed and debubbled. The electronic head (E-head), a 48-channel transimpedance amplifier, moved around the PatchPlate™ performing a hole-test to determine if the holes in each of the PatchPlate™ wells were open or blocked. This consisted of a small voltage waveform, during which the current was measured and thus the resistance calculated. The F-head then deposited 3.5 µL cell suspension into each well of the PatchPlate™, which was given a 200 s period to allow a cell to reach (under differential pressure) the hole in each well and form a high resistance seal.

The E-head then used a voltage waveform to determine the resistance across each hole in the PatchPlate™. The solution on the underside (the “intracellular” side) of the PatchPlate™ was changed to “access” solution, which contained 100 µg/ml amphotericin B (Sigma-Aldrich) to perforate the patch of cell exposed to it. 9 min was allowed for this to occur. The E-head then moved around the PatchPlate™ and applied a voltage protocol to measure the precompound hERG current. To ensure that currents were recorded post-compound addition, 3.5 µl from each well of the compound plate was added to 4 wells of the PatchPlate™ via the F-head. Following roughly 3.5 min incubation the E-head then moved around the PatchPlate™ to record the post compound hERG currents. The exclusion criteria for measured hERG currents were $>60 \text{ M}\Omega$ pre and post-scan seal resistance and a hERG tail current amplitude $>150 \text{ pA}$. hERG inhibition was measured by using the post compound current as a fraction of the pre compound current.

Although still described as a high resistance seal, comparatively the seal formed between a cell and the hole in a PatchPlate™ well is small when compared to other methods; in the order of tens of $\text{M}\Omega$ instead of the $\text{G}\Omega$ values normally encountered when using a patch clamp. This can result in a large amount of leak current which may interfere with current amplitudes and thus necessitates the use of leak subtraction. Thus, during voltage clamp protocols leak subtraction was calculated upon the assumptions that any changes in current amplitude during a 10 mV step from -70 mV to -60 mV resulted not from the activation of any channels, but from leak current, and that this leak current behaved in a linear manner (ie . according to Ohm’s law, see Equation 2.1). In this manner, the proportion of current produced in response to a voltage step (in absence of channel opening) could be calculated and subtracted from the measured current.

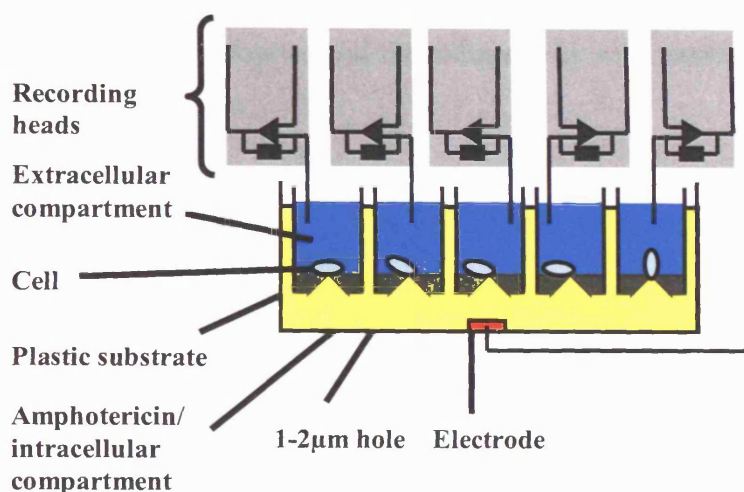


Figure 2.7. Illustration of the basic principles of recording hERG current from cloned cell lines in the ionworks™ HT.

Schematic of the ionworks design; a representation of cells positioned on microholes is shown. Each hole acts as the equivalent of the tip of a microelectrode in more classical patch clamps. The intracellular electrode is grounded, whilst the voltage command is applied through the headstage for each well.

2.3. hERG binding protocols.

Test compounds were diluted to 100x the final concentration in DMSO, prior to being diluted a further tenfold in assay buffer. 20 μL of each test concentration was then added to a Costar polypropylene round-bottomed 96 well plate. In addition to this, a control for calculating the total binding was added, which consisted of 20 μL of assay buffer containing 10 % DMSO; as well as 20 μL 10 μM astemizole in assay buffer to test for non-specific binding. Following this 160 μL of a 1:32 dilution in assay buffer of hERG-transfected cell membranes was added to each well. The radioligand, [³H]-AR-C160051XX, which was stored in a stock solution of 20 μM, was diluted 2000 fold in assay buffer, of which 20 μL was added to each well. This provided a final volume of 200 μL and a final concentration of 1 nM of [³H]-AR-C160051XX, which had a K_d of 1 nM, per well. The plate was then agitated for 1 min prior to 3 hours incubation at room temperature.

During the incubation, GF/B plates were immersed for 20 min in coating solution at 4 °C. Following the incubation, the compound plates were harvested using either a Tomtec or Filter harvester and repeatedly washed using wash buffer.

Plates were then dried overnight or for 2 hours at 57 °C. A backseal was then adhered to the base of each plate and 40 μL Microscint was added to each well. Following this, the plate was sealed with a topseal and the radioactivity was counted using a Packard Topcount liquid scintillation counter.

2.4. Optical recording methods.

Initial experiments to determine conditions for loading isolated myocytes with di-4-ANEPPS and di-8-ANEPPS are described in Chapter 3. Following this, during recordings of drug-induced changes in morphology, myocytes were loaded with either di-8-ANEPPS or di-4-ANEPPS at a concentration of 5 μM for 20 min at room temperature, prior to washing in normal Tyrode. This concentration and incubation period was found to give a consistent signal/noise ratio, which was able to resolve the action potential configuration without the need for filtering and with minimal averaging required (2–20 APs, depending upon the dye used). Recordings using cells loaded with di-4-ANEPPS also had a maintenance dye concentration of 200 nM.

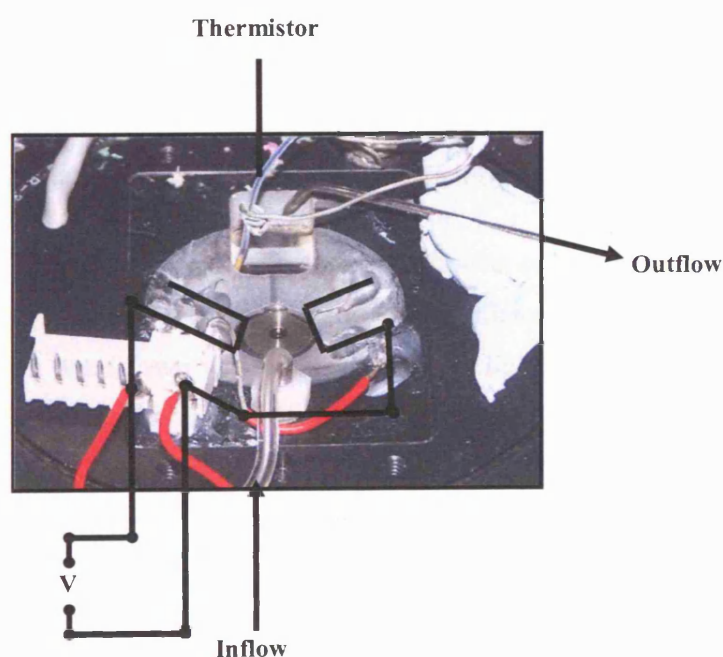


Figure 2.8. Picture of the heated tissue bath used for optical recordings.

The Dagan heated tissue bath is overlaid with a schematic of the two platinum stimulating electrodes.

Similar to electrophysiological measurements of AP morphology, myocytes were placed in a 400- μ l heated chamber mounted on the stage of an inverted microscope and continuously superfused with normal Tyrode at 3 ml/min at 36 ± 1 °C. Action potentials were evoked by electrical field stimuli of 4 ms duration at 1 Hz through bath-mounted platinum wire electrodes using a constant voltage isolated stimulator (Digitimer), at 200% of the threshold (see Figure 2.8) for causing the studied cell to contract.

A schematic of the optical apparatus used in this study is shown in Figure 2.9 which includes numbered regions to identify different functional units of the apparatus.

1. Myocytes loaded with Di-4-ANEPPS or di-8-ANEPPS were excited by wavelengths in the region of 488 nm. The light source used for this was a 75W Xenon arc lamp housed in a high stability Optosource arc lamphouse (Cairn Research Ltd.). This was coupled via light source output coupling for Cairn lamphouse, which includes iris diaphragm to limit the intensity of excitation light reaching the tissue bath. In front of the iris was a shutter (not visible in figure 2.9), which allowed for a rapid and complete block of excitation light from the specimens in the tissue bath. This allowed for the exposure of myocytes to excitation light to be limited to discrete periods of time.

2. The excitation light (unfiltered at this point) was directed into the back of the microscope via a UV liquid light guide (1.5 metre long, 2mm core diameter, Cairn Research Ltd. The light was filtered to between 460 and 500 nm wavelength and reflected toward the tissue bath by a narrowpass filter (di-8-ANEPPS exciter, DC/480/30x, Cairn Research Ltd.) and chromatic reflector (di-8-ANEPPS dichroic, DC/505/DCLP, Cairn Research Ltd.).

3. Light emitted from loaded cells was collected using a $\times 40$ oil immersion objective (NA = 1.3, Nikon) and directed toward the microscope prism. The microscope prism could be angled in one of two ways: either to reflect light from the tissue bath through the eyepieces, which allowed for initial viewing of the cells prior to recording, or out the side of the microscope, toward the photomultiplier tubes (PMTs) for data acquisition and toward an infrared CCD camera (Watec).

4. Between the prism and the PMTs was a movable and rotatable holder with rectangular diaphragm. This allowed for adjustment of the field of view on the monitor to isolate recordings to regions occupied only by the cell being studied.

5. Light reflected by the prism toward the infrared camera was then filtered and separated toward the two different PMTs. The first PMT, was a rubidium alkali PMT, which was more sensitive in the blue/green wavelengths detects light that is reflected toward it by a

lowpass filter, <590 nm, (emission dichroic, DC/590DCLP, Cairn Research Ltd.) and filtered by a narrow bandpass filter, 540-580 nm, (di-8-ANEPPS emitter, DC/560/30, Cairn Research Ltd.). The second PMT, an S20 PMT, which was more sensitive to red/infrared wavelengths detects light that was reflected toward it by a lowpass filter, <700 nm (Cold dichroic mirror for fluorescence / IR viewing (700nm cut-off; 25 x 40 mm) and filtered by a narrow bandpass filter, 600-640 nm (di-8-ANEPPS emitter, DC/620/30, Cairn Research Ltd.). Collection of two different emitted wavelengths allowed for ratiometric recordings to be made for elimination and reduction of artefacts arising from photobleaching, wash-off and movement (see Chapter 3).

6. Light from the tissue bath of wavelengths greater than 700 nm, was detected by the infrared CCD camera (Watec) for viewing on the monitor. This allowed for continual monitoring of a myocyte to ensure that it was still contracting in time with the stimulus, that it had not died (as determined by contracture) and that it had not moved out of the region of view as a result of the perfusion. This also allowed for observations when other cells moved into the field of view, at which point the diaphragm (described in 4.) would be adjusted to exclude the rogue cell from the field of view.

7. Longer wavelength (>700 nm) light for viewing on the infrared camera was produced by the microscope (halogen) lamp. To prevent interference from the shorter wavelengths this lamp also produced, light it produced was passed through an infrared filter (780 nm longpass) prior to reaching the tissue bath.

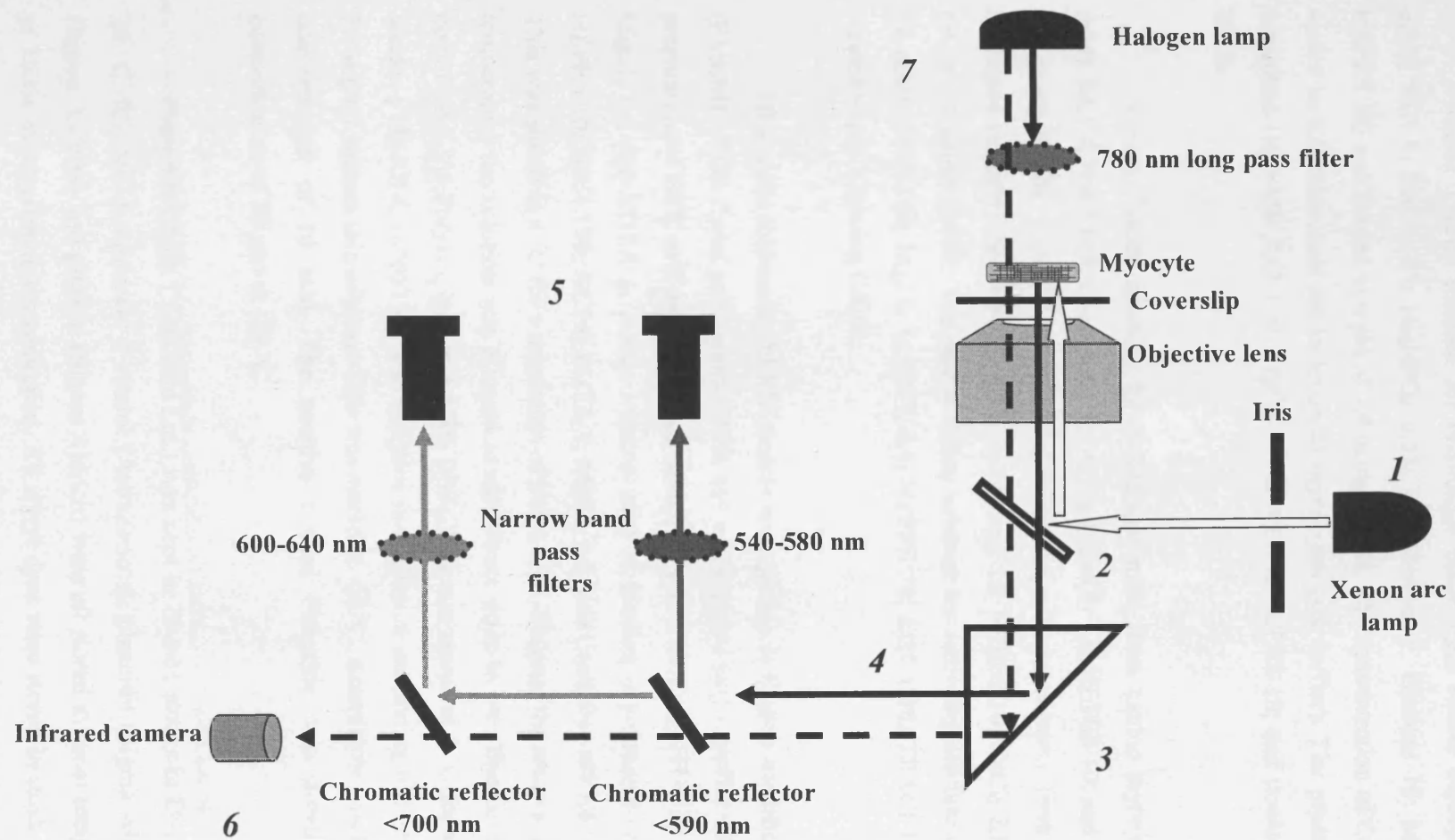


Figure 2.9. Schematic showing the set-up of the optical apparatus used for recording cardiac action potentials from isolated myocytes.

2.5. Drugs and Solutions.

Normal Tyrode solution for recordings made from rodent myocytes contained (in mM): KCl 6; NaCl 135; Na₂HPO₄ 0.33; Na Pyruvate 5; Glucose 10; MgCl₂ 1; CaCl₂ 2; HEPES 10; and titrated to a pH of 7.4 using NaOH. The concentration of CaCl₂ was however varied in solutions used for isolation of myocytes (see earlier). The pipette filling solution contained (in mM): KCl 130; MgCl₂ 5; Na ATP 3; HEPES 10; and titrated to pH 7.2 using KOH.

Normal Tyrode solution for recordings made from canine myocytes contained (in mM): KCl 4; NaCl 145; Glucose 11.1; MgCl₂ 1; CaCl₂ 1.8; HEPES 10; and titrated to a pH of 7.4 using NaOH. External solution for recording calcium currents from canine myocytes contained (in mM): NaCl 140; MgCl₂ 1; Glucose 10; HEPES 10; CaCl₂ 2.8; and titrated to a pH of 7.4 using NaOH. The pipette filling solution for recording calcium currents contained (in mM): CsCl 130; MgCl₂ 1; CaCl₂ 0.4; HEPES 20; EGTA 10; TEACl 10; MgATP 5; and titrated to pH 7.2 using CsOH.

HEK cells expressing hERG protein were grown in Eagle's modified Eagle's medium (EMEM) + 10% foetal calf serum + 10% M1 + 400 µg/ml G418. Buffer solution used for the preparation of HEK cell membranes contained (in mM): HEPES pH7.4 10; NaCl 130; KCl 5; MgCl₂ 0.9 and EGTA 1. Assay solution used in binding experiments contained (in mM): HEPES 10; NaCl 130; KCl 5; EGTA 1; MgCl₂ 0.8; and titrated to pH 7.4 using 10 M NaOH. This was stored at 4 °C for a maximum of two weeks. Because the assay is performed at room temperature the solution was allowed to equilibrate prior to use. The GF/B coating solution contained 0.3% Polyethylene and 0.2% BSA. This was stored at 4 °C for a maximum of two weeks. [³H]-AR-C160051XX was supplied in a solution containing 67% ethanol, 33% water 3.3 mg/ml sodium thiosulphate. This was stored at -20 °C. Astemizole was kept in DMSO at a concentration of 10 mM. The positive control Pimozide was stored in DMSO at a concentration of 30 µM at -20 °C.

Cisapride (Apin Chemicals Ltd.) was kept in 10 mM stocks in DMSO and stored at -20 °C. Blinded compounds, d-sotalol (AstraZeneca), pinacidil (Sigma Aldrich), terfenadine (Sigma Aldrich) and glucose (Sigma Aldrich) were all stored at room temperature in DMSO at 1000x the maximum concentration. All styryl dyes were stored in stock solutions of 5 mM (or 3 mM for binding experiments) stored at 4 °C, with the exception of di-12-ANEPPS, which was stored at -20 °C. Di-8-ANEPPS and di-4-ANEPPS were obtained as solids from

Molecular Probes and dissolved into DMSO containing 5% pluronic acid by weight. Di-4-ANEPPS was also stored in ethanol as were di-3-ANEPPDHQ and di-4-ANNEPDHQ. Di-12-ANEPPS was stored in DMSO containing 20% pluronic acid by weight. Di-3-ANEPPDHQ, di-4-ANNEPDHQ and Di-12-ANEPPS were obtained from Professor Loew of The University of Connecticut Health Centre.

2.6. Data analysis and statistics.

All data is expressed as means \pm SEM. Statistical analysis was performed using either Sigmaplot 8.0 or Graphpad Prism version 4. Action potential durations at different stages of AP repolarisation were calculated according to the diagram in Figure 2.10. Calculations of the resting membrane potential are averages of the data points obtained from the final 200 ms of recordings/averages that are 1 s in duration, where an AP was stimulated 15 ms from the beginning of the sweep.

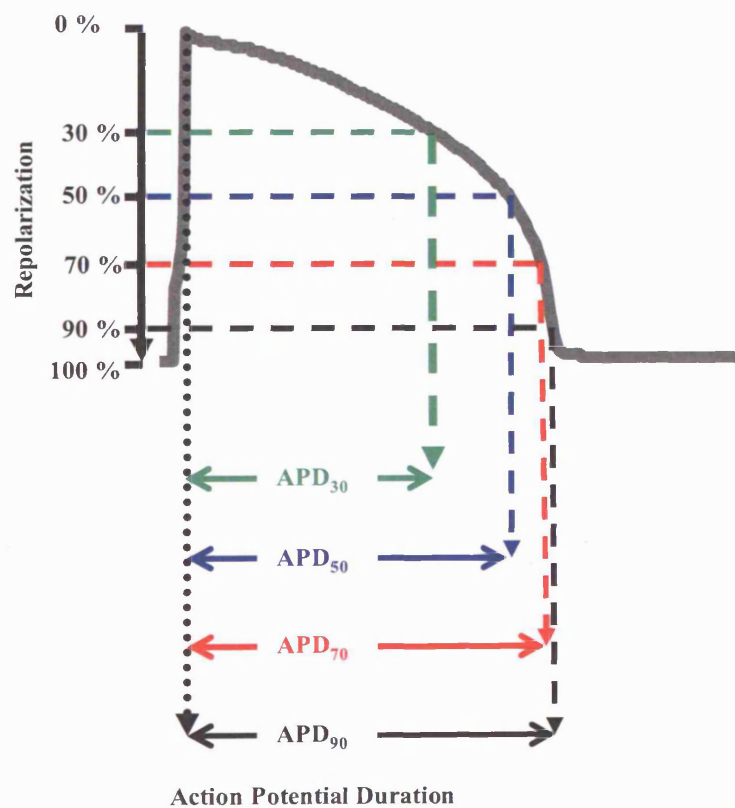


Figure 2.10. Illustration displaying the calculation of different action potential durations.

Example taken from a representative guinea pig ventricular action potential, by virtue of the percentage of repolarization where: 0 % repolarization is calculated as the maximum depolarization and 100 % repolarization is equal to the resting membrane potential.

Chapter 3:

**Considerations in recording action potentials optically from
isolated ventricular myocytes.**

Chapter 3: Considerations in recording action potentials from isolated ventricular myocytes.

The cardiac action potential (AP) is largely determined by the response of a number of voltage-sensitive ion channels to changes in the electric fields across the cell membrane, thus monitoring cardiac function and dysfunction requires measurement of the membrane potential. Fast voltage-sensitive dyes have been used previously to measure electrical activity in a wide range of different preparations including both neuronal tissue and cardiac muscle (Baker *et al.*, 2000; Brunner *et al.*, 2003; Bullen & Saggau, 1999; Obaid *et al.*, 2004; Salama & Choi, 2000; Zhang *et al.*, 1998). For studies of cardiac muscle potentiometric dyes have a variety of applications, including studies of arrhythmias in isolated intact hearts, which have also been performed simultaneously with monitoring of calcium transients, for example during alternans (Pruvot *et al.*, 2004; Salama & Choi, 2000).

Both di-4-ANEPPS and di-8-ANEPPS have been used to monitor membrane potential in isolated cardiac myocytes (Windisch *et al.*, 1995) and it has been demonstrated that using di-8-ANEPPS it is possible to record fluorescent changes from an area as small as 14 μm in diameter (Sharma & Tung, 2002; Sharma *et al.*, 2002; Sharma *et al.*, 2005). Recent studies using di-8-ANEPPS demonstrated that it is possible to record action potentials (APs) from isolated cardiac myocytes (Klauke *et al.*, 2005).

In this chapter practical variables were identified to obtain the optimum conditions for detecting action potential durations (APDs) using these dyes. These included the use of ratiometric recordings to reduce artefacts caused by movement, photobleaching and dye wash-off. Additional experiments were undertaken to demonstrate the relationship between the emitted fluorescence of these dyes and the membrane potential of isolated cardiac myocytes, including using electrophysiological techniques to control membrane potential whilst monitoring emitted fluorescence intensity. Additionally, using the proarrhythmic compound cisapride, drug-induced alterations in APD were monitored in isolated myocytes using either a patch electrode, di-8-ANEPPS or both simultaneously.

3.1. Results I: Recording cardiac action potentials.

3.1.1. Optically recording cardiac action potentials.

The fluorescence intensity emitted by styryl dyes is dependent upon both the dye concentration present in the cell membrane and the intensity of excitation light. However, dye molecules may become bleached during excitation or may be washed out of the membrane during superfusion, which results in degradation of the emitted signal. In addition, continued excitation of some fluorochromes can result in production of reactive oxygen species (ROS), which are toxic to the cell and may influence some ion channels. Thus a balance must be obtained between these factors. Initial experiments to obtain the optimum conditions for recording cardiac APs were performed on rodent myocytes, although the ultimate aim was to transfer the protocol into canine midmyocardial cells (M cells), which bear a more similar ion channel expression to human ventricular cells.

Both di-4-ANEPPS and di-8-ANEPPS display a number of properties which are advantageous in the study of membrane characteristics: they display no appreciable fluorescence in solution; they exhibit a relatively large Stokes shift; and they emit at two different spectral wavelengths that are dependent upon voltage (Loew, 1999; Loew, 2001). Thus, using a set-up of optical filters and reflectors, it is possible to remove the majority of scattered and reflected light and obtain fluorescent recordings at wavelengths emitted from dye only when it is bound in the membrane.

Studies were performed on isolated guinea pig and rat ventricular myocytes, which had been incubated at room temperature with differing concentrations of di-4-ANEPPS or di-8-ANEPPS for variable durations. Myocytes were field-stimulated at 1 Hz to produce visible contractions, thus providing APs with a fast change in membrane potential with which to monitor the response of either dye and data was sampled at 1 kHz. Figure 3.1 is a confocal image through a single plane of an isolated myocyte, which had been stained for 20 min with di-8-ANEPPS; the edge of the cell and t-tubules are visible, which demonstrates the localization of emitted fluorescence to the membrane.

Figure 3.2 shows quantitative recordings of the emitted fluorescence during an AP from an isolated guinea pig ventricular myocyte loaded with di-8-ANEPPS for 20 min at room temperature. Fluorescence was emitted at two wavelengths which showed divergence in response to the change in membrane potential; light detected at 560 nm increased in intensity during depolarisation of the membrane and decreased as the cell repolarised, whilst light

emitted at 620 nm did the opposite. The ratio of these two wavelengths showed a morphology similar to that of a guinea pig ventricular AP.

Brette *et al.*, (2002) incubated isolated ventricular myocytes in 5 μM di-8-ANEPPS for 2 min to visualise t-tubules. However, even using an oil immersion lens of relatively high numerical aperture, 1.3, at x40 magnification this was insufficient to record a clear enough fluorescent signal to determine cardiac APDs in response to stimulation, despite the myocytes contracting visibly. Increases in the duration of incubation with di-8-ANEPPS were beneficial. Figure 3.3 demonstrates that a clearer visualisation of rat APs could be obtained by increasing the incubation period of di-8-ANEPPS from 5 to 20 min. In practice, APs recorded from myocytes incubated with 5 μM di-8-ANEPPS for 5-10 min were of variable quality and a more consistent signal was obtained with a 20 min loading regimen. Longer incubations, up to 40 min did not visibly improve the signal: noise (S/N) ratio. Using the loading regimen of 5 μM di-8-ANEPPS for 20 min it was possible to visualise a change in fluorescence using a non-immersion x40 objective of lower NA, 0.6, but not with sufficient signal strength to be able to detect changes in AP morphology.

Previously it has been demonstrated that di-4-ANEPPS can cause photodynamic damage to myocytes (Schaffer *et al.*, 1994). To avoid this, excitation light intensity was minimised by limiting the opening of the iris in front the arc lamp to 1 cm. Additional reduction in light intensity was achieved by the placement of two neutral density filters in front of the arc lamp. Although increases in the loading concentration of di-8-ANEPPS up to 20 μM did cause an increase in S/N ratio, APD prolongation due to phototoxicity was more rapid. Ultimately, using guinea pig myocytes loaded with 5 μM di-8-ANEPPS for 20 min and reducing exposure times to 30s in every 3 minutes allowed for recordings of APD with steady duration to be made up to a period of 24 min. Figure 3.4 shows averages of 20 APs recorded using this protocol during the first exposure and after 24 min.

To characterise the conditions required for recording APD morphology from isolated myocytes with di-4-ANEPPS, attempts were made using the same protocol that were successful using di-8-ANEPPS; cells were incubated at room temperature for 20 min with a dye concentration of 5 μM . However, the emitted fluorescence declined too quickly to be able to maintain recordings and so a maintenance dose of dye was placed in the superfusate. In practice, sufficient light intensity was emitted to maintain a signal using the same loading protocol, but with 200 nM di-4-ANEPPS in the perfusate.

Cells loaded with di-4-ANEPPS in this manner displayed increases in APD when subjected to excitation light for periods of 30 s every 3 min. However, by limiting this exposure to 5 s in every four minutes it was possible to record steady state APDs for a minimum of 28 min. Figure 3.4 shows APs recorded from an isolated myocyte using di-4-

ANEPPS during the first exposure as well as during a sixth exposure after 28 min. Curiously, attempts to adopt the same protocol for recordings APs from isolated canine myocytes produced an increased signal:noise ratio, but pronounced phototoxicity; AP prolongation was visible within seconds of exposure to excitation light and following exposures resulted in an unstable membrane potential and loss of AP induction. This is shown by the AP sweeps in Figure 3.5.

Recordings of a single AP were often subject to too much noise to allow for accurate determination of APD. However, averaging multiple APs increased the signal-to-noise ratio appreciably. Figure 3.6 shows a single AP recorded using di-8-ANEPPS that can be compared to averages of 5 and of 20 consecutive APs from the same cell. Whilst determination of the APD₉₀ from the single AP would be difficult and inaccurate, analysis became easier as more APs were averaged.

Previous work by Klauke *et al.*, 2005, has demonstrated that it is possible to record APs from isolated myocytes using di-8-ANEPPS, however their optical system only recorded light emitted at a single wavelength and thus would have been subject to motion artefacts. Previously, in whole rabbit hearts stained with di-4-ANEPPS, Knisley *et al.*, (2000) used emission ratiometry to reduce drift and motion artifacts. When myocytes were subjected to suprathreshold stimuli they would contract, sometimes causing movement artefacts when regions of the cell moved in and out of focus or view. Figure 3.7 shows an average of 5 APs during which the contraction of the cell resulted in an increase in the fluorescence intensity detected at both 560 and 620 nm. However, the ratio of these signals was not altered by this artefact. Additionally, ratiometric recordings also minimised artefacts that arose from photobleaching or wash-off of the dye.

Studies utilising voltage-sensitive dyes in whole hearts have been used to measure the upstroke velocity of the cardiac AP. However, because the fluorescent signal received in whole heart studies is from the emission of a large number of cells, it is likely that the response would be slower than that recorded from a single cell. Figure 3.8 shows the upstroke of an average of 5 APs from a cell loaded with 5 μ M di-4-ANEPPS (with 200 nM maintenance in the perfusate), simultaneously recorded with a patch electrode at a sampling frequency of 10 kHz to allow for measurement of the rapid upstroke (other recordings in this chapter were sampled at 1 kHz). APs were stimulated using a relatively brief stimulus duration of 0.1 ms[†]. The ratio emission of di-4-ANEPPS does not change with a rate as fast as the recordings using a patch electrode.

[†] In the majority of patch electrode recordings of APs in this thesis, a longer stimulus duration of 4 ms was used. However, this would interfere with measurement of the upstroke of the AP (see later in section 3.1.3).

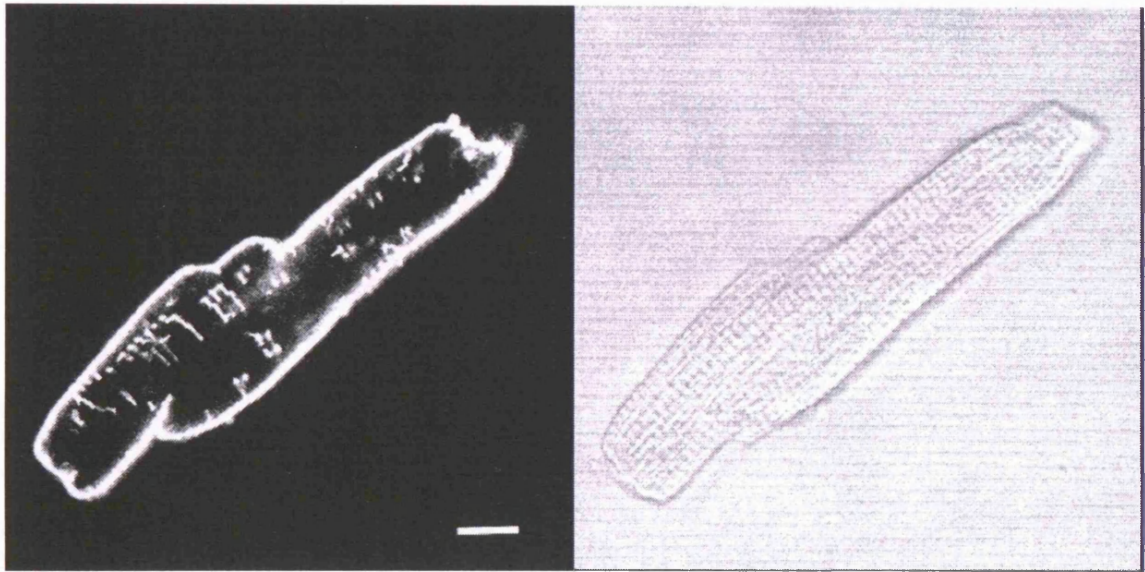


Figure 3.1. A confocal image through a single plane of an isolated myocyte.

An isolated guinea pig ventricular cell incubated with $5 \mu\text{M}$ di-8-ANEPPS for 20 minutes at room temperature. Confocal image showing fluorescence emitted at 560 nm (left) from the myocyte when excited with a 488 nm laser and the same myocyte viewed under bright field illumination (right). Bar inset is equal to $10 \mu\text{m}$.

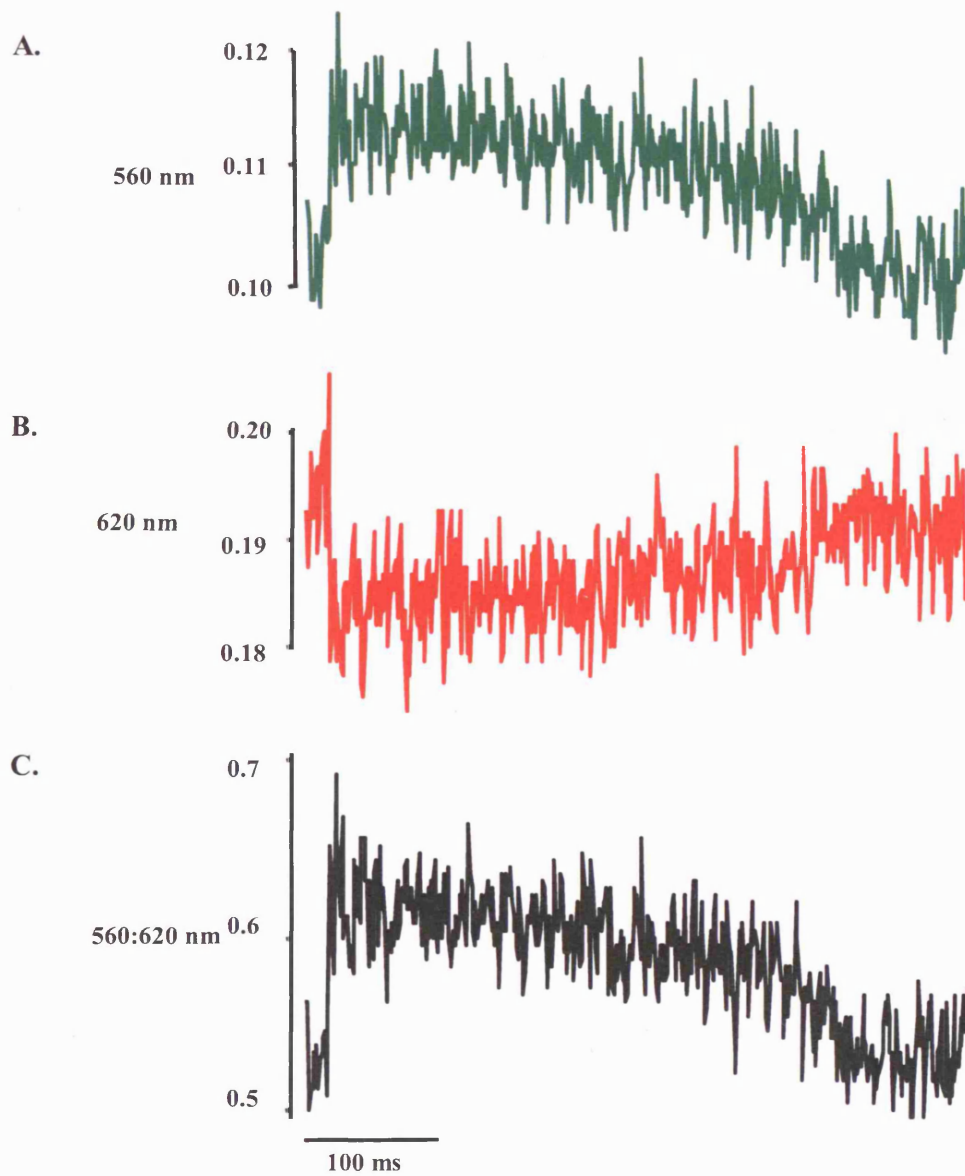


Figure 3.2. A ventricular cardiac action potential recorded with di-8-ANEPPS

A single action potential recorded from an isolated guinea pig myocyte loaded with di-8-ANEPPS for 20 min at room temperature and excited with wavelengths between 460-500 nm. (A) The fluorescent intensity (arbitrary units) emitted at 560 nm. (B) The fluorescent intensity emitted at 620 nm. (C) The ratio of the fluorescence intensities 560:620 nm, used to derive the action potential.

A.



B.

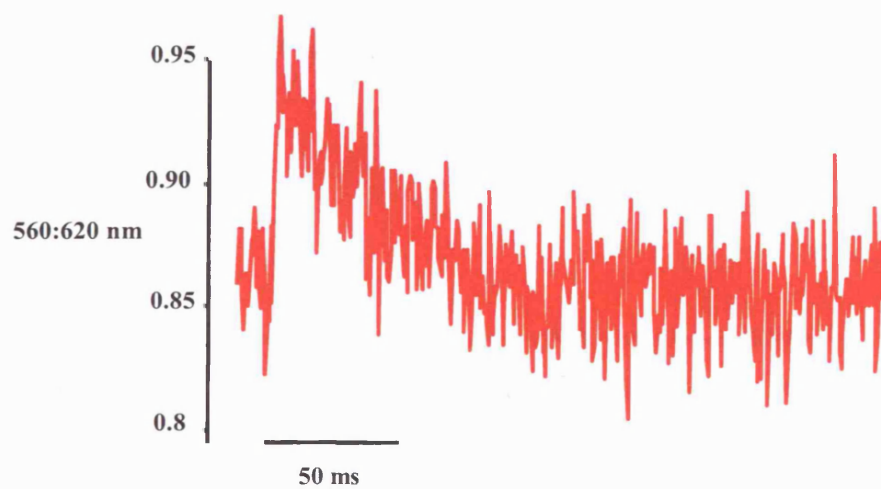


Figure 3.3. Cardiac action potentials recorded from cells with different incubation periods in di-8-ANEPPS.

Individual action potentials recorded from isolated rat myocytes incubated with 5 μ M di-8-ANEPPS for 5 min (A) and 20 min (B) excited with wavelengths between 460-500 nm.

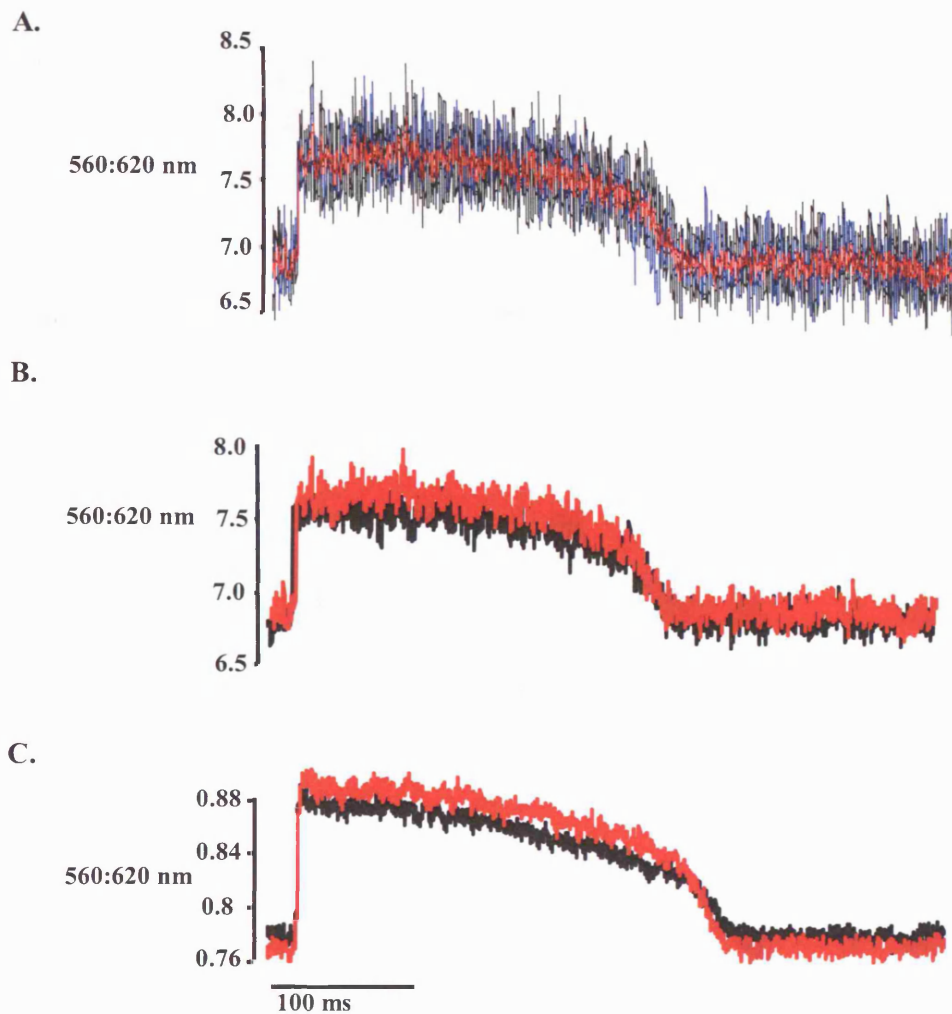


Figure 3.4. Stability of action potential durations recorded with di-4-ANEPPS

(A, B) Optical action potentials recorded from a single guinea pig ventricular myocyte incubated with $5 \mu\text{M}$ di-4-ANEPPS for 20 min and superfused with 200 nM di-4-ANEPPS. The cell was exposed to excitation light for 5 consecutive seconds in every 4 min. (A) the first exposure after 4 min of stimulation at 1 Hz. The first sweep is in blue and the following 4 are in black. An average of the 5 traces is superimposed in red. (B) The average of 5 action potentials (black) recorded after 28 min with the average of the traces in (A), recorded during the first exposure, overlaid. (C) A single guinea pig ventricular myocyte incubated with $5 \mu\text{M}$ di-8-ANEPPS for 20 min. The cell was exposed to excitation light for 30 consecutive seconds in every 3 min. The average of 20 action potentials (black) recorded after 24 min with the average of 20 traces recorded during the first exposure overlaid (red).

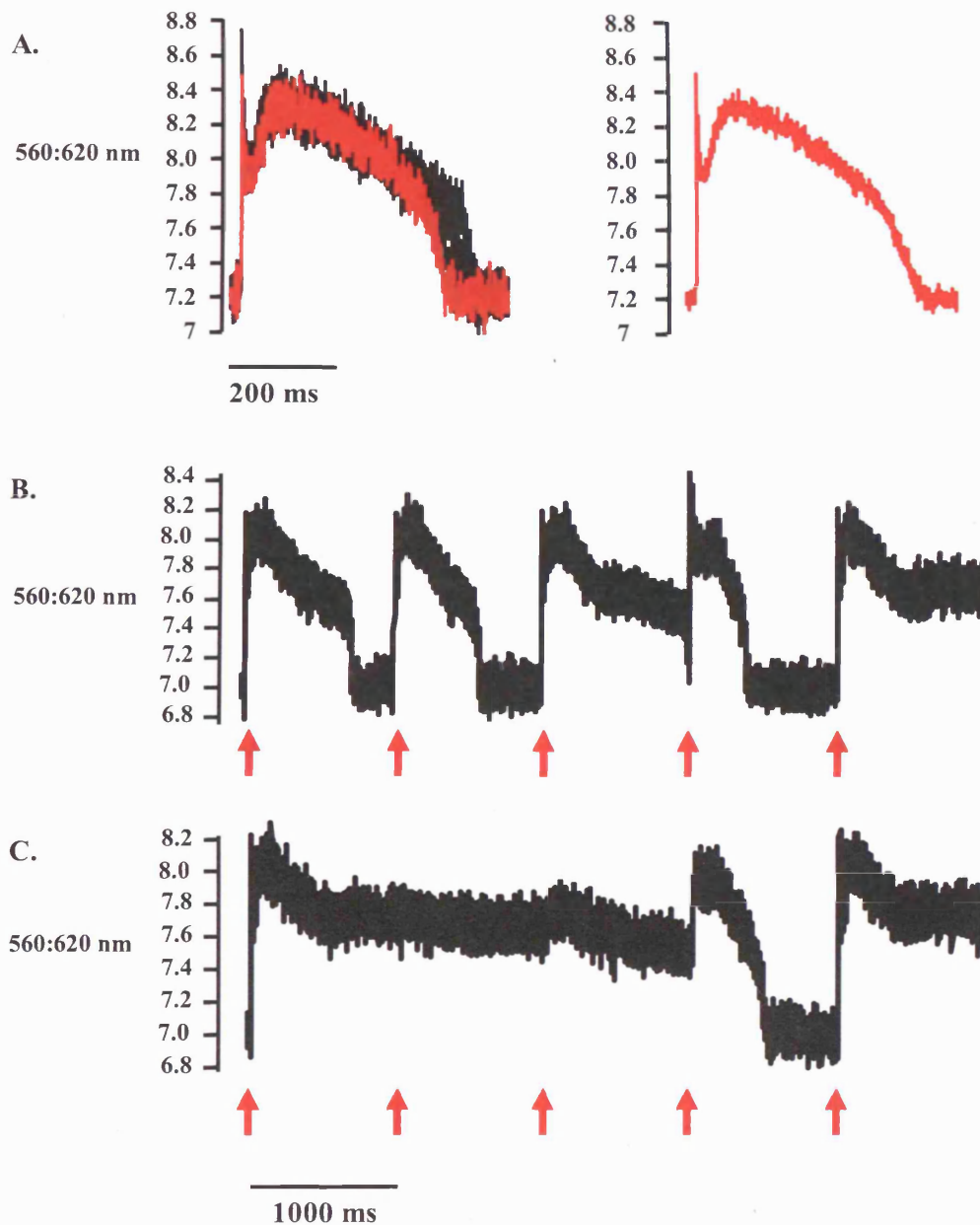


Figure 3.5. Phototoxic effects upon canine cardiac action potentials.

A single canine M cell loaded with 5 μM di-4-ANEPPS for 20 min and superfused with 200 nM di-4-ANEPPS. The cell was exposed to excitation light for 5 consecutive seconds in every 4 min. (A) 5 consecutive action potentials stimulated at 1 s intervals show prolongation during a 5 second exposure to excitation light (left) and the average of those sweeps (right) showing relatively large signal:noise ratio. The first action potential is shown in red. (B) 5 s exposure following the sweeps in (A) at 4 min intervals show further APD prolongation and EADs. (C) 5 s exposure after 8 min shows a loss of excitation with stimulus (stimuli are marked by red arrows).

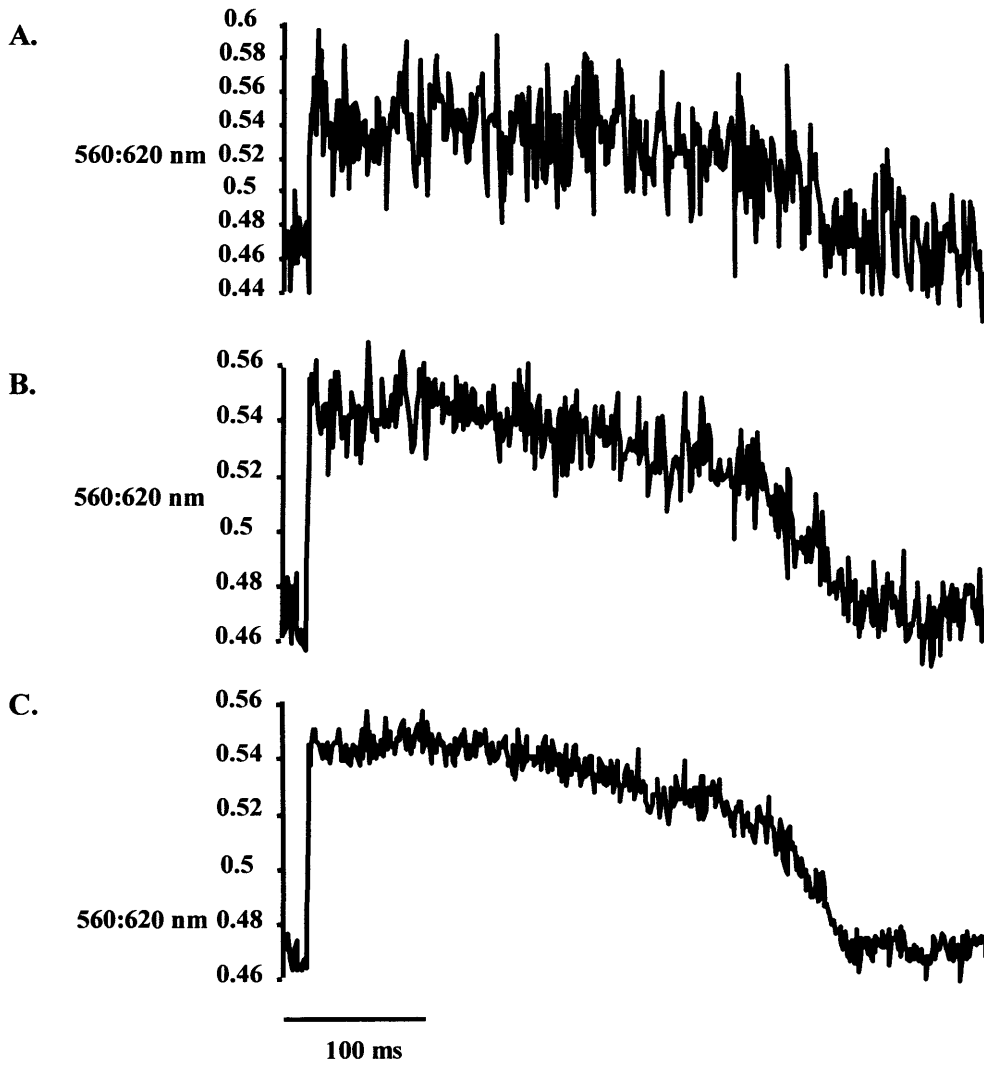


Figure 3.6. Averaging multiple cardiac action potentials to reduce noise.

The fluorescence ratio 560:620 nm recorded from an isolated guinea pig ventricular myocyte incubated for 20 min with di-8-ANEPPS. Recordings are from a single action potential (A) and the averages of 5 (B) and 20 (C) consecutive action potentials.

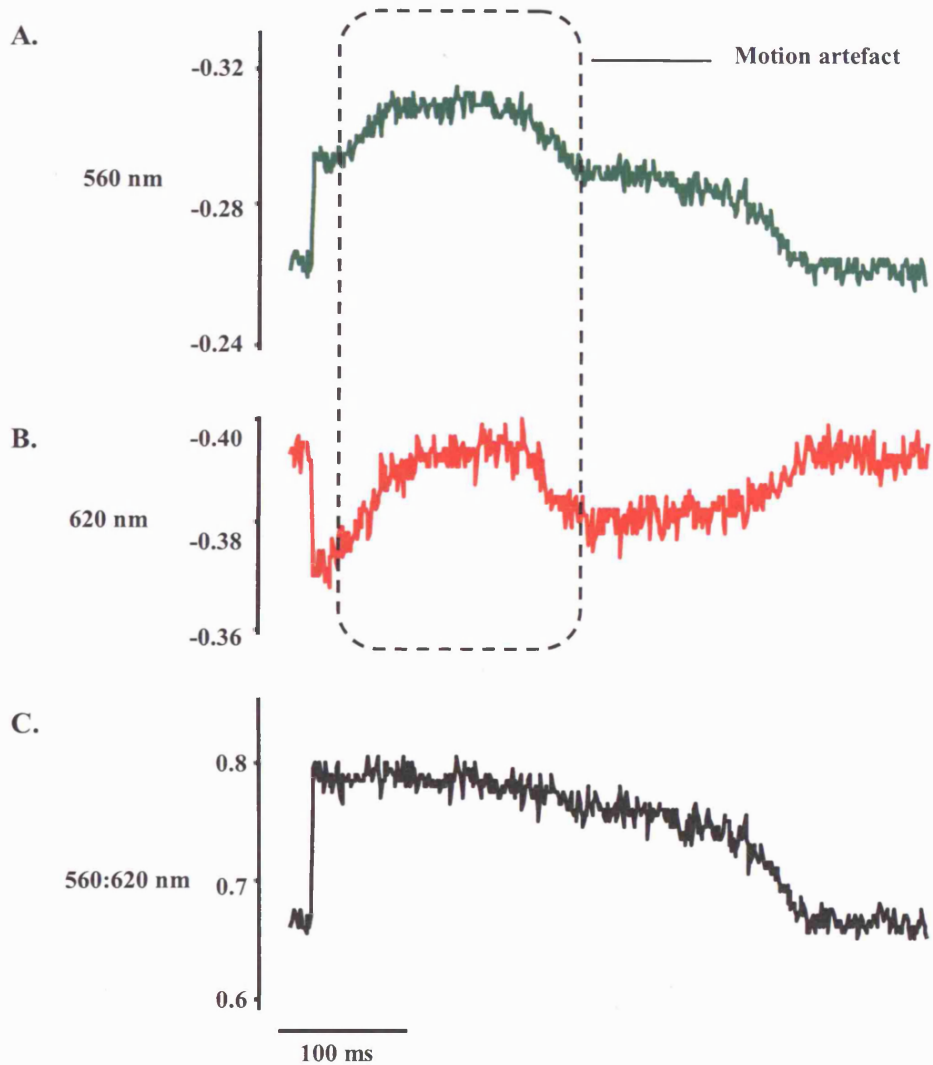


Figure 3.7. The removal of a motion artefact by ratio emission fluorescence.

An average of 5 consecutive action potentials recorded from an isolated guinea pig ventricular myocyte loaded for 20 min with di-8-ANEPPS. Contraction of the myocyte produced motion artefacts in the fluorescence emitted at 560 nm (A) and 620 nm (B). However, in the ratio of 560:620 nm, the motion artefact is removed.

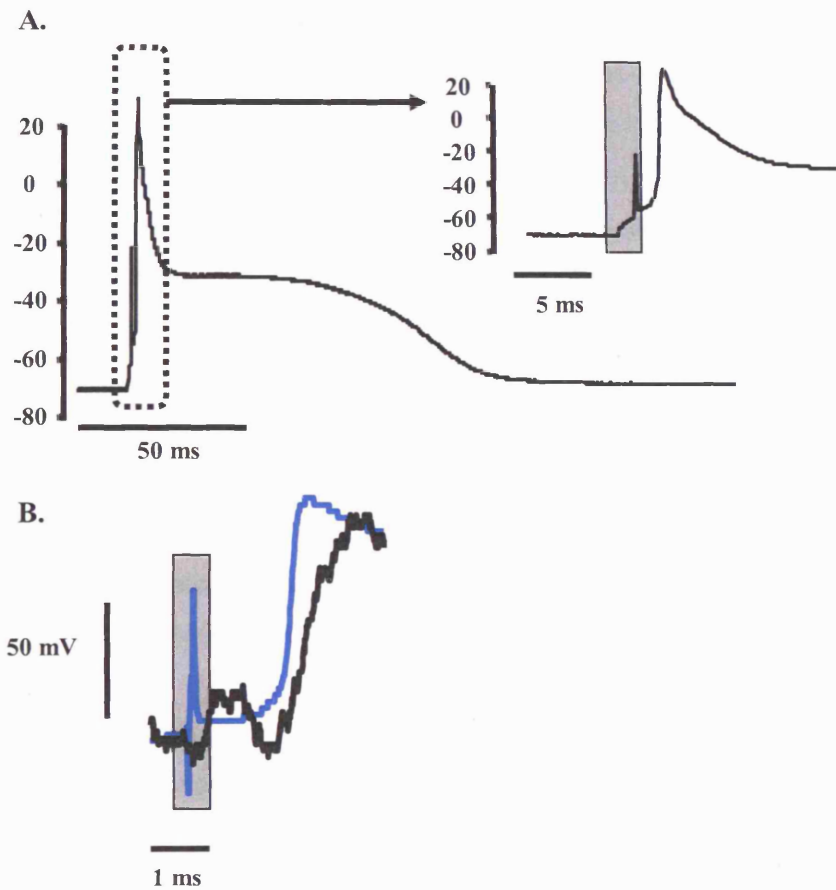


Figure 3. 8. Changes in fluorescence of di-4-ANEPPS during the upstroke of a rat action potential.

(A) An average of 5 action potentials recorded from a single isolated rat cardiac myocyte using a brief suprathreshold stimulus. The presence of a stimulus artifact distinct from the upstroke is displayed (inset – artifact shown with a grey background). (B) An average of 5 upstroke velocities recorded simultaneously using a patch electrode and optically after staining with di-4-ANEPPS. The optically recorded AP displays a longer rise time than the electrically recorded AP.

3.1.2. Calibrating the optical response of di-8-ANEPPS and di-4-ANEPPS to membrane potential.

Previously in cell types other than the cardiac myocytes, it has been demonstrated that the fluorescence emission of di-8-ANEPPS has a linear relationship with membrane potential (Staub et al., 1994; Beach et al., 1996; Huser et al., 1996). To ensure that the fluorescent signal we obtained using di-8-ANEPPS and di-4-ANEPPS was equivalent to the membrane potential of isolated ventricular myocytes, it was necessary to record optical signals whilst simultaneously using whole cell patch-clamp recordings to control and measure the membrane potential.

This was achieved using a voltage-clamp protocol with a holding potential of -70 mV and 300 ms test pulses, 10 mV apart, between -80 mV and +60 mV. 10 records were recorded and averaged at each potential from cells which had been loaded for 20 min with either di-8-ANEPPS or di-4-ANEPPS with additional superfusion of 200 nM. By employing the discontinuous single electrode voltage-clamp (dSEVC), it was possible to record the membrane potential as well as the command potential. Thus, any differences between the command potential and the membrane potential could be detected and accounted for during analysis.

Both di-4-ANEPPS and di-8-ANEPPS loaded myocytes emitted fluorescence with a linear relationship to membrane potential. Di-4-ANEPPS demonstrated a percentage change in the ratio of 560:620 nm of 7.4% per 100 mV, compared to the change of 8.6% exhibited by di-8-ANEPPS. During calibration of both dyes, values were obtained after excluding outlying responses from two cells, which showed a much smaller shift in fluorescence compared to the other cells studied. Figure 3.9 shows the changes in ratio emission for both dyes, for each individual cell in response to changes in membrane potential. This is expressed as both the raw fluorescence and as a percentage change. When the change in fluorescence was expressed as a percentage it was easier to identify the outlying cells. All of the cells studied, including outliers, demonstrated linearity between membrane potential and emitted fluorescence ratio ($r > 0.99$ for each cell). Inclusion of all the cells studied showed changes in emitted fluorescence of 7.4% and 5.8% per 100mV for di-8-ANEPPS and di-4-ANEPPS respectively. These results suggest two things: firstly, because the emitted fluorescence of some cells was not as pronounced as with others, there may be a requirement for exclusion criteria; and secondly, in isolated guinea pig ventricular myocytes, di-8-ANEPPS exhibits a greater change in emitted fluorescence than di-4-ANEPPS.

Figure 3.10 shows averages of 10 records from a single guinea pig myocyte loaded with di-8-ANEPPS. Parameters monitored included the fluorescence emitted at both wavelengths, the emitted ratio as well as the membrane potential. This showed that when the

voltage was stepped to potentials that did not activate the sodium current, for example from -70 mV to +60 mV, the recorded voltage was not subject to large deviations. However, during steps from -70 mV to -30 mV, a transient positive deflection can be seen in the recorded potential, which is also detected by both of the emitted fluorescent signals and is present in the resultant 560:620 nm emission ratio. Close inspection of the deflection in figure 3.9 demonstrates that the optical signal is marginally slower than the electrical one. During the voltage steps used in the calibration protocol, recording from the last 200 ms of the averaged sweeps avoided the fluctuations in membrane potential caused by the sodium current. Additionally, as can be seen in Table 3.1, which shows means of the recorded and command potentials from the 10 cells loaded with di-8-ANEPPS, there is a deviation between the recorded potential and the command potential. Although this is only slight, data analysis was performed using the recorded potential for greater accuracy. In this way, the linearity of the change in fluorescence emitted by di-8-ANEPPS and di-4-ANEPPS in the membrane could be evaluated: a linear increase in fluorescence emitted at 560 nm signal accompanied by a decrease in at 620 nm during a positive shift in membrane potential.

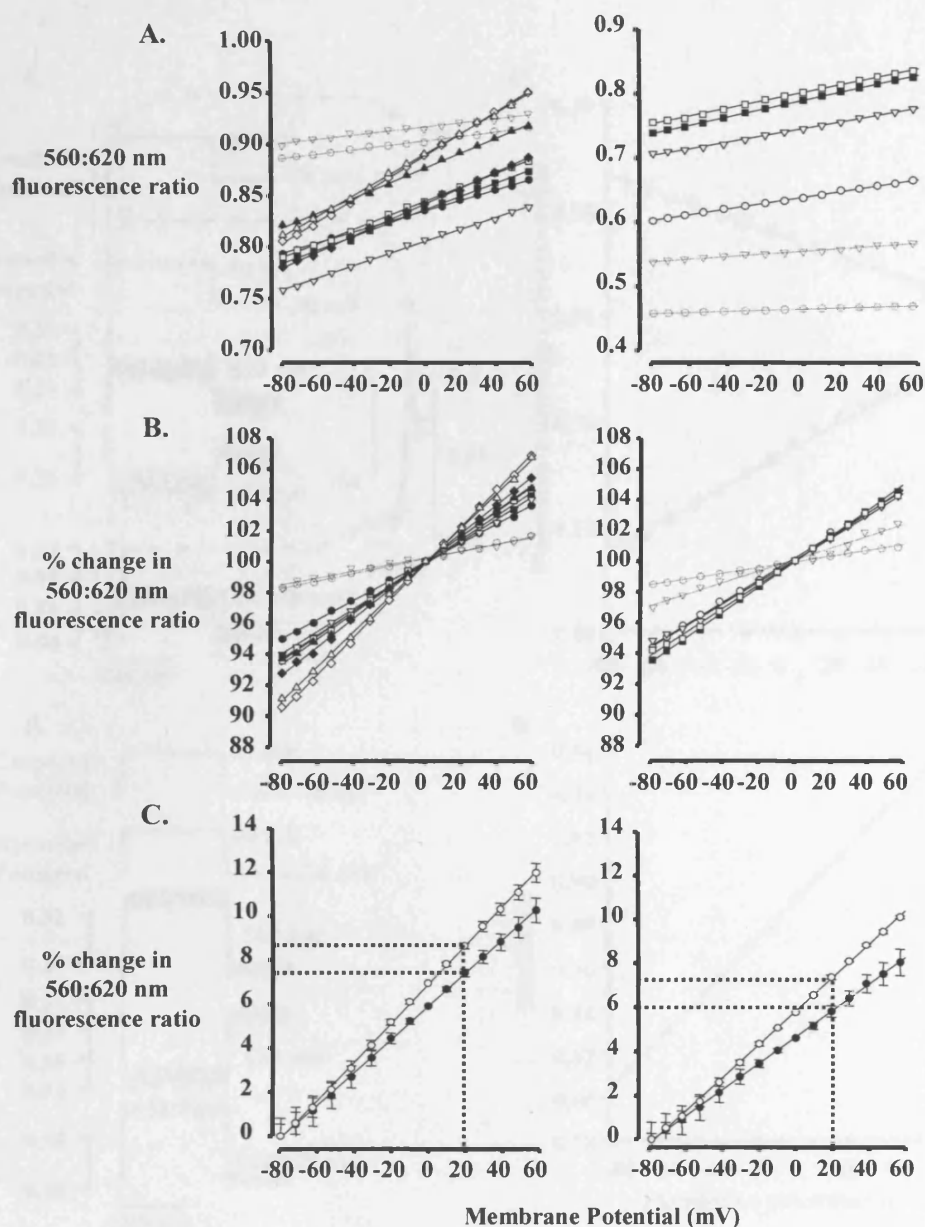


Figure 3.9. The relationships between membrane potential and the emitted fluorescence of di-8-ANEPPS and di-4-ANEPPS.

Changes in emitted fluorescence from myocytes loaded with di-8-ANEPPS (left, $n = 10$) or di-4-ANEPPS (right, $n = 6$). (A) Graphs showing the ratio of the emitted fluorescence at 560 and 620 nm for individual myocytes. (B) Graphs showing the change in ratio emission at 560:620 nm expressed as a percentage normalised to 0 mV. (C) Graphs showing the mean \pm SEM percentage change. For clarity 0% change is taken from -80 mV. Two estimates of percentage change are exhibited for both di-8-ANEPPS and di-4-ANEPPS; one plot shows all the mean of all of the cells (open circles) and the other plot with outliers (dotted lines in (A) and (B)) removed (closed circles).

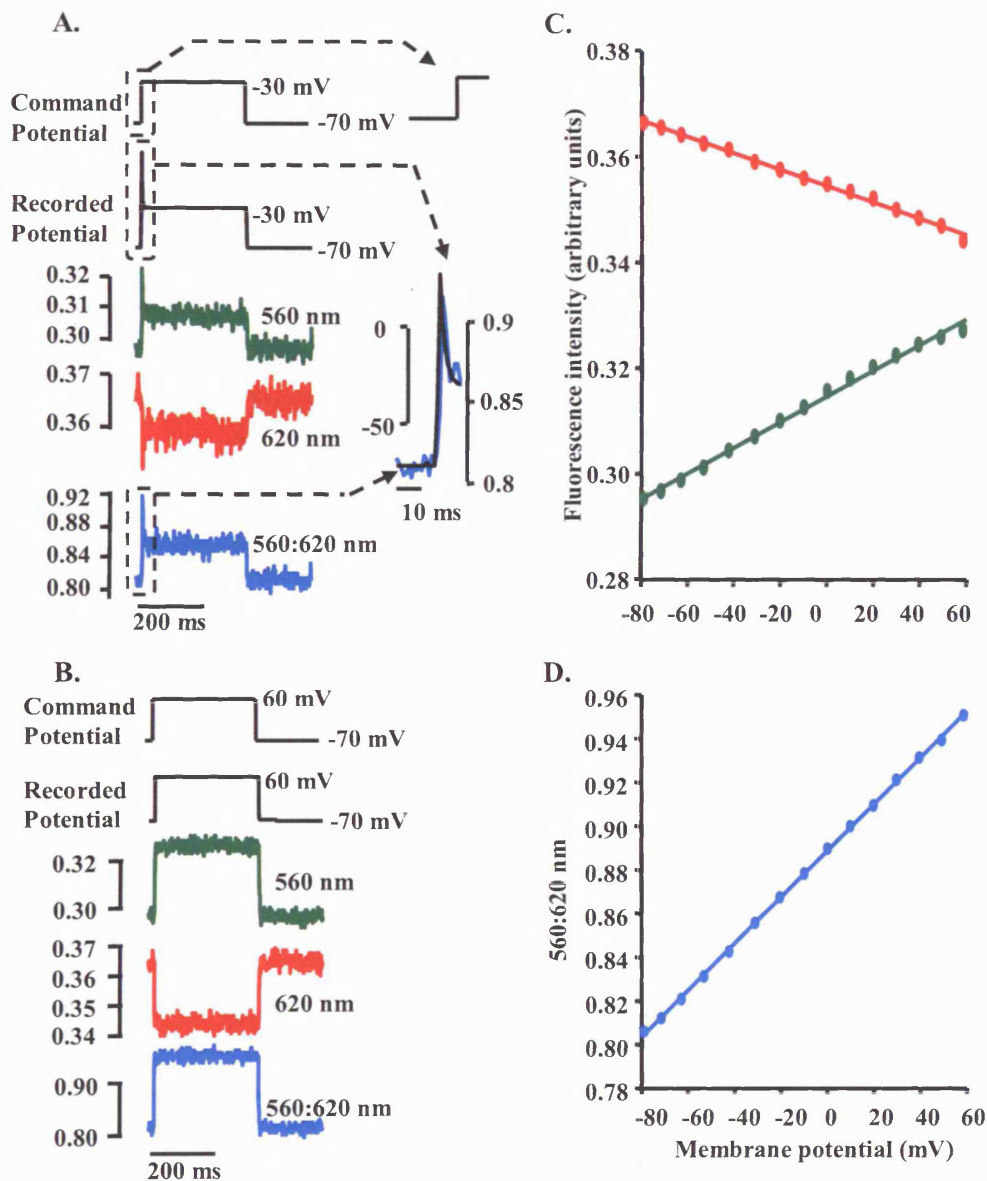


Figure 3.10. Calibrating the ratiometric emission of di-8-ANEPPS using dSEVC.

Fluorescence emission recorded from an isolated guinea pig myocyte loaded with di-8-ANEPPS. (A) Averages of 10 records showing loss of voltage control when the sodium current is activated during a 300 ms step from -70 mV to -30 mV. A transient is visible in both the optical recordings and the recorded membrane potential, but this is brief enough to allow for accurate recordings at -30 mV. The ratio of the 560:620 emission ratio is inset overlaid with the recorded membrane potential. (B) Averages of 10 records showing optical and electrical recordings during 300 ms step from -70 mV to 60 mV. (C) Graph showing the increase in fluorescence emitted at 560 nm and the corresponding decrease at 620 nm as membrane potential becomes more positive. (D) Graph showing the increase in the ratio of emitted fluorescence at 560:620 nm.

Command Potential (mV)	Recorded Potential (mV)		
-80	-79.30	±	0.09
-70	-71.23	±	0.11
-60	-62.12	±	0.18
-50	-52.08	±	0.24
-40	-41.37	±	0.23
-30	-30.62	±	0.22
-20	-20.04	±	0.18
-10	-9.77	±	0.15
0	0.17	±	0.13
10	10.09	±	0.14
20	20.01	±	0.13
30	29.89	±	0.11
40	39.64	±	0.11
50	49.28	±	0.12
60	58.85	±	0.15

Table 3.1. Comparing the recorded membrane potential with the command potential.

Table displaying values of command potential and recorded membrane potential from isolated guinea pig ventricular myocytes voltage-clamped for 300 ms durations using dSEVC (n = 10). The values are taken as the mean value of the last 200 ms of an average of 10 records.

3.1.3. Recording cardiac action potentials with sharp electrodes and patch pipettes.

Previously, studies monitoring APD in isolated myocytes have used microelectrodes, either using a sharp electrode or a patch pipette. Therefore, to assess the accuracy of monitoring APD using fast voltage-sensitive dyes, APDs were also monitored electrically. Initially, optical measurements from proarrhythmic compounds were to be recorded from isolated guinea pig myocytes, so assessment of AP morphology in this cell type was also necessary using electrophysiological techniques. (*Rat myocytes were not used for validations using proarrhythmic compounds because of their lack of sensitivity toward many APD prolonging compounds – see below and McDermott *et al.*, (2002)).

APs were recorded from isolated guinea pig myocytes using the whole-cell patch clamp configuration in Bridge mode on an Axoclamp 2A amplifier. APs were elicited using suprathreshold stimuli of 4 ms duration. Figure 3.11 shows the appearance of a guinea pig ventricular action potential recorded using this method. Practically, this was a relatively simple approach for recording action potentials from isolated myocytes; using a bridge balance circuit to balance the resistance at the tip of the glass pipette provided a relatively noise-free method for recording membrane potentials, provided there was no current being injected through the microelectrode. However, during the stimulus and whilst the capacitance discharged, the potential difference value at the tip of the electrode was not the same as the potential difference across the cell membrane. As a result, the value recorded for the membrane potential during this period was erroneous and appeared as an artefact. This error can be derived from Ohm's law ($V=IR$), whereby, when the current passing through the tip of the electrode is equivalent to zero, the resistance at the tip of the pipette has no effect. However as the current increases, a voltage is produced that is recorded cumulatively with the membrane potential. Thus, when compensation using the Bridge balance circuit was not perfect, for example if the tip of an electrode became occluded throughout the duration of an experiment, a stimulus artefact became apparent. In such cases, the maximum depolarisation was calculated as the first point of the AP following the artefact (example is shown inset in Figure 3.11).

Use of this technique demonstrates that there are differences in guinea pig ventricular morphology in cells stimulated at different frequencies. Isolated guinea pig myocytes were paced at 0.1, 0.2, 0.5, 1.0 and 2.0 Hz and found to have a biphasic response to increases in pacing rate. Figure 3.12 shows two averages of 10 action potentials recorded at 0.1 and 2 Hz. The action potential average recorded at the faster pacing frequency has a shorter duration. Increasing the stimulation frequency from 0.1 Hz to 0.5 Hz caused an increase in APD from 365 ± 19 ms to 412 ± 24 ms, $n = 13-15$. Although this was not found to be significant ($p >$

0.05, ANOVA, Tukey's post test, $n = 13-15$), a biphasic response to pacing frequency in APD has been reported previously in guinea pig papillary muscles (Ravens & Wettwer, 1998). Further increases in pacing frequency up to 2 Hz caused a reduction in APD (273 ± 10 ms at 2 Hz). Statistical analysis against values of APD₉₀ recorded at 2 Hz yielded significance at all the other pacing frequencies monitored ($p < 0.05$ at 0.1, 0.2, 1.0 Hz, $p < 0.01$ at 0.5 Hz, ANOVA, Tukey's post test, $n = 13-15$). This can be viewed in the graph in Figure 3.12 and also occurred at APDs at 30, 50 and 70 % repolarisation. Monitoring the last 200 ms of each averaged AP allowed for estimation of the resting membrane potential (RMP). Increasing the stimulation rate from 0.1 Hz to 0.5 Hz caused a small shift in RMP to more positive potentials from -72.7 ± 0.7 mV to -71.9 ± 0.7 mV, although this was not significant. Further increases in pacing rate did not appear to alter the RMP.

Presently, a number of other tissues and species are used to monitor for proarrhythmic potential in test compounds in the pharmaceutical industry. These include the canine Purkinje fibre (Gintant *et al.*, 2001) and studies have been performed on isolated canine M cells (Liu *et al.*, 1993; Liu & Antzelevitch, 1995). In the current study, rat cells were also used to help obtain suitable conditions for recording APs optically, as were guinea pig myocytes. Comparisons can therefore be made between APs from these different species.

Figure 3.13 shows typical individual APs recorded with a patch electrode from a ventricular rat cell and a guinea pig ventricular myocyte as well as sharp electrode recordings from a canine M cell. In each example, cells had been stimulated at 1 Hz and allowed to reach steady state. Ventricular myocytes isolated from rat ventricles displayed a much briefer APD than either guinea pig or canine myocytes, which had relatively comparable APDs. Canine M cells displayed a "notch and dome" morphology – an initial incomplete repolarisation, prior to a gradual depolarisation and the plateau phase of the AP. In addition, canine M cells also maintained a more negative RMP, implying that, at rest, these cells possess a membrane more permeable to potassium ions than either rat or guinea pig cells.

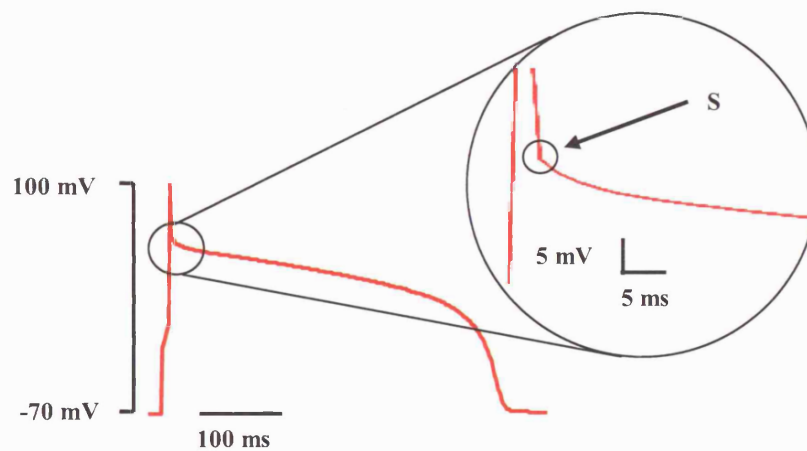


Figure 3.11. A single action potential recorded from an isolated guinea pig cardiac myocyte with a patch electrode.

A single recording of an action potential clearly demonstrates the presence of an artifact resulting from a voltage drop at the electrode tip during a 4 ms pulse. "S" indicates where measurement of the maximum depolarization was sampled, which was measured at 56 mV for this trace.

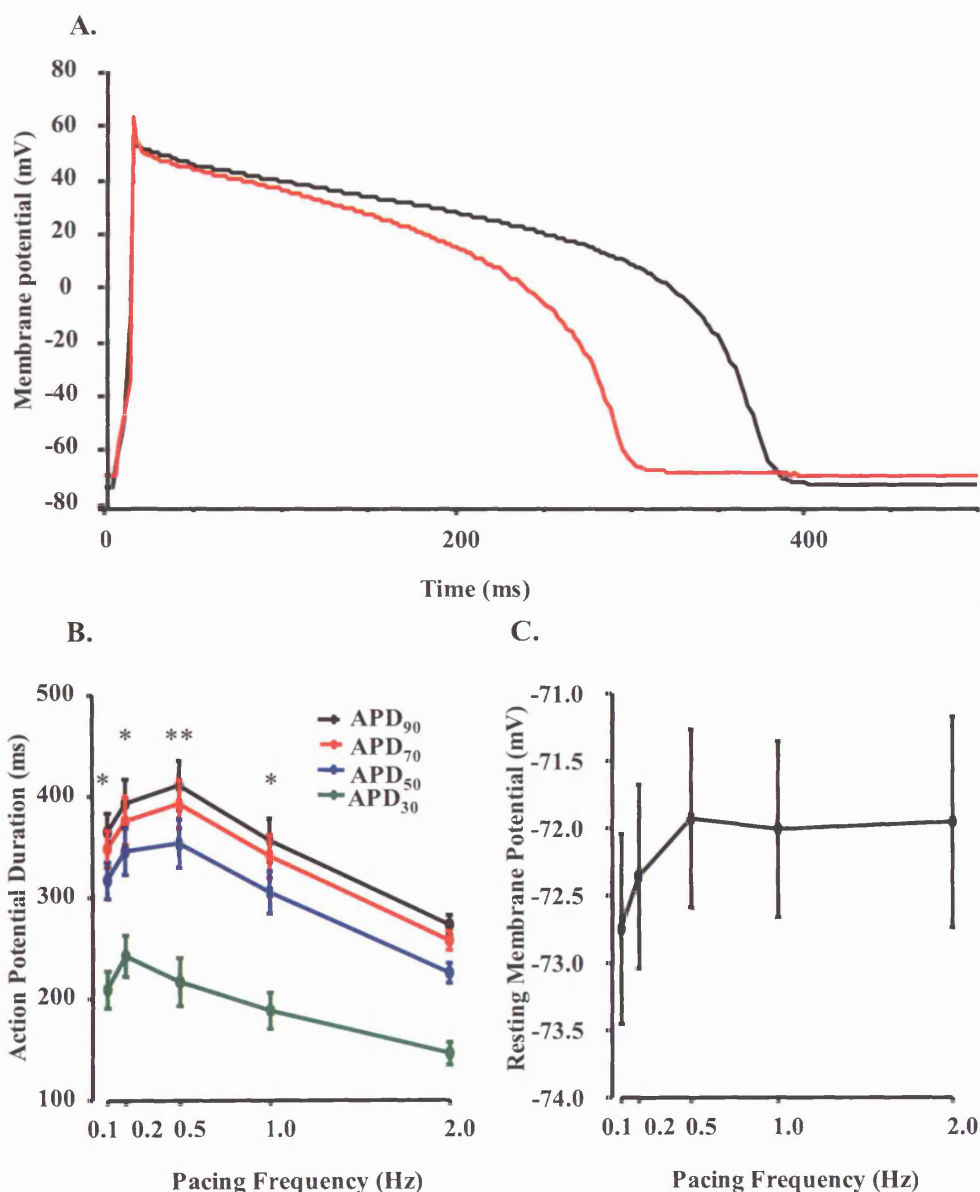


Figure 3.12. The effects of increased pacing rate upon ventricular guinea pig action potentials.

Action potentials were recorded with a patch electrode from isolated guinea pig ventricular myocytes paced at 0.1, 0.2, 0.5, 1.0 and 2.0 Hz. (A) Averages of 10 action potentials recorded from a single myocyte paced at 0.1 Hz (black) and 2 Hz (red). (B) Graph displaying action potential durations recorded from averages of 10 action potentials at 30, 50, 70 and 90% repolarisation at different pacing frequencies. (C) Graph displaying resting membrane potentials recorded from the last 200 ms of each averaged trace. Data are expressed as mean \pm SEM, * indicates $p < 0.05$, ** indicates $p < 0.01$ vs. APD₉₀ recorded at 2 Hz, ANOVA, Tukey's post test, $n = 13-15$.

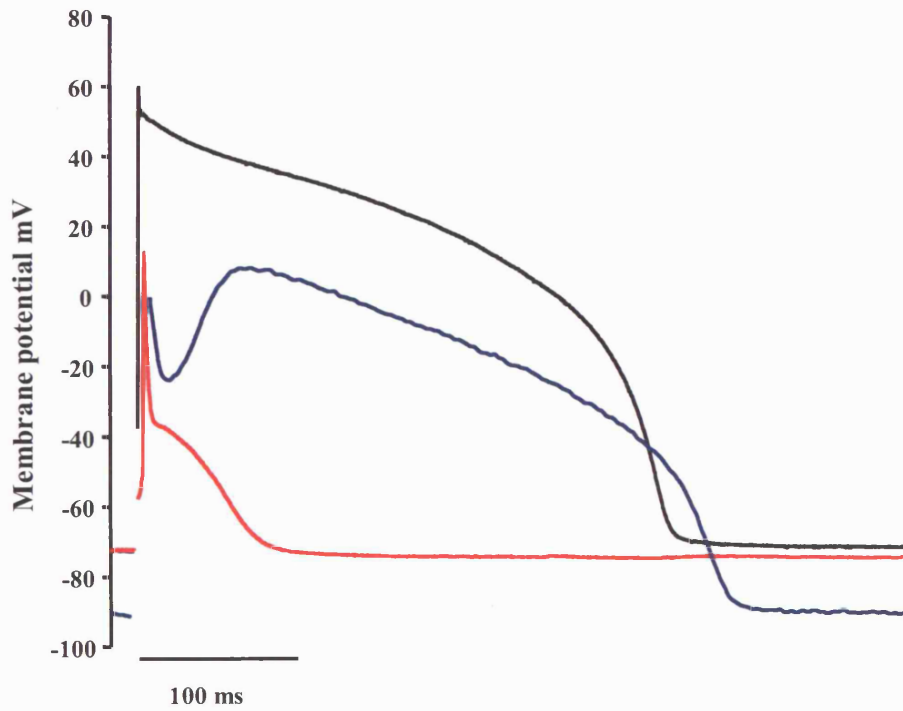


Figure 3.13. Figure displaying single action potentials from isolated ventricular myocytes.

Action potentials recorded from rat (red) and guinea pig (black) isolated ventricular myocytes and canine isolated midmyocardial cells (blue), all stimulated at 1 Hz. Stimulus artefacts have been removed for clarity.

3.1.4. The effects of Penicillin/Streptomycin solution on cardiac action potential durations.

During the development of this project data were published that demonstrated the effects of streptomycin sulphate upon AP morphology in isolated guinea pig ventricular myocytes (Belus & White, 2002). This was of concern because a solution containing streptomycin was used to maintain an infection-free suspension of cells in my work and because the reported effects were due to inhibition of a number of cardiac ion currents, including I_{Kr} , which is largely implicated in acquired LQTS. Therefore, the effects of the antibiotic solution in use were also ascertained.

To assess the effects of the antibiotic solution, action potentials were recorded from isolated guinea pig myocytes stimulated at 1 Hz using patch electrode and the APD at 30, 50, 70 and 90 % repolarisation was monitored during the acute application of normal Tyrode containing penicillin-streptomycin solution.

The antibiotic solution used (Sigma) contained 10, 000 units/ml penicillin and 10 mg/ml streptomycin, of which 1 ml was added to 30 ml myocyte suspension. The resultant solution therefore contained 457 μ M streptomycin. This was lower than the concentration shown to have an effect upon cardiac AP morphology (2 mM) in the study by Belus and White (2002), but considerably larger than the other concentration used which had no effect (50 μ M). Figure 3.14 demonstrates the effects of an equivalent concentration of Pen-Strep solution and the following wash-off upon the AP morphology of isolated guinea pig myocytes. Examples are shown of APs recorded before addition, as well during perfusion with an antibiotic solution and following wash-off. Whilst there was a significant increase in APD at 50, 70 and 90 % repolarization (APD_{90} increased from 262 ± 11 to 293 ± 17 ms, $n = 7$), the prolongation caused by the antibiotic solution was reversible upon wash-off. Since antibiotic solution was washed off before the measurements were made, it should not have had a detrimental effect upon the results in the current study.

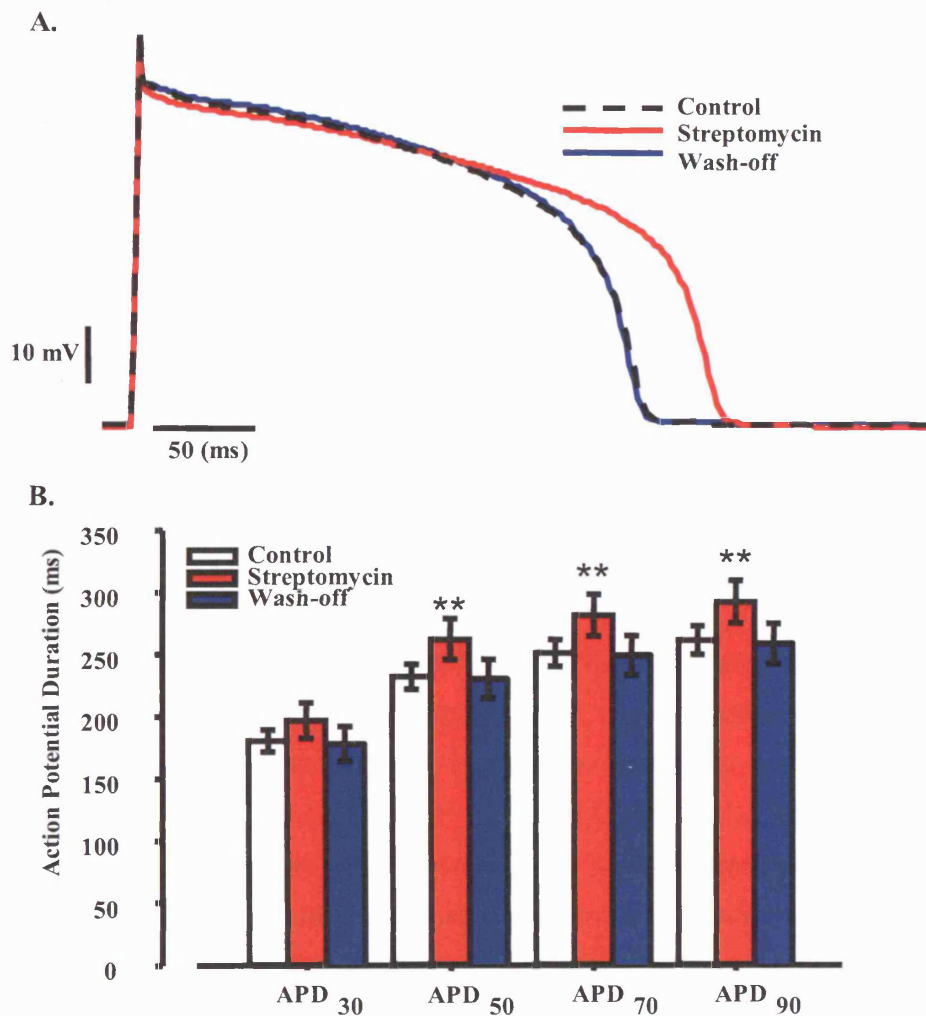


Figure 3.14. The effects of Pen-Strep solution upon the action potential morphology of guinea pig ventricular myocytes.

(A) Averages of 10 APs from a single myocyte demonstrating the increase in APD from control (dashed) in the presence of Pen-Strep (red) and after wash-off (blue). (B) Bar chart showing the increases in APD at 30, 50, 70 and 90 % repolarisation following addition of Pen-Strep (red) and wash-off (blue). Data are presented as mean \pm SEM ** represents statistical significance $p < 0.01$ versus control, paired t-test, $n = 7$.

3.1.5. Drug-induced changes in APD prolongation monitored with di-8-ANEPPS and a patch electrode.

Use of dSEVC whilst simultaneously recording ratio emission from either di-8-ANEPPS or di-4-ANEPPS demonstrated the linear relationship between the fluorescent properties of both dyes and membrane potential. Di-8-ANEPPS demonstrated a number of advantages over di-4-ANEPPS, including a larger relative change in fluorescence with alterations in membrane potential, less wash-off or bleaching and lesser phototoxic effects. Di-8-ANEPPS also allowed for recordings to be performed from isolated myocytes for 30 simultaneous APs in every 3 minutes, which allowed for a maximum of 30 APs to be averaged for different doses of test compound. In comparison, di-4-ANEPPS would have only allowed for a maximum average of 5 consecutive APs. Therefore di-8-ANEPPS was selected to monitor drug-induced changes in APD.

As yet drug-induced alterations in APD had not yet been assessed using either dye. Therefore experiments were performed using a compound upon which effects upon APD were already well documented. Cisapride has previously been shown to have arrhythmic properties and can cause Torsade de Pointes (TdP) (Ahmad & Wolfe, 1995). Additionally, the effects of cisapride have been demonstrated in isolated guinea pig myocytes on individual ion currents; in guinea pig myocytes cisapride is known to block both I_{Kr} and I_{Ks} with IC_{50} values of 15 nM and $> 10 \mu\text{M}$, respectively (Drolet *et al.*, 1998), as well as to cause inhibition of I_{CaL} with an IC_{50} of $46.9 \mu\text{M}$ (Chiang *et al.*, 2004).

Cisapride-induced alterations in APD were recorded at concentrations of 1, 3, 10, 30, 300 nM and $1 \mu\text{M}$. Fluorescent recordings were made from isolated guinea pig myocytes that had been loaded with $5 \mu\text{M}$ di-8-ANEPPS for 20 min at room temperature. Cells were stimulated at 1 Hz and exposed to excitation light for 30 s in every 3 minutes, at which point optical recordings were made. Averages of 20 APs were used for analysis. Because drug-induced alterations in APD have not previously been demonstrated using optical techniques in isolated myocytes, patch electrode recordings were also made from cells that had not been loaded with dye to provide a standard for comparison and to validate optical measurements.

Additional measurements were made using a patch electrode from cells that had been loaded with di-8-ANEPPS at concentrations of cisapride of 30 and 300 nM, as well as during wash-off. In this way it was possible to record APs with a patch electrode whilst simultaneously recording APs using fluorescence emitted from di-8-ANEPPS.

Figure 3.15 compares action potential morphology and durations from the maximum depolarization to repolarization values of 40; 50; 70; and 90%. As can be seen in traces A and B, as well as in the graphs C, it is possible to detect alterations in AP morphology using either

the fluorescent ratio emission produced by di-8-ANEPPS, or by using a patch electrode. Half-log increases in cisapride concentration induced a prolongation of APD which was maximal at 300 nM. Recordings made optically from 10 cells demonstrated an absolute increase in APD₉₀ from the control value of 355 ± 11 ms, to 382 ± 11 ms in the presence of 300 nM cisapride ($p < 0.01$, paired Student's t test, $n = 10$), whilst recordings made electrically from 10 cells increased the APD₉₀ values from 301 ± 14 ms to 334 ± 17 ms ($p < 0.001$, paired Student's t test, $n = 10$). Conversely, at concentrations of cisapride above 300 nM a reduction in APD values was detected in both assays. APD₉₀ values recorded in the presence of 1 μ M cisapride produced values similar to control values when recorded optically or electrically, 369 ± 11 ms and 300 ± 14 ms. APDs calculated at repolarisation values closer to the plateau phase of APs recorded with a patch electrode demonstrated a decrease in duration from control values in the presence of 1 μ M cisapride, which were not detected in recordings made using di-8-ANEPPS. APD₄₀ values recorded electrically were 242 ± 11 ms which decreased to 205 ± 10 ms in 1 μ M cisapride, whilst values recorded optically at the same concentrations were 290 ± 9 ms and 291 ± 6 ms, respectively.

In addition to the alterations in morphology of cardiac APs in response to increasing concentrations of cisapride, differences were also detected in APD between the two different recording methods. The graphs in Figure 3.15C, which are on the same scale, show APD values recorded with either a patch electrode or using di-8-ANEPPS throughout the cisapride dose response measurements. These clearly show that optical recordings display an increased basal duration at all the parameters measured. The longer basal APD recorded optically is proven to be a result of optical recording methods by data obtained from APs recorded simultaneously with di-8-ANEPPS and a patch electrode. During simultaneous measurements, APD₉₀ values recorded under control conditions were 360 ± 18 ms when recorded with a patch electrode and 360 ± 17 ms when recorded optically. These data are comparable to APD₉₀ values obtained previously in optical recordings (355 ± 11 ms) and are statistically different to control values obtained with a patch electrode (301 ± 14 ms, $p < 0.05$, unpaired Student's t-test). These data are also displayed in Figure 3.18 and described in more detail later.

Figure 3.16 compares the percentage change in APD of optical recordings with di-8-ANEPPS against those made with a patch electrode. Comparing the difference between absolute APD₉₀ values recorded at the lowest concentration of 1 nM, versus those recorded at 300 nM cisapride (mean increases of 22 ms and 43 ms for optical and electrical assays, respectively) demonstrates a larger response to cisapride in recordings made with a patch electrode. This is possibly as a consequence of the increased basal duration observed in optically recorded APs. Similarly, values obtained for the APD₅₀ and APD₇₀ also displayed a

smaller increase in duration when measured optically, while APD₄₀ values did not lengthen using either recording method. However, despite these differences, both assays provided similar values for an IC₅₀ apparent (displayed in Table 3.2). These were obtained by plotting a Hill curve to the data excluding the final concentration of 1 μ M (at which point the APDs had begun to decrease). This was despite the requirement for constraining the minimum of the curve-fit to 0% for optical data recorded at the parameters APD₅₀ and APD₇₀, which may have resulted in an overestimate of the concentration of the IC₅₀ apparent.

Superimposing averaged APs recorded with a patch electrode onto the averages of simultaneously recorded optical traces shows that, aside from the stimulus artefact present on the electrical recordings, the waveforms display an exact match (see Figure 3.17). However, as is illustrated in the bar chart in Figure 3.18C,D, despite the similarity between these waveforms, differences are apparent in the durations when measured at values of repolarization during which the voltage gradient is still relatively shallow: APD₄₀ and APD₅₀. For example, values of APD₄₀ detected from patch electrode recordings were 284 ± 14 ms compared to 300 ± 15 ms when recorded optically in normal Tyrode ($p < 0.001$, paired Student's *t* test, $n = 10$). This shows an overestimation of the APD₄₀ when utilising the optical data. Despite this, alterations in APD in response to 30 and 300 nM cisapride could still be detected optically, demonstrating maximal mean increases of 33 ms and 59 ms for APD₄₀ and APD₅₀ parameters, respectively. Measurements taken at APD₇₀ and APD₉₀ recorded similar durations using either set of data, similarly showing mean maximal increases in duration at 300 nM cisapride of 90 ms (electrical) and 94 ms (optical).

Figure 3.19 shows an average of 20 APs recorded from the same myocyte with both recording techniques; the optical trace has been scaled to fit the patch electrode recording. In addition, the magnitude of the overshoot and 40% repolarisation, as measured by the respective analysis of the corresponding traces is also shown. The value of overshoot, at 0% repolarization, is underestimated in the optical trace, when compared to the value obtained by the patch electrode AP. This has a consequence that the calculated value of APD₄₀ is at a more negative membrane potential when compared to the electrical recording and is therefore at an increased duration. In this example the measurement of APD₄₀ from the optical data is 61 ms longer than that obtained from the patch electrode recording. This demonstrates that the differences in values of APD₄₀ and APD₅₀ may arise from differences in analysis. Although this artefact is detectable at values of repolarisation of 40 and 50%, it does not have a significant effect upon the durations measured at APD₇₀ and APD₉₀. This is probably because, whilst the APD₄₀ and APD₅₀ are measured during the plateau phase of the AP, the gradient of the AP is comparatively shallow, whereas, as the membrane potential approaches the RMP,

the gradient becomes much steeper. Thus, whilst during the plateau small differences in estimates of membrane potential can separate values by a large number of milliseconds, during the steep repolarisation phase, similar differences in estimates are not separated by the same temporal distance.

Fortuitously, a single cell for which the APD was being monitored simultaneously with a patch electrode and optically with di-8-ANEPPS, underwent an early afterdepolarisation (EAD). This is displayed in Figure 3.20 thus demonstrating that the optical assay is sensitive enough to detect EADs, provided they occur during periods of exposure to excitation light.

Previously, it has been demonstrated in myocytes isolated from the ventricles of dogs with chronic atrioventricular block (which made them more susceptible to arrhythmia), that I_{Kr} block can result in an increased beat-to-beat variability in APD (Thomsen et al., 2004). By plotting the value of APD from a single AP against the value of APD from the previous AP (a Poincaré plot), it is possible to visualise this. Figure 3.21 shows that it is possible to demonstrate this in an isolated guinea pig ventricular myocyte in response to 300 nM cisapride. However, because optical recordings necessitate the use of averaging a number of APs, it is not possible to accurately determine beat-to-beat variability using those techniques.

Interestingly, when the values obtained from the simultaneous optical and electrical recordings are compared to the values obtained in the cisapride dose-responses using each recording method separately, additional differences are apparent. During simultaneous measurements the increase in APD_{90} from control measurements recorded in response to 300 nM cisapride was significantly larger when measured simultaneously (means between 90 and 94 ms, depending upon the recording method), than when measured using either method independently (between 27 and 33 ms). An increased number of doses at lower concentrations (1, 3 10 and 100 nM) were used during the experiments performed independently than during simultaneous measurements (30 and 300 nM). This may suggest that exposure to lower concentrations of cisapride provided myocytes resistance to the APD prolonging effects of further increases in concentration.

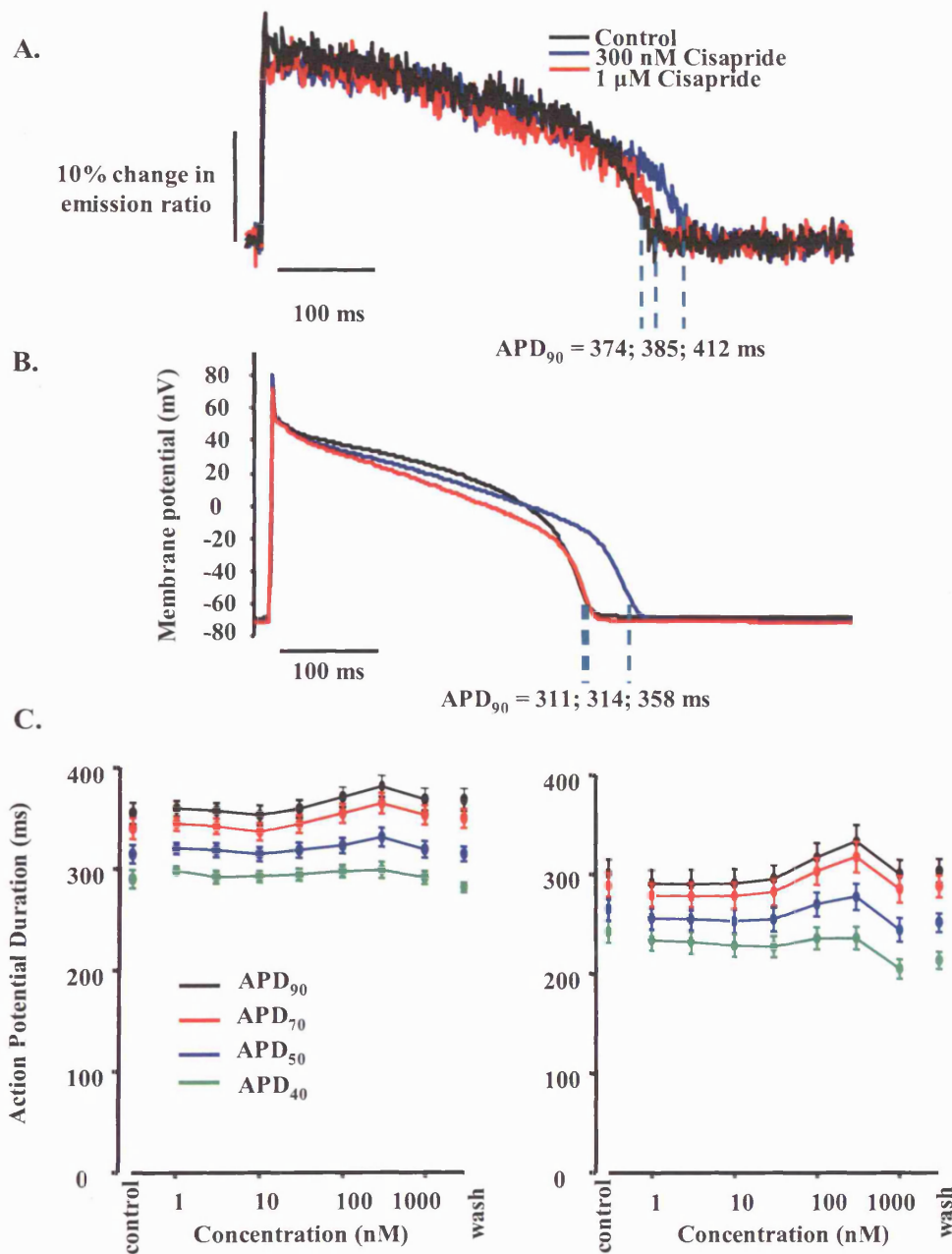


Figure 3.15. Changes in cardiac action potential duration recorded using a patch electrode or optically with di-8-ANEPPS.

Example traces of averages of 20 action potentials recorded at steady-state from isolated guinea pig ventricular myocytes using emitted fluorescence from di-8-ANEPPS (A) or using a patch electrode (B). Traces show control action potentials and action potentials recorded in the presence of 300 nM and 1 μM cisapride. C. Graphs showing 40; 50; 70; and 90% repolarisation times recorded using di-8-ANEPPS (left) or with a patch electrode (right) for myocytes for control values, increasing concentrations of cisapride and the following wash-off. Data are presented as mean ± SEM, n=10.

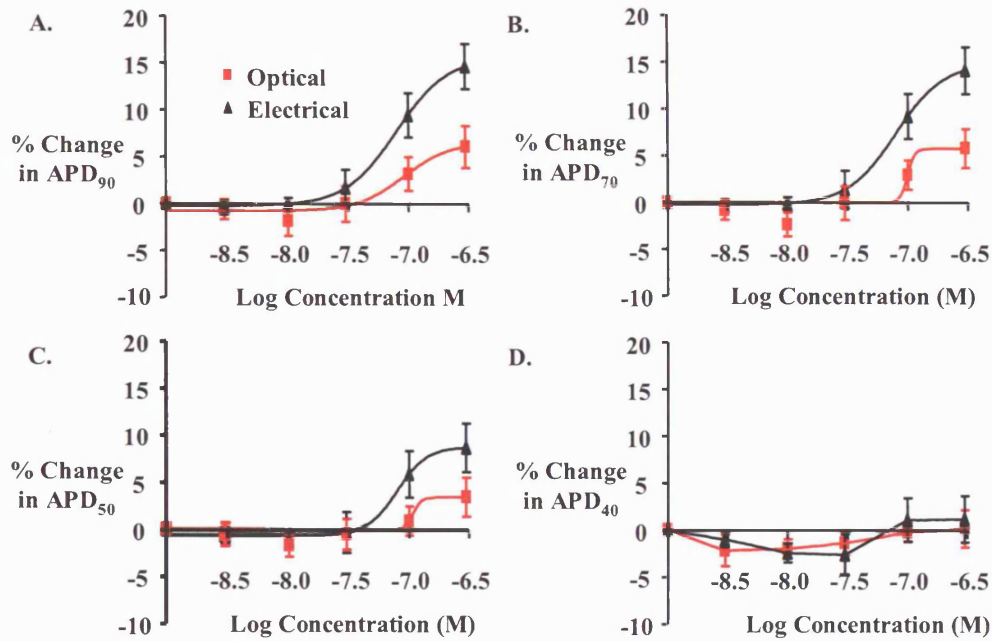


Figure 3.16. Relative changes in action potential durations as measured by using different values of repolarisation.

Graphs displaying the changes in action potential duration in response to increasing concentrations of cisapride in isolated guinea pig ventricular myocytes when measured at 90 (A); 70 (B); 50 (C); and 40% (D) repolarisation. Data are presented as mean \pm SEM, $n = 10$.

Parameter	Optical IC_{50} apparent (with di-8-ANEPPS)	Electrical IC_{50} apparent (with a patch electrode)
APD ₅₀	95.2 nM	79.7 nM
APD ₇₀	99.8 nM	79.2 nM
APD ₉₀	92.4 nM	80.5 nM

Table 3.2. Comparing the IC_{50} apparent values as measured using di-8-ANEPPS or a patch electrode in response to changes in action potential duration caused by cisapride.

Table displaying the IC_{50} apparent values obtained from Hill curve-fits to changes in action potential duration in response to increasing concentrations of cisapride when measured at 90; 70; and 50% repolarisation. It was not possible to obtain a curve fit for either electrical or optical data for the duration measured at 40% repolarization. In order to obtain a curve-fit, the parameters at APD₅₀ and APD₇₀ were constrained to a minimum value of 0% for optical recordings.

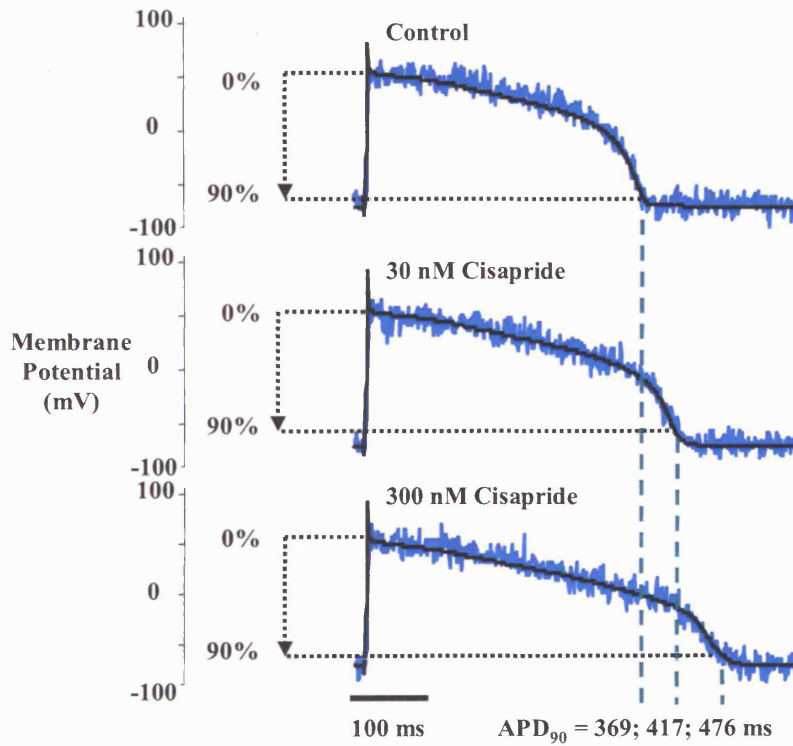


Figure 3.17. Measurements of action potential durations recorded simultaneously with di-8-ANEPPS and a patch electrode.

Averages of 20 action potentials recorded from a single guinea pig ventricular myocyte simultaneously with a patch electrode (dashed) and with the emitted fluorescence ratio of di-8-ANEPPS (blue). The different traces were recorded in the presence of either normal Tyrode alone, or containing 30 nM or 300 nM cisapride.

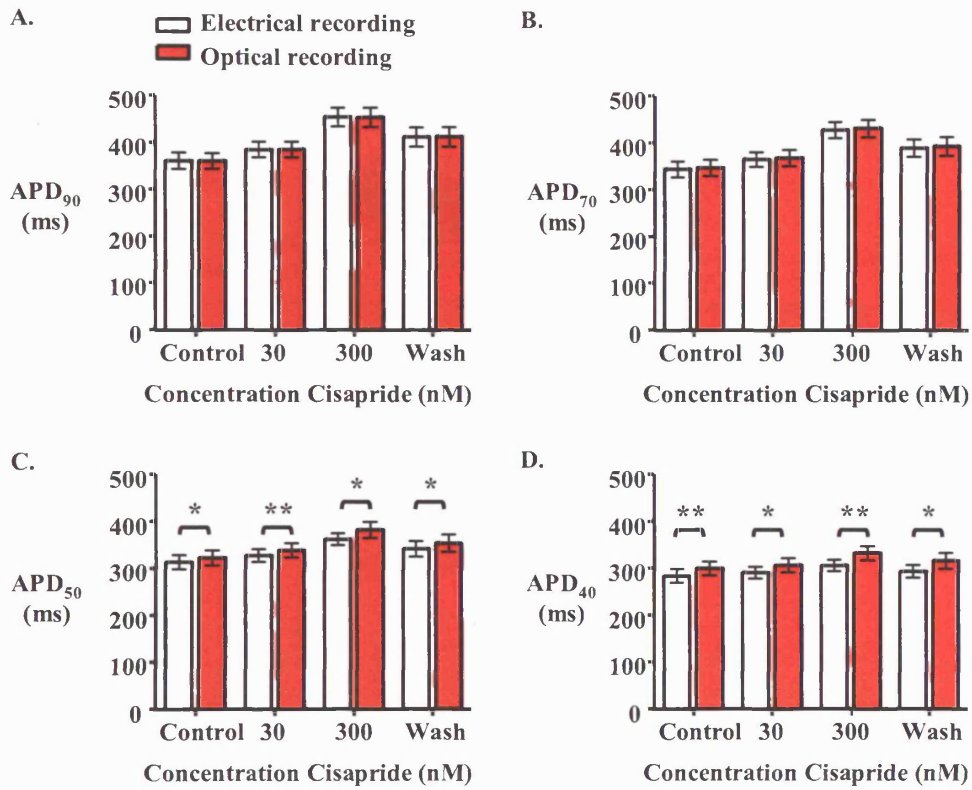


Figure 3.18. Comparing measurements of action potential durations recorded simultaneously with di-8-ANEPPS and a patch electrode.

Bar charts displaying the changes in action potential duration recorded from optical traces and patch electrode traces recorded simultaneously in response to increasing concentrations of cisapride in isolated guinea pig ventricular myocytes when measured at 90 (A); 70 (B); 50 (C); and 40% (D) repolarisation. ($p < 0.05$ indicated by *, $p < 0.01$ indicated by ** from a two-tailed, paired Student's t-test, $n = 10$).

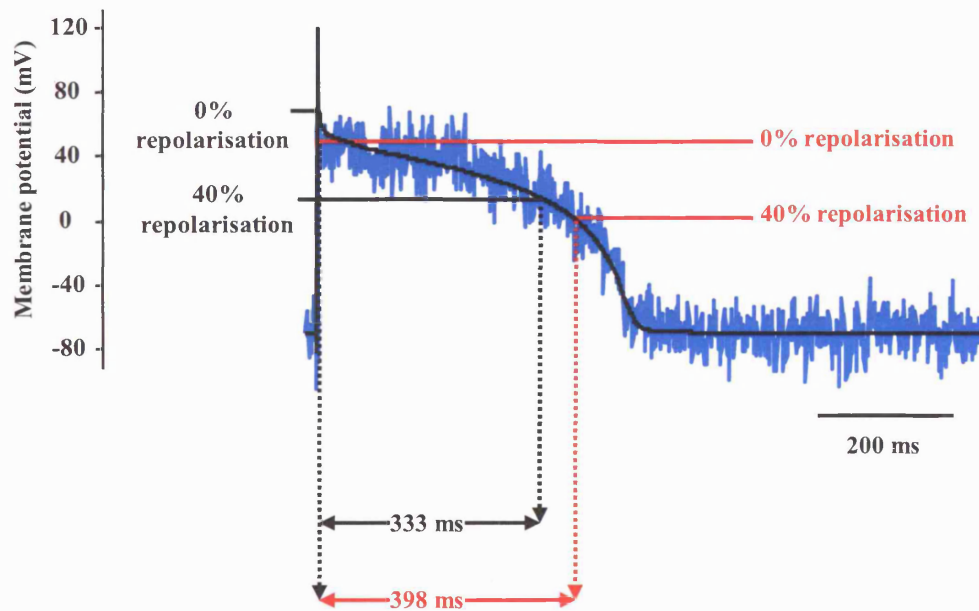


Figure 3.19. Measurements of action potential durations at 40% repolarisation recorded simultaneously with di-8-ANEPPS and a patch electrode.

An average of 20 action potentials recorded from a single guinea pig ventricular myocyte simultaneously with a patch electrode (black) and with the emitted fluorescence ratio of di-8-ANEPPS (blue). Illustrated are the values recorded at 0% and 40% repolarisation as determined from the electrical (black) and optical (red) traces and the time difference between them.

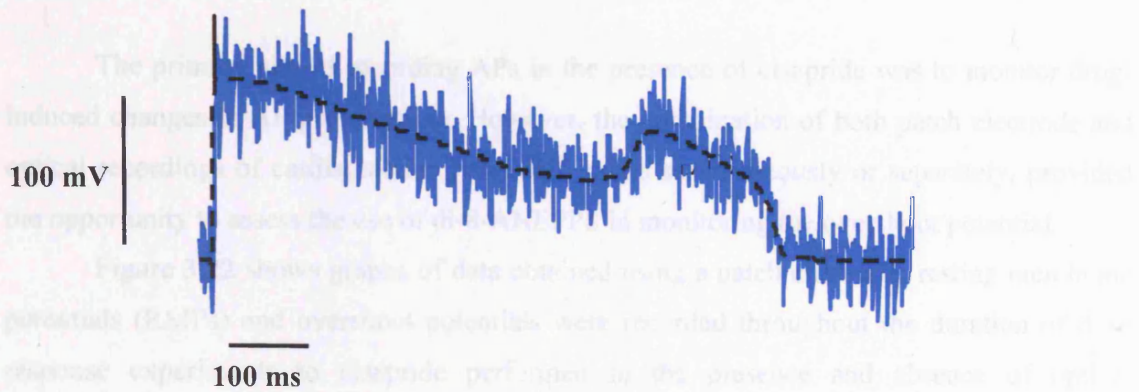


Figure 3.20. An early afterdepolarisation.

A single action potential recorded simultaneously with a patch electrode and with fluorescence emission from an isolated guinea pig ventricular myocyte loaded with di-8-ANEPPS during perfusion with 300 nM cisapride.

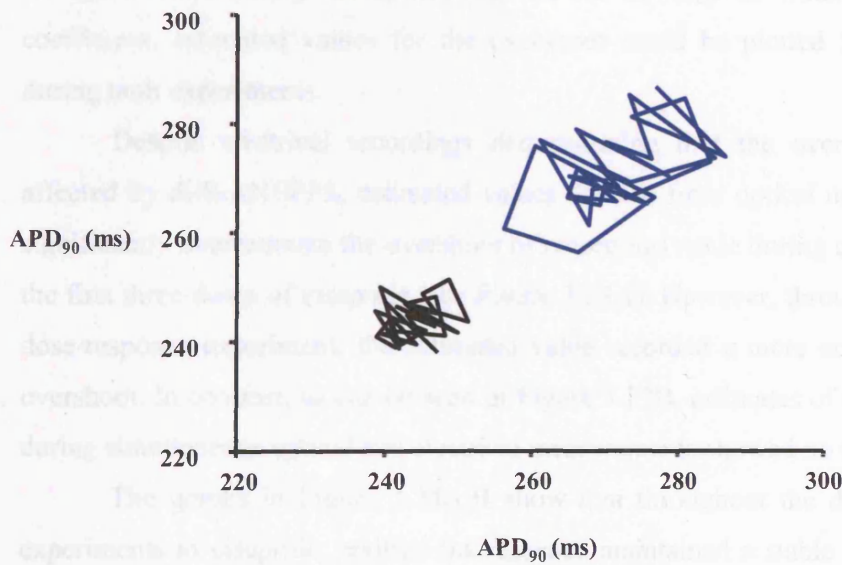


Figure 3.21. Beat-to-beat variability in isolated guinea pig ventricular myocytes.

Poincaré plot of action potentials stimulated at 1 Hz recorded with a patch electrode under control conditions (black) and in response to 300 nM cisapride (blue). Points were plotted as the 90% repolarization value (y-axis) against the 90% repolarization value of the previous action potential.

3.1.6. Can di-8-ANEPPS be used to monitor overshoot potential in isolated cardiac myocytes?

The primary aim of recording APs in the presence of cisapride was to monitor drug-induced changes in AP prolongation. However, the combination of both patch electrode and optical recordings of cardiac action potentials, made simultaneously or separately, provided the opportunity to assess the use of di-8-ANEPPS in monitoring the overshoot potential.

Figure 3.22 shows graphs of data obtained using a patch electrode: resting membrane potentials (RMPs) and overshoot potentials were recorded throughout the duration of dose response experiments to cisapride performed in the presence and absence of optical recordings with di-8-ANEPPS. During neither experiment were changes in overshoot potential or RMP (recorded with a patch electrode) observed in response to increases in cisapride concentration. Because the RMP did not change, this allowed for the assumption that a single value (the mean RMP calculated via a patch electrode from cells loaded with di-8-ANEPPS) could be used to normalise the values for RMP in optically recorded data. Thus, using the calibration coefficient calculated during simultaneous optical and dSEVC measurements (8.6% per 100 mV), and excluding cells that did not demonstrate a percentage change in ratio during the upstroke of the AP as large as would be expected using this coefficient, estimated values for the overshoot could be plotted for optical data obtained during both experiments.

Despite electrical recordings demonstrating that the overshoot potential was not affected by di-8-ANEPPS, estimated values derived from optical measurements appeared to significantly overestimate the overshoot of recordings made during control measurements and the first three doses of cisapride (see Figure 3.23A). However, throughout the duration of the dose-response experiment, the estimated value recorded a more accurate assessment of the overshoot. In contrast, as can be seen in Figure 3.23B, estimates of overshoot potential made during simultaneous optical and electrical measurements showed no significant differences.

The graphs in Figure 3.24A,B show that throughout the duration of dose-response experiments to cisapride, emitted fluorescence maintained a stable intensity at both 560 nm and 620 nm wavelengths. However, measurements of the maximum change in the fluorescent intensity at 560 nm, calculated during the upstroke of the AP, show a significant decrease throughout experiments made optically with di-8-ANEPPS, in the absence of a patch electrode. Thus, the inaccurate assessment of overshoot potentials during earlier measurements did not arise because of an effect of wash-off or bleaching of the dye, but rather a reduced response to changes in membrane potential.

A possible explanation for this result is that dye molecules flipped within the membrane, so that they were positioned on the inner leaflet of the phospholipid bilayer.

Molecules in this position would produce the opposite fluorescent change to those in the outer leaflet of the membrane, thus the perceived result may be a decrease in the change in fluorescent signal. Other important considerations include the use of the calibration coefficient. This was obtained following the exclusion of cells which exhibited a fluorescent change with voltage that was small relative to other cells. This provided exclusion criteria for monitoring the overshoot. However, cells were only excluded if they did not demonstrate a large enough change in fluorescence ratio, whilst there was no cut-off for cells which displayed an abnormally large fluorescence change.

Incidentally, changes in fluorescence during the upstroke that were detected during the last 4 doses to cisapride in optical measurements were similar to those detected during simultaneous measurements. Similarly, these values produced the most accurate estimation of overshoot potential. During measurements of calibration and simultaneous APs, cells were superfused in the tissue bath whilst the whole-cell configuration was obtained. It seems feasible that the delay in measurements of fluorescent recordings in these experiments is the reason that optical estimates of overshoot potential during simultaneous measurements were more accurate. In experiments monitoring APs optically with field stimulation, a minimum of 10 min was required before values of overshoot were not statistically different from those obtained separately with a patch electrode.

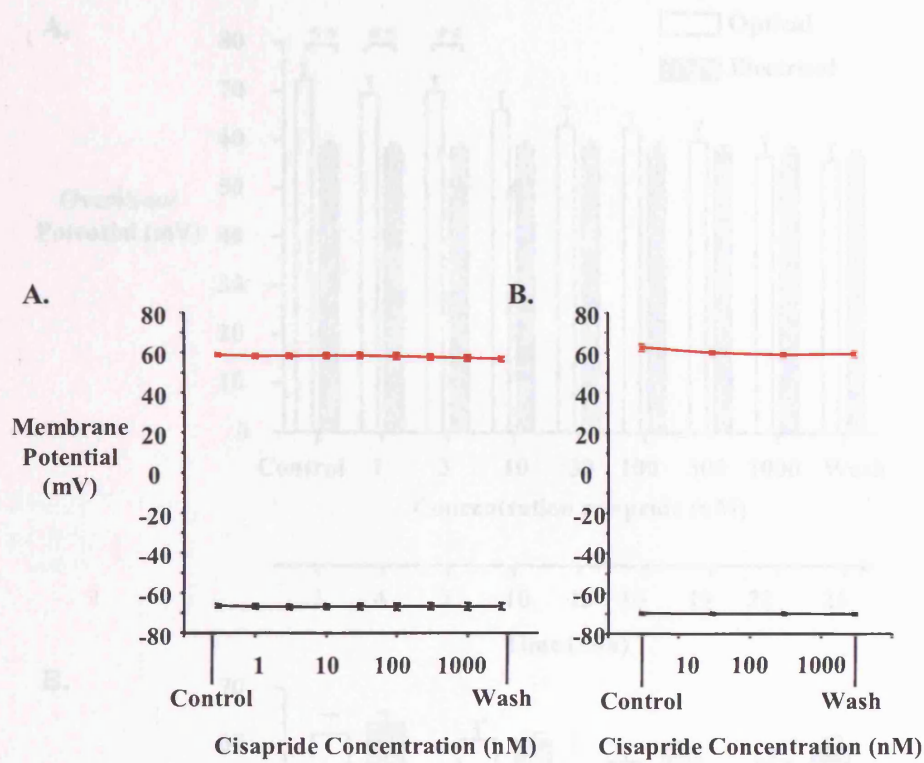


Figure 3.22. Values of the resting membrane potential and overshoot measured with a patch electrode.

Graphs displaying the resting membrane potential, recorded from the last 200 ms of averages of 20 records, and overshoot for action potentials recorded from guinea pig ventricular myocytes with a patch electrode. The data are displayed from recordings performed independently (A) or simultaneously with di-8-ANEPPS (B) during perfusion with different concentrations of cisapride. Data are expressed as means \pm SEM, $n = 10$ in both graphs.

Figure 3.23. Estimates of overshoot values for using di-8-ANEPPS compared to patch electrode values.

Bar charts displaying the overshoot for action potentials, measured with a patch electrode (black) and guinea pig ventricular myocytes with di-8-ANEPPS (grey) and compared with a patch electrode. Data displayed from experiments during a dose-response experiment to determine effects of cisapride from optical experiments and patch electrode experimental performed separately (A) or simultaneously (B). Data values are means from 10 cells (n=10) and 7 cells (n=7) respectively from averages of 20 action potentials recorded during the 30s prior to the wash value in each of the charts. ($p < 0.01$ indicated by ** from a two-tailed paired Student's t test)

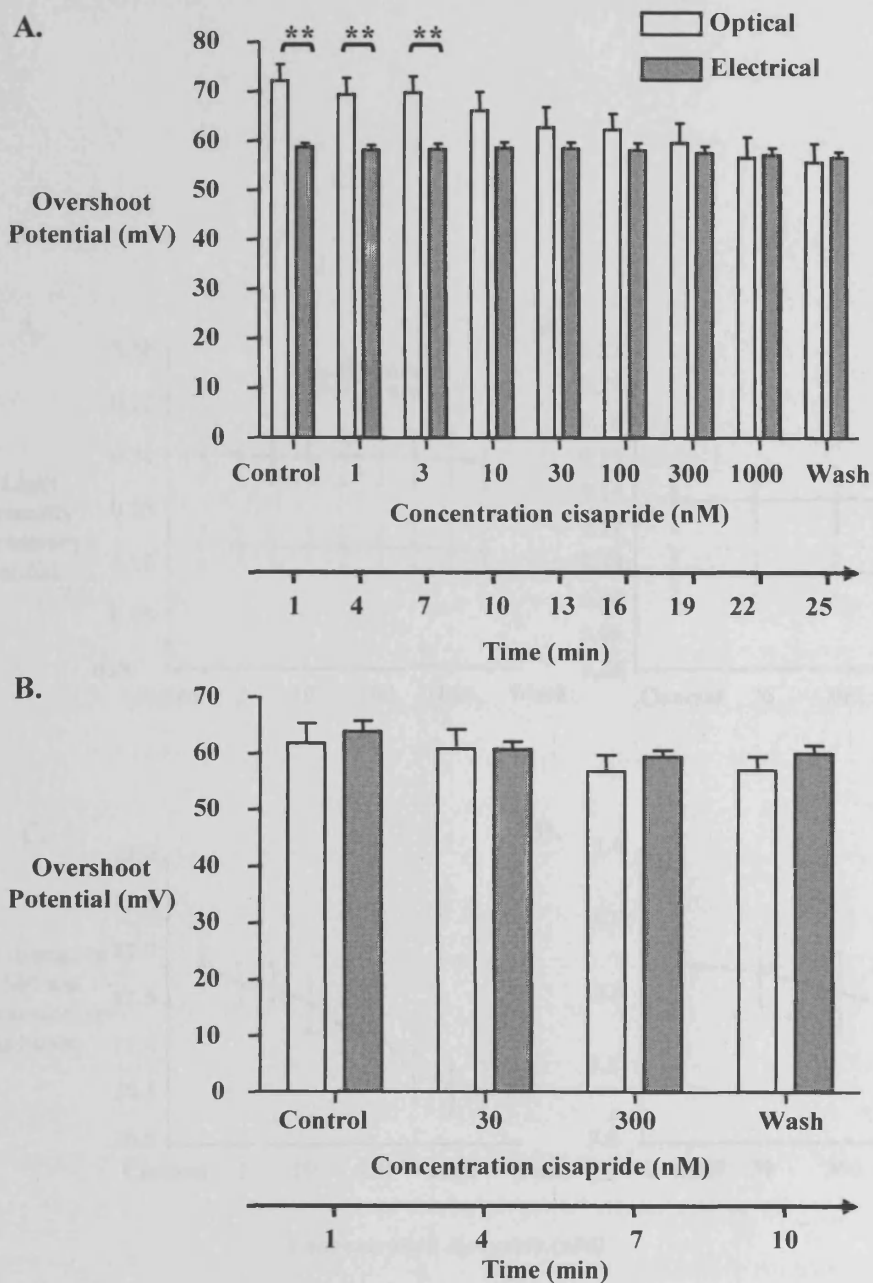


Figure 3.23. Estimates of overshoot potentials using di-8-ANEPPS compared to patch electrode values.

Bar charts displaying the overshoot for action potentials estimated with a calibration coefficient from guinea pig ventricular myocytes with di-8-ANEPPS (grey) and recorded with a patch electrode (clear). Data displayed from experiments during a dose-response experiment to increasing concentrations of cisapride from optical experiments and patch electrode experiment performed separately (A) and simultaneously (B). Data values are means from 10 cells in (A) and 7 cells in (B) of the overshoot from averages of 20 action potentials recorded during the 30s prior to the time value displayed beneath the chart. ($p < 0.01$ indicated by ** from a two-tailed, paired Student's t-test).

3.2. Discussion I: Recording cardiac action potentials

3.2.1. Underlying physiology for species differences in ventricular action potential morphology

Figure 3.13 shows a control trace and traces after application of cisapride to the APs. These differences arise from

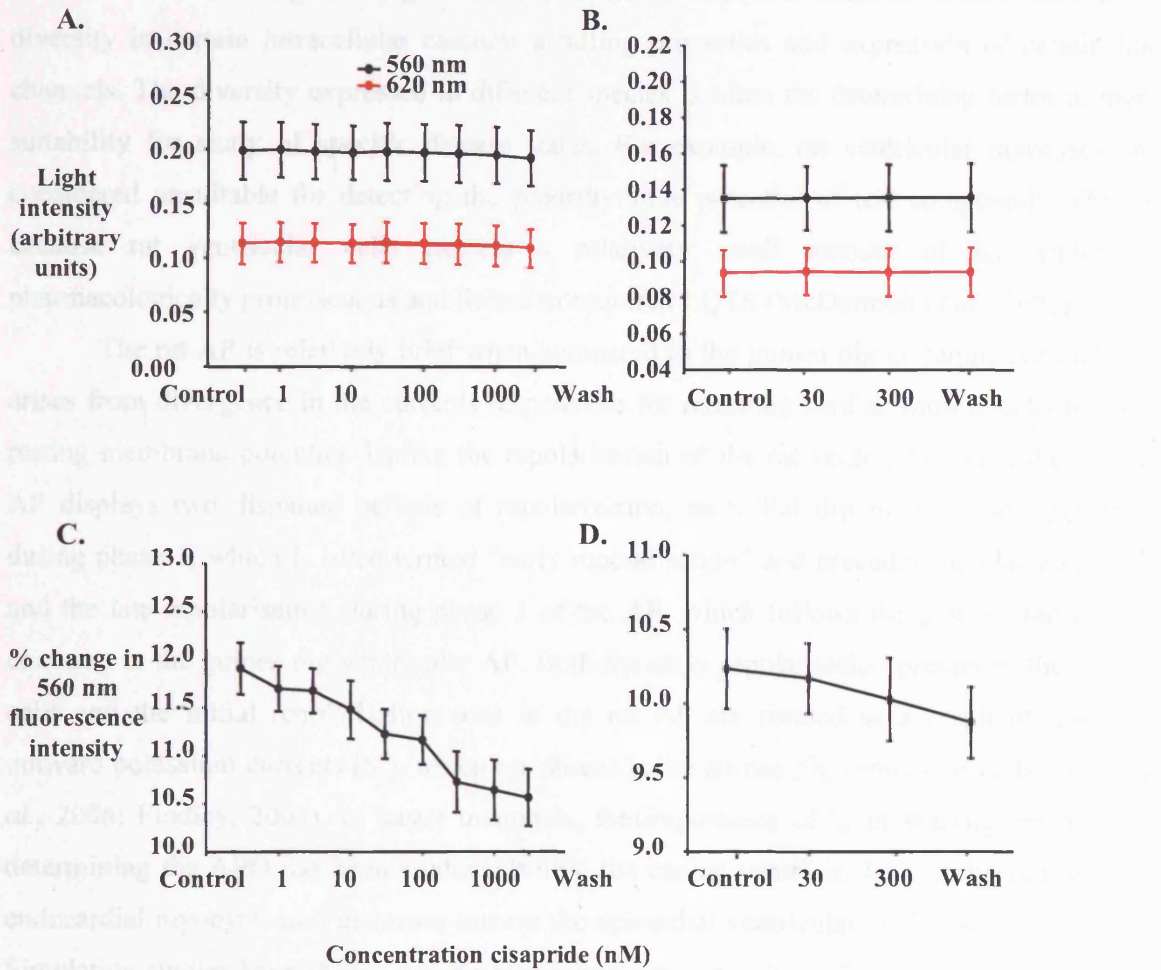


Figure 3.24. The baseline levels and peak change in fluorescence emitted by di-8-ANEPPS during a dose response to cisapride.

Graphs displaying the fluorescence levels during diastole of the fluorescence emitted at 560 nm (black) and 620 nm (red) during dose responses to cisapride measured using bath electrodes as the stimulus (A) and a patch pipette (B). (C) Graph showing the change in fluorescence emitted at 560 nm during the upstroke action potentials analysed in (A) (n = 10). (D) Graph showing the change in fluorescence emitted at 560 nm during the upstroke action potentials analysed in (B) (n = 7). Data are expressed as means ± SEM.

3.2. Discussion I: Recording cardiac action potentials.

3.2.1. Underlying physiology for species differences in ventricular action potential morphology.

Figure 3.13 shows a number of characteristic differences between action potentials recorded from rodent; guinea pig or rat, and canine cardiac APs. These differences arise from diversity in certain intracellular calcium handling properties and expression of certain ion channels. The diversity expressed in different species is often the determining factor in their suitability for study of specific disease states. For example, rat ventricular myocytes are considered unsuitable for detecting the proarrhythmic potential of test compounds. This is because rat ventricular cells express a relatively small amount of I_{Kr} , which is pharmacologically promiscuous and linked to acquired LQTS (McDermott *et al.*, 2002).

The rat AP is relatively brief when compared to the guinea pig or canine AP and this arises from divergence in the currents responsible for returning cardiac muscle cells to their resting membrane potential. Unlike the repolarisation of the rat ventricular cells, the canine AP displays two disparate periods of repolarization; an initial dip in membrane potential during phase 1, which is often termed “early repolarisation” and precedes the plateau phase, and the late repolarisation during phase 3 of the AP, which follows the plateau and is also common to the guinea pig ventricular AP. Both the early repolarisation present in the canine cells and the initial repolarisation seen in the rat AP are formed as a result of transient outward potassium currents (I_{to}), which are absent in the guinea pig ventricular cells (Dong *et al.*, 2006; Findlay, 2003). In larger mammals, the importance of I_{to} in shaping the AP and determining the APD has been studied. Within the canine ventricle, I_{to} is expressed least in endocardial myocytes and increases toward the epicardial ventricular wall (Liu *et al.*, 1993). Simulation studies have shown that the transmural heterogeneity of I_{to} causes the presence of the J wave, a positive deflection that is sometimes visible immediately following the QRS complex on an ECG (Gima & Rudy, 2002). The diversity of I_{to} current expressed within the canine ventricle wall does not result in any significant alteration to the APD (Sun & Wang, 2005) and is, therefore, more likely to affect mechanical characteristics upon myocyte contraction, via secondary effects upon I_{CaL} and sarcoplasmic reticulum (SR) calcium release. In contrast, I_{to} in the rat ventricle is relatively large and thus, instead of displaying a notch and dome morphology, once repolarisation during a rat AP has begun there is no further depolarisation until the next beat. Simulating I_{to} in guinea pig ventricular myocytes has demonstrated that there is a threshold (roughly 40 pA/pF) that separates two distinct consequences of the I_{to} current (Dong *et al.*, 2006). Below this, a visible spike and dome

morphology is present, with a decreasing prominence at lower levels of I_{to} . However, above this threshold, APs exhibit complete repolarisation and spike-like morphology. The mechanism responsible is probably due to the ensuing membrane potential at the end of the phase 1 notch occurring further from the activation potentials of calcium channels, thus suppressing the plateau.

At 37 °C it is estimated that the inward calcium flux contributes roughly 50% of the calcium accounting for the contraction of a guinea pig ventricular myocyte during an AP (Mackiewicz & Lewartowski, 2006). In contrast, because of the succinct plateau and relatively low amplitude of I_{Ca} in rat myocytes, the proportion of calcium released from intracellular stores is roughly 89% of the calcium transient, as determined by the contribution of reuptake by SERCA to relaxation. The plateau itself is retained as long as the inward currents, primarily consisting of calcium ion flux, remain equal to the outward currents, which are predominated by movement of potassium ions. Thus, a relatively small inward calcium current in the presence of larger outward currents results in the formation of a relatively brief AP in rat ventricular muscle. Therefore, in the rat ventricle, a larger proportion of the calcium contributing to contraction is released from intracellular organelles compared to the influx of calcium during the AP.

In each cell type, the plateau eventually terminates and returns to the resting membrane potential as a result of repolarising potassium currents: I_{Kr} , I_{Ks} and I_{K1} . Whilst it has been demonstrated that mRNA for ERG is present throughout the myocardium of all three of the species discussed here (Wymore *et al.*, 1997), I_{Kr} current within the rat ventricle is of comparably small amplitude. This may seem inconsistent with the results of certain studies demonstrating significant QT prolongation in rat electrocardiograms during exposure of known I_{Kr} blocking macrolides such as erythromycin (Ohtani *et al.*, 2000). However, the lack of efficacy in isolated rat myocytes of more specific inhibitors, such as E4031 and dofetilide, would indicate that these were not I_{Kr} specific effects (McDermott *et al.*, 2002). It is generally assumed that, at least for studies of LQT2 and acquired LQTS; use of rat ventricular tissue does not provide an adequate testing medium. Additionally, the Food and Drug Administration states that the use of adult rats and mice is not appropriate for nonclinical evaluation of cardiac repolarisation (U.S. Department of Health and Human Services, 2005). This is because of differing mechanisms of repolarisation from other species, for example, that I_{to} is the primary current controlling repolarisation in these species.

Although the species differences in AP morphology I have described here are supported in the literature, some of the values obtained may rely on differences in recording techniques. The recording techniques used for rat and guinea pig APs are identical and thus the APs of both of those species are directly comparable. However, the constituents of

external Tyrode used for experiments with canine mid-myocardial cells were different. Additionally, the use of a sharp electrode, as opposed to a patch electrode, will have prevented the dialysis of internal constituents of the cells which may have had a small effect upon AP configuration in rodent myocytes.

3.2.2. Changes in action potential morphology in response to different pacing frequencies.

Figure 3.12 shows alterations in APD for myocytes being paced at different frequencies. The effects of different stimulation rates arise from a number of factors. Firstly, pacing myocytes at increasing rates can affect the amount of time some ion channels have to recover from inactivation, thus at faster pacing rates certain families of channels will remain inactivated and pass less current. Secondly, increased pacing rates can result in increased concentrations of specific ions and molecules in regions close to the sarcolemma, for example in the microdomains between the SR and the L-type calcium channels (often referred to as the “fuzzy” space (Lederer *et al.*, 1990), or in microdomains outside the sarcolemma, contained within the tubular system. The modulation these ions and molecules exert upon ion channels and transporters is thus escalated and they can also affect the electrochemical driving force. Finally, there are frequency-dependent effects upon the intracellular stores of calcium, which also have effects upon the modulation of channels across the membrane.

The inward sodium current is responsible for the upstroke of a ventricular AP and calcium currents are responsible for the plateau phase. Cardiac I_{Na} consists of a TTX sensitive component, generally referred to as slow I_{Na} , and a TTX insensitive component, fast I_{Na} . Whilst channels that undergo fast inactivation recover very rapidly (within 10ms) during the hyperpolarisation between stimuli, prolonged depolarization can generate a slow inactivated state, from which the channel may take 100s of milliseconds to recover (Balsler, 2001; Cannon, 1996). Therefore, fast I_{Na} will only contribute to AP shortening in the event of an extrasystole. However, slow I_{Na} will not completely recover at faster pacing rates and this can result in a reduced persistent sodium current at quicker pacing rates with a subsequent shortening of the APD.

Ca^{2+} ions have an important and complex role in the function of cardiac muscle. It has been demonstrated that increased pacing can potentiate L type calcium currents in human myocytes as a result of a slowed inactivation process (Lemaire *et al.*, 1998). This is proposed to be due to time, calcium and voltage mediated effects, which boost reactivation of the L-type channels (Lederer *et al.*, 1990). For example, following a rest period, using a holding potential of -90 mV, voltage steps to 0 mV repeated every 2 min cause an increase in peak

current (Hryshko & Bers, 1990). However, similar experiments using a holding potential of -40 mV results in a progressive decline of peak current (Hryshko & Bers, 1990; Tseng, 1998). The increase in calcium current observed during repeated steps from -90 mV are calcium dependent and inhibited by 20 mM BAPTA. Thus, the effect can also be amplified by calcium release from the SR (Delgado *et al.*, 1999). However, the presence of an increased concentration of calcium within the fuzzy space may also serve to promote inactivation of these channels.

One of the net results of an increased influx of certain ions at faster pacing rates is the formation of ion concentration gradients within the cell. The characterization of the increases in calcium concentration in the subsarcolemmal region, referred to as the fuzzy space, has been firmly demonstrated, whilst the effects of increases in sodium current are, to a certain extent, still debated.

Observations that E-C coupling can still occur in the apparent absence of L-type calcium current only under conditions when I_{Na} is active (Leblanc & Hume, 1990) have led to the subsequent suggestion that this would require an increased concentration of sodium ions within the subsarcolemma. It was proposed that the effects of an increased sodium concentration in the fuzzy space would be to elicit a larger gross outward NCX current; thus allowing for an associated influx of calcium ions as sodium ions are expelled (Barry, 2006).

Heterogeneity of ion channels across the ventricular wall may influence alterations in response to changes in cardiac pacing. For example, a modelling study has demonstrated that, whilst maintaining the same density of I_{Kr} current, in cells with reduced I_{Ks} current, the APD is relatively long and displays a steep dependence on rate (Viswanathan *et al.*, 1999). This helps to explain why the APD of M cells (see section 1.3.2) may prolong disproportionately compared to other ventricular myocytes. Mechanistically, this is attributed to both an accumulation of I_{Ks} current at faster pacing rates, as well as increased NCX current arising from sodium accumulation. The same study also showed that decreases in I_{Kr} current density also caused an increased lengthening of the APD, although not to the same extent as decreases in I_{Ks} density. Differences in the dependence of APD upon pacing rate in different regions of the ventricular wall are important in circumstances when certain ion channels are dysfunctional, for example in acquired LQTS, when I_{Kr} is frequently inhibited.

The results I have shown reveal an initial increase in APD in isolated guinea pig myocytes for increases in pacing between 0.1 and 0.5 Hz, and a decrease at faster pacing rates than these, a variation that is supported by previous studies (Ravens & Wettwer, 1998). This would indicate that the physiological process detailed here have different implications at different pacing rates, i.e. mechanisms that contribute to prolongation of a guinea pig myocyte have more of an impact when increasing stimulation frequency between

0.1 and 0.5 Hz, but beyond those pacing rates, changes in factors that influence APD shortening predominate. The results I have displayed are also only applicable to the guinea pig myocyte (there are species dependent differences), which I studied because guinea pig myocytes were the cell type commonly used throughout this project.

3.2.3. The effects of antibiotic solutions upon cardiac AP morphology.

To prevent bacterial infection in myocytes isolated from rodent species in our laboratory a mixture of streptomycin and penicillin was used. Therefore, the effect of this mixture upon guinea pig AP morphology was assessed. Streptomycin sulphate has previously been reported to reduce calcium transients in rat cardiac muscle cells (Belus & White, 2001). This was considered attributable to a decreased inward calcium current because inhibition of I_{CaL} has been observed in other muscle types (Haws *et al.*, 1996; Miller & Langton, 1998). The report of the effects of streptomycin sulphate upon guinea pig isolated ventricular myocytes demonstrated inhibition of the L type calcium current and of both the delayed and rapid rectifier currents, reduced intracellular calcium transients and reduced contractility at a concentration of 2 mM, although these effects were not found at a concentration of 50 μ M (Belus & White, 2002). Furthermore, at a concentration of 2 mM, the increases in APD were significant at 20%, 50% and 90% repolarisation. In contrast, there is little published data available for the effects of penicillin upon APD in guinea pig myocytes, although in a rabbit heart Langendorff proarrhythmia model penicillin was not found to increase monophasic APDs (Hondeghe *et al.*, 2003).

Perfusion with normal Tyrode containing an antibiotic mixture (in which the concentration of streptomycin was 457 μ M) showed a significant increase in APD at 50, 70 and 90 % repolarization. Following wash-off the APD of isolated guinea pig myocytes returned to their control values. Thus the presence of the antibiotic solution did not confound the effects of compounds applied thereafter.

3.2.4. Optical recordings of action potentials from isolated myocytes.

Both di-4-ANEPPS (Windisch *et al.*, 1995) and di-8-ANEPPS (Sharma *et al.*, 2002; Sharma *et al.*, 2005) have been used to monitor membrane potential in isolated cardiac myocytes. In the instances described here, I have used the styryl dyes: di-8-ANEPPS and di-4-ANEPPS to study alterations in membrane potential, either as a result of physiological processes (an AP) or via voltage clamp. Furthermore, cisapride-induced alterations in APD were monitored using di-8-ANEPPS and compared to results obtained with a patch electrode.

By utilizing the calibration protocols described above, I have demonstrated the linear relationship of both the red and the green emitted signals for both dyes with changes over a physiological range in membrane potential of isolated cardiac myocytes. Additionally, in the present study, utilizing a single excitation wavelength of 488 nm and two distinct emission spectra from which the ratio is calculated, it was possible to obtain ratiometric recordings from isolated myocytes. In this way, artefacts that may arise from wash-off, photobleaching or contractile movements were removed from experiments, as well as reducing any noise which originated from the light source.

Reports of phototoxicity in isolated myocytes with di-4-ANEPPS have been shown using concentrations of dye at 30 μM and 60 μM and incubation periods of 10 min (Schaffer *et al.*, 1994). These were significantly larger concentrations of dye than I incorporated and attempts to increase the dye concentration to 20 μM did show toxic effects. However, the current study suggests that by limiting exposure to excitation to discrete periods of time and by obtaining a suitable trade-off between excitation light intensity and dye concentration (5 μM), it is possible to obtain stable measurements of APD over periods of time that allow for measurements of dose-response curves. However, monitoring overshoot potentials with di-8-ANEPPS over time periods up to 25 min demonstrated a reduction in peak fluorescence change. This may be a result of dye molecules flipping into the inner leaflet of the cell membrane, which could reduce the ratiometric fluorescent response.

3.2.5. Alterations in action potential duration in response to cisapride.

Previous work on different guinea pig cardiac electrophysiological parameters has demonstrated that, during patch clamp experiments on isolated myocytes, cisapride blocks I_{Kr} current with an IC_{50} value of 15 nM and I_{Ks} with an estimated IC_{50} of $> 10 \mu\text{M}$ (Drolet *et al.*, 1998). In the current study, the highest concentration of cisapride tested was 1 μM , less than

the IC_{50} for block of I_{Ks} ; therefore, the increase in APD observed at concentrations up to 300 nM is likely attributable to block of I_{Kr} .

However, cisapride has also been shown to inhibit channels other than repolarising potassium channels. In particular, Chiang *et al.*, (2004) showed that cisapride blocks L-type calcium channels in both a tonic and use-dependent manner. In addition to this, cisapride also delays the recovery from inactivation in these channels. Because the effect of calcium channels upon the membrane potential during an AP is to sustain the plateau, inhibition of these channels causes a reduction in APD, particularly at levels of repolarization that depict the plateau (APD_{40} and APD_{50}). This is further confirmed in the experiments reported here with a patch electrode (in the absence of di-8-ANEPPS), where at a concentration of 1 μ M a significant decrease in APD_{40} could be recognised. This was also emulated in optical recordings, although the effect was less pronounced.

In addition to voltage clamp recordings, both these studies also monitored guinea pig APDs: the study by Drolet *et al.*, (1998) used monophasic APDs to demonstrate an increase in APD_{90} during exposure to 100 nM cisapride; and the study by Chiang *et al.* (2004) recorded similar biphasic effects to those that were observed in the studies here, an increase in APD at lower concentrations of cisapride, coupled with a decrease at higher concentrations. Results from both optical recordings using di-8-ANEPPS and patch electrode recordings showed that increasing the concentration of cisapride up to 300 nM caused a prolongation of the AP in guinea pig ventricular myocytes, which was most prominent at APD values of repolarisation nearing the resting membrane potential.

Thus, based upon the previous observations of Drolet *et al.* (1998) and Chiang *et al.* (2004), the biphasic change in APD observed in response to cisapride using both optical and electrical recordings was to be expected. However, differences between the two recording methods also became apparent. Independent measurements of cardiac APs from isolated guinea pig ventricular myocytes demonstrated two things: firstly, the alterations in AP morphology in response to differing concentrations of cisapride, which demonstrated the characteristic biphasic changes in AP duration; and secondly, an increased basal APD in myocytes loaded with di-8-ANEPPS, which resulted in a decreased sensitivity to drug-induced APD changes. In particular, this reduced sensitivity was observed as a decrease in the relative prolongation recorded at repolarisation times between 50 and 90%, and a failure to detect AP shortening to below basal levels at higher concentrations of cisapride.

In contrast, simultaneous measurements allowed the opportunity to examine firstly, whether APs recorded optically with di-8-ANEPPS demonstrated a similar shape to those recorded with an electrode and secondly, what errors may then arise from analysing optical APs, which are relatively noisy and do not give a direct measurement of membrane potential.

By scaling the ratio values of optically recorded APs to electrical APs recorded simultaneously, it was clear that both recording methods gave similar representation of the AP. However, underestimates of the overshoot potential as a result of the increased noise inherent to the optical signal caused overestimates of APD parameters measured at 40 and 50% repolarization. This demonstrated an error that is an artefact of the analysis technique and not due to alterations in the ratio emission produced by the dye.

3.2.6. Application of optical dyes in the pharmaceutical industry.

The ability to accurately measure fast changes in membrane potential from a single cardiac myocyte using optical techniques provides a non-invasive method to study changes in cardiac AP configuration. Within the pharmaceutical industry this provides an easy method to monitor drug-induced AP prolongation, which is associated with LQTS (Redfern *et al.*, 2003). Importantly, the experiments demonstrated here show that recordings of AP morphology using the fast voltage sensitive dye, di-8-ANEPPS, demonstrate a similar morphology to electrically recorded APs and that it was possible to record drug-induced changes in APD. Additionally, the resemblance of electrical and optical measurements made simultaneously indicates that another proarrhythmic marker may also be identified, triangulation (Hondeghem *et al.*, 2001).

However, the use of a single cell excludes monitoring of certain arrhythmic aspects, including spiral wave formation, re-entry and transmural dispersion of repolarisation. Additionally, the nature of the dyes requires that measurements be made during discrete periods of time. Despite the ability of optical recordings to detect EADs, these cannot be guaranteed to occur during time periods when recordings are being made. The requirement for averaging a number of APs to obtain a large enough S/N ratio for analysis also limits the ability of an optical assay to detect beat-to-beat variability. Furthermore the current study shows that the ability to accurately monitor overshoot potential requires further evaluation.

The ability to monitor changes in AP duration, which was the primary aim of this project, has been demonstrated. However, this ability was limited in part by pharmacological effects of di-8-ANEPPS, which caused a significant increase in the basal duration of APs. Due to the manufacture of other styryl dyes and the promising results also obtained using di-4-ANEPPS, further studies were necessary to find a more appropriate dye for use in screening for proarrhythmic potential in test compounds.

Chapter 4:
**Testing the suitability of different “styryl” dyes for use with
cardiac myocytes.**

Chapter 4: Testing the suitability of different “styryl” dyes for use with cardiac myocytes.

In chapter 3, recordings of action potentials (APs) were obtained from isolated guinea pig myocytes stained with either di-4-ANEPPS or di-8-ANEPPS, from which action potential durations (APDs) were determined. However, comparisons demonstrated an increase in basal APD from myocytes stained with di-8-ANEPPS versus those recorded with a patch electrode in absence of dye. Furthermore, possibly as a result of the prolongation of basal APD, increases in APD in response to cisapride were reduced in recordings made using the fluorescence emission from di-8-ANEPPS, when compared to recordings made using a patch electrode.

Previously, it has been shown that a variety of chemicals which bind to the phospholipid membrane have effects upon ion channel currents. For example, in cardiac cells, the application of a number of antiarrhythmic ω -3 polyunsaturated fatty acids (n-3-PUFAs) produced a concentration dependent inhibition of the L-type calcium current (I_{CaL}) (Xiao *et al.*, 1997). In addition, n-3-PUFAs have been shown not only to inhibit the sodium current (I_{Na}), but also to shift the voltage-dependent inactivation of sodium channels to more hyperpolarised values (Xiao *et al.*, 1995). Furthermore, these effects may not arise from direct binding with the ion channels concerned. n-3-PUFAs do not bind to the same site as lidocaine, which has similar effects upon I_{Na} (Leaf *et al.*, 2003). Additionally, they also have effects upon a range of different cardiac currents; these include repolarising potassium currents, sodium currents and calcium currents, which all share considerable amino-acid homology, but also the ligand-gated cAMP-activated chloride current and ACh-activated potassium currents (Leaf & Xiao, 2001; Rodrigo *et al.*, 1999). Klausner *et al.*, (1980) showed that high concentrations of n-3-PUFAs could affect the “packing” of phospholipids in the bilayer; thus effecting the fluidity of the membrane. Similarly, Andersen and colleagues have postulated that the conformational state of an ion channel may be altered if the hydrophobic thickness of the membrane around it is altered. This hypothesis has been tested on the cation-permeable short gramicidin channel using the non-ionic detergents Triton X-100 and β -octyl glycoside. Interestingly, both these detergents also inhibit the cardiac sodium current and shift the inactivation potential to more hyperpolarised potentials (Leaf & Xiao, 2001; Leaf *et al.*, 2003).

It therefore seemed reasonable (because styryl dyes also bind to the cell membrane) that the APD prolonging effects of di-8-ANEPPS may also arise from alterations in the properties of cardiac ion channel currents. To determine whether or not a more suitable dye

for recording APDs from isolated myocytes could be identified, a series of experiments examining the effects of different fast voltage-sensitive dyes on APD and different cardiac ion currents were conducted.

Since the development of voltage-sensitive dyes, a number of different dyes have become available. Due to the success in detecting APD changes in response to cisapride using di-8-ANEPPS (refer to chapter 3), other dyes utilizing the styryl chromophore were selected for screening. Other ANEPPS dyes were selected to ascertain if there was a link between carbon chain length in the tail end of the molecule and the increase in APD. In addition, due to favourable use in recent literature (Obaid *et al.*, 2004), two ANEPPDHQ dyes were also selected, which retained the chromophore of ANEPPS but had an altered head group within their structure (see Figure 4.1).

In this chapter, the effects of certain styryl dyes upon the APD of paced isolated guinea pig myocytes are evaluated. I_{Kr} is known to be pharmacologically promiscuous, and inhibition of this current causes AP prolongation (Mitcheson *et al.*, 2000a). To assess this, hERG currents were monitored using the planar patch clamp array of Ionworks HT™. Additionally, the affinity of the different dyes for hERG protein was also assessed using a radioligand binding assay. Calcium regulation is of vital importance in the cardiac cell (Bers, 2001), and release of calcium from the intracellular stores is initiated by influx of calcium through ion channels. Furthermore, calcium currents are responsible for maintaining the plateau of the cardiac AP and alterations in the voltage dependence of inactivation or inhibition of this current can have effects upon the APD. Therefore, voltage-clamp experiments were also used to monitor the peak current, voltage dependent inactivation and recovery from inactivation of native I_{CaL} from canine M cells in response to the different dyes.

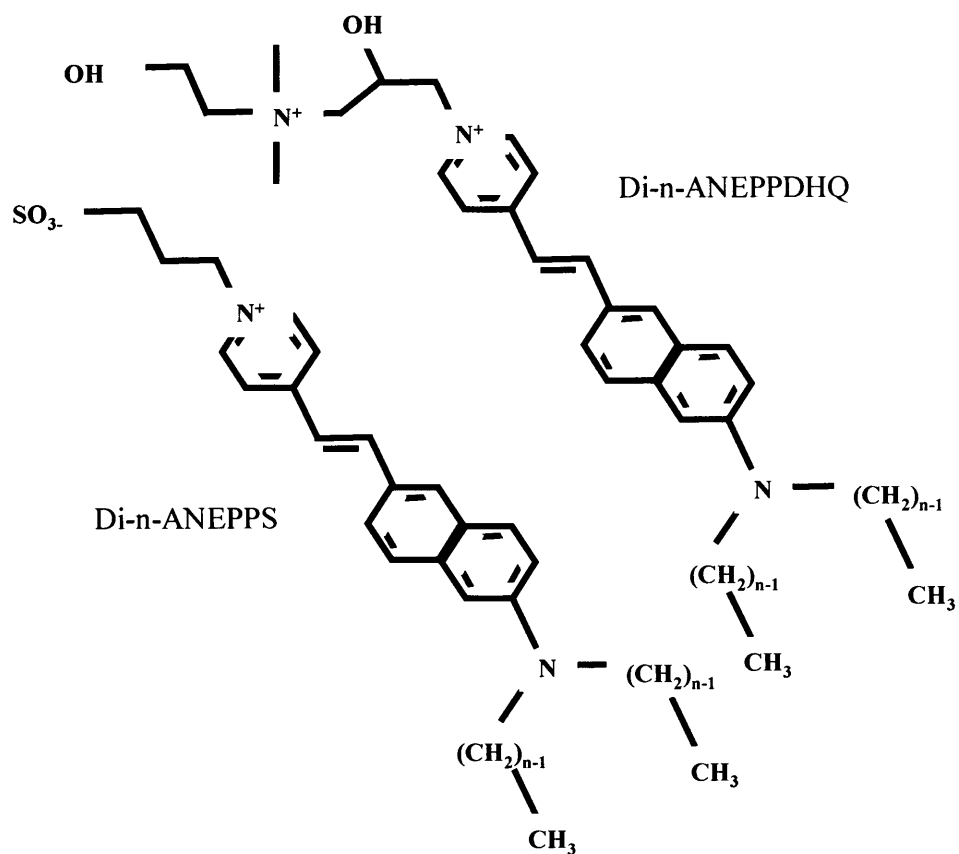


Figure 4.1. The chemical structures of ANEPPS and ANEPPDHQ fast voltage-sensitive dyes.

4.1.1. The effects of acute application of “styryl” dyes upon guinea pig cardiac action potential duration.

Increased APD in cardiac myocytes can result from phototoxicity (Schaffer *et al.*, 1994). Therefore, preliminary experiments were designed to assess the direct effects of different styryl dyes upon APD in the absence of excitation light. Isolated guinea pig myocytes were stimulated with a patch electrode at 1 Hz and the APD at 50% and 90% repolarisation was monitored during 5 min superfusion with normal Tyrode containing the loading concentration (5 μ M) of di-4-ANEPPS, di-8-ANEPPS or di-4-ANEPPDHQ. The traces shown in Figure 4.2 are averages of 10 traces made under control conditions and during perfusion with dyes. Di-4-ANEPPDHQ had the largest effect upon the APD of the three dyes tested; the APD₉₀ was reduced by $19 \pm 5\%$. Comparing APD₉₀ values recorded after 1 min of stimulation under control conditions versus values recorded after 5 min perfusion with di-4-ANEPPDHQ showed that the reduction in APD was significant ($p < 0.05$, paired Student's t-test, $n = 6$). Di-4-ANEPPS also caused a decrease in APD₉₀ of $7 \pm 5\%$, although this was not found to be significant. Conversely, di-8-ANEPPS caused an increase in APD₉₀ of $16 \pm 5\%$. Comparing APD₉₀ values recorded under control conditions and after 5 min perfusion with the dye showed that the increase in APD caused by di-8-ANEPPS was very significant ($p < 0.01$, paired Student's t-test, $n = 10$).

In addition to determining the effects of different styryl dyes upon cardiac APD, different vehicle solutions were also examined. The solute for di-8-ANEPPS was DMSO into which the detergent Pluronic F127 had been dissolved at a concentration of 5% by weight. Both di-4-ANEPPS and Di-4-ANEPPDHQ were dissolved in ethanol. Therefore, each of these vehicle solutions was diluted 1000-fold in normal Tyrode to obtain the equivalent concentration as to that present during incubation with dye. The graphs in Figure 4.3 show that neither of these carrier solutions had any effect upon the APD₅₀ or APD₉₀. Although there was a reduction in the average APD recorded through the experiments made upon cells acutely perfused with 0.1% ethanol, this was consistent throughout the experiment and was not altered by the presence of ethanol.

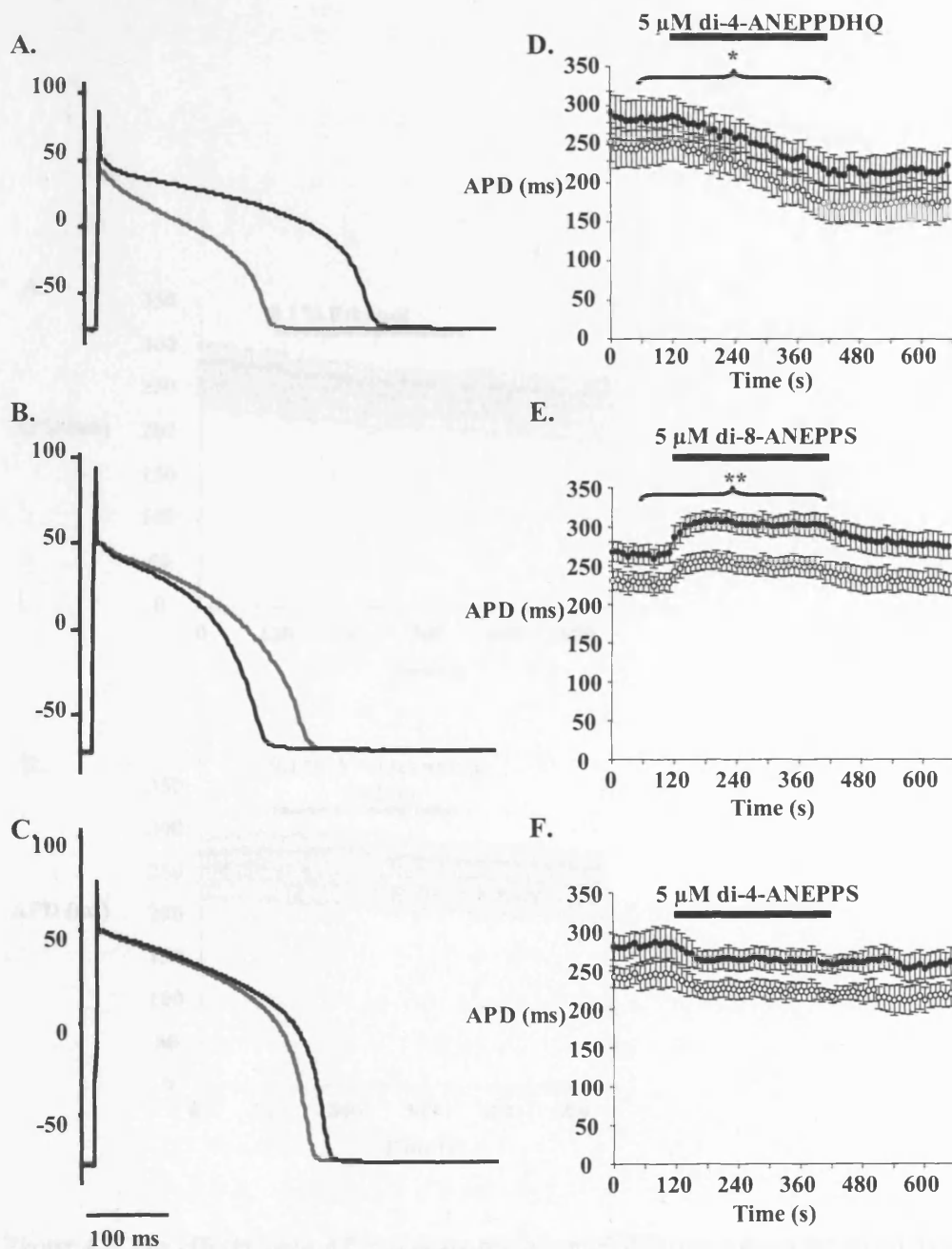


Figure 4.2. The effects upon APD of acute perfusion of different styryl dyes upon action potential duration.

Averages of 10 action potentials recorded from isolated guinea pig ventricular myocytes stimulated at 1 Hz under control conditions (black) and during perfusion with either: 5 μ M di-4-ANEPPDHQ (A), di-8-ANEPPS (B) or di-8-ANEPPS (C) (red). Graphs displaying the APD₅₀ (open circles) and APD₉₀ (closed circles) of isolated guinea pig ventricular myocytes perfused with either 5 μ M di-4-ANEPPDHQ (D), $n = 6$, di-8-ANEPPS (E), $n = 10$ or di-4-ANEPPS (F), $n = 6$. Comparison between data recorded after 60 s of stimulation and 300 s following the addition of dye showed a significant decrease in APD caused by 5 μ M di-4-ANEPPDHQ ($p < 0.05$, paired Student's-test) and a significant increase in APD caused by di-8-ANEPPS ($p < 0.01$, paired Student's-test). Data are expressed as means \pm SEM.

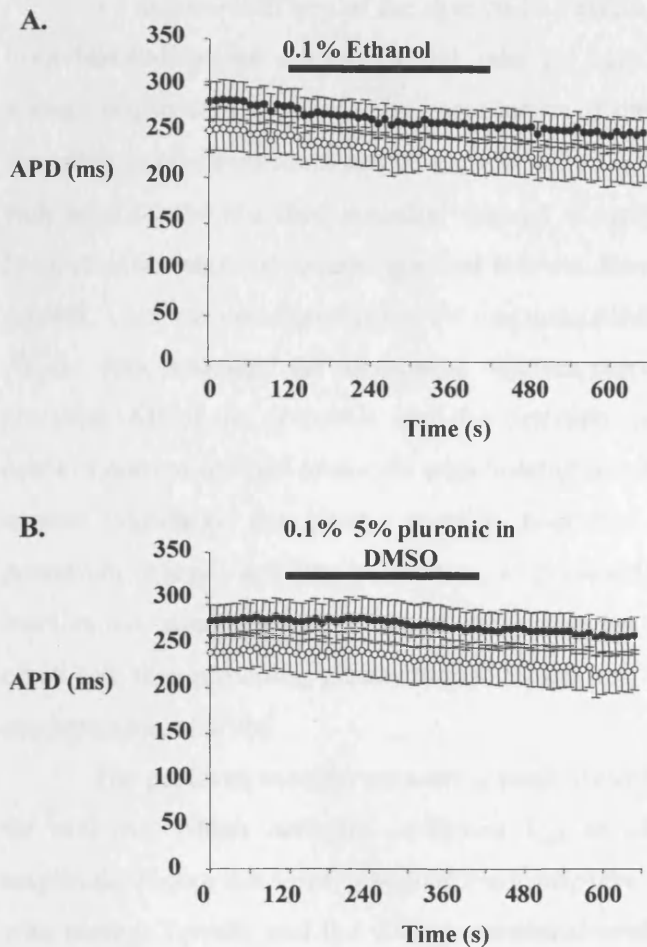


Figure 4.3. The effects upon APD of acute perfusion of different solutes for styryl dyes.

Graphs displaying the APD₅₀ (open circles) and APD₉₀ (closed circles) of isolated guinea pig ventricular myocytes perfused with either (A) normal Tyrode containing 0.1% ethanol (n = 5) or (B) normal Tyrode containing 0.1% DMSO into which 5% by weight pluronic F127 had been dissolved (n = 7). Data are expressed as means \pm SEM.

4.1.2. The effects of different “styryl” dyes upon canine cardiac L-type calcium currents.

In mammalian ventricular myocytes, the L-type calcium current is responsible for maintaining the plateau. Thus, either increasing or attenuating I_{CaL} can result in prolongation or shortening of the AP respectively.

To determine if any of the dyes had an effect on I_{CaL} , calcium currents were measured from isolated canine midmyocardial cells (M cells) using a patch electrode in whole-cell voltage clamp configuration. The constituents of the internal and external solutions used for recording calcium currents can be viewed in section 2.5. When the pipette was placed in the bath solution the recorded potential was set at zero using pipette offset controls. However, because of the electrochemical gradient between these solutions there was a junction potential present. This was calculated using the junction potential calculator in pCLAMP 9.2 as -4 mV. All the data presented for monitoring calcium currents has been corrected for this junction potential. All of the protocols used for determining alterations in the characteristics of the calcium current utilized protocols with holding potentials of -44 mV to inactivate the sodium current. Similarly, the pipette solution contained 130 mM caesium chloride to inhibit potassium channel activity. In addition, to prevent the effects of calcium-dependent channel inactivation, sweeps were performed at 8 s intervals. Dyes were spot-tested at a concentration of 16 μ M, thus providing greater than a 0.5 log unit safety margin against the normal loading concentration of 5 μ M.

The protocol used for measuring peak inward current utilized a voltage step to +6 mV for 400 ms, which activated sufficient I_{CaL} to allow for the detection of peak current amplitude. Figure 4.4 shows a typical recording taken from an individual myocyte, superfused with normal Tyrode, and the voltage command used to elicit it. Peak current was calculated by subtracting the average current during the last 10 ms of the test pulse from the maximal inward current.

Each cell was superfused with external solution, prior to superfusion with vehicle and then dye, and allowed to reach steady state prior to measurement. Figure 4.5 shows individual records monitoring the peak inward current during perfusions with vehicle solutions and then either di-4-ANEPPS or di-8-ANEPPS. Di-4-ANEPPS did not have a significant effect upon peak inward current. In contrast, di-8-ANEPPS caused a significant reduction in peak current ($p < 0.01$, $n = 4$, paired Student's t-test) reducing the current from 330 ± 22 pA under control conditions, to 257 ± 18 pA (See Figure 4.5E).

To ensure that L type calcium channels were responsible for the inward currents measured, cells that had been treated with di-4-ANEPPS or di-8-ANEPPS were superfused with 30 μ M of the specific inhibitor diltiazem (Hockerman et al., 1997). Figure 4.6 shows

individual traces of cells treated with di-8-ANEPPS or di-4-ANEPPS, wash-off of the dye and perfusion with 30 μ M diltiazem. In both sets of experiments diltiazem produced a significant decrease in inward current compared to values following wash-off. ($p > 0.05$ cells treated with di-4-ANEPPS, $n = 4$ and $p > 0.05$ in cells treated with di-8-ANEPPS, $n = 3$, paired Student's *t* test).

Di-4-ANEPPDHQ appeared to cause an increase in peak current from 311 ± 144 pA under control conditions, to 803 ± 220 pA, however this was not significant. Additionally, during the test pulse, the time taken to reach the peak current was abbreviated in cells during perfusion with di-4-ANEPPDHQ from 17.5 ± 2 ms to 3 ± 1 ms. Although this may indicate a reduction in the activation time for cardiac calcium channels caused by this dye, the timecourse of the current is arguably not dissimilar from that of the capacitance transient (see Figure 4.7A) and the kinetics of the current appear to be altered in such a way that this may have arisen from a lack of control of voltage, although this effect was consistent in all of the three cells examined. As such I could not determine the precise effects of Di-4-ANEPPDHQ upon I_{CaL} , but did deem them to be too severe to merit continued testing upon this current as it was unlikely that this dye would be selected as optimum for recording cardiac action potentials.

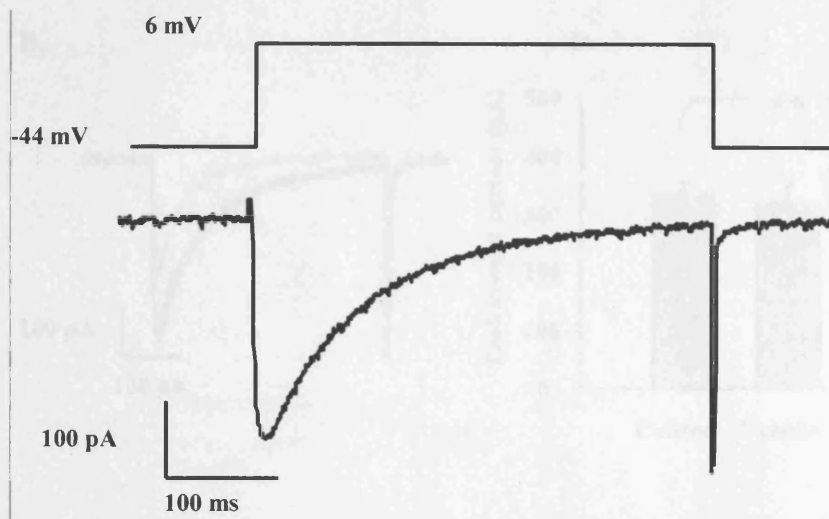


Figure 4.4. The voltage protocol and associated current obtained from patch clamp recordings of the L-type calcium current from an isolated midmyocardial canine cell.

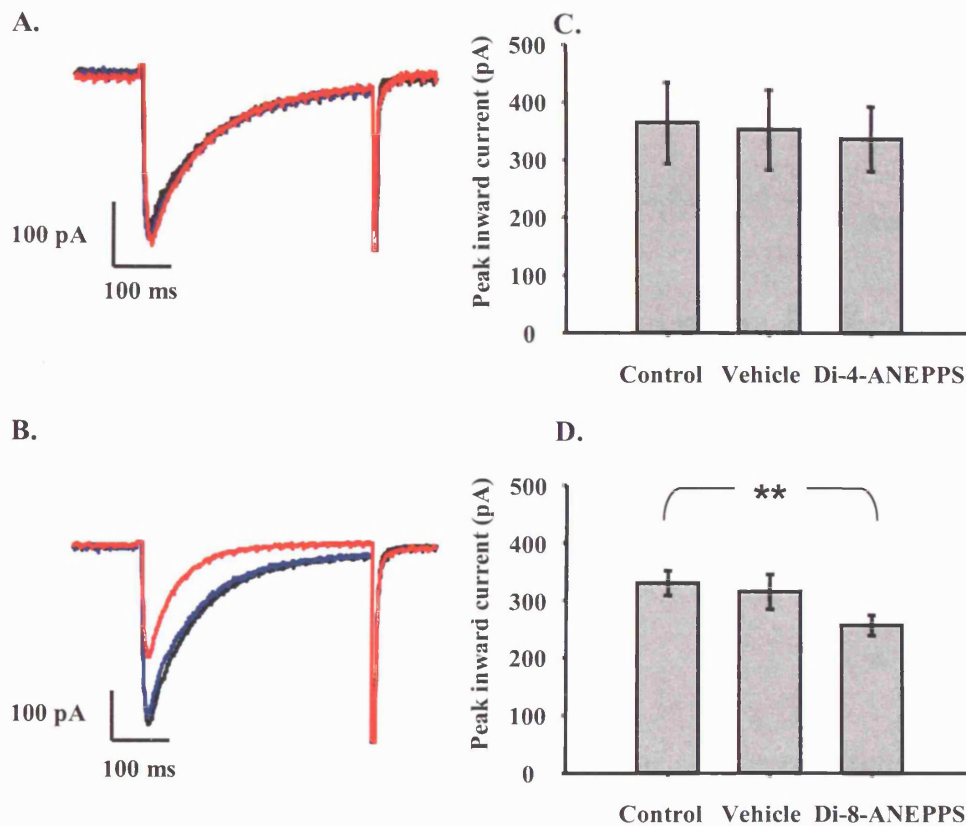


Figure 4.5. The effects of di-4-ANEPPS and di-8-ANEPPS on peak L-type calcium current in isolated canine M cells.

(A,B) Single records of L-type calcium currents recorded from canine M cells during a 400 ms voltage step from -44 mV to +6 mV, under control conditions (black), during perfusion with a vehicle solution (blue) and during perfusion with 16 μ M dye (red) which was either di-4-ANEPPS (A) or di-8-ANEPPS (B). (C, D) Graphs displaying the peak inward calcium currents of isolated canine M cells perfused with either 16 μ M di-4-ANEPPS (C), $n = 4$ or di-8-ANEPPS (D), $n = 4$. Data are expressed as means \pm SEM, ** denotes $p > 0.01$, paired Student's t test.

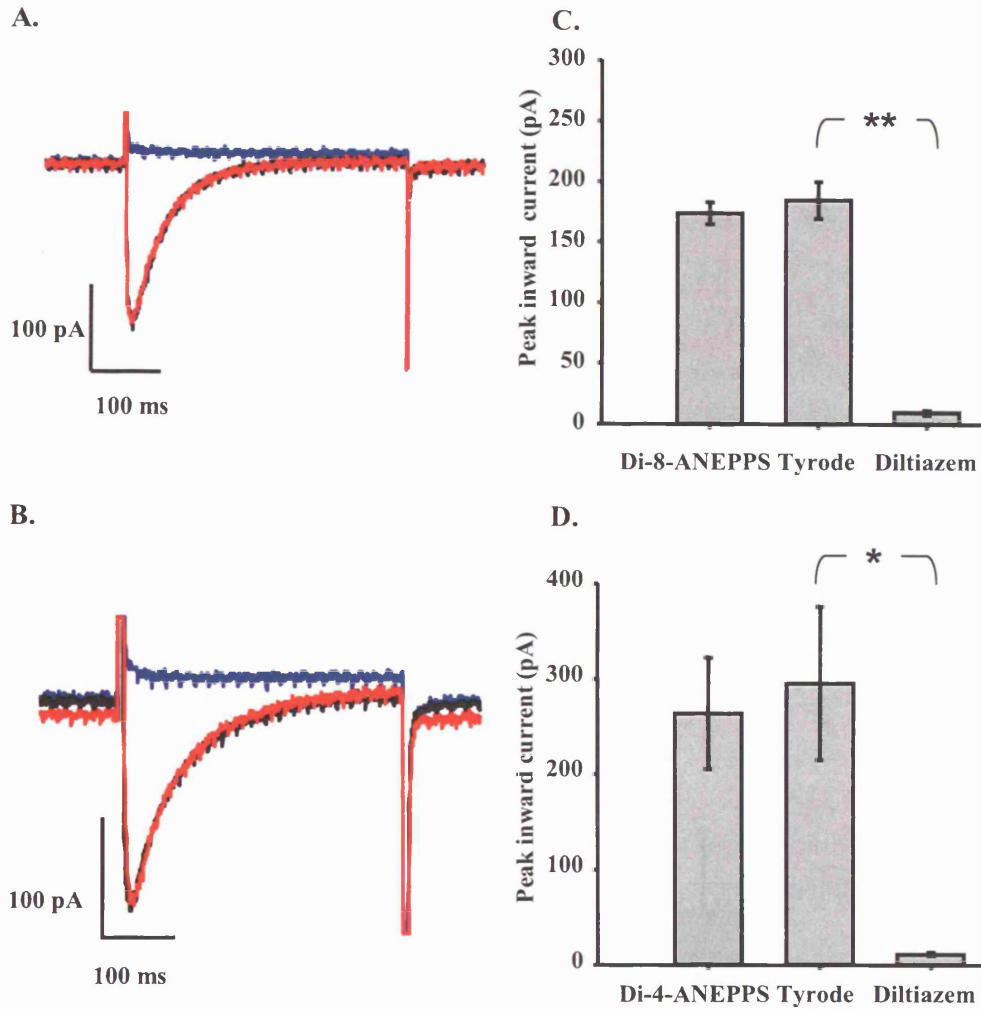
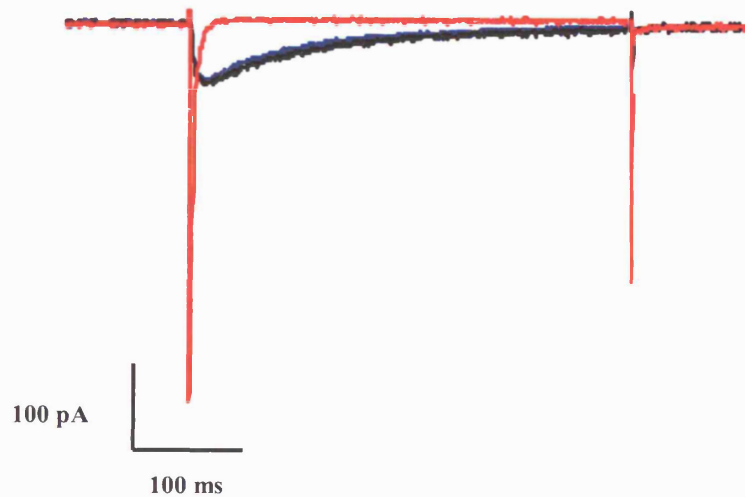


Figure 4.6. Application of diltiazem during measurements of peak L-type calcium current in isolated canine M cells.

(A,B) Single records of L-type calcium currents recorded from canine M cells during a 400 ms voltage step from -44 mV to +6 mV, during perfusion with 16 μ M dye (red) which was either di-8-ANEPPS (A) or di-4-ANEPPS (B), wash-off (black) and during application of 30 μ M diltiazem. (C,D) Graphs displaying the peak inward calcium currents of isolated canine M cells perfused with either di-8-ANEPPS (C), n = 3, or di-4-ANEPPS (D), n = 4, and during wash-off and during application of 30 μ M diltiazem. Data are expressed as means \pm SEM, * denotes p > 0.05 ** denotes p < 0.01, paired Student's t test).

A.



B.

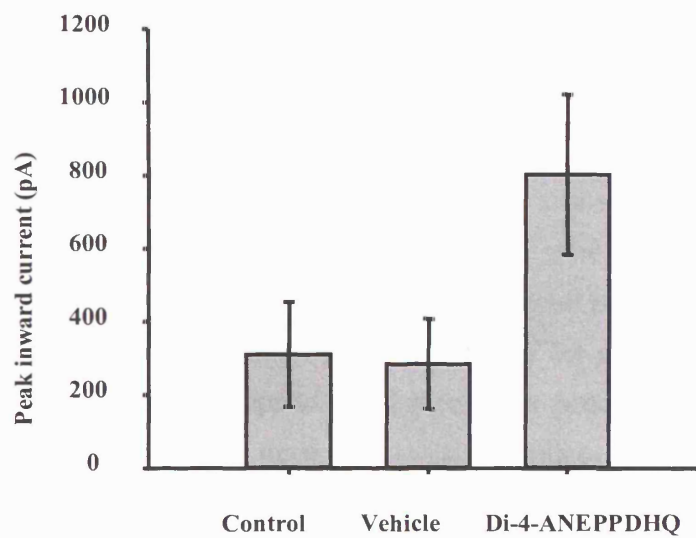


Figure 4.7. The effects of di-4-ANEPPDHQ on peak L-type calcium current in isolated canine M cells..

(A) Single records of L-type calcium currents recorded from canine M cells during a 400 ms voltage step from -44 mV to +6 mV, during perfusion with normal Tyrode (black) or during with 16 μM di-4-ANEPPDHQ (red). (B) Graph showing the peak inward calcium currents of isolated canine M cells perfused with di-4-ANEPPDHQ, n = 3.

The L-type calcium channel is known to be voltage dependent and activates during positive shifts in membrane potential (Hess, 1988). Therefore, experiments were performed to determine if di-8-ANEPPS or di-8-ANEPPS would alter the current voltage relationship of this channel.

The current-voltage relationship of the peak calcium current was determined under control conditions and during perfusion with dye. This was achieved with 400 ms voltage steps, increasing by 10 mV with each sweep, between -34 mV and +56 mV from a holding potential of -44 mV. Figure 4.8 demonstrates both the protocol used and the resultant current from this protocol for a single myocyte prior to the addition of any test compound. This could be fit using a modified Boltzman relationship (see Equation 4.1), where $V_{1/2}$ is the value at which half of the channels were inactivated, k is the slope of the activation curve (when plotted as a sigmoidal relationship (see later and equation 4.2)[‡], G_{max} is the peak of the curve, V_m is the membrane potential and V_{rev} is the reversal potential.

$$I_{CaL} = G_{max} (V_m - V_{rev}) / \{1 + \exp[(V_{1/2} - V_m)/k]\}$$

Equation 4.1. A modified Boltzman relationship.

I_{CaL} began to activate between -34 and -24 mV and the largest current was recorded during a test pulse to +6 mV, which is not dissimilar to the voltage relationship previously shown in canine M cells (Cordeiro *et al.*, 2004). At more positive potentials, the current approaches zero at potentials which are below the reversal potential of calcium. Although L type calcium channels are roughly 1000-fold selective for calcium ions over caesium ions (which was contained in the pipette solution to block potassium efflux), at more positive potentials the outward driving force for caesium increases. The result is that the current voltage relationship for L-type calcium channels approaches zero when the caesium efflux becomes equal with the calcium influx. This has been demonstrated using fluorescent indicators to monitor calcium influx, whilst simultaneously measuring I_{CaL} (Zhou & Bers, 2000).

By fitting the modified Boltzman relationship (Equation 4.1) to the IV relationships of the calcium current recorded from each cell under control conditions and in the presence of

[‡] k refers to the slope obtained by plotting a Boltzman curve to the voltage dependence of inactivation or activation. For an activation curve this slope is positive, unlike in equation 4.2 where the slope is negative because it plots the inactivation against voltage for L-type calcium channels.

either 16 μM di-4-ANEPPS or 16 μM di-8-ANEPPS, it was possible to ascertain if either of these dyes had effects upon the voltage dependent activation of the L-type calcium channels (See Figure 4.9 and Figure 4.10). Di-4-ANEPPS did not have a significant effect upon either $V_{1/2}$ or k (-4.2 ± 1.6 mV under control conditions vs. -2.4 ± 0.8 mV, $p = 0.08$ and 5.4 ± 0.1 vs. 5.2 ± 0.2 , $p = 0.64$ respectively, paired Student's t-test, $n = 4$). Di-8-ANEPPS caused a significant alteration to $V_{1/2}$, shifting the activation of these channels to more negative potentials. $V_{1/2}$ was -5.3 ± 0.6 mV under control conditions and was shifted to -10.6 ± 1.6 mV ($p < 0.05$, paired Student's t-test, $n = 4$). However, di-8-ANEPPS did not have a significant effect upon k (4.5 ± 0.4 vs. 4.8 ± 0.5 , $p = 0.37$ respectively, paired Student's t-test, $n = 4$).

Additionally, similarly to the experiments in the previous section that showed a decrease in inward calcium current recorded during voltage steps from -44 mV to $+6$ mV, di-8-ANEPPS caused a significant decrease in the peak current measured at voltages between $+16$ mV and $+46$ mV ($p < 0.05$, paired Student's t test, $n = 4$) (see Figure 4.9).

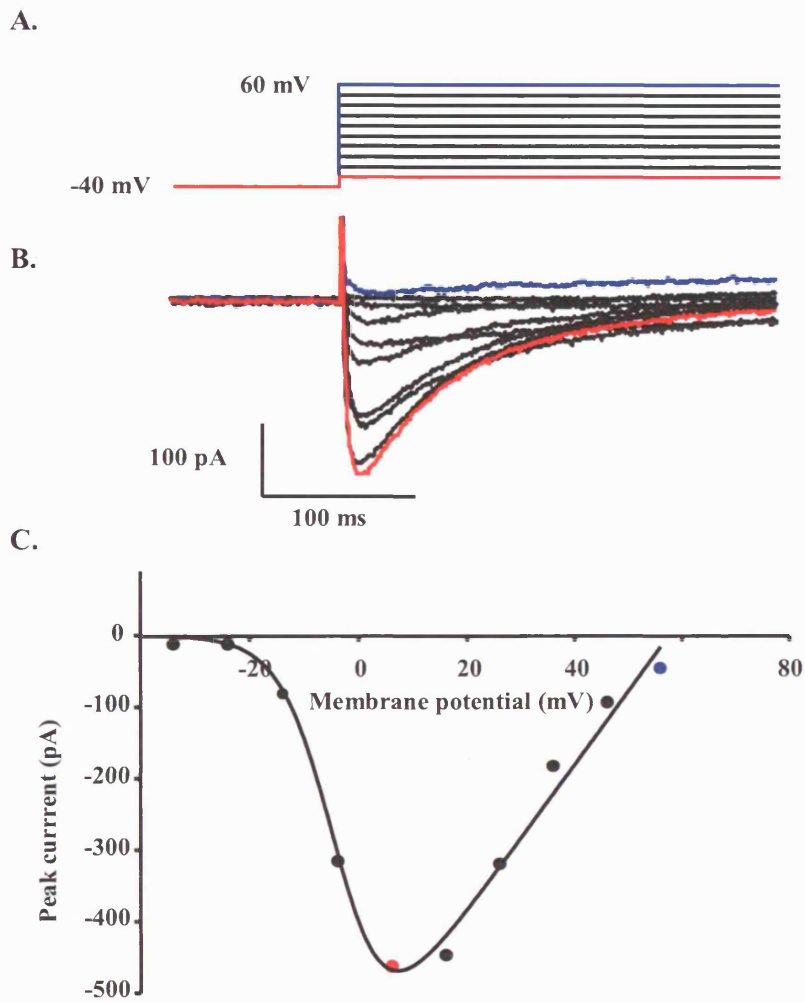


Figure 4.8. The IV relationship for cardiac L-type calcium channels.

(A) The voltage waveform used to obtain peak current responses at different holding potentials and (B) the resultant current traces recorded from a single canine M cell. (C) Graph displaying current-voltage relationship from the data displayed in A and B fit using a modified Boltzman relationship. Red traces/symbols show the current/voltage values at +6 mV. Blue traces/symbols show the current/voltage values at +56 mV.

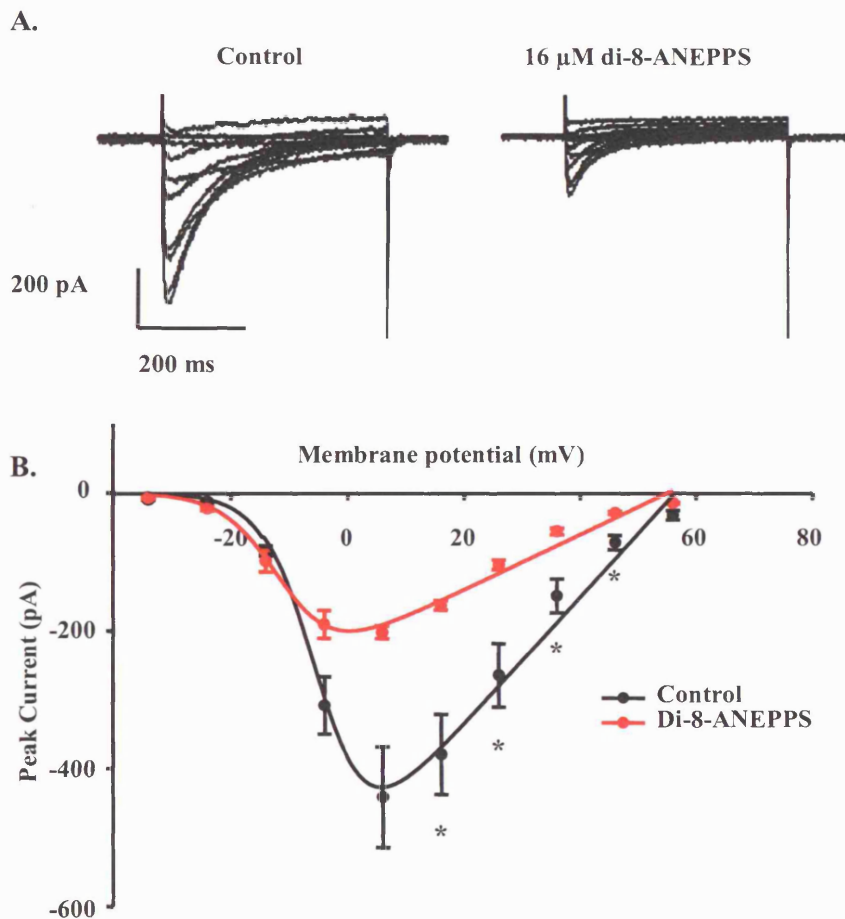


Figure 4.9. The effects of di-8-ANEPPS on the IV relationship of cardiac L-type calcium channels.

(A) Current traces displaying control currents (left) and currents following treatment with 16 μ M di-8-ANEPPS recorded from an isolated canine M cell. (B) Graph showing the IV relationship for currents before (black) and after treatment with 16 μ M di-8-ANEPPS (red), fit using a modified Boltzman relationship. Data are expressed as means \pm SEM, * signifies $p < 0.05$, paired Student's t-test, $n = 4$.

In addition to the effects of di-4-ANEPPS on voltage-dependent activation, voltage-dependent kinetics of inactivation were also altered in the presence of di-4-ANEPPS. Figure 4.10 shows the degree of inactivation at different holding potentials. When holding potentials of -40 mV and $+10$ mV were used, the degree of inactivation was similar in both conditions. However, when holding potentials of -20 mV and $+30$ mV were used, the degree of inactivation was significantly reduced in the presence of di-4-ANEPPS. This effect was not observed when holding potentials of -60 mV and $+70$ mV were used. The effect of di-4-ANEPPS on the IV relationship of cardiac L-type calcium channels is shown in Figure 4.11. The relationship between peak current and membrane potential was fitted using a modified Boltzmann relationship. Data are expressed as means \pm SEM, $n = 4$.

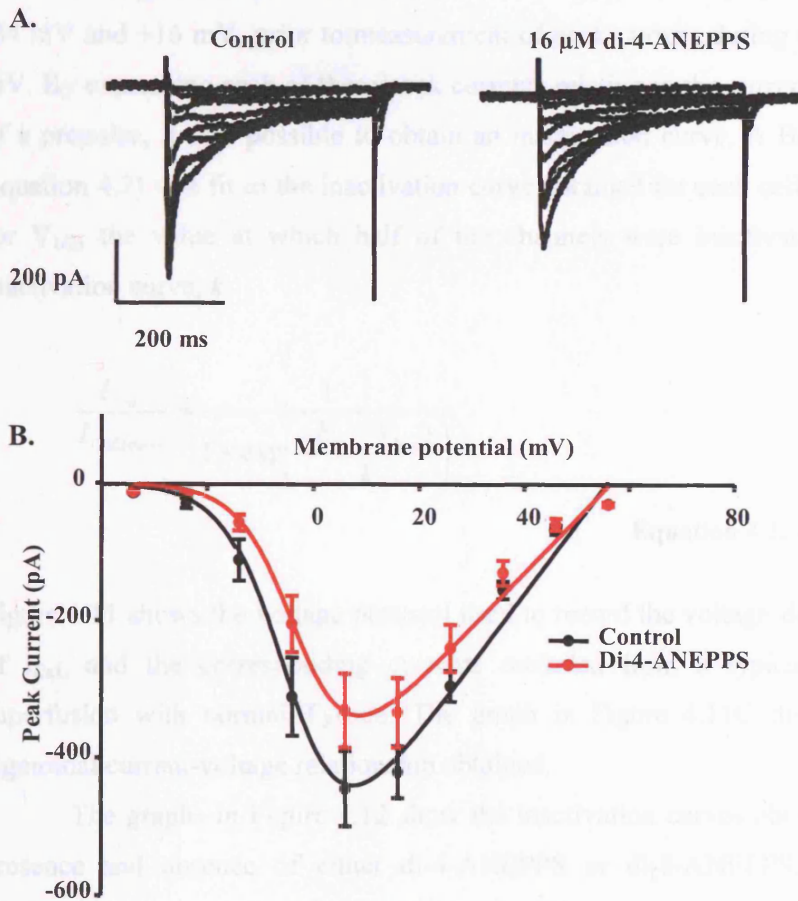


Figure 4.10. The effects of di-4-ANEPPS on the IV relationship of cardiac L-type calcium channels.

(A) Current traces displaying control currents (left) and currents following treatment with 16 μ M di-4-ANEPPS recorded from an isolated canine M cell. (B) Graph showing the IV relationship for currents before (black) and after treatment with 16 μ M di-4-ANEPPS (red), fit using a modified Boltzmann relationship. Data are expressed as means \pm SEM, $n = 4$.

In addition to the effects of the dye upon voltage dependent activation, voltage-dependent kinetics of inactivation were also altered in the presence of di-8-ANEPPS. To assess the degree of inactivation at different voltages, 400 ms prepulses were applied between -34 mV and +16 mV, prior to measurement of peak current during a 400 ms test pulse to +6 mV. By expressing each of these peak currents relative to the current recorded in the absence of a prepulse, it was possible to obtain an inactivation curve. A Boltzman relationship (see Equation 4.2) was fit to the inactivation curve obtained for each cell in order to obtain values for $V_{1/2}$, the value at which half of the channels were inactivated and the slope of the inactivation curve, k .

$$\frac{I_{CaL}}{I_{CaL(max)}} = \frac{1}{1 + \exp\left(\frac{(E_m - V_{1/2})}{k}\right)}$$

Equation 4.2. The Boltzman relationship

Figure 4.11 shows the voltage protocol used to record the voltage-dependence of inactivation of I_{CaL} and the corresponding currents recorded from a typical canine M cell during superfusion with normal Tyrode. The graph in Figure 4.11C displays the corresponding sigmoidal current-voltage relationship obtained.

The graphs in Figure 4.12 show the inactivation curves obtained from M cells in the presence and absence of either di-4-ANEPPS or di-8-ANEPPS. Di-4-ANEPPS did not significantly alter the kinetics of inactivation. However, di-8-ANEPPS shifted the dependence of inactivation to more negative potentials, the value at which half of the channels were inactivated, $V_{1/2}$, was modified from -14.5 ± 0.9 mV to -22.7 ± 1.0 mV ($p < 0.05$, paired Student's t test, $n = 4$). Additionally, the slope of the inactivation curve was altered from -4.1 ± 0.4 to -5.1 ± 0.4 ($p < 0.01$, paired Student's t test, $n = 4$).

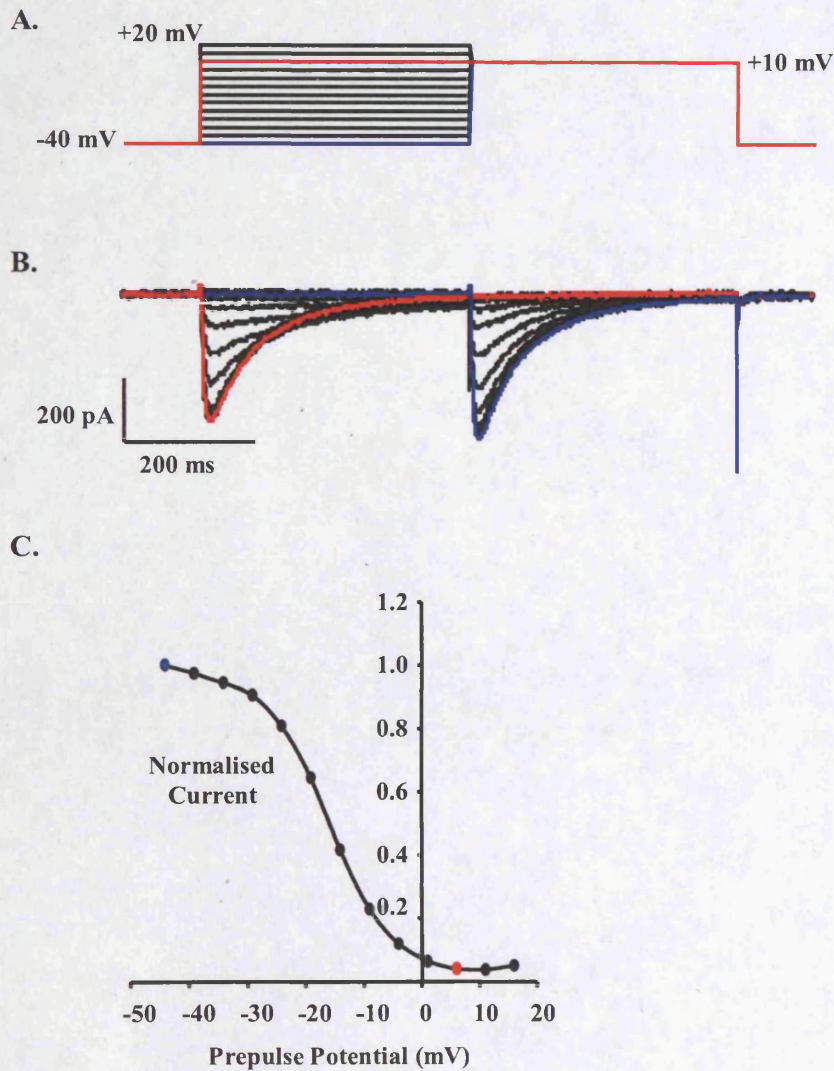


Figure 4.11. The inactivation IV relationship for cardiac L-type calcium channels.

(A) The voltage waveform used to obtain peak current responses at +10 mV following different prepulse potentials and (B) the resultant current traces recorded from a single canine M cell. (C) Graph displaying current-voltage relationship for the peak current recorded during the +6 mV test pulse from the data displayed in B, normalised to the peak current obtained in the absence of a prepulse. Blue traces/symbols show the current/voltage values at +6 mV in the absence of a prepulse. Red traces/symbols show the current/voltage values at +6 mV in the absence of a test pulse.

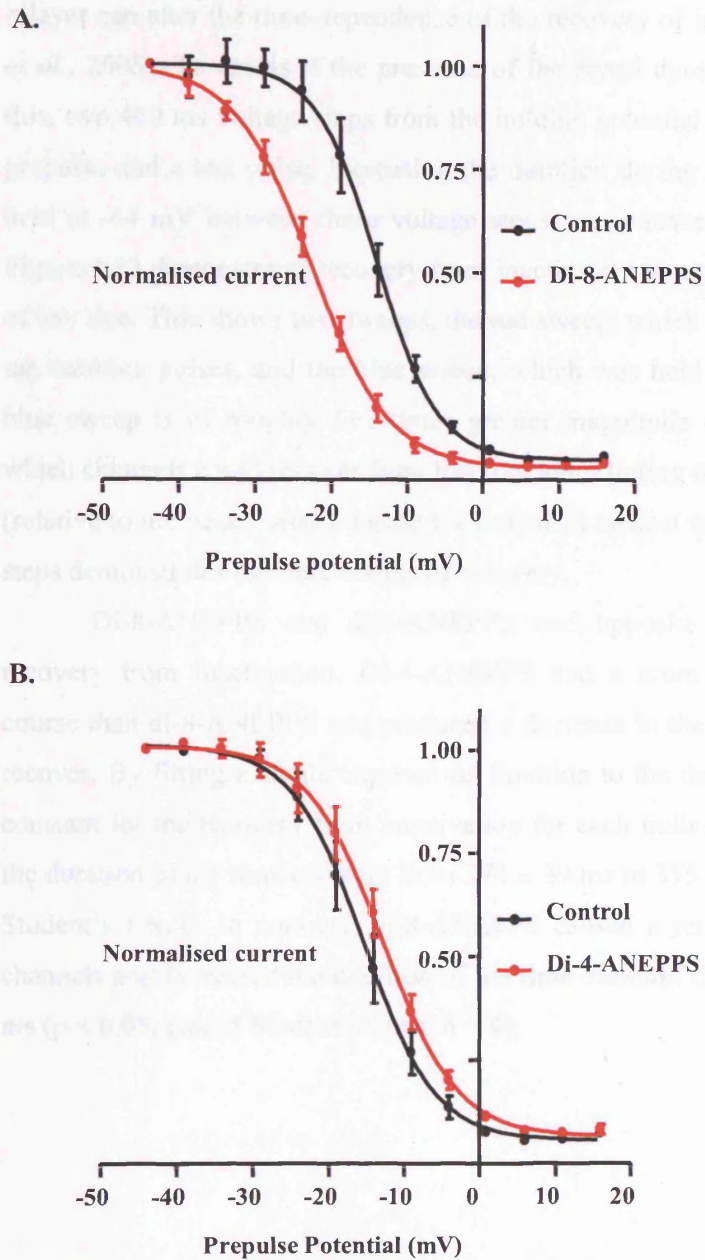


Figure 4.12. The effects of different styryl dyes upon the inactivation IV relationship of cardiac L-type calcium channels.

Graphs showing the effects of 16 μM di-8-ANEPPS ($n = 3$) (A) or di-4-ANEPPS ($n = 4$) upon the voltage dependence of inactivation of L-type calcium channels in canine M cells. Values were obtained by plotting the peak current, obtained during a 400 ms pulse at +6 mV, against the voltage of a 400 ms prepulse. Peak currents are expressed as a fraction of the current recorded in the absence of a prepulse. Data are expressed as mean \pm SEM.

Previously, it has been demonstrated that the presence of n-3-PUFAs in the lipid bilayer can alter the time-dependence of the recovery of ion channels from inactivation (Leaf *et al.*, 2003). To assess if the presence of the styryl dyes under investigation may modulate this, two 400 ms voltage steps from the holding potential of -44 mV to +6 mV were used: a prepulse and a test pulse. Increasing the duration during which the membrane potential was held at -44 mV between these voltage steps, an increased the current during the test pulse. Figure 4.13 demonstrates recovery from inactivation in a canine myocyte prior to the addition of any dye. This shows two sweeps, the red sweep, which was at the holding potential for 100 ms between pulses, and the blue sweep, which was held for 1600 ms between sweeps. The blue sweep is of roughly five times greater magnitude due to the increased duration with which channels could recover from inactivation. Plotting the peak current during the test pulse (relative to the peak current during the prepulse) against the duration between the two voltage steps demonstrates the time course of recovery.

Di-8-ANEPPS and di-4-ANEPPS had opposite effects upon the time course of recovery from inactivation. Di-4-ANEPPS had a more pronounced effect upon the time course than di-8-ANEPPS and produced a decrease in the time taken for calcium channels to recover. By fitting a single exponential function to the data, it was possible to obtain a time constant for the recovery from inactivation for each individual cell. Di-4-ANEPPS shortened the duration of the time constant from 574 ± 39 ms to $375 \text{ ms} \pm 21$ ms ($p < 0.05$, $n = 4$, paired Student's *t* test). In contrast, di-8-ANEPPS caused a reduction in the number of available channels and increased the duration of the time constant from 651 ± 62 ms to $1001 \text{ ms} \pm 118$ ms ($p < 0.05$, paired Student's *t* test, $n = 4$).

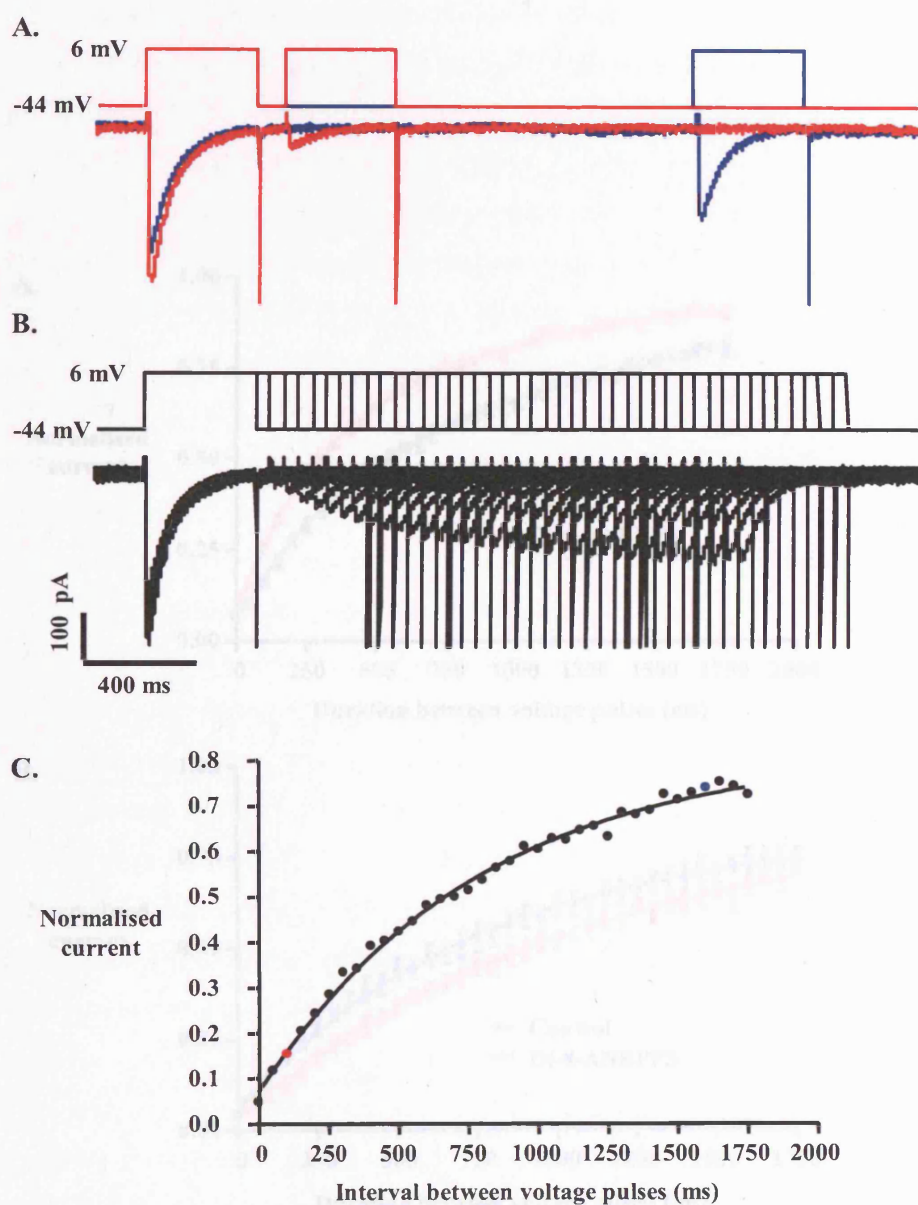


Figure 4.13. Recovery from inactivation for cardiac L-type calcium channels.

(A) Voltage waveforms and resultant current traces for intervals between pulses of 100 ms (red) and 1600 ms (blue). (B) The voltage waveform and peak current responses recorded from a single canine M cell; two 400 ms pulses to 6 mV were used per sweep, a prepulse and the test pulse; the time between these was varied to obtain the time course for recovery from inactivation. (C) Graph displaying recovery from inactivation from the data displayed in (B), normalised to the peak current obtained during the prepulse. The current recorded at 0 ms was during a single 800 ms pulse to +6 mV after the complete decay of the calcium current.

4.1.4. The effects of different styryl dyes upon the recovery from inactivation of cardiac

Owing to the large number and variety of compounds which block I_{CaL} currents (Sutton *et al.*, 2003), one of the primary concerns for studying AP arrhythmias is to ensure the experiments performed with di-4-ANEPPS was the most appropriate method for the study of I_{CaL} currents (Pitts). To assess if different styryl dyes had effects upon I_{CaL} recovery, we used a medium diameter paper patch clamp system (Rigbi, 1998) to measure

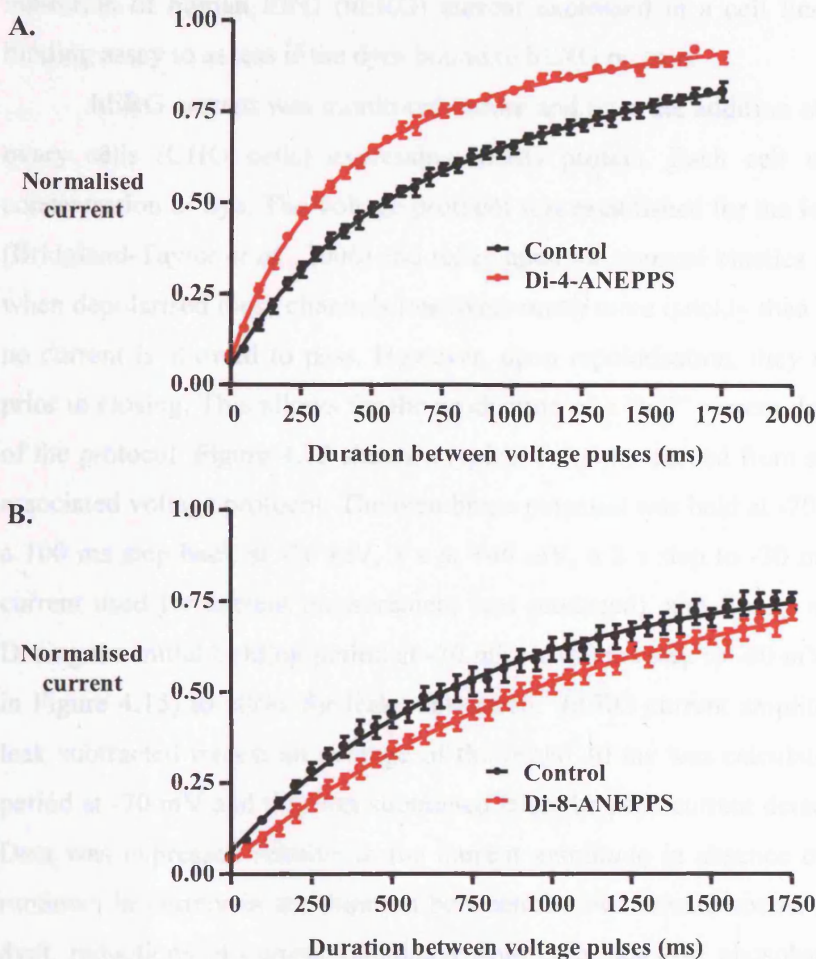


Figure 4.14. The effects of different styryl dyes upon the recovery from inactivation of cardiac L-type calcium channels.

Graphs showing the effects of di-4-ANEPPS (A) and di-8-ANEPPS (B) on the recovery from inactivation of L-type calcium channels in canine M cells. Data are expressed as means \pm SEM, $n = 4$ in both graphs.

4.1.3. The effects of different “styryl” dyes upon hERG current and binding.

Owing to the large number and variety of compounds which block I_{Kr} current (Redfern *et al.*, 2003), one of the primary candidates for inducing AP prolongation in guinea pig myocytes perfused with di-8-ANEPPS was the potassium channel encoded for by the ether-a-go-go related gene (ERG). To assess if different styryl dyes had effects upon ERG, two assays were used: a medium throughput planar patch clamp system, the Ionworks HT™, to monitor inhibition of human ERG (hERG) current expressed in a cell line; and also a radioligand binding assay to assess if the dyes bound to hERG protein.

hERG current was monitored before and after the addition of dye, in Chinese hamster ovary cells (CHO cells) expressing hERG protein. Each cell was exposed to a single concentration of dye. The voltage protocol was established for the Ionworks HT™ previously (Bridgland-Taylor *et al.*, 2006) and relies upon the unusual kinetics of the hERG ion channel; when depolarised these channels inactivate much more quickly than they can open, so little or no current is allowed to pass. However, upon repolarisation, they recover from inactivation prior to closing. This allows for the production of a “tail” current during the repolarising step of the protocol. Figure 4.15 shows a typical current recorded from a single CHO cell and the associated voltage protocol. The membrane potential was held at -70 mV for 20 s followed by a 100 ms step back at -70 mV, 1 s at +40 mV, a 2 s step to -30 mV (during which the tail current used for current measurement was produced), and finally a 500 ms step to -70mV. During the initial holding period at -70 mV, a 160 ms step to -60 mV was applied (not shown in Figure 4.15) to allow for leak subtraction. hERG current amplitude was calculated using leak subtracted traces; an average of the initial 40 ms was calculated from the first holding period at -70 mV and this was subtracted from the peak current detected from the tail current. Data was expressed relative to the current amplitude in absence of dye. To adjust for any rundown in current in the duration between the two measurements (pre and post addition of dye), reductions in current calculated from cells that had phosphate buffered saline (PBS) alone added were subtracted from dye-induced values of inhibition.

Di-4-ANEPPS, di-8-ANEPPS, di-12-ANEPPS, Di-3-ANEPPDHQ and Di-4-ANEPPDHQ were assessed for inhibition of hERG current in the Ionworks HT™ at concentrations of 0.03, 0.1, 0.3, 1, 3, 10 and 30 μ M. None of the dyes tested in the Ionworks HT™ produced inhibition of hERG current great enough to accurately predict an IC_{50} value using nonlinear regression (see Figure 4.16). Inhibition of hERG current was greatest in the dyes with shorter carbon tail lengths. At 30 μ M, di-3-ANEPPDHQ caused an inhibition of $40 \pm 7\%$ ($n = 7$), di-4-ANEPPDHQ inhibited the current by $30 \pm 5\%$ ($n = 3$) and di-4-ANEPPS caused an inhibition of $35 \pm 2\%$ ($n = 7$). Di-8-ANEPPS and di-12-ANEPPS at 30 μ M reduced

hERG current by $27 \pm 2\%$ and $17 \pm 3\%$, respectively, however at this concentration both dyes were seen to precipitate in solution, which may have caused a reduction in the observed effects.

In addition to monitoring hERG current, the affinity of different dyes for hERG protein was also examined. This was achieved using human embryonic kidney (HEK) cell membranes obtained from cells expressing hERG protein and monitoring the inhibition of the binding of the radioligand [^3H]-AR-C160051XX (which had a K_d of 1 nM). Following subtraction of non-specific binding, this was calculated as a percentage of the total binding according to equation 4.2, where *Value* equals the number recorded from the well containing test compound and NSB equals non-specific binding.

$$\text{Binding}(\%) = 100 - \left(\frac{100 * (\text{Value} - \text{NSB})}{\text{TotalBinding}} \right)$$

Equation 4. 3. Calculation for hERG binding.

Figure 4.17 shows the percentage of inhibition exhibited by Di-4-ANEPPS, di-8-ANEPPS, di-12-ANEPPS, Di-3-ANEPPDHQ and Di-4-ANEPPDHQ at concentrations of 0.3, 1, 3, 10 and 30 μM . Data are plotted using linear regression of a four-way parametric equation with upper and lower limits of 100% and 0 % imposed. Di-12-ANEPPS exhibited the lowest affinity for hERG. At the maximal concentration of 30 μM di-12-ANEPPS inhibited the binding of the radioligand by $49.5 \pm 3.3\%$. Di-3-ANEPPDHQ and di-4-ANEPPDHQ exhibited the largest affinity for hERG protein; each dye inhibited binding of radioligand with in IC_{50} of 0.7 μM and 1.4 μM , respectively. Di-4-ANEPPS and di-8-ANEPPS each had an IC_{50} of 2.2 μM and 3.5 μM , respectively.

Comparisons between data on the efficacy of dyes for inhibiting hERG current, as detected in the Ionworks HTTM, and hERG binding data showed differences in the data obtained using the two methods. Table 4.1 shows the percentage of inhibition of hERG current detected in Ionworks HTTM at the same concentration used to incubate myocytes with dye, 5 μM (calculated from the least squares fit from the graphs in Figure 4.16) for di-4-ANEPPS di-8-ANEPPS, di-3-ANEPPDHQ and di-4-ANEPPDHQ. These data are compared to values calculated at the same concentration for inhibition of the binding of radioligand. The binding data shown in Table 4.1 has been corrected for the concentration of radioligand used with the Cheng-Prusoff equation (Cheng & Prusoff, 1973). In the case of each of these dyes,

binding of radioligand was inhibited substantially more than hERG current. For example, di-8-ANEPPS inhibited the binding of radioligand by 78%, whilst only inhibiting hERG current by 17%.

Positive controls were also examined in both the Ionwork HT™ and the radioligand binding assay. Cisapride, which has previously been shown to inhibit hERG current expressed in HEK cells with an IC_{50} of 44.5 nM was tested in the Ionworks HT™ at concentrations of 0.01, 0.03, 0.1, 0.3, 1, 3 and 10 μ M (Rampe *et al.*, 1997). This inhibited hERG current with an IC_{50} of 318 nM (n = 3-4). Similarly, pimozone, which has previously been shown to inhibit hERG current expressed in CHO cells with an IC_{50} of 18 nM (Kongsamut *et al.*, 2002), was tested in the radioligand assay at concentrations of 1, 3, 10, 30, and 100 nM. This inhibited the binding of [³H]-AR-C160051XX with an IC_{50} of 55 nM (22.5 nM following correction for radioligand concentration).

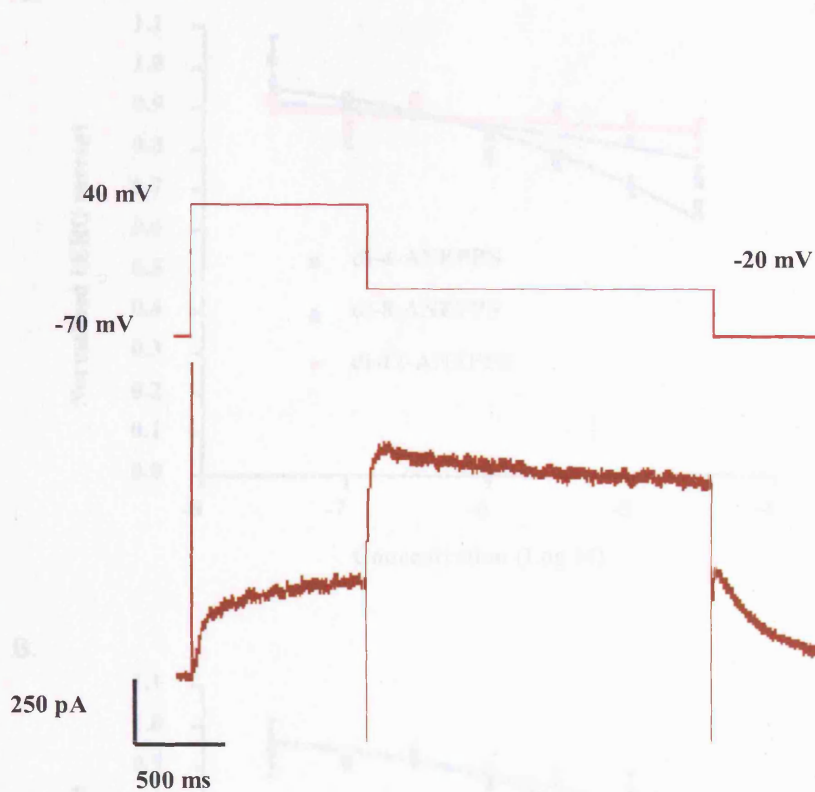


Figure 4.15. The voltage protocol and associated current recorded from CHO cells expressing hERG protein in the Ionworks®.

The upper trace shows the voltage protocol used to produce a tail current in CHO cells expressing hERG ion channels. The lower trace shows the resultant current. The peak of the tail current produced following the step from 40 mV to -20 mV was measured.

Figure 4.16. The inhibitory effects of different "dye" dyes upon hERG current in CHO cells expressing hERG protein in the Ionworks HT™. Graphs showing the hERG current expressed in CHO cells following the application of the concentrations of 0.1 μM ANEPDS (black), 0.5 μM ANEPDS (blue) and 0.1 μM ANEPDS (red) and 0.1 μM ANEPDS (green) and 0.1 μM ANEPDS (purple). Data are expressed as mean ± SEM (n = 3-8).

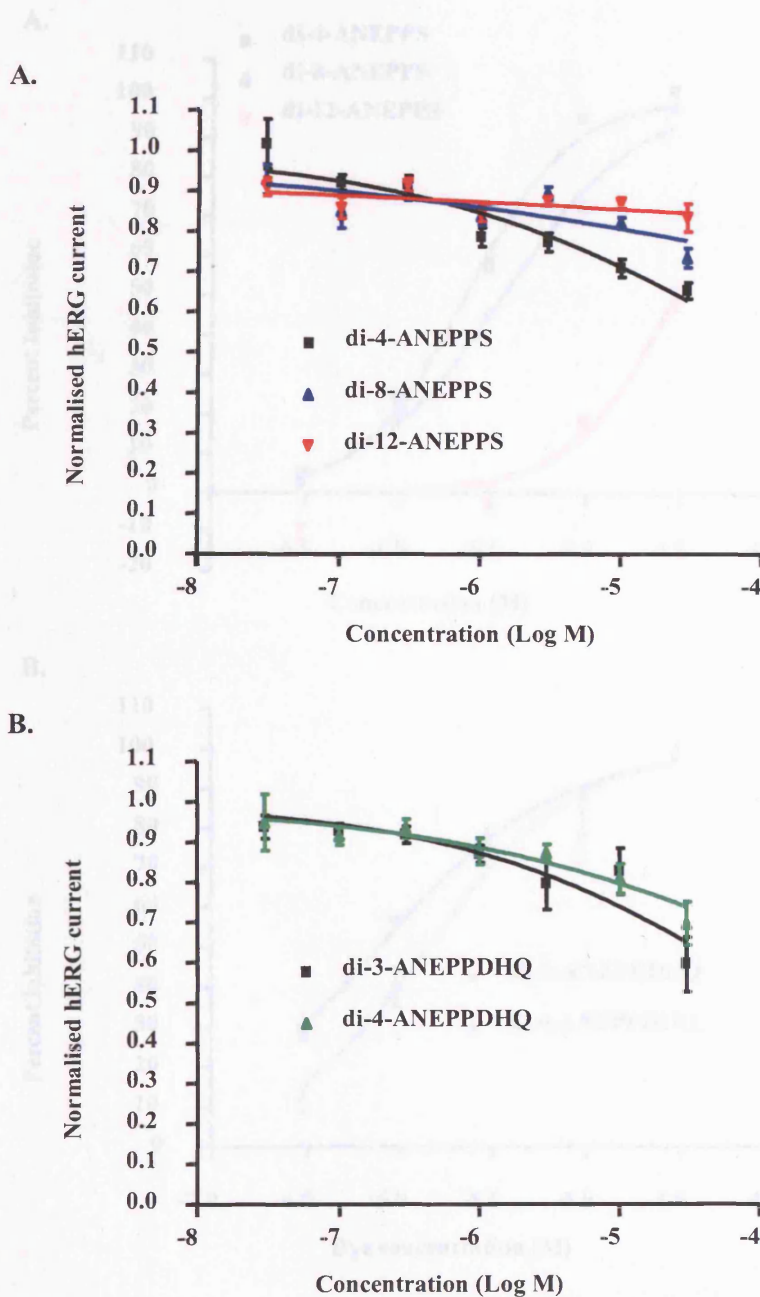


Figure 4.16. The inhibitory effects of different “styryl” dyes upon hERG current measured using Ionworks HT™.

Graphs showing inhibition of hERG current expressed in CHO cells following the addition of different concentrations of di-4-ANEPPS (black), di-8-ANEPPS (blue) and di-12-ANEPPS (red) (A), as well as di-3-ANEPPDHQ (black) and di-4-ANEPPDHQ (green) (B). Data are expressed as means \pm SEM, $n = 3-8$.

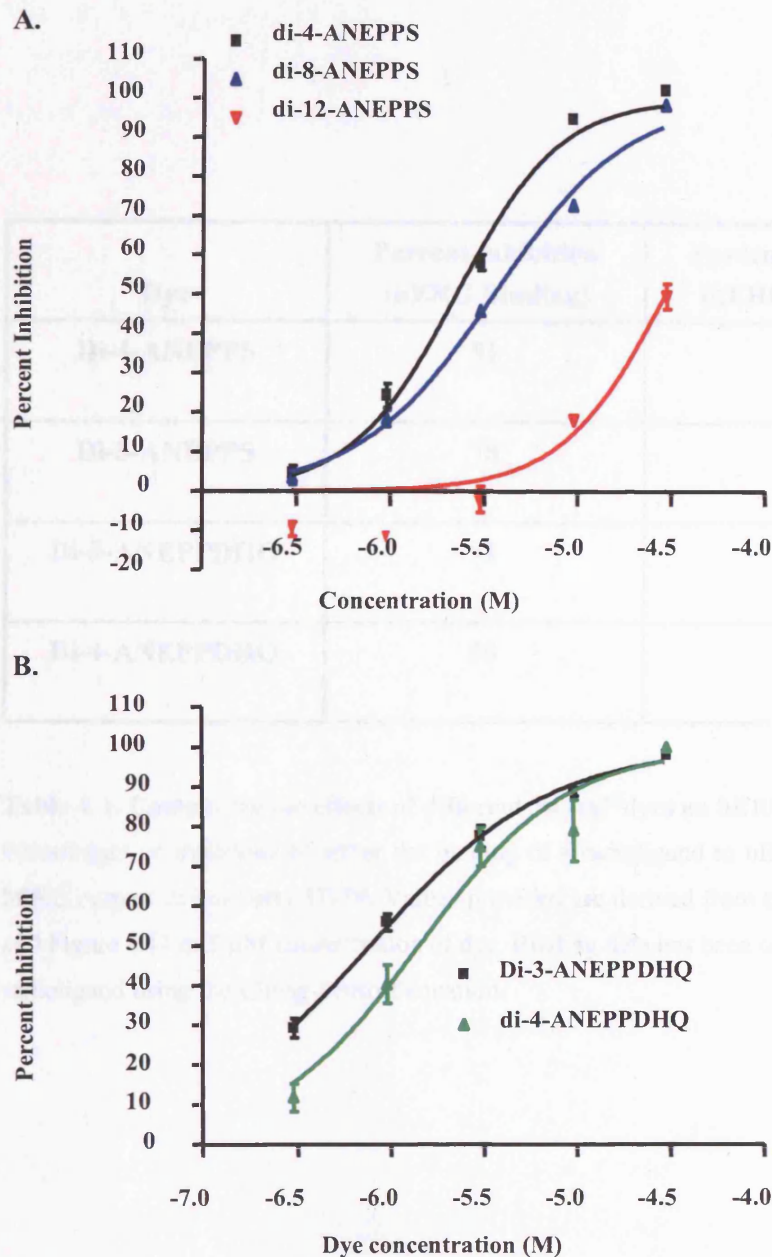


Figure 4.17. The inhibitory effects of different “styryl” dyes upon inhibition of a radioligand binding to hERG protein.

Graphs showing inhibition of the binding of [3 H]-AR-C160051XX to hERG protein expressed in HEK cell membranes following the addition of different concentrations of di-4-ANEPPS (black), di-8-ANEPPS (blue) and di-12-ANEPPS (red) (A), as well as di-3-ANEPPDHQ (black) and di-4-ANEPPDHQ (green) (B). Data are expressed as means \pm SEM, $n = 3-4$ in both graphs.

Dye	Percent inhibition (hERG Binding)	Percent inhibition (hERG Current)
Di-4-ANEPPS	91	24
Di-8-ANEPPS	78	17
Di-3-ANEPPDHQ	91	27
Di-4-ANEPPDHQ	90	17

Table 4. 1. Comparing the effects of different “styryl” dyes on hERG binding and hERG current. Percentages of inhibition of either the binding of a radioligand to hERG protein or the inhibition of hERG current in Ionworks HT™. Values provided are derived from the graphs shown in Figure 4.16 and Figure 4.17 at 5 μ M concentration of dye. Binding data has been corrected for the concentration of radioligand using the Cheng-Prusoff equation.

4.1.4. The effect of different vehicle solutions upon hERG.

Stocks of the different dyes that were examined for effects on hERG current and binding were prepared in different carrier solutions. Both di-3-ANEPPDHQ and di-4-ANEPPDHQ were dissolved in ethanol. Di-n-ANEPPS dyes were dissolved into DMSO containing concentrations of the non-ionic detergent pluronic F127 measured as a percentage of the total weight of solute. Di-4-ANEPPS and di-8-ANEPPS were prepared in DMSO that contained 5% pluronic F127. Di-12-ANEPPS, which was less soluble, was dissolved into DMSO containing 20% pluronic F127. Therefore, hERG current in the presence of different carrier solutions was monitored using both the Ionworks HT™ assay and hERG binding was examined in the radioligand binding assay.

Current was measured in cells exposed to phosphate buffered saline (PBS) containing 0.6% by volume of carrier solution, which was the maximum volume present during examination of the different dyes in both the Ionworks HT™ and radioligand binding assay. Data were then expressed relative to the level of current prior to the addition of the carrier solutions (i.e. when the cells were in PBS alone). As with the measurement of inhibition of hERG current produced by different dyes, to adjust for any rundown in current in the duration between the two measurements (pre and post addition of vehicle), reductions in current calculated from cells that had phosphate buffered saline (PBS) alone added were subtracted from vehicle-induced values of inhibition.

The bar chart in Figure 4.18 shows the effect of the different vehicle solutions on hERG current. Following addition of PBS alone, current had rundown by $9 \pm 1\%$ ($n = 15$). Neither ethanol nor DMSO caused any further reduction in the current. However, the addition of pluronic F127 to DMSO did cause significant reduction in hERG current. DMSO containing 5% pluronic F127, caused a reduction in current of $28 \pm 3\%$, which was statistically different from the value obtained in PBS alone ($p < 0.01$, Student's t test, $n = 14$). Similarly, DMSO containing 20% pluronic F127 caused a reduction in current of $29 \pm 2\%$ ($p < 0.001$, Student's t test compared to PBS, $n = 15$).

Similarly, DMSO containing pluronic F127 also caused the largest effects in the radioligand binding assay. Figure 4.19 shows the effects of the three carrier solutions upon the binding of the radioligand to hERG. DMSO containing 5% pluronic F127, enhanced the binding of radioligand by $13 \pm 5\%$ and DMSO containing 20% pluronic F127, enhanced the binding of radioligand by $12 \pm 2\%$. Ethanol did not affect binding and gave a value of $-2 \pm 2\%$ ($n = 4$ for each carrier solution).

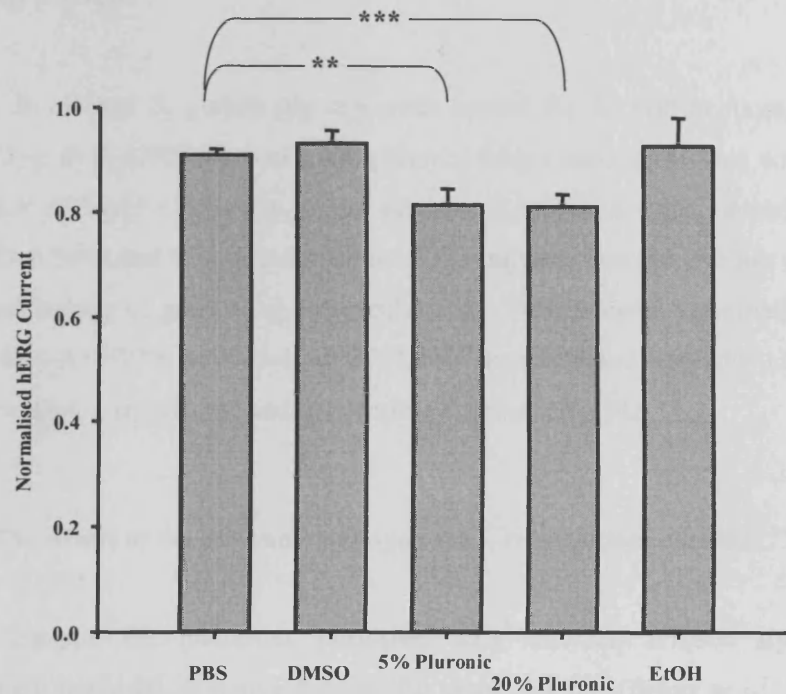


Figure 4.18. The effects of different vehicles for “styryl” dyes on hERG current measured using Ionworks HT™.

Bar chart showing normalised tail current amplitudes measured in CHO cells expressing hERG ion channels following the addition of 0.6% by volume different vehicle solutions or PBS as control. Both carrier solutions of DMSO containing 5% and 20% pluronic F127 caused a significant inhibition in hERG current. Data are expressed as means \pm SEM, ** indicates $p < 0.01$, *** indicates $p < 0.001$. Student's t test, $n = 10-15$.

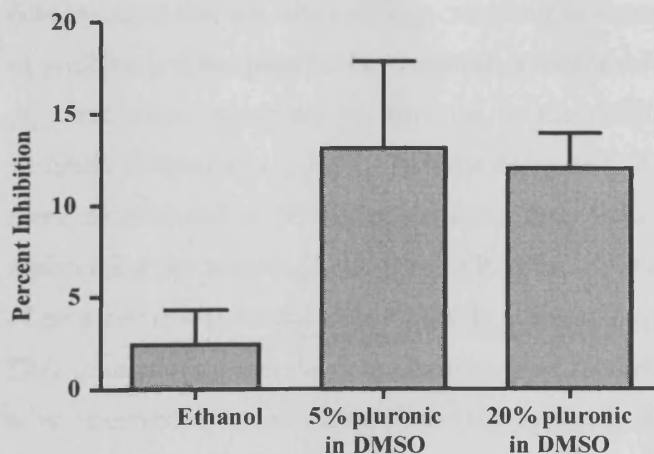


Figure 4.19. The effects of different vehicles for “styryl” dyes upon hERG binding.

Bar chart showing enhancement of binding of a competitive radioligand measured in HEK cells expressing hERG ion channels following the addition of 0.6% by volume different vehicle solutions; either ethanol or DMSO into which 5% or 20% by weight pluronic F127 had been dissolved. Data are expressed as means \pm SEM, $n = 4$.

4.1. Discussion.

In chapter 3, guinea pig myocytes loaded for 20 min at room temperature with the styryl dye, di-8-ANEPPS, had a significantly longer basal APD than control myocytes. Acute perfusion of 5 μ M of this dye, in the absence of excitation light, caused a significant increase in APD at 50% and 90% repolarisation. This suggests that the dye has direct effects upon the AP morphology of guinea pig ventricular cells. Furthermore, examination of two other styryl dyes, di-4-ANEPPS and di-4-ANEPPDHQ demonstrated opposite effects upon APD, the latter causing a significant and irreversible decrease in APD.

4.2.1. The effects of the different dyes upon the L-type calcium current.

Despite the numerous published data that has utilised styryl dyes to monitor membrane potential in native tissues (for examples see (Baker *et al.*, 2000; Brunner *et al.*, 2003; Bullen & Saggau, 1999; Obaid *et al.*, 2004; Salama & Choi, 2000), there has been no prior research to assess the direct effect of any of these dyes upon individual ion channels. In particular, the data shown here demonstrate significant effects of the fast voltage sensitive dyes, di-4-ANEPPS, di-8-ANEPPS and di-4-ANEPPDHQ upon the L type calcium current in isolated canine M cells.

For an optical assay designed to detect alterations in cardiac APD, the importance of the dye effects on inward calcium current cannot be overemphasised. Numerous studies have demonstrated that inhibition of I_{CaL} can result in shortening of the APD, most likely as a result of inhibition of the plateau. For example, a recent study reported a decrease in APD in guinea pig ventricular myocytes in response to the calcium channel antagonists nifedipine and verapamil (Terrar *et al.*, 2007). That the decrease in APD reported by Terrar *et al.*, (2007) was more pronounced at 50% repolarisation than 90% is indicative of the role I_{CaL} plays in maintaining the plateau phase of the AP. If the APD is being monitored to allow for detection of proarrhythmic potential in compounds this may have relevance to the outcome of the assay. That triangulation (see later in Chapter 5) of the action potential can be proarrhythmic, has been observed in several laboratories (Champeroux *et al.*, 2005; Hondeghem *et al.*, 2001; Lu *et al.*, 2002) and this can be caused by inhibition of the calcium current. In addition, a number of proarrhythmic compounds are known to block cardiac calcium currents, such as cisapride (Chiang *et al.*, 2004) and terfenadine (Liu *et al.*, 1997; Ming & Nordin, 1995).

The present study assessed the effects of a single concentration of different dyes upon the peak calcium current, the current voltage relationship of activation and recovery from

inactivation in canine M cells. A significant reduction in peak I_{CaL} was observed in M cells that were acutely superfused with di-8-ANEPPS, together with a shift in activation and inactivation kinetics to more negative membrane potentials and slower recovery from inactivation. The combination of these effects could reduce the calcium influx into a cell during an AP as a result of direct inhibition of the current, a reduction in the availability of channels owing to inactivation at more negative membrane potentials and a failure of a proportion of them to recover following the previous AP. The peak calcium current may also occur earlier during the AP as the channels are activated at more negative potentials in the presence of di-8-ANEPPS. Previously (refer to Chapter 3), alterations in APD in response to cisapride were monitored in guinea pig myocytes stained with di-8-ANEPPS and compared to results obtained using a patch electrode. An example of when dye-induced inhibition of I_{CaL} may affect the ability to detect drug-induced changes in APD was highlighted in Chapter 3. At 1 μ M cisapride a reduction in APD was observed at 40% repolarisation using a patch electrode. However, this was not detected in cells where the APD was recorded optically using di-8-ANEPPS. One possible reason for this may be that a reduction in I_{CaL} had occurred as a result of the presence of di-8-ANEPPS in the cell membrane. This could have reduced the sensitivity of the assay to drug-induced inhibitions in inward calcium current. Reduction in I_{CaI} has been shown to cause a decrease in APD (Terrar *et al.*, 2007), which is inconsistent with the observed increase in APD during acute perfusion of 5 μ M di-8-ANEPPS on guinea pig myocytes and the prolonged basal APD observed in guinea pig myocytes loaded with di-8-ANEPPS in Chapter 3 (Figure 3.15). Therefore, di-8-ANEPPS is likely to have effects upon multiple ion channels; the global effects of which cause an increase in APD. Similarly, although di-4-ANEPPS did not have significant effects upon the voltage dependence of inactivation or peak current magnitude, the dye did cause a significant decrease in the time taken for channels to recover from inactivation. This may result in increased availability of calcium channels during an AP, which would not correspond with the decrease in APD observed during acute perfusion of the dye in guinea pig myocytes.

These observations are limited by a certain experimental conditions. Experiments on calcium currents were made using myocytes isolated from the midmyocardium of the canine left ventricle, whereas alterations in APD during acute perfusion of the dyes were observed in guinea pig ventricular cells. The former were selected to initiate screening for suitable dyes in a cell type amenable for drug screening, using a species that was already in use in pharmaceutical laboratories (Abi-Gerges *et al.*, 2004; Abi-Gerges *et al.*, 2006). Guinea pig myocytes were used to monitor APD to assess if the increased basal APD observed in cells

loaded with di-8-ANEPPS (see Chapter 3) was a direct result of the dye, as well as to ascertain if other dyes (di-4-ANEPPS and di-4-ANEPPDHQ) would have similar effects.

Furthermore, experiments were performed using different concentrations of dyes; I_{CaL} measurements being made during perfusion of dyes at a concentration of 16 μM , whilst APDs were monitored at a concentration of 5 μM . I_{CaL} measurements were performed using 16 μM of each dye, because that allowed for a 0.5 log unit safety margin against the loading concentration of 5 μM . Logically, if no effect was observed at that concentration, it was unlikely that lower concentrations would produce any side-effects. In contrast, experiments to monitor APD in isolated guinea pig cells purposefully used the same concentration of dye that was used to for making optical measurements of membrane potential.

Therefore, some differences that were observed between the effects of the dyes upon I_{CaL} in canine M cells, versus those upon APD measurements in guinea pig myocytes may arise from differences between species and dye concentration. For example, acute perfusion of di-4-ANEPPDHQ on guinea pig myocytes caused a significant reduction in APD that was maintained during wash-off. Yet attempts to monitor I_{CaL} during perfusion with this dye showed that the differences observed in the recorded current washed off rapidly.

Both di-4-ANEPPS and di-8-ANEPPS were observed to have significant effects upon the time course of recovery from inactivation of L type calcium channels. However, under more physiological conditions, I_{CaL} recovery from inactivation is dependent upon voltage while peak currents can also be affected by calcium dependent facilitation. It has been shown in rabbit myocytes that increasing the frequency of voltage clamp steps from -40 mV causes a gradual decrease in peak current, whilst in similar experiments using a more physiological holding potential, around -80 mV, increases in pacing frequency increases the current (Hryshko & Bers, 1990). This facilitation is calcium dependent, but was still observed in the presence of 10 mM EGTA (but not 20 mM BAPTA (Hryshko & Bers, 1990)) and has been shown to be due to Calmodulin protein kinase II phosphorylation (Anderson *et al.*, 1994; Xiao *et al.*, 1994; Yuan & Bers, 1994). Additionally, recovery from inactivation has been shown to be slower at more positive membrane potentials in rat and guinea pig myocytes (Josephson *et al.*, 1984) and calf purkinje fibres (Kass & Sanguinetti, 1984). The protocol I used here was a twin-step voltage-clamp protocol, stepping from a holding potential of -44 mV (at which sodium channels were inactivated) to +6 mV to elicit inward calcium current and using a pipette solution containing 10 mM EGTA. Therefore, observed differences only assessed changes in recovery from inactivation at -44 mV and not at other membrane potentials. Additionally, the effects of calcium-induced facilitation were not considered.

4.2.2. The reliability of hERG binding versus hERG current data as measured in the Ionworks HT™.

Both the binding assay and the Ionworks HT™ assays demonstrated that the di-n-ANEPPS dyes exhibited an increased likelihood to interact with the hERG protein as the carbon chain length in the tails decreased. This trend was also emulated by the di-n-ANEPPDHQ dyes in the electrophysiological assay, although, both these dyes had a similar level of binding. Similarly, both assays showed that di-12-ANEPPS, followed by di-8-ANEPPS had least effect upon hERG current or binding and that di-3-ANEPPDHQ had the most. Di-4-ANEPPS and di-4-ANEPPDHQ both had similar effects. This is contrary to what would be expected for data obtained during acute perfusion of these dyes on guinea pig ventricular myocytes. Inhibition of I_{Kr} results in AP prolongation. Yet, at the same concentration, di-8-ANEPPS caused a significant increase in APD, unlike di-4-ANEPPS and di-4-ANEPPDHQ, which both caused a reduction. However, di-8-ANEPPS also showed a lower affinity for hERG protein and inhibited hERG current less than either of the other two dyes.

Data obtained from the Ionworks HT™ showed values for inhibition of hERG current that did not correspond well to the levels of binding demonstrated in the radioligand binding assay. None of the dyes tested exhibited enough inhibition of hERG current to reliably estimate an IC_{50} . Yet, IC_{50} values for di-4-ANEPPS, di-8-ANEPPS and di-4-ANEPPDHQ estimated in the binding assay, were all outside a 0.5 log unit margin compared to the final concentration tested in both assays (i.e. the IC_{50} values for hERG current inhibition are at considerably higher concentrations than those in the binding assay). In context, the level of competitive binding showed a higher affinity of all of the dyes tested for the hERG ion channel than the level of current inhibition measured in the Ionworks HT™ would indicate. The possible reasons for this must arise from either a physiological phenomenon, or as a result of the differences between the two assays.

The assays were performed on different cell types, the Ionworks HT™ utilising CHO cell lines while the binding assay incorporated HEK cells. In addition to this, cells used in the binding assay were homogenised and the resultant membranes were used. If the differences between the results from the two different methods do not arise from the different cell type, it is feasible that using non-intact cell membranes gave dye molecules access to the intracellular side of protein, which is where the binding region of the majority of hERG inhibiting compounds is located (Mitcheson *et al.*, 2000a). Previously, a binding assay using [³H]-dofetilide as a radioligand has been used to examine differences between affinity of a variety of different compounds for hERG expressed in both intact HEK cells and homogenised HEK

cell membranes (Diaz *et al.*, 2004). Although no clear differences were observed between in compound affinities for homogenised versus intact cells, a general trend for increased potency was noted in HEK cell membranes.

Similarly, dyes were applied to intact cells in the Ionworks HT™, and hence access to the intracellular region of protein would therefore have been limited. To block hERG channels, dye molecules would have to cross the lipid bilayer. This may explain why the current inhibition was higher in dyes with a shorter carbon chain length in the tail; as the length of the tail is related to the lipophilic nature of these compounds. For example, di-4-ANEPPS, which has a shorter carbon chain length than di-8-ANEPPS, has been reported to internalise more readily than di-8-ANEPPS (Rohr & Salzberg, 1994). If this caused the differences between the binding and the electrophysiological assays, the Ionworks HT™ would be more likely to resemble the effects in a cardiac ventricular cell, because both preparations use an intact cell. Alternatively, the trend seen with increasing chain length may arise from the increasing hydrophobicity of the dye molecules. Both di-8-ANEPPS and di-12-ANEPPS came out of solution at their highest concentrations in the Ionworks HT™ extracellular solution (PBS).

Another possibility is that the excitation spectra of the dyes could be responsible for a perceived increase in the binding affinity of the dyes. The binding assay is reliant upon measuring radioactivity by counting in a liquid scintillation counter. If dyes were still bound in the membrane and their excitation spectra overlap with the wavelengths emitted in the scintillation fluid it is possible that the dyes could absorb the light wavelengths that would otherwise be detected by the photocathode tubes in the scintillation counter. Whilst there is little published data detailing the exact spectra examined in the scintillation counter, the majority of scintillators emit in the blue spectrum (Burle Industries,), in which the excitation wavelengths used to excite di-8-ANEPPS, di-4-ANEPPS and di-4-ANEPPDHQ fall (460-500 nm). This would imply that di-12-ANEPPS requires different excitation wavelengths to be excited, which, although the spectra are unpublished, would be corroborated by the lack of signal I obtained with the dye when using the same optical filters as for di-8-ANEPPS, di-4-ANEPPS and di-4-ANEPPDHQ. To determine if the dyes do quench the signal, the binding assay would need to be repeated using membranes from HEK cells which had not been transfected with hERG (although these were unavailable during my work).

The differences between the two assays may also arise from a direct effect upon the hERG protein. If the dyes do bind to hERG with the affinities indicated by the binding assay, they do not necessarily have to block the channel. Instead, this would demonstrate allosteric hindrance; instead of blocking the pore, dye molecules would cause a conformational change preventing the binding of the radioligand. If this is the case it could however mean that the

dyes were unsuitable for this type of assay, because they may also prevent the binding of other ligands and therefore their detection as AP prolonging compounds. If it transpired that the compounds which inhibited hERG were being prevented access to a binding site in a number of experiments, further tests could be performed to ascertain if this is the cause of the differences between the assays. Testing could be performed in the Ionworks HT™, performing dose responses to the radioligand in the presence and absence of high concentrations of the dyes.

4.2.3. Possible causes for the effects of styryl dyes on cardiac ion channels.

Previously, screening suitable voltage-sensitive dyes for applications in biological experiments has largely been confined to studying their fluorescent properties (Tsau *et al.*, 1996; Wolff *et al.*, 2003). However, the present study demonstrates that some of these dyes have side-effects associated with them when used in isolated ventricular myocytes. Significant effects from all of the dyes examined were observed on the L type calcium channel, which suggests that these effects may not be limited to cardiac cells, since this channel is expressed in a wide variety of cell types including smooth muscle, endocrine cells, neuronal cell bodies and proximal dendrites (Catterall *et al.*, 2005b).

Modulation of the membrane electrical properties by the styryl dyes tested may arise from a number of different causes: either direct modulation of an ion channel(s) or associated β subunits, indirect modulation resulting from either interference with a second messenger pathway, or alterations in the dynamics of the lipid membrane. Interference with any second messenger pathways is possible, particularly as some membrane bound molecules exert modulation upon a large number of ion channels, either directly or indirectly. For example, PIP₂ has been reported to modulate I_{K1}, I_{KACH}, and I_{Kr} (Bian *et al.*, 2001; Cho *et al.*, 2002; Tamargo *et al.*, 2004), alterations in each of which may cause changes in APD.

It has also been shown previously that addition of the non-ionic detergents Triton X-100 and β -octyl glucoside dose dependently inhibit the sodium current and shift the steady state of inactivation to more hyperpolarized potentials, an effect which is thought to be resultant of alterations in sarcolemmal membrane characteristics and is likely to also be the reason for the similar effects upon the sodium current caused by ω -3-polyunsaturated fatty acids (Leaf *et al.*, 2003). Leifert *et al.*, (1999) also demonstrated effects of ω -3-polyunsaturated fatty acids upon the cardiac sodium current such as inhibition, shifts of activation and inactivation to more positive and negative potentials, respectively. Fluorescence anisotropy also showed that ω -3-polyunsaturated fatty acids increased the

fluidity of the membrane. Additionally, the membrane fluidising agent, benzyl alcohol also had similar effects upon the voltage dependence of activation and inactivation in sodium channels (Leifert *et al.*, 1999). Although inhibition of the sodium current would not lead to AP prolongation, these studies demonstrate that alterations in membrane dynamics can cause changes in ion channel function.

A final possibility for the actions of di-8-ANEPPS upon the cardiac AP may be via an indirect effect upon the membrane. For example, it has been shown that anchoring proteins may modulate ion channels, such as the effect of actin in modulation of cortical sodium channels (Cantiello *et al.*, 1991).

4.2.4. Choosing a suitable carrier solution for the dyes.

In addition to examining the styryl dyes, different vehicles into which stock solutions of the dyes were made were also examined. These included DMSO, DMSO containing (by weight) either 5% or 20% pluronic F127, as well as ethanol. Of these, DMSO and ethanol alone performed more favourably in the Ionworks HT™, as neither caused a significant inhibition of hERG current. However, the presence of 5% and 10% pluronic F127 by volume in DMSO caused inhibition of the hERG current and enhancement of the binding of a radioligand to hERG. Although it should be noted that DMSO containing 5% pluronic F127 did not cause any detectable alteration to the APD when perfused acutely on guinea pig ventricular cells. Ultimately, because DMSO alone was not examined in the binding assay, ethanol was selected as the more suitable carrier solution.

4.2.5. Summary.

The primary concern of the assays used to screen for suitable dyes in this chapter was to select a dye that causes the least interference to the physiology of the cardiac myocyte. The data collected in hERG binding and current assays and screens on APDs in guinea pig ventricular myocytes and calcium currents in canine M cells present a variety of different effects of both the styryl dyes tested, and the vehicle solutions into which they are dissolved. Consideration of these different effects is required to select the optimum dye and vehicle solution for further use in an assay measuring cardiac AP morphology. Di-3-ANEPPDHQ and di-4-ANEPPDHQ were not considered fit for use in an assay in cardiac myocytes. Firstly, when examined for effects upon hERG currents and binding, neither dye demonstrated

benefits compared to di-4-ANEPPS and di-8-ANEPPS, which have both been used in cardiac myocytes, either by myself or in earlier reports (Sharma & Tung, 2002; Sharma *et al.*, 2002; Sharma *et al.*, 2005; Windisch *et al.*, 1995). Secondly, although di-3-ANEPPDHQ remains untested, the severe effect of di-4-ANEPPDHQ upon both L-type calcium currents in canine M cells and guinea pig APD clearly indicates that it is unsuitable for monitoring cardiac AP morphology. Di-12-ANEPPS was selected to assess if there was a relationship between carbon tail length and effects on hERG. This dye demonstrated little affinity or efficacy for hERG. However it did present problems in terms of solubility, which may make it a poor choice. In addition, it is commercially unavailable and has no published excitation or emission spectra.

In chapter 3, di-8-ANEPPS was used successfully to record alterations in APD in response to cisapride. However the response was diminished, most probably as a result of a longer basal APD. In addition, di-8-ANEPPS significantly inhibited L-type calcium currents and had significant effects upon both voltage dependent inactivation and recovery from inactivation. In contrast, di-4-ANEPPS displayed the smallest effect on the APD of guinea pig ventricular myocytes of the three dyes tested and did not significantly alter peak calcium current or inactivation kinetics, which makes it a more suitable choice for further study.

Chapter 5:

Using di-4-ANEPPS to monitor cardiac action potential duration.

Chapter 5: Using di-4-ANEPPS to monitor cardiac action potential duration.

In Chapter 3, the relationships between the emitted fluorescence ratio and membrane potential of both di-4-ANEPPS and di-8-ANEPPS were demonstrated to be linear. Furthermore, using the set-up described in Chapter 2, I showed that it is possible to use both dyes to record action potentials (APs) from isolated guinea pig ventricular myocytes and recorded cisapride-induced alterations in APD using di-8-ANEPPS. However, using di-8-ANEPPS to optically record APs also increased the basal APD and the response to cisapride was diminished compared to that detected using a patch electrode. In Chapter 4, acutely applying di-8-ANEPPS in the tissue bath, in absence of excitation light, increased the APD, confirming that the dye had pharmacological side effects. Screening different styryl dyes demonstrated that di-4-ANEPPS did not have such a pronounced effect upon APD in guinea pig myocytes, although APs were shortened marginally during acute perfusion of the dye. Additionally, in canine myocytes, di-8-ANEPPS significantly reduced the inward calcium current and altered the voltage-dependence of inactivation and timescale of recovery from inactivation. In contrast, di-4-ANEPPS only had significant effects upon recovery from inactivation in L-type calcium channels. Based upon these observations, di-4-ANEPPS was selected for further use in monitoring drug-induced alterations in APD.

This project aims to develop an optical technique that has the potential to be used as a screen for proarrhythmic potential in pharmaceutical candidate compounds by assessing their effects upon APD. Currently, a number of *in vitro* assays have been developed for this purpose and have demonstrated success in recording drug-induced alterations in APD. These include sharp electrode recordings from canine midmyocardial cells (M cells) and Purkinje fibres; both of which have been shown to be sensitive to drug-induced alterations in APD morphology (Abi-Gerges *et al.*, 2004; Champeroux *et al.*, 2005; Gintant *et al.*, 2001; Liu & Antzelevitch, 1995). Essentially, the optical assay is intended for generation of data similar to both these assays, but with a reduction in labour and an increase in throughput; all three of these assays monitor AP morphology and use measurements of APD and triangulation in assessment of potential risk.

One of the difficulties of monitoring AP morphology using voltage-sensitive dyes is that recordings are subject to substantially more noise when compared to more conventional electrophysiological techniques. Detection of the APD at different levels of repolarisation requires calculation of the values for zero and maximum repolarisation. From optically derived data, the latter of these presents little difficulty and can be calculated from an average

of data sampled between APs, the resting membrane potential (RMP). However, zero repolarisation occurs at the peak of the upstroke of an AP, which is brief in duration and therefore more difficult to accurately assess. Similarly, durations calculated in and around the plateau phase of an AP are subject to more interference from noise and can be difficult to assess. This made analysis of APDs from optical recordings in Chapter 3 difficult and time-consuming. Thus, whilst recordings of APs using optical techniques used a practical technique that was easier and quicker to achieve compared to standard electrode techniques, data analysis was substantially more time consuming.

To test the potential of the optical technique to identify proarrhythmic compounds, di-4-ANEPPS was used to assess changes in APD induced in guinea pig ventricular cardiomyocytes by a group of four well-characterised double-blinded compounds. Additionally, to assess the value of using di-4-ANEPPS to monitor APD morphology, changes in APD detected optically were compared to those obtained using sharp electrodes from canine Purkinje fibres and M cells. To make analysis of optical data more efficient, APDs generated from the fluorescence emission of di-4-ANEPPS were calculated using a computer-based spreadsheet.

5.1. Optically detecting drug-induced alterations in APD and comparing them to results from sharp electrode techniques.

Pharmaceutical preclinical screens used to detect changes in APD often analyse test compounds at predetermined concentrations. These can be based upon the limit of solubility or to assess safety at concentrations relevant to plasma levels expected clinically. Additionally, the effect of a candidate drug upon APD will not previously have been assessed, hence the requirement for the screen. However, to assess the feasibility of using di-4-ANEPPS to monitor APD, compounds selected were required to have either a known effect or lack thereof upon cardiac AP morphology. Therefore APs were recorded using di-4-ANEPPS from cells exposed to well-characterised compounds supplied at prearranged concentrations. This was performed in a double-blinded manner. I was not aware of the identity of the compounds being examined for their effects upon APD and records were assigned random numbers prior to analysis to avoid bias.

APs were recorded from isolated guinea pig myocytes using the methods developed in Chapter 3. Cells were incubated with 5 μ M di-4-ANEPPS (prepared from a stock solution in ethanol) for 20 min at room temperature. Additionally, throughout the duration of an experiment, cells were superfused with normal Tyrode containing a maintenance dose of 200

nM of the dye. The amount of time taken for solution to reach the tissue bath was roughly 1 min. Myocytes were field stimulated at 1 Hz and exposed to excitation light for 5 s in every 4 min; this allowed 1 min for changes of solution to reach the tissue bath and 3 min for changes in compound or concentration to take effect, prior to optical recordings being made. This also allowed the sampling of a maximum of 5 action potentials at each concentration, which were averaged for the determination of APD. Additionally, each cell was exposed to 300 nM cisapride following the final dose of test compound as a positive control.

Previously, in Chapter 3, APs were sampled at 1 kHz. However, sampling at 10 kHz provided greater flexibility for developing a computer based spreadsheet to analyse APs. An algorithm was developed to detect specific regions of the AP for calculation of APDs at differing repolarisation values. These included the baseline, the value considered to be 100% repolarisation, and 0% repolarisation. Time-points were also calculated for the start of the AP. The details of the algorithm used to determine APDs can be seen in Appendix A.

Additionally, APDs obtained using the emitted fluorescence from di-4-ANEPPS in response to test compounds were compared to data obtained from current preclinical safety pharmacology screens: sharp electrode recordings from canine M cells and Purkinje fibres*. M cells were stimulated using a sharp electrode containing 3M potassium chloride. Recordings of APs from Purkinje fibres were also obtained using a sharp electrode, but cells were stimulated via electrodes pinned through the ventricular muscle at each end of the fibre bundle. There were also differences between the stimulation protocols used between optical and sharp electrode recordings. Optical recordings were made from isolated myocytes that were stimulated at 1 Hz throughout the duration of the experiment and doses were changed once every four min. In contrast, because the duration of acquisition using sharp electrodes was not limited by photo-effects, doses were only altered once the APD was determined to have reached a steady state. Additionally, reverse-use dependence was assessed using sharp electrode recordings, so that at each dose, cells were paced at 1 Hz until steady state was obtained, then at 0.5Hz (data not shown) and then at 1 Hz, during which APDs used for analysis were acquired. Additionally, because the number of exposures to excitation was limited to avoid phototoxicity, optical data were compared to values during perfusion with Tyrode, whereas APDs recorded from Purkinje fibres and M cells were compared to values obtained in Tyrode containing the vehicle (0.1% DMSO).

The degree of triangulation caused by each compound was also evaluated for data obtained optically from guinea pig ventricular myocytes and compared to those obtained with sharp electrodes from canine M cells and Purkinje fibres. Triangulation from canine APDs

* Data obtained from sharp electrode recordings from Purkinje fibres and canine M cells was donated by the Dept. of Safety Pharmacology, AstraZeneca.

was determined by the difference in duration between the APD at 50% and 90% repolarisation. To allow for comparisons between different assays, triangulation was expressed as a percentage of values recorded under control conditions according to equation 5.1, where $Test(APD_{90} - APD_{50})$ is the triangulation in the presence of a known concentration of compound and $Control(APD_{90} - APD_{50})$ is the triangulation in control conditions.

$$Triangulation(\%control) = \frac{100 * Test(APD_{90} - APD_{50})}{Control(APD_{90} - APD_{50})}$$

Equation 5.1. Calculation for triangulation.

Previously (refer to Chapter 3), APDs calculated at 40 and 50% repolarisation were found to be longer in duration from optical records of APs, when compared to less noisy electrical data that was recorded simultaneously. Therefore, triangulation from optical records from guinea pig myocytes was calculated as the difference between the APD_{90} and APD_{50} , as well as between APD_{90} and APD_{40} . Terrar *et al.*, (2007) also demonstrated triangulation using the difference between APDs measured at 40 and 50% repolarisation. To allow for comparison between the different methods and tissue types, these data were expressed as a change in triangulation, relative to the duration obtained under control/vehicle conditions.

Compounds selected for analysis were d-sotalol, terfenadine, pinacidil and glucose.

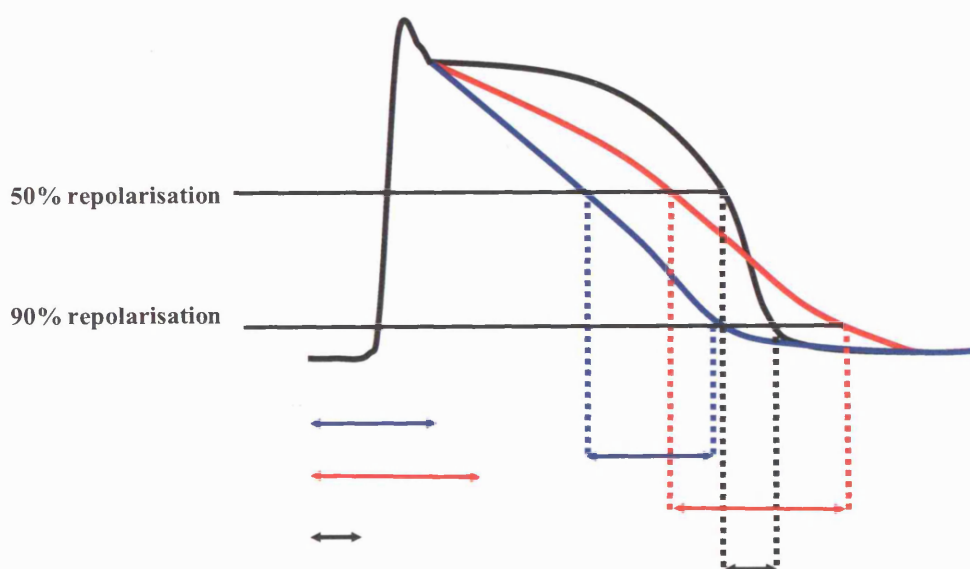


Figure 5. 1. Illustrating the measurement of triangulation.

Illustrations of three action potentials showing increases in the duration between action potential durations measured at 50 and 90% repolarisation. A normal action potential is shown in black. Two triangulated action potentials are also shown: the red action potential is triangulated such that the APD increases and the blue action potential such that the APD shortens. In both examples the difference between the APD_{90} and APD_{50} is increased compared to the normal action potential.

5.1.1. The effects on APD of d-sotalol

Figure 5.2A shows two averages of 5 APs recorded using the fluorescence emission of di-4-ANEPPS in response to increasing concentrations of d-sotalol, which is an I_{K_r} specific blocker (Advani & Singh, 1995). The red record, which was made in the presence of 100 μM d-sotalol, is longer in duration than the averaged AP recorded under control conditions. Figure 5.2B is a graph of the absolute values of APDs recorded at 40, 50, 70 and 90% repolarisation from 6 cells under control conditions and with increasing concentrations of d-sotalol (0.01, 0.1, 1.0, 10.0 and 100.0 μM). This caused a significant increase in APD_{90} from 221 ± 27 ms under control conditions, to 291 ± 16 ms in the presence of 100 μM d-sotalol (mean \pm SEM, $p < 0.01$, repeated measures ANOVA, Dunnett's post test, $n = 7$). Expression of the same data as a percentage of the values measured under control conditions (Figure 5.2C), shows that values of APD_{40} , APD_{50} , APD_{70} , and APD_{90} all prolonged by the same relative duration. At the maximum concentration of d-sotalol, values of APD measured at 40% repolarisation increased by $46 \pm 30\%$, which are similar to values recorded at 90% repolarisation, $43 \pm 21\%$.

Sharp electrode recordings from canine Purkinje fibres and M cells also demonstrated an increase in APD in response to increases in concentration of d-sotalol. Both these preparations were exposed to 1, 10, 30 and 100 μM d-sotalol. Figure 5.3A shows individual records made with a sharp electrode from canine Purkinje fibres. At 100 μM d-sotalol, APDs at 90% repolarisation recorded from Purkinje fibres increased from 269 ± 8 ms in the presence of 0.1% DMSO to 430 ± 40 ms and increases in APD were very significant at 30 and 100 μM (mean \pm SEM, $p < 0.01$, repeated measures ANOVA, Dunnett's post test, $n = 3$). Similarly, values of APD_{90} recorded from M cells significantly increased from 364 ± 21 ms in the presence of 0.1% DMSO to 467 ± 35 ms in 100 μM d-sotalol (mean \pm SEM, $p < 0.01$, repeated measures ANOVA, Dunnett's post test, $n = 4$). Figure 5.3B and Figure 5.3C show the relative increases in APD recorded from M cells and Purkinje fibres. M cells had a similar relative increase in APD at different stages of repolarisation; compared to values obtained in the presence of 0.1% DMSO; APDs at 50 and 90% repolarisation increased by $27 \pm 5\%$ and $28 \pm 3\%$, respectively. Relative increases in APD recorded at 50 and 90% repolarisation from canine Purkinje fibres were also similar ($54 \pm 14\%$ and $59 \pm 12\%$).

Figure 5.4 compares values obtained in response to increasing concentrations of d-sotalol recorded using the three different tissue types. Figure 5.4A shows the relative increases in APD_{90} . All three different assays clearly demonstrate an increase in APD with increasing concentrations of d-sotalol. At 100 μM d-sotalol, there was no significant difference between the relative increases observed with canine M cells, Purkinje fibres or

optical measurements from guinea pig cells. However, at 30 μ M d-sotalol, Purkinje fibres did display an increased sensitivity compared to M cells (means \pm SEM, $14 \pm 4\%$, $n = 3$, vs. $36 \pm 7\%$, $n = 4$, respectively, $p < 0.05$, unpaired Student's t test).

The degree of triangulation in response to increasing concentrations of d-sotalol from optical recordings from guinea pig cells were determined as the change in duration between APD₉₀ and APD₅₀ and between APD₉₀ and APD₄₀. Both the different calculations of triangulation showed significance at the highest concentration of d-sotalol tested, 100 μ M (APD₉₀₋₄₀: $p < 0.01$; APD₉₀₋₅₀: $p < 0.05$, repeated measures ANOVA, Dunnett's posthoc test, $n = 6$). Similarly, increases in concentration of d-sotalol caused a significant increase in triangulation at 100 μ M to APs recorded from Purkinje fibres, from 84 ± 10 ms in vehicle to 153 ± 34 ms (APD₉₀₋₅₀: $p < 0.05$, repeated measures ANOVA, Dunnett's posthoc test, $n = 3$). However, although there was a trend toward an increase in triangulation in APDs recorded from M cells this was not significant.

Figure 5.4B compares the relative values of triangulation for the three different assays as a percentage of the control values (for optical recordings) or of the vehicle. In each assay there is an increase in triangulation caused by increases in the concentration of d-sotalol. Statistical analysis between the different assays at the highest concentration of d-sotalol firstly showed that increases in triangulation in Purkinje fibres, $77 \pm 18\%$, were significantly greater than increases in M cells, $28 \pm 20\%$ ($p < 0.01$ repeated measures ANOVA, Tukey's posthoc test) and increases recorded from guinea pig myocytes 37 ± 18 ($p < 0.05$) using the difference in durations between 90 and 50% repolarisation. Optical measurements of triangulation calculated using the difference in APDs between 90 and 40 % repolarisation ($52 \pm 12\%$) were not statistically different from either assay.

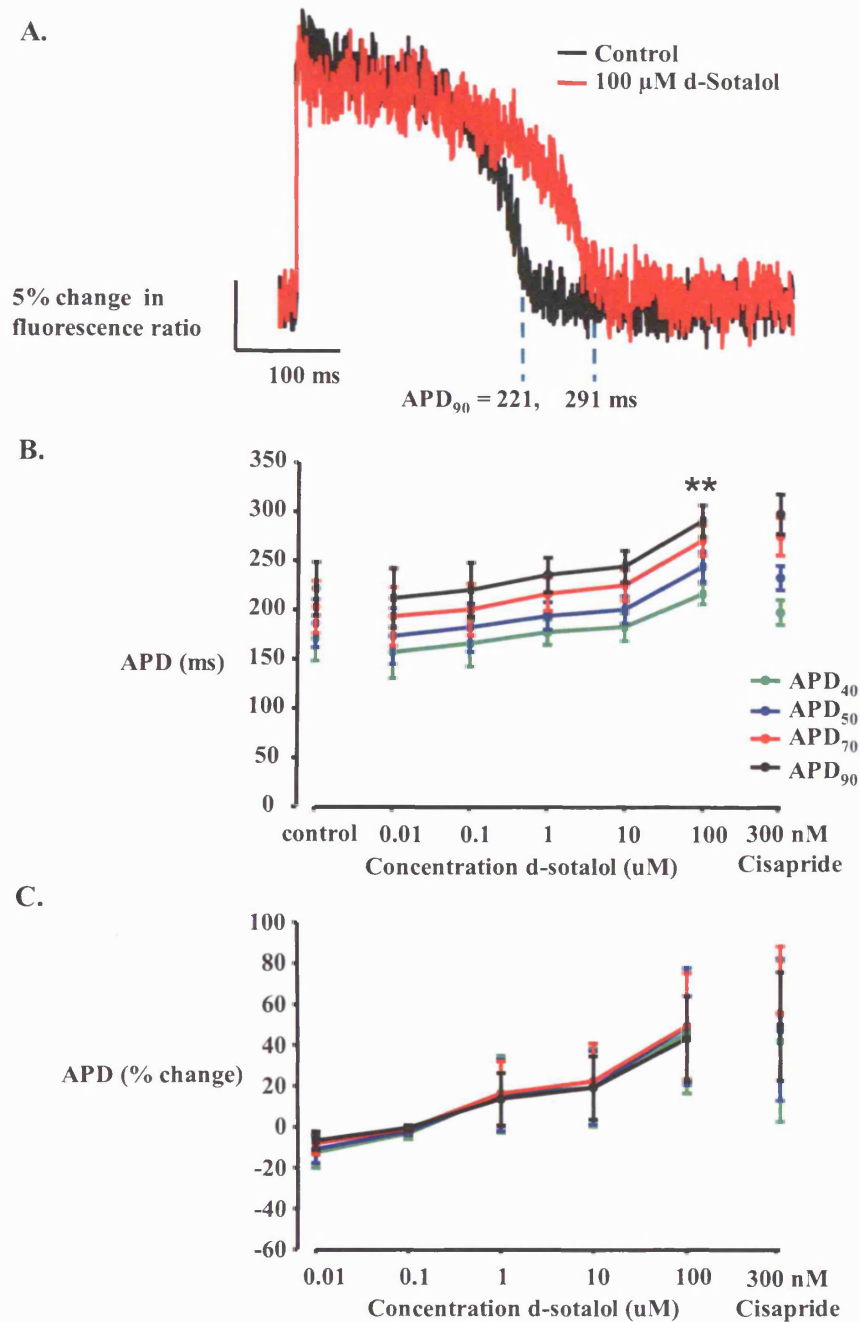


Figure 5.2. Increases in APD recorded optically from guinea pig myocytes in response to increasing concentrations of d-sotalol.

(A) Averages of 5 action potentials recorded from isolated guinea pig ventricular cells using di-4-ANEPPS under control conditions (black) and in the presence of 100 μM d-sotalol (red). (B) graph showing the absolute action potential durations from 6 cells exposed to increasing concentrations of d-sotalol. Durations are shown for repolarisation stages at 40, 50, 70 and 90%. Data are expressed as means ± SEM, APD₉₀ values are significant at 100 μM d-sotalol compared to control, $p < 0.01$, repeated measures ANOVA, Dunnett's posthoc test. (C) Data from (B) expressed as a percentage change. At repolarisation stages between 40% and 50%, action potential durations all express the similar relative changes.

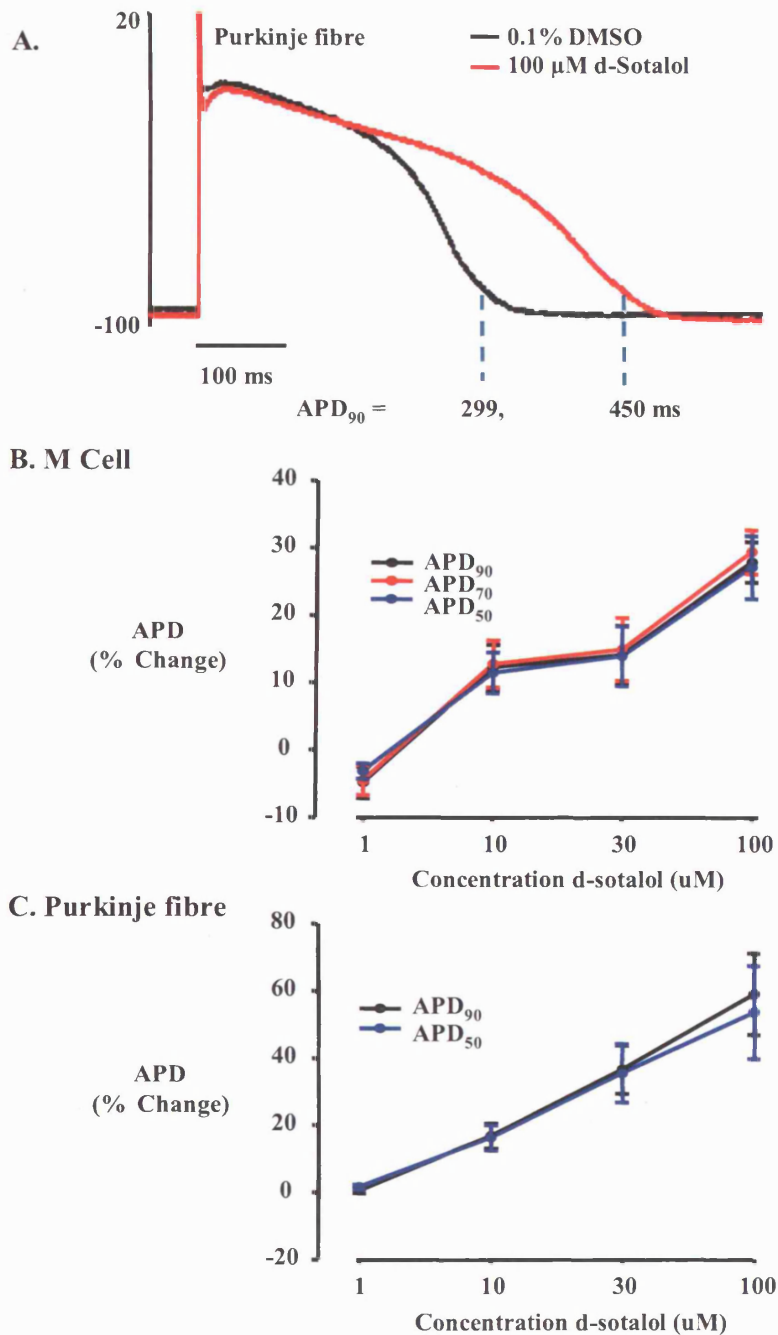


Figure 5.3. Increases in APD recorded with a sharp electrode from canine M cells and Purkinje fibres in response to increasing concentrations of d-sotalol.

(A) Individual records recorded from a canine Purkinje fibre in the presence of 0.1% DMSO (black) and in the presence of 100 μ M d-sotalol (red). (B) Graph showing the percentage change in action potential durations recorded from canine M cells exposed to increasing concentrations of d-sotalol. Values are shown for repolarisation stages at 50, 70 and 90%. Data expressed as means \pm SEM, n = 4. (C) Graph showing the percentage change in action potential durations recorded from canine M cells exposed to increasing concentrations of d-sotalol. Values are shown for repolarisation stages at 50 and 90%. Data expressed as means \pm SEM, n = 3.

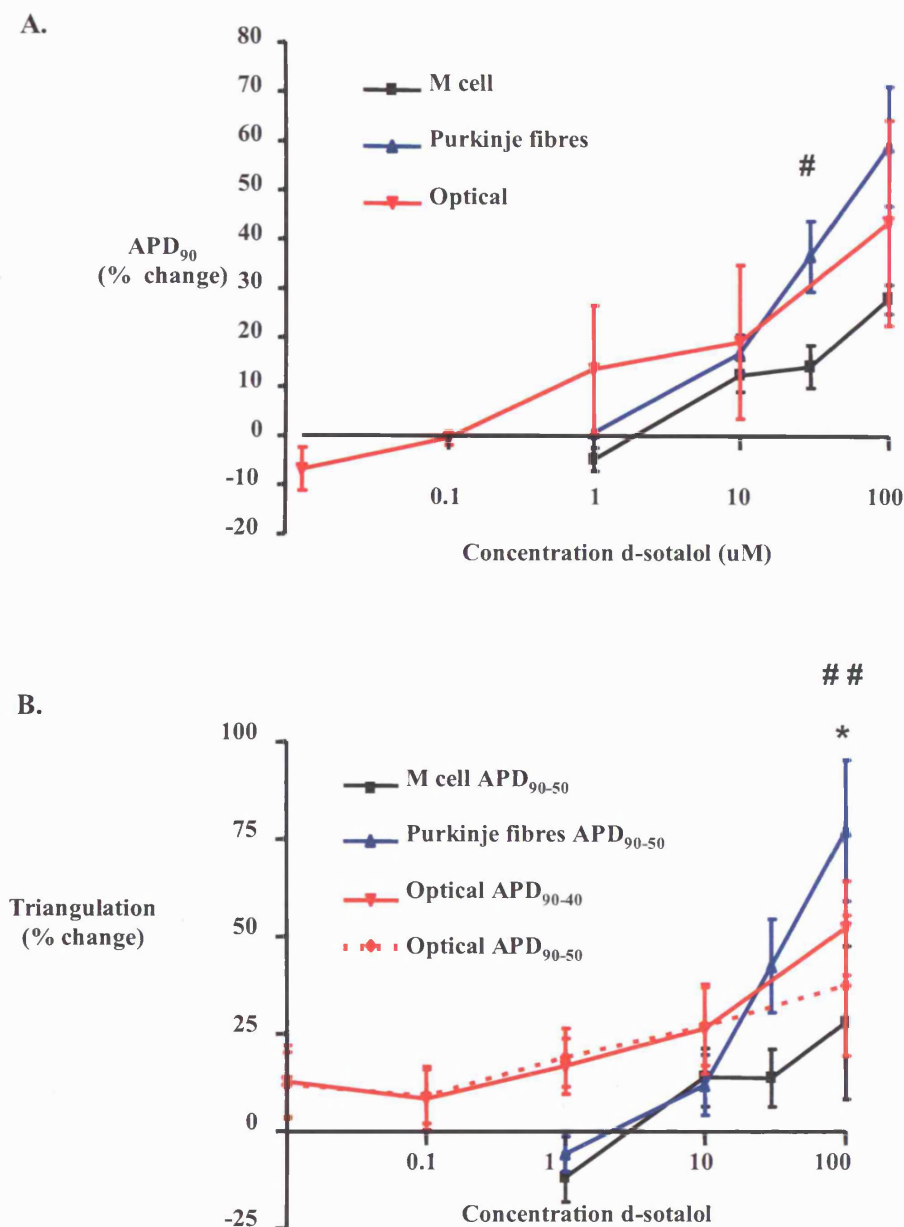


Figure 5.4. Changes in APDs and triangulation recorded optically from guinea pig myocytes or with a sharp electrode from canine M cells and Purkinje fibres in response to increasing concentrations of d-sotalol.

(A) Graph showing the relative increases in APD₉₀ recorded with di-4-ANEPPS from guinea pig ventricular myocytes (red triangles, $n = 6$), canine M cells (black squares, $n = 4$) and canine Purkinje fibres (blue triangles, $n = 3$) in response to increasing concentrations of d-sotalol. # indicates statistical significance between M cell and Purkinje fibre data, $p < 0.05$, unpaired Student's t test. (B) Graph showing changes in triangulation relative to control for optical measurements and 0.1% for sharp electrode measurements. Data are recorded from the same cells/fibres treated in (A). Data are expressed as means \pm SEM, ## indicates statistical significance between M cell and Purkinje fibre data, $p < 0.01$. * indicates statistical significance between M cell and optical data APD₉₀₋₄₀, $p < 0.05$, ANOVA, Tukey posthoc test.

5.1.2. The effects on APD of terfenadine.

Previously, terfenadine has been shown to have effects upon multiple ion channels (Li *et al.*, 2006; Ming & Nordin, 1995). Optical measurements of APDs at stages of repolarisation between 40 and 50% revealed a decrease in duration at the maximum concentration of terfenadine, 3 μM (see Figure 5.5A). This can be seen in the graph in Figure 5.5B; at 90% repolarisation, APDs recorded during perfusion of 3 μM terfenadine were significantly shorter than control values (252 ± 12 ms versus 188 ± 21 ms, mean \pm SEM, $p < 0.01$, $n = 6$, repeated measures ANOVA, Dunnett's post test). Terfenadine concentrations of 0.1 and 0.3 μM did not produce a significant effect, although the mean duration was increased compared to control at all of the stages of repolarisation measured. Figure 5.5C shows the changes in APD in response to increasing concentrations of terfenadine expressed as a percentage. Relative to control values, changes in APD_{40} were less than those recorded between 50 and 90% repolarisation at concentrations of terfenadine between 0.1 and 1 μM , however this was not significant.

Canine Purkinje fibres and M cells were exposed to concentrations of terfenadine of 0.01, 0.1, 1 and 10 μM . Sharp electrode recordings from canine M cells had similar changes in APD duration in response to increasing concentrations of terfenadine as were observed in optical recordings from guinea pig myocytes. Exposure to 0.1 μM terfenadine produced a small increase in APD_{90} from 369 ± 16 ms, in the presence of 0.1% DMSO, to 391 ± 21 ms, although this was not significant. However, at 1 and 10 μM there was a very significant reduction in APD ($p < 0.01$, ANOVA, Dunnett's post test, $n = 8-10$) At the highest concentration tested, 10 μM , the APD_{90} was reduced to 96 ± 10 ms (means \pm SEM). As can be seen in Figure 5.6B, the relative changes in APD were similar at repolarisation stages between 50 and 90%. For example, at 10 μM terfenadine, APD_{50} and APD_{90} had reduced to $27 \pm 5\%$ and $28 \pm 3\%$ of the value in 0.1% DMSO. In contrast to values obtained from guinea pig ventricular myocytes and canine M cells, there was no observed effect upon the APD_{90} recorded from canine Purkinje fibres at any of the concentrations of terfenadine tested. However, at the highest concentration of terfenadine, 10 μM , the APD_{50} was significantly reduced from 217 ± 16 ms to 192 ± 13 ms (mean \pm SEM, $p < 0.05$, repeated measures ANOVA, Dunnett's post test, $n = 7$).

Figure 5.7 shows graphs of the relative APD_{90} and triangulation obtained in response to terfenadine from canine M cells and Purkinje fibres, as well as optically from guinea pig ventricular myocytes. The decrease in APD_{90} was greater when recorded from M cells with a sharp electrode than when recorded with the fluorescence emission of di-4-ANEPPS from

guinea pig cells. In the presence of 1 μ M terfenadine, optically recorded values of APD₉₀ in guinea pig myocytes were reduced from control by $10 \pm 7\%$, compared to a value of $34 \pm 7\%$ in canine M cells ($p < 0.05$, Student's t-test).

At the highest concentration of terfenadine, a significant decrease in triangulation was detectable in sharp electrode recordings from M cells, from 48 ± 4 ms to 25 ± 4 ms ($p < 0.05$, ANOVA, Dunnett's post test, $n = 8-10$). In contrast, at the same concentration of terfenadine, an increase in triangulation was detected in sharp electrode recordings from Purkinje fibres, from 82 ± 8 ms in the presence of 0.1% DMSO to 110 ± 13 ms ($p < 0.01$, repeated measures ANOVA, Dunnett's post test, $n = 8-10$). Measurements of triangulation recorded optically from guinea pig ventricular myocytes displayed a similar trend to those observed in canine M cells. However, changes in triangulation recorded in this manner were not significant, although the maximal concentration tested was 3 μ M as compared to 10 μ M in canine tissues. Figure 5.7 compares changes in triangulation recorded using the three different tissue types relative to measurements taken under control or vehicle conditions. These are expressed as percentages to allow for comparison between the tissue types. That terfenadine had significantly opposite effects upon triangulation in Purkinje fibres compared to M cells is shown clearly ($p < 0.001$, Student's t-test).

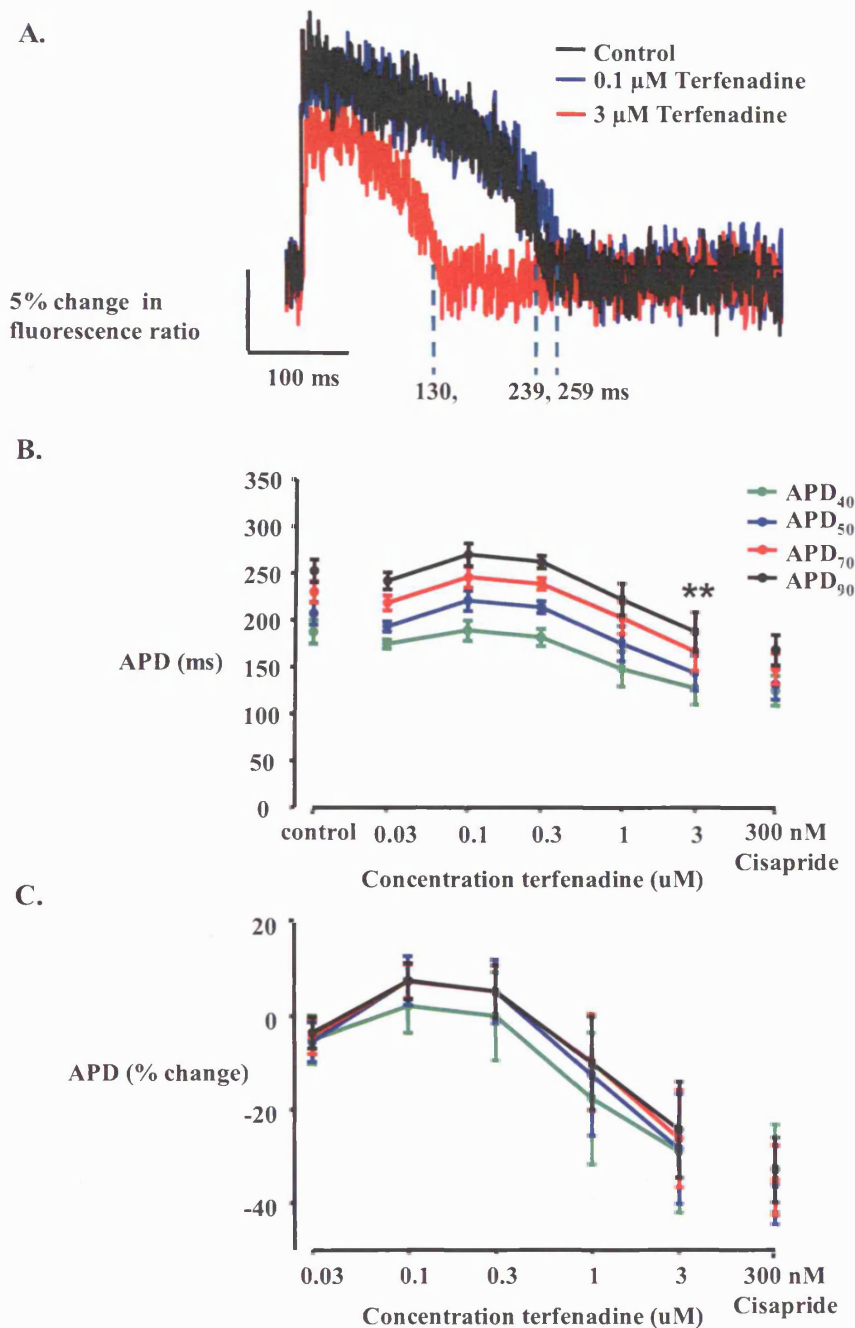


Figure 5.5. Changes in APD recorded optically from guinea pig myocytes in response to increasing concentrations of terfenadine.

(A) Averages of 5 records recorded from isolated guinea pig ventricular cells using di-4-ANEPPS under control conditions (black), 0.1 μM terfenadine (blue) and in the presence of 3 μM terfenadine (red). (B) Graph showing the absolute action potential durations from 7 cells exposed to increasing concentrations of terfenadine. Durations are shown for repolarisation stages at 40, 50, 70 and 90%. Data are expressed as means ± SEM, APD₉₀ values are significant at 3 μM terfenadine compared to control, $p < 0.01$, repeated measures ANOVA, Dunnett's posthoc test. (C) Data from (B) expressed as a percentage change.

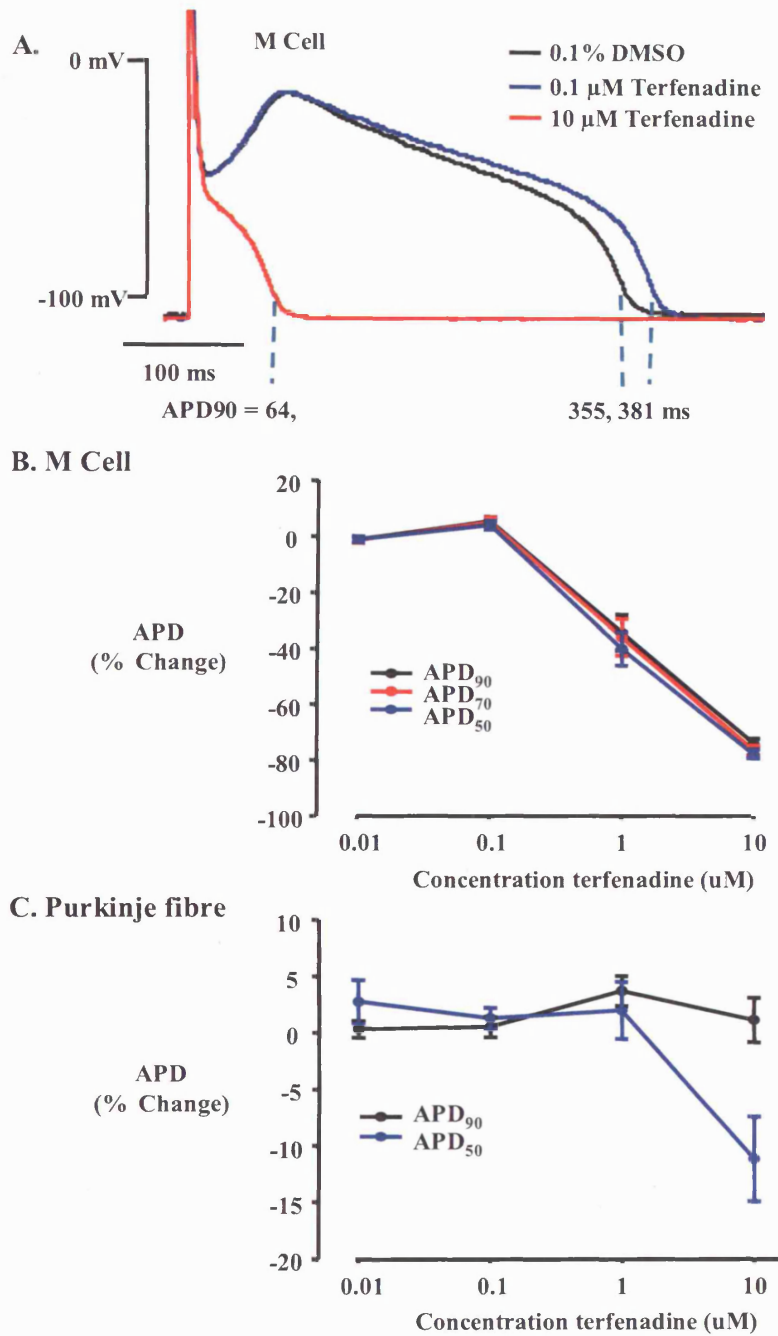


Figure 5.6. Changes in APD recorded with a sharp electrode from canine M cells and Purkinje fibres in response to increasing concentrations of terfenadine.

(A) Individual records recorded from a canine M cell in the presence of 0.1% DMSO (black) and in the presence of 0.1 (blue) and 10 μM terfenadine (red). (B) Graph showing the percentage change in action potential durations recorded from canine M cells exposed to increasing concentrations of terfenadine. Values are shown for repolarisation stages at 50, 70 and 90%. Data are expressed as means ± SEM, n = 8-10. (C) Graph showing the percentage change in action potential durations recorded from canine M cells exposed to increasing concentrations of d-sotalol. Values are shown for repolarisation stages at 50 and 90%. Data are expressed as means ± SEM, n = 7.

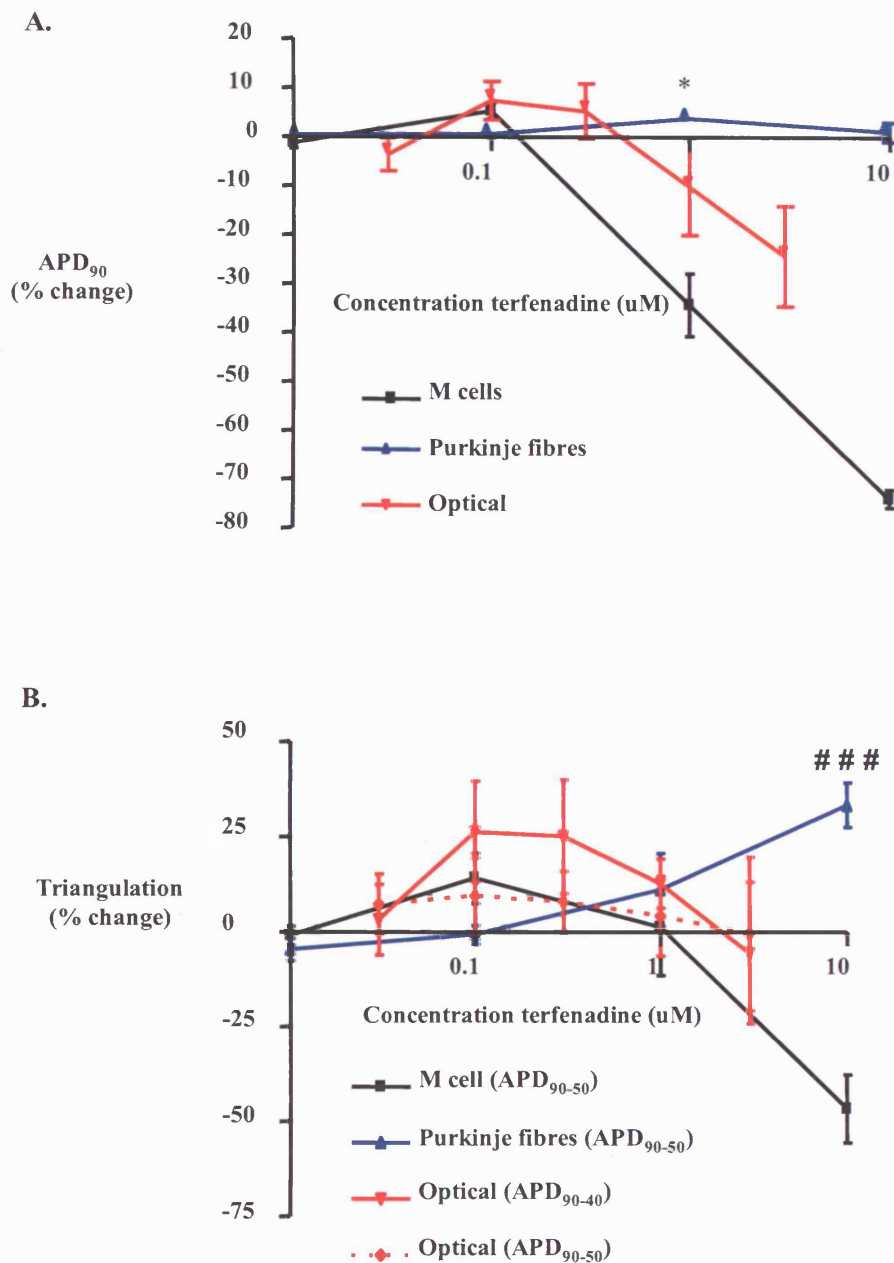


Figure 5.7. APDs and triangulation recorded optically from guinea pig myocytes or with a sharp electrode from canine M cells and Purkinje fibres in response to increasing concentrations of terfenadine.

(A) Graph showing the relative increases in APD₉₀ recorded with di-4-ANEPPS from guinea pig ventricular myocytes (red triangles, n = 6), canine M cells (black squares, n = 8-10) and canine Purkinje fibres (blue triangles, n = 7) in response to increasing concentrations of terfenadine. * indicates statistical significance between M cell and optical data, p < 0.05, Student's t-test. (B) graph showing changes in triangulation relative to control for optical measurements and 0.1% for sharp electrode measurements. Data are recorded from the same cells/fibres treated in (A). Data are expressed as means ± SEM, ### indicates statistical significance between M cell and Purkinje fibre data, p < 0.05, Student's t-test.

5.1.3. The effects on APD of pinacidil.

APDs were recorded optically from guinea pig myocytes at increasing concentrations of 0.03, 0.1, 0.3, 1 and 3 μM of pinacidil, which is an activator of $I_{K(ATP)}$ channels (Hermsmeyer, 1988). Even at the maximum concentration of 3 μM pinacidil, no effect upon APD was observed at repolarisation stages of 40, 50, 70 and 90% (see Figure 5.8). Values of APD_{90} were 253 ± 8 ms under control conditions versus 261 ± 11 ms during perfusion with 3 μM pinacidil (mean \pm SEM, $n = 10$). However, following the application of the highest concentration of pinacidil, cells were superfused with 300 nM cisapride, which caused a significant increase in APD. At 90% repolarisation, the mean APD was 326 ± 19 ms (mean \pm SEM, $p < 0.001$ versus control, paired Student's t test, $n = 10$). This suggests that pinacidil had no effect in this assay at the concentrations tested.

Figure 5.9 shows individual records recorded from Purkinje fibres and canine M cells in the presence of differing concentrations of pinacidil as well as graphs showing the relative changes in APD for each tissue type. 3 μM pinacidil caused a small reduction in APDs recorded from canine M cells (9 ± 2 % reduction in APD_{90}). However, this was a relatively small reduction in APD comparative to that observed in recordings from canine Purkinje fibres, which were 42 ± 6 %. Increases in the concentration of pinacidil to canine M cells did produce significantly larger decreases in APD which were equal to 86 ± 1 % at the maximal concentration tested (30 μM) ($p < 0.01$, Student's t -test, $n = 3-4$).

Figure 5.10 compares values for APD_{90} obtained from each of the three different assays. This clearly shows that at lower concentrations of pinacidil there was a much larger decrease in APD_{90} in Purkinje fibres (41.6 ± 6.2 %, $n = 4$), than was present in M cells (8.6 ± 1.8 %, $n = 7$), as well as the lack of response observed with guinea pig ventricular cells in the optical assay (an increase of 3.2 ± 2.4 %, $n = 10$). Each of the different assays was significantly different ($p < 0.001$, ANOVA in each case).

Measurements of triangulation failed to demonstrate any trend in any of the three assays being evaluated up to a concentration of 10 μM . However, at 30 μM pinacidil there was a 40 ± 11 % reduction in triangulation recorded from canine M cells, which were the only cell type examined at this concentration, although this was not significant.

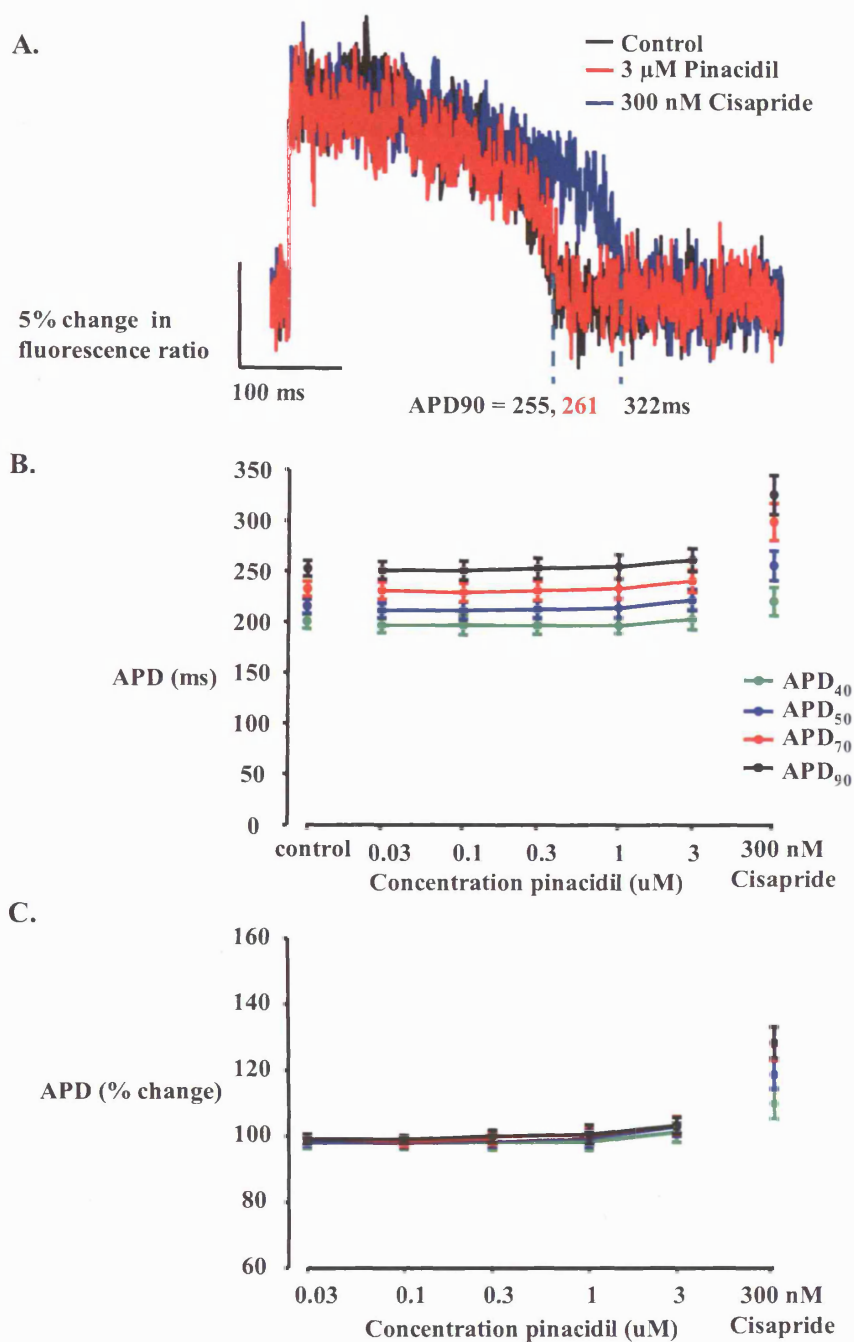


Figure 5.8. APDs recorded optically from guinea pig myocytes in response to increasing concentrations of pinacidil.

(A) Averages of 5 records recorded from isolated guinea pig ventricular cells using di-4-ANEPPS under control conditions (black), 3 μM pinacidil (red) and in the presence of 300 nM cisapride (blue).

(B) Graph showing the absolute action potential durations from 10 cells exposed to increasing concentrations of terfenadine. Durations are shown for repolarisation stages at 40, 50, 70 and 90%. Data are expressed as means \pm SEM.

(C) Data from (B) expressed as a percentage change.

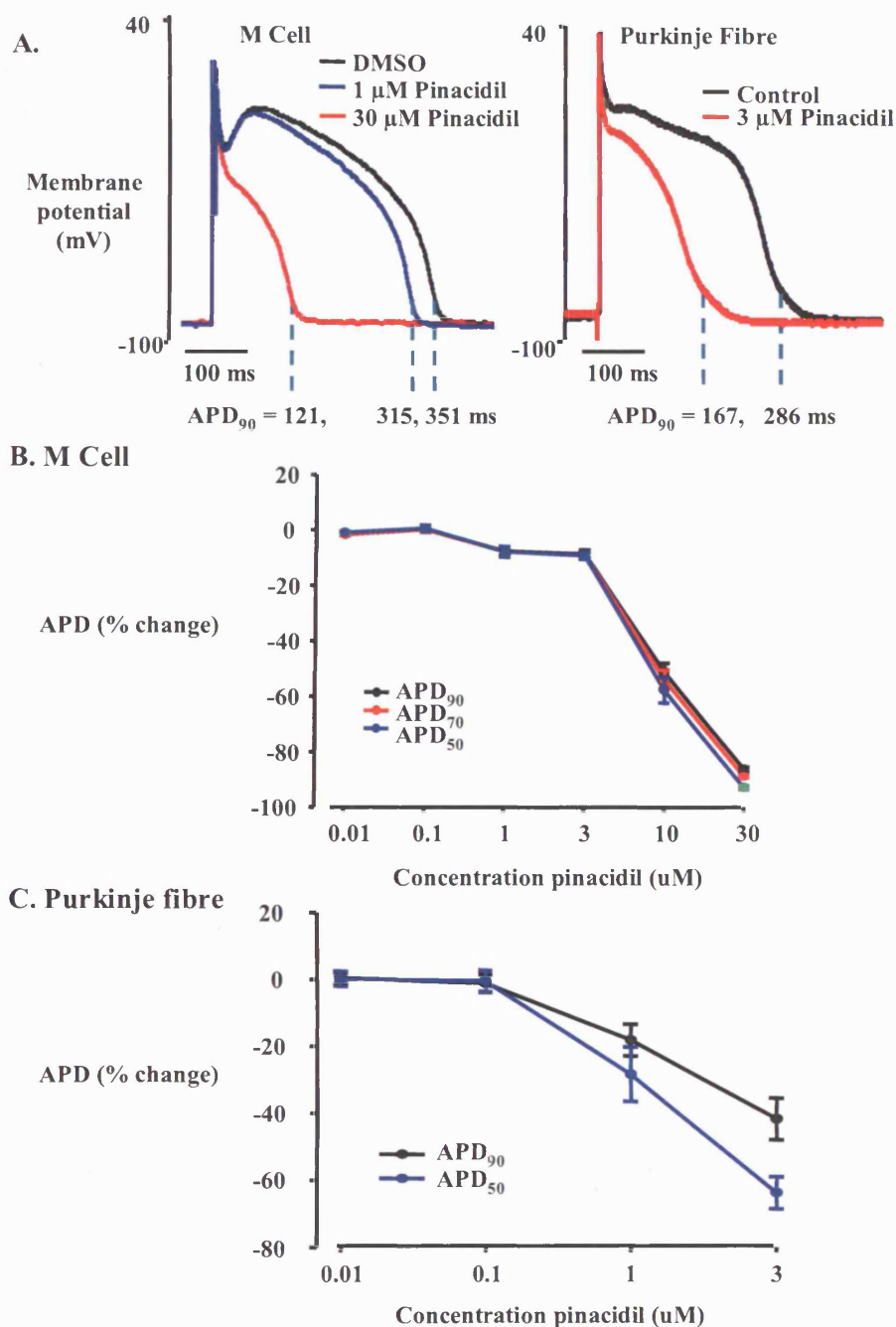


Figure 5.9. Changes in APD recorded with a sharp electrode from canine M cells and Purkinje fibres in response to increasing concentrations of pinacidil.

(A) Individual records recorded from a canine M cell (left) in the presence of 0.1% DMSO (black) and in the presence of 1 (blue) and 30 μ M pinacidil (red). Records from a canine Purkinje fibre (right) under control conditions (black) and in the presence of 3 μ M pinacidil (red). (B) graph showing the percentage change in action potential durations recorded from canine M cells exposed to increasing concentrations of pinacidil. Values are shown for repolarisation stages at 50, 70 and 90%. Data expressed as means \pm SEM, $n = 3-7$. (C) graph showing the percentage change in action potential durations recorded from canine M cells exposed to increasing concentrations of pinacidil. Values are shown for repolarisation stages at 50 and 90% Data expressed as means \pm SEM, $n = 4$.

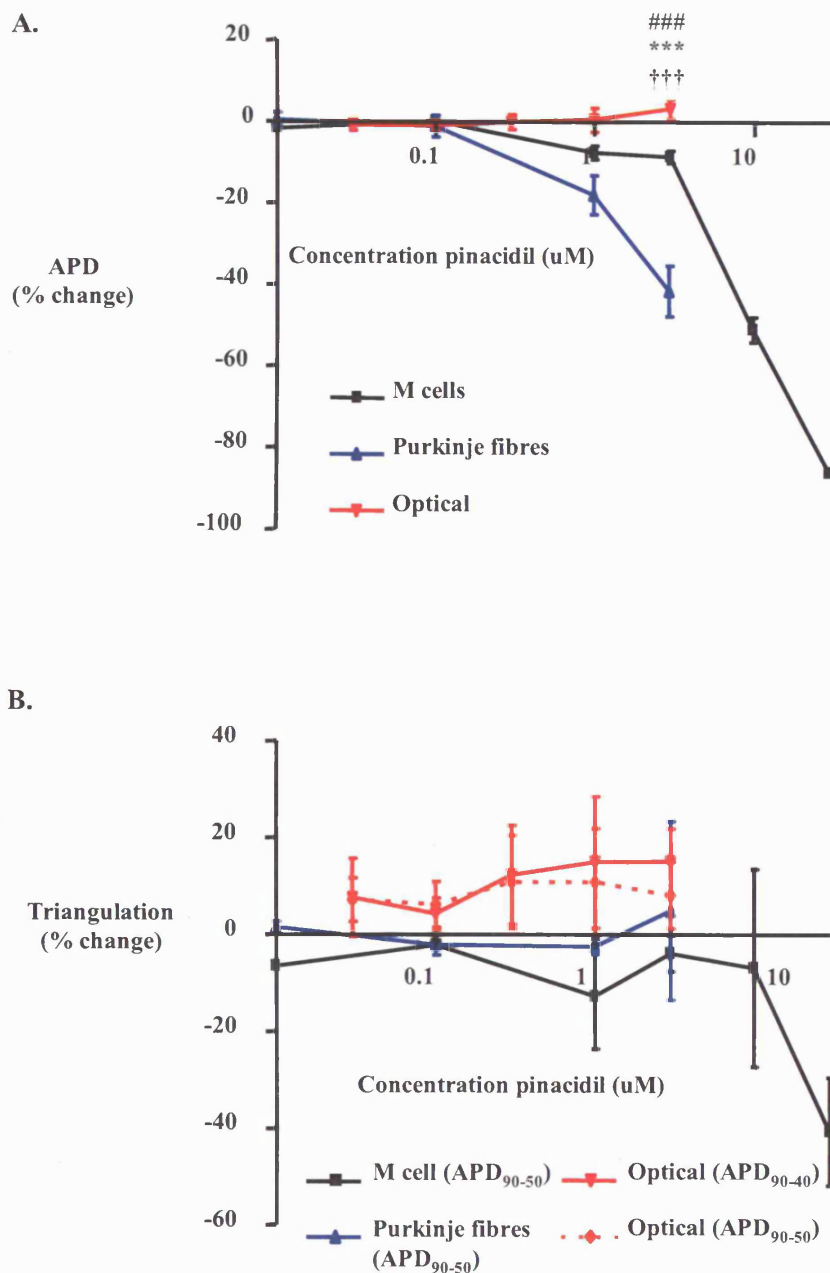


Figure 5.10. APDs and triangulation recorded optically from guinea pig myocytes or with a sharp electrode from canine M cells and Purkinje fibres in response to increasing concentrations of pinacidil.

(A) Graph showing the relative increases in APD₉₀ recorded with di-4-ANEPPS from guinea pig ventricular myocytes (red triangles, n = 10), canine M cells (black squares, n = 3-7) and canine Purkinje fibres (blue triangles, n = 4) in response to increasing concentrations of pinacidil. Data are expressed as means ± SEM, ###, *** and ††† indicates statistical significance between M cell and Purkinje fibre data, Purkinje and optical data and M cell and optical data, p < 0.001, indicates statistical significance between M cell and Purkinje fibre data, p < 0.001, ANOVA. (B) Graph showing changes in triangulation relative to control for optical measurements and 0.1% for sharp electrode measurements. Data is recorded from the same cells/fibres treated in (A).

5.1.4. Negative and positive controls.

Cells were superfused with concentrations of glucose of 0.0045, 0.045, 0.45, 4.5 and 45 μM glucose. Since the normal Tyrode that was used as superfusate already contained 10 mM glucose, it was unlikely that these additional concentrations would elicit changes in APD and therefore these experiments served as a negative control. Figure 5.11A shows averages of 5 traces recorded from a single myocyte under control conditions and in response to 45 μM glucose or 300 nM cisapride. Values of APD_{90} recorded under control conditions and in the presence of 45 μM glucose were 263 ± 12 ms and 269 ± 19 ms, respectively (mean \pm SEM, $n = 8$). The presence of 300 nM cisapride caused a significant increase in APD_{90} to 366 ± 47 ms (see Figure 5.11B, $p < 0.05$ versus control, paired Student's t test, $n = 8$).

The use of cisapride as a positive control also clearly demonstrates an increase in triangulation. Compared to control values, the APD_{90-40} and the APD_{90-50} increased to 1.7 ± 0.6 and 1.9 ± 1.0 relative to control (see Figure 5.12). With the exception of cells that had previously been perfused with terfenadine, where values for both the APD and triangulation remained decreased compared to control, indicating that terfenadine did not wash-off before the application of cisapride, application of cisapride caused an increase in triangulation. For example, following the application of 100 μM d-sotalol, which caused an increase in triangulation of 0.5 ± 0.1 relative to control, application of cisapride still produced a value of 1.0 ± 0.2 ($n = 6$).

5.1.5. Practical considerations in recording APs from myocytes using optical techniques.

Generally, optical measurements were comparatively easy to obtain relative to sharp electrode recordings. Difficulties in obtaining access to the cell with an electrode were absent, which reduced the amount of time taken to achieve a dose-response experiment from a given cell. However, optical measurements did present other challenges that were not present when using standard microelectrode techniques. For example, whilst superfusing guinea pig myocytes with terfenadine, higher concentrations reduced the contractile response such that on occasion, it was difficult to ascertain if an AP was being produced in response to stimulus. This could present a dilemma, in that, whilst stimuli that are too large can prevent the excitation of cardiac cells (Sharma *et al.*, 2005), the stimuli may need to be increased to ensure that an AP is evoked. In one instance, during the acquisition of the highest concentration of terfenadine an average of only 2 records was used because APs were not present during the other three stimuli.

Also, on 4 occasions early-afterdepolarisations were recorded during the brief exposure to excitation light during the application of 300 nM cisapride, which would often prevent the measurement of APDs from that AP and the following AP 1 s later if the EAD caused sufficient prolongation. This would reduce the number of APs that would be averaged during a single exposure. Fortunately, in none of the instances when this occurred was the resultant average too noisy to obtain accurate measurements, although in one instance an average of only 2 APs was used.

Another example of interference in optical measurements occurred when detritus from dead cells (which fluoresce very intensely) moved into view during the acquisition as a result of the perfusion. Although it was possible to remove them from the field of view using the rotating diaphragm (see Methods, Section 2.4), if this occurred during acquisition interference in measurements of APD was unavoidable. In a single instance this resulted in the averaging of only 4 records instead of five. Other problems associated with perfusion could occur if the cell blew away prior to the completion of an experiment, which is less likely to occur with the presence of an electrode that may help to hold the cell in position.

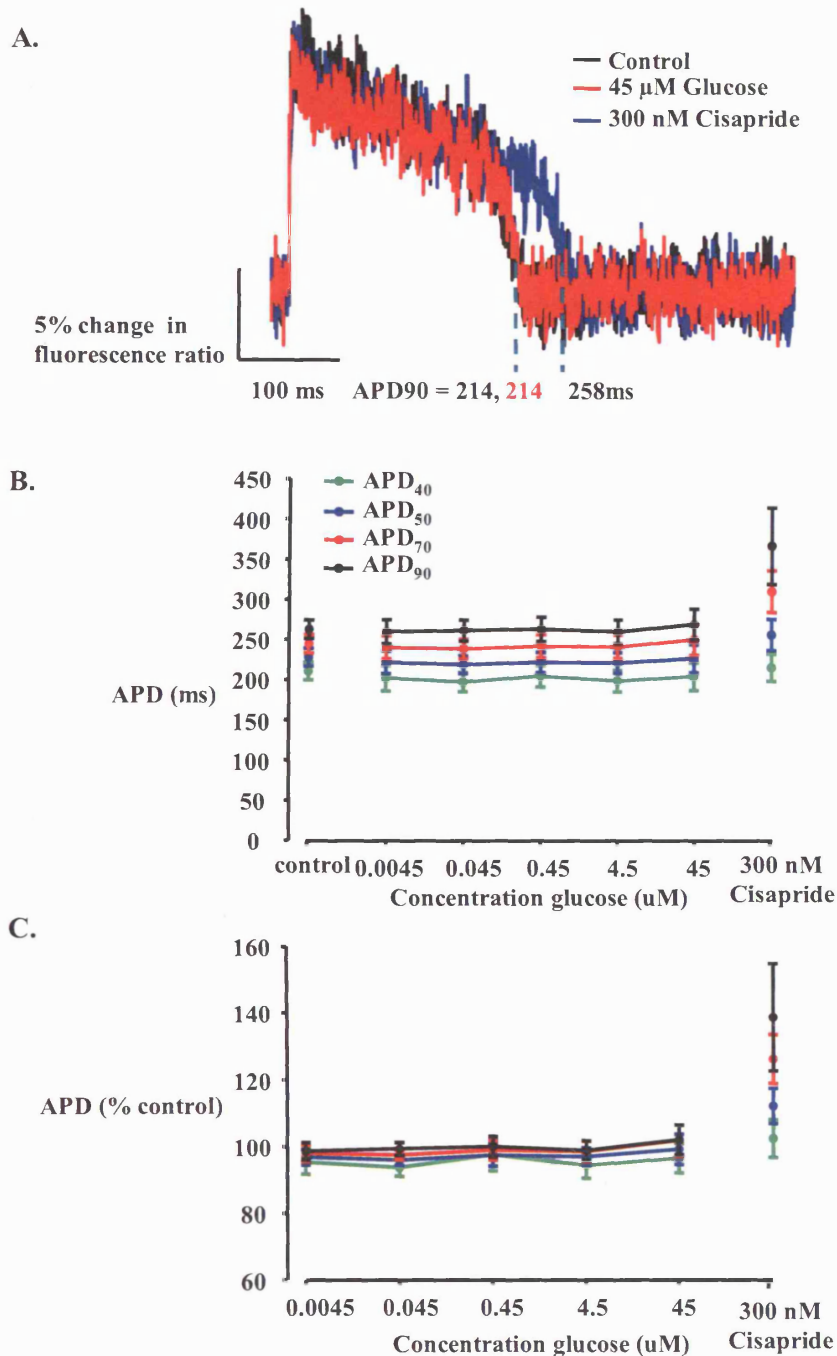


Figure 5.11. APDs recorded optically from guinea pig myocytes in response to increasing concentrations of glucose.

(A) Averages of 5 records recorded from isolated guinea pig ventricular cells using di-4-ANEPPS under control conditions (black), 45 μ M glucose (red) and in the presence of 300 nM cisapride (blue). (B) graph showing the absolute action potential durations from 10 cells exposed to increasing concentrations of glucose. Durations are shown for repolarisation stages at 40, 50, 70 and 90%. (data expressed as means \pm SEM) (C) Data from (B) expressed as a percentage change.

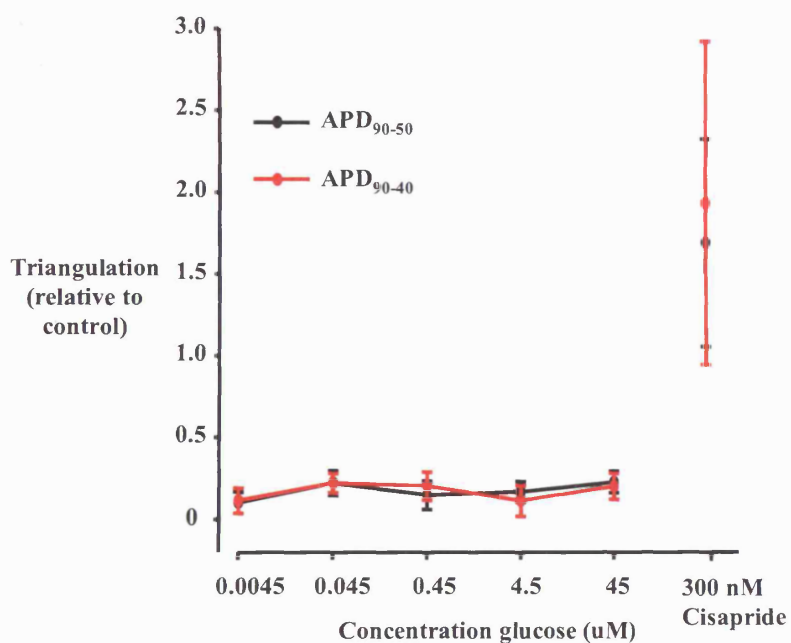


Figure 5.12. Triangulation in the presence of increasing concentrations of glucose (placebo) and in the presence of 300 nM cisapride.

Triangulation recorded from isolated guinea pig myocytes using the fluorescence emission of di-4-ANEPPS. Calculations were made as either the $APD_{90} - APD_{40}$ (APD_{90-40} , red) or $APD_{90} - APD_{50}$ (APD_{90-50} , black) expressed relative to control. The presence of 300 nM cisapride caused an increase in triangulation. Data are expressed as means \pm SEM.

5.2.1. Discussion.

In this chapter, the effects of three different compounds were assessed upon the repolarisation of cardiac APs recorded with a sharp electrode from two different types of canine cardiac tissue: Purkinje fibres and M cells. These data were used for comparison, to evaluate the efficiency of an optical assay for recording cardiac APDs from isolated guinea pig myocytes. However, because three different tissue types were examined, different effects upon repolarisation were also observed in response to certain compounds.

Optical measurements of APD allowed for the measurement of two parameters used in preclinical assessment of cardiac risk in test compounds: APD and triangulation. Increases in APD are often associated with proarrhythmic potential because of the large number of compounds which inhibit repolarising potassium currents that are associated with long QT syndrome and sudden death (Redfern *et al.*, 2003). However, it has also been argued that in the absence of triangulation or instability, APD prolongation is antiarrhythmic (Hondeghem *et al.*, 2001). Therefore, the ability of the optical assay to detect triangulation is also an important characteristic in determination of proarrhythmic potential.

5.2.2. The underlying cause of the effects of d-sotalol, terfenadine and pinacidil on cardiac repolarisation.

The ventricular cardiac AP is generated by a variety of different ionic currents and transporters (see Introduction for more details). Therefore, the effects that different compounds exert upon cardiac AP duration are a result of interference with these ionic pathways. Sotalol exists as two isomers: d-sotalol and l-sotalol. The racemic mixture of sotalol has antagonistic effects upon β -adrenoceptors and I_{Kr} current. However, the (d)-isomer, which was used in the present study, is specific for I_{Kr} inhibition only (Advani & Singh, 1995). It is therefore expected that the effects of this compound are to cause an increase in APD, which is consistent with inhibition of repolarising potassium currents. D-sotalol caused an increase in APD in the sharp electrode recordings from canine M cells and Purkinje fibres, as well as in guinea pig APs using the optical assay. All three methods also demonstrated that d-sotalol-induced increases in APD were consistent between the three different tissue types at repolarisation stages between 50 and 90%. At the highest concentration tested, there was no significant difference in d-sotalol induced APD prolongation between the different assays, although at lower concentrations the Purkinje fibre

assay may have increased sensitivity versus the canine M cell. Increases in triangulation with increasing concentrations of d-sotalol were also identified using the three different assays.

In contrast to the results obtained in response to d-sotalol, different effects upon APD were apparent between the different assays in the presence of terfenadine or pinacidil. In both canine and guinea pig myocytes, pronounced decreases in APD were observed at higher concentrations of terfenadine. Similarly, in canine M cells, significant decreases in triangulation were detected at higher concentrations of terfenadine, although no significant change was detected in the optical assay. In contrast to results obtained from both types of myocyte, values of APD₉₀ in Purkinje fibres were unaltered at any of the concentrations tested. However, a decrease in APD₅₀ was detectable at 10 μ M terfenadine that was also associated with an increase in triangulation. These data are difficult to interpret for two reasons: firstly, because of differing results upon APD between ventricular myocytes and Purkinje fibres; and secondly, because clinically, terfenadine has been associated with increases in the QT interval on an ECG (Honig *et al.*, 1993; Pratt *et al.*, 1996), which is contrary to what would be expected by the decrease in APD observed in ventricular tissue. Previously, it has been demonstrated that terfenadine blocks multiple cardiac ion channels. In guinea pig myocytes, blockade of I_{CaL} , I_{Na} and I_K has been demonstrated at terfenadine concentrations greater than 0.03 μ M (Li *et al.*, 2006; Ming & Nordin, 1995). It is the multiple ion channel blockade that explains the biphasic effect of terfenadine upon cardiac AP in M cells and guinea pig ventricular myocytes. A reduction in repolarising potassium current is likely responsible for the increases in APD observed at lower concentrations of terfenadine. Although these were not significant in the experiments in the present study, they occurred in both types of myocytes studied and a previous study has found this increase to be statistically significant (see Terrar *et al.*, (2007) and below). This is also likely to be responsible for increases in the QT interval in response to terfenadine observed clinically. At higher concentrations, reductions in calcium and sodium currents are the probable cause for reductions in APD.

Pinacidil is a specific activator of the K_{ATP} cardiac ion channel (Hermsmeyer, 1988). Whilst no effects were observed in guinea pig myocytes at the concentrations tested, decreases in APD were detected in both canine M cells and Purkinje fibres. This is consistent with the opening of potassium channels, which would be associated with an increased efflux of potassium ions, with consequential increased rapidity of repolarisation.

5.2.3. Comparison of drug effects upon different preparations.

Using optical recordings from guinea pig myocytes, it was possible to detect both a significant increase in APD at repolarisation stages between 40 and 50%, as well as significant increases in triangulation in response to increasing concentrations of d-sotalol. Measurements of APD using sharp electrodes in canine M cells and Purkinje fibres also showed similar responses (although increases in triangulation from M cells did not reach significance), which would indicate that using this type of compound, an I_{Kr} specific inhibitor, it is possible to detect increases in both APD and triangulation in all three tissue types, as well as using optical measurements of APs from guinea pig myocytes.

In contrast, the compounds tested that have effects upon other ion channels than I_{Kr} had varied effects in different tissue types. In both the optical assay in guinea pig myocytes and sharp electrode recordings in canine M cells, terfenadine caused a decrease in APD at higher concentrations. However, at concentrations lower than 0.3 μM there was an increase in APD. This was not significant in either assay, but is consistent with previous studies. Terrar *et al.* (2007) also demonstrated a biphasic effect upon APD using sharp electrode recordings from isolated guinea pig ventricular myocytes paced at 1 Hz, with a significant increase in APD at 0.1 and 1 μM terfenadine which was reversed at higher concentrations. Furthermore, similar to the data displayed here, the same study also did not find any significant effect upon the APD in canine Purkinje fibres and other studies using canine Purkinje fibres have failed to realise the proarrhythmic potential of terfenadine (Gintant *et al.*, 2001). Sharp electrode recordings from canine M cells, however, had a similar response to terfenadine as optical measurements from guinea pig myocytes; a small, but insignificant increase in APD at lower concentrations accompanied by a decrease in APD at higher concentrations. Gintant *et al.*, (2001) found no effect upon APD using sharp electrode recordings in canine midmyocardial slices and 1 μM terfenadine, although the current study observed a decrease in at the same concentration in canine M cells. This may reflect differences in the use of multicellular preparations. Use of isolated cells may have allowed for easier access of terfenadine to the ion channels it inhibits when compared to the wedge preparation. Similarly, it might be argued that the reason there was no observed effect upon the APD_{90} in Purkinje fibres in the current study was because the drug did not have access to the fibre being monitored, as there were multiple Purkinje fibres within each bundle. However, there were terfenadine-induced alterations in V_{max} that were present in both M cells and Purkinje fibres would suggest that this was not the case.

The absence of effects upon APD of terfenadine observed in Purkinje fibres contrasted with the biphasic response observed in ventricular muscle can present a dilemma for

preclinical assessment of proarrhythmic risk. Data obtained from Purkinje fibres in the present study would indicate that terfenadine would be unlikely to have proarrhythmic potential, whilst the observed effects upon APD and triangulation observed in ventricular myocytes would indicate the opposite. However, it is likely that the difference in response to terfenadine between the two tissue types is responsible for the arrhythmic incidences that have been associated with the drug. Alterations in APD in ventricular muscle that occur in the absence of effects upon the Purkinje fibre AP, provide an environment for re-entry (see Introduction): an occurrence when one region of cardiac tissue may be in its refractory period, whilst another is prone to excitation from an ectopic beat.

Increasing concentrations of pinacidil caused a significant decrease in APD in canine Purkinje fibres. However, this effect was not observed at the concentrations tested in guinea pig myocytes using di-4-ANEPPS. Sharp electrode recordings from canine M cells revealed a modest decrease in APD at 3 and 10 μM (concentrations which produced no effect in the optical assay), but larger concentrations of pinacidil were required to cause equivalent decreases in APD to those observed in Purkinje fibres. Previously, pinacidil has been used in experiments upon a variety of guinea pig cardiac tissues. Microelectrode recordings from guinea pig papillary muscles revealed a decrease in APD at concentrations of pinacidil above 30 μM (Hirai *et al.*, 1990). However, the same study only identified effects of pinacidil upon APD at concentrations below 30 μM in the presence of high external potassium (27 mM) and 0.2 mM barium. In the present study, the maximum concentration of pinacidil examined using guinea pig myocytes was 3 μM in physiological Tyrode (6 mM potassium and absence of barium), and concentrations were selected to reflect those examined in canine Purkinje fibres at which a decrease in APD was observed. Previous studies have used pinacidil in the study of a variety of conditions at concentrations greater than 3 μM ; APD shortening has been demonstrated in canine papillary muscles at a concentration of 10 μM (Takacs *et al.*, 2003). The decrease in APD in the presence of 3 μM pinacidil reported from sharp electrode recordings from canine M cells was also substantially smaller than that observed in canine Purkinje fibres. Yet concentrations greater than 3 μM of pinacidil did cause decreases in APD equivalent and greater to those observed in Purkinje fibres at 3 μM . Similarly, an earlier study on the effects of K_{ATP} openers on canine Purkinje fibres demonstrated APD shortening effects of pinacidil at concentrations between 0.3 and 10 μM (Sato, 1993). Thus, from the observed results in the present study, combined with data from previous studies, it is reasonable to conclude that canine Purkinje fibres are more sensitive to the APD shortening effects of pinacidil, when compared to myocytes from either canine or guinea pig myocardium.

5.2.4. Summarising the effects of different compounds upon repolarisation in canine Purkinje and M cells and guinea pig ventricular myocytes.

The primary findings of this chapter are that optical measurements of APs from isolated guinea pig myocytes using di-4-ANEPPS represent a feasible methodology for measuring drug-induced alterations in APD and triangulation. Although some differences were observed between the responses of guinea pig myocytes to compounds when compared with sharp electrode recordings, both terfenadine and d-sotalol invoked similar alterations in APD. The I_{Kr} specific inhibitor d-sotalol caused an increase in both types of myocyte, whilst terfenadine produced responses consistent with a multi-channel drug effect. The exception to this, pinacidil, had no effect upon APD in the optical assay. However, The APD shortening effect of pinacidil at concentrations similar to those monitored optically were diminished in M cells compared to those recorded from Purkinje fibres, and the lack of effect observed in guinea pig myocytes is consistent with a previous study in guinea pig myocytes that also did not observe shortening of the APD at the concentrations tested when using standard electrode techniques.

More prominent differences were observed in the responses of Purkinje fibres to terfenadine and pinacidil when compared with either the optical assay in guinea pig ventricular cells or sharp electrode recordings from canine M cells. Terfenadine did not alter the APD_{90} in Purkinje fibres at any of the concentrations tested. In contrast, Purkinje fibres were much more sensitive to the effects of pinacidil than either type of myocyte. This clearly demonstrates a difference between the preparations. Therefore, whilst using di-4-ANEPPS to record APDs from isolated guinea pig myocytes is a viable alternative to using electrodes, the acquired data must only be used in conjunction with other appropriate screens in assessing proarrhythmic risk.

Chapter 6:
Conclusions and Future Work.

Chapter 6: Conclusions and future work.

6.1. Final discussion.

The work in this thesis provides good evidence to support the use of optical techniques in determining drug-induced alterations in cardiac action potential (AP) morphology from isolated cardiac ventricular myocytes. Both di-4-ANEPPS and di-8-ANEPPS were used to successfully monitor drug-induced alterations in action potential duration (APD) recorded from isolated guinea pig myocytes.

In Chapter 3, I have demonstrated that the change in emitted fluorescence of both di-4-ANEPPS and di-8-ANEPPS has a linear relationship with the membrane potential of isolated guinea pig myocytes. Further experiments using the dyes to record APs over longer time periods showed that continuous exposure of isolated guinea pig myocytes to excitation light, using light intensities and dye concentrations at levels that were sufficient to record APs, resulted in phototoxic effects. However, by limiting the duration of exposure to excitation light, it proved possible to maintain consistent recordings using both dyes. Initially, it appeared that di-8-ANEPPS was superior to di-4-ANEPPS in this regard, allowing for longer periods of excitation as well as having a larger change in emitted fluorescence with changes in membrane potential. Changes in APD in response to increasing concentrations of cisapride were monitored using di-8-ANEPPS and compared to results obtained using a patch electrode. Whilst the biphasic response of guinea pig ventricular myocytes to increasing concentrations of cisapride was correctly identified using di-8-ANEPPS and the IC_{50} apparent was similar using both techniques, recordings made using the dye had an increased basal APD and decreased sensitivity versus a patch electrode.

In Chapter 4, the effects of di-8-ANEPPS upon cardiac ion currents was further examined and compared with those of other styryl dyes, including di-4-ANEPPS. Experiments using a patch electrode to monitor APD during acute applications of dyes showed that the AP prolonging effect of di-8-ANEPPS was directly due to the dye and not induced by phototoxicity. Furthermore, di-4-ANEPPS caused a moderate decrease in APD and the effects of another styryl dye, di-4-ANEPPDHQ, caused a pronounced and irreversible shortening in APD. Voltage-clamp experiments using the same three dyes also revealed some significant effects upon the L type calcium current (I_{CaL}) in canine midmyocardial cells (M cells). Di-4-ANEPPDHQ consistently altered the perceived current, appearing to cause an increase in peak inward current accompanied by large alterations in the activation and inactivation kinetics. However, the timescale of activation and inactivation were altered to

such a degree that capacitance transients could arguably interfere with analysis, so further investigations of the electrophysiological effects of this dye may be necessary. Di-8-ANEPPS caused a significant increase in peak I_{CaL} , as well as significantly shifting the voltage-dependence of activation and inactivation to more negative potentials and delaying recovery from inactivation. Of the three dyes tested, di-4-ANEPPS exhibited the smallest effect upon I_{CaL} ; no significant effects upon the peak current or the voltage dependence of inactivation were detectable, but this dye did decrease the time taken for channels to recover from inactivation. When considering the direct effects these dyes may have upon ion channels, the only aspect in which di-8-ANEPPS performed favourably over di-4-ANEPPS was that it interacted with the ion channel encoded by the human ether-a-go-go related gene (hERG) to a lesser extent. This was determined by monitoring inhibition of hERG current using the planar microelectrode array, Ionworks HT™, and also by utilizing a radioligand binding assay. It is also worth noting that whilst none of the dyes exhibited a large enough inhibition of hERG current to determine an IC_{50} , radioligand binding studies would indicate that the dyes had relatively more affinity for hERG protein.

In Chapter 5, APDs were recorded from guinea pig ventricular myocytes using di-4-ANEPPS. This was done in response to 4 blinded compounds and compared to results obtained from two other assays used to monitor APD: sharp electrode recordings from canine M cells and Purkinje fibres. The results showed two things: firstly, that optical recordings from isolated guinea pig myocytes compared favourably with sharp electrode recordings from canine M cells; both these assays obtained similar alterations in response to the compounds terfenadine, d-sotalol and pinacidil at the concentrations tested. Secondly, these experiments also demonstrated differences in response to drugs between different tissue types. For example, they showed an increased sensitivity of Purkinje fibres to the APD shortening effects of pinacidil.

This chapter aims to address the implications of these results. Firstly, it will illustrate the advantages and disadvantages of using voltage-sensitive dyes for recording APs from isolated myocytes. This will place particular emphasis on the role such an assay may play in current safety pharmacology screening profiles. Secondly, the short-term and long-term future of this technique will be focused on. This includes the options of using other dyes, perhaps with increased signal to noise ratio (S/N) or reduced pharmacological and phototoxic effects. Additionally, the possibilities for further development of optical methods to increase throughput are discussed, with brief details of recent technological advances that may make this possible.

6.1.1. What are the advantages and disadvantages of using optical means to acquire cardiac action potentials?

The previous chapter compared the APDs acquired by three different means whilst being treated with a variety of well-characterised compounds. Whilst the optical assay demonstrated success in identifying expected changes in APDs, differences between results obtained using electrodes and using voltage-sensitive dyes became apparent.

In practice, APs recorded using voltage-sensitive dyes were much easier to obtain than sharp electrode recordings from either M cells or Purkinje fibres and this may allow for an increase in throughput. However, sharp electrode techniques also demonstrated a greater versatility; they allowed for continuous monitoring of membrane potential over long periods of time, where (to avoid phototoxic effects) optical measurements were limited to discrete durations every few minutes. This has several consequences. Firstly, as was observed whilst monitoring the APD of guinea pig myocytes being superfused with terfenadine, high concentrations of this compound could reduce the contractile response to stimulation such that it was not visually identifiable. In recordings made with a sharp electrode this presented less of a problem because it was still possible to observe whether APs were being elicited. However, during optical recordings, it was more difficult to judge whether the stimulus needed to be increased or if this was just an effect of the drug. This is further complicated, because very high intensity pulses are known to cause a loss of stimulation in isolated myocytes (Sharma *et al.*, 2005), which presents the dilemma of whether to risk increasing the magnitude of the voltage-stimulus and causing a loss of excitation or to maintain the same intensity stimulus and hope that APs are still being elicited. Similarly, sampling only a few APs every few minutes also limits the ability to detect other proarrhythmic markers. For example, early afterdepolarisations (EADs) are associated with arrhythmia (Choi *et al.*, 2002; Sicouri & Antzelevitch, 1993). In this thesis, EADs were detected with both di-4-ANEPPS and di-8-ANEPPS. However, in experiments where no EADs were observed using optical recordings, it is possible that extrasystoles did arise, but during periods when cells were not illuminated with excitation light.

In a study on rabbit Langendorff-perfused hearts, one of the indicators of proarrhythmic potential identified by Hondeghem *et al.*, (2004) was instability of APD. Furthermore, recent studies in anaesthetised dogs with electrically remodelled hearts have demonstrated that short-term variability in monophasic APD is associated with Torsades de Pointes and that this was both detectable in isolated myocytes with block of I_{Kr} and highest in cells that subsequently showed EADs. In Chapter 1 using a patch electrode, I have

demonstrated that it is possible to detect increases in beat-to-beat variability of repolarisation in isolated guinea pig myocytes in response to 300 nM cisapride. Thus, whilst continuous monitoring of APD using a microelectrode allows for identification of changes in short-term variability of repolarisation, discontinuous monitoring using voltage-sensitive dyes does not. This is particularly true because APs recorded optically are often subject to noise and require averaging to prior to measurement of APD; a process that removes beat-to-beat variability (BVR).

However, optical recordings using guinea pig ventricular myocytes loaded with di-4-ANEPPS did demonstrate the ability for detection of two important indicators of proarrhythmia: APD prolongation and triangulation. Furthermore, once the conditions for recording APs optically were identified (correct concentration of dye, excitation light intensity and duration of exposure to excitation light), recording APs was both easier and substantially quicker using di-4-ANEPPS than using an electrode.

6.1.2. Can optical recordings of APD be used as a predictor of proarrhythmic potential?

Clinical experience has demonstrated the need for reliable preclinical screens to assess proarrhythmic potential. It is widely accepted that AP prolongation manifests as an increase in the duration between the Q and T deflections recorded on an ECG. Additionally, dose-dependent prolongation of the QT interval has been reported for a variety of compounds, including sotalol (Wang *et al.*, 1986), dofetilide (Pfizer Inc., 2004), terfenadine (Honig *et al.*, 1993; Pratt *et al.*, 1996), and cisapride (Wysowski & Bacsanyi, 1996). Additionally, sotalol (MacNeil *et al.*, 1993; MacNeil, 1997), dofetilide (Pfizer Inc., 2004) and terfenadine (Woosley *et al.*, 1993) all appear to induce TdP dose-dependently. Taken alone, these reports would suggest that QT prolongation is directly linked to incidences of arrhythmia; that the QT interval is directly related to APD would suggest that this was a suitable surrogate for assessing proarrhythmic potential *in vitro*. However, this is not always the case. Sub-therapeutic concentrations of quinidine have been shown to cause excessive QT prolongation and TdP (Roden *et al.*, 1986), thus monitoring increases in APD in a dose-dependent manner may not provide the increase in APD that might otherwise be expected. Additionally, both sharp electrode recordings from M cells and optical measurements of APD in guinea pig ventricular myocytes (refer to Chapter 5) demonstrate that higher concentrations of terfenadine caused a decrease in APD. At lower concentrations both assays did detect a comparatively small (and insignificant) increase in APD that, although it may be associated with the increase in APD seen in patients, would probably not have been considered a

potential risk during regular preclinical screens. In contrast, the pronounced decrease in APD observed in both guinea pig myocytes and canine M cells in the presence of higher concentrations of terfenadine would generate more concern. Similarly, comparisons between published data for a variety of compounds, which included activity at I_{Kr} , ability to delay repolarisation and reports of increased QT interval and incidences of TdP, concluded that drugs that interact with multiple ion channels may mitigate or exacerbate increases in APD arising from block of I_{Kr} (Redfern *et al.*, 2003). Therefore, delays in ventricular repolarisation may not necessarily reflect Torsadogenic potential. Indeed Hondeghem *et al.* (2000) measured the effects of 702 compounds on multiple parameters in Langendorff-perfused rabbit hearts and concluded that, in the absence of triangulation and instability, AP prolongation is antiarrhythmic.

However, studies of AP duration still provide a valuable tool for screening test compounds for proarrhythmic potential for a variety of reasons. Early pre-screens such as the Ionworks HT™ (Bridgland-Taylor *et al.*, 2006; Schroeder *et al.*, 2003), rubidium efflux assay (Chaudhary *et al.*, 2006; Rezazadeh *et al.*, 2004) and hERG binding assay (Diaz *et al.*, 2004), only allow for evaluation of drug-potency at a single ion channel. These assays were largely designed to detect activity at hERG or I_{Kr} . This is logical because the majority of compounds associated with LQTS and TdP also inhibit hERG at concentrations close to or overlapping the free plasma concentrations found in clinical use (Redfern *et al.*, 2003). However, these screens do not address the proarrhythmic risk presented by compounds that have effects on multiple ion channels or channels that are not screened for. Furthermore, *in vitro* assays available for assessing proarrhythmic potential are often limited in throughput and need a high degree of technical expertise in the operator, as well as being resource intensive. This is particularly true of some assays which measure multiple proarrhythmic indicators, such as the canine ventricular wedge model that can assess transmural dispersion, APD, instability and a pseudo ECG (Shimizu & Antzelevitch, 1999; Yan *et al.*, 1998). Although this assay provides a large number of parameters with which to assess proarrhythmic potential, it is not feasible for use as a high throughput screen. However, studies of APD and triangulation in isolated cardiac tissues have demonstrated success in identifying drugs associated with QT prolongation or TdP. In a study that assessed the effect of 12 compounds upon APD in canine Purkinje fibres, six of seven drugs linked to LQTS or TdP caused an increase of >15%, and cleared five drugs not associated with arrhythmia (Gintant *et al.*, 2001). The only compound that was not correctly identified in this model was terfenadine, which also did not significantly alter the APD in sharp electrode recordings from canine Purkinje fibres reported in Chapter 6. That terfenadine did cause changes in APD in both guinea pig ventricular myocytes and canine M cells, using optical and sharp electrode techniques, respectively, is an

indication of its proarrhythmic potential; changes in APD in ventricular muscle cells that are not present in Purkinje fibres will produce dispersion in repolarisation across the two different tissue types.

Using alterations in APD as a marker for proarrhythmic potential, optical recordings of APD in guinea pig myocytes successfully identified the proarrhythmic compounds d-sotalol and terfenadine, using di-4-ANEPPS. Furthermore, glucose was correctly identified as placebo (refer to Chapter 5). Additionally, in Chapter 3, the emitted fluorescence ratio of di-8-ANEPPS correctly identified the well-characterised biphasic change in APD in response to increasing concentrations of cisapride. That no change in APD was observed with pinacidil using di-4-ANEPPS is concordant with the reduced sensitivity of myocytes to that compound versus the effects seen on Purkinje fibres (Hirai *et al.*, 1990). Furthermore, these conclusions could be reached without any additional evaluation of markers for proarrhythmia. For example, the study by Gintant and colleagues (2001) in canine Purkinje fibres used a slow pacing rate of 0.5 Hz compared to 1 Hz used in the current study. This used the knowledge that proarrhythmic drugs can exhibit reverse-use dependence and hence cause larger increases in APD at slower cycle lengths; something that I did not attempt to assess in the optical measurements made with di-4-ANEPPS. It is also of note, that optical recordings of APD in guinea pig myocytes in response to d-sotalol and cisapride did detect statistically significant changes in triangulation. This means that optically recording APDs at different percentages of repolarisation can identify one of the markers for proarrhythmia that Hondeghem *et al.* (2004) suggest must accompany AP prolongation: triangulation.

Although it is not possible to assess the degree of transmural dispersion of repolarisation across the ventricular wall from a single cell, recording APs from cells isolated from different regions of the heart may allow one can give an indication of heterogeneity across the ventricular wall. For example, it has been demonstrated that M cell APs can prolong disproportionately compared to those of epicardial or endocardial cells isolated from the canine left ventricle (Liu & Antzelevitch, 1995). This is not addressed in the present study, but hypothetically, recording APs from myocytes using higher throughput techniques presents the possibility of recordings APs from different regions of the ventricular wall as part of a screening process. Using optical techniques to achieve this would present an easier method than using conventional microelectrode techniques.

Thus, optically measuring APDs provides a higher throughput tool for monitoring APD and triangulation from isolated ventricular myocytes. However, this assay does not generate data required for assessing BVR. Additionally, its use in assessing reverse-use dependence and transmural dispersion has not been addressed. AP prolongation is associated with proarrhythmia, but only in the presence of other risk factors that cannot always be

addressed in this assay. Therefore the use of an optical assay to monitor APD needs to be in conjunction with preclinical screens that may identify other markers for proarrhythmia.

6.1.3. Implications for safety-pharmacology.

In 1996, following a recent spate of incidences of TdP, the first draft of a document on QT prolongation by the European Medicines Agency's Committee for Proprietary Medicinal Products (CPMP), which was later issued as the official document (CPMP/986/96), advised that all non-cardiac drugs should be screened for effects on cardiac AP parameters *in vitro* (Committee for Proprietary Medicinal Products., 1997; Redfern *et al.*, 2002). The result of this has been twofold: firstly, generating debate as to the most appropriate tests for predicting proarrhythmia, and secondly leading to the development of assays that could be placed earlier within the screening process. These assays may remove compounds that present a risk prior to their introduction into a whole animal proarrhythmia model and could help to address the 3Rs (Replacement, Reduction & Refinement) of laboratory animal welfare (Russel & Burch, 1959). This requirement for more in depth safety-pharmacological profiling also coincided with increased numbers of chemical entities being synthesised during pharmaceutical development. Advances in combinatorial chemistry and high throughput screening allow for the production of roughly 10^4 lead compounds per annum; an approximate 200-fold increase on the number of candidate compounds being evaluated 25 years ago (Wakefield *et al.*, 2002). Thus the desirability of front-loading compounds becomes apparent; a process that would eliminate test compounds from the development process and is therefore more cost and labour effective.

In the assessment of the proarrhythmic potential of candidate drugs, medium throughput techniques are largely limited to studies on ion channels expressed in cloned cell lines. These include binding assays, rubidium efflux assays and planar-patch clamp arrays and are often directed at assessing compound interactions with hERG (Bridgland-Taylor *et al.*, 2006; Chaudhary *et al.*, 2006; Diaz *et al.*, 2004). Studies on native tissues provide numerous advantages, including the ability to assess ion channels in a more physiological environment, where they will be associated with their respective subunits and membrane potential can be monitored in a system expressing multiple ion currents. However, studies on native tissue can be limited in throughput. For example, studies utilizing sharp electrode recordings from Purkinje fibres (Champeroux *et al.*, 2005; Gintant *et al.*, 2001) are limited by the relatively small number of viable fibres that can be obtained from a single heart (Wakefield *et al.*, 2002). Even studies on native cell types that are numerous, such as the ventricular myocyte,

have the drawback that electrophysiological techniques that use sharp or patch electrodes can be time-consuming and require highly skilled operators. Thus, it is often the case that an isolation will produce thousands of individual cells of which very few are actually used for screening.

However, using voltage-sensitive dyes to record cardiac action potentials provides a means by which a larger number of cells can be examined from a viable isolation. Although the technique is not as versatile as more standard electrophysiological techniques i.e. it does not provide adequate measurements of V_{max} and is yet untested for examining reverse-use dependence, it does provide information on APD and triangulation. Thus the optical assay demonstrates some of the requirements for being a suitable precursor to sharp electrode techniques in the isolated myocyte or Purkinje fibres. If test compounds exhibit excessive AP prolongation and/or triangulation in an optical assay, they can be deemed inappropriate for further study and so time, labour and further animal usage is not necessary.

6.1.4. Is di-4-ANEPPS the optimum dye for use in screening for drug-induced alterations in cardiac action potential morphology?

In Chapters 3 & 4, the benefits of using di-4-ANEPPS, instead of di-8-ANEPPS, for recording cardiac APs from isolated myocytes were demonstrated; this is due to side-effects exhibited by di-8-ANEPPS upon the L-type calcium current and an increased basal APD in myocytes loaded with the dye. That either of these dyes may have direct pharmacological actions on cardiac tissue is worthy of note because they have both been used in a variety of cardiac preparations. Di-4-ANEPPS has been used in optical mapping studies in whole hearts (for examples see Baker *et al.*, 2000; Girouard *et al.*, 1996; Knisley *et al.*, 2000; Nygren *et al.*, 1922). Di-8-ANEPPS has also been used in multicellular preparations using heart cell cultures (Entcheva *et al.*, 2004; Rohr & Salzberg, 1994) as well as for recording fluorescence from isolated myocytes (Sharma & Tung, 2002; Sharma *et al.*, 2002; Sharma *et al.*, 2005). Drawbacks were demonstrated in the use of other dyes, including pronounced shortening of the APD and effects upon calcium channels resulting from the use of di-4-ANEPPDHQ, which is also now commercially available (Invitrogen, 2007). Additionally, the current project demonstrated that in order to record APs over long time-periods using di-4-ANEPPS or di-8-ANEPPS, for example during a dose-response experiment, exposure to excitation light was limited by phototoxic effects. Phototoxicity has also previously been reported with considerably higher concentrations of di-4-ANEPPS (30 or 60 μM ; incubated for 10 min) with effects upon the AP including AP prolongation, early afterdepolarisations, reduction of

the membrane resting potential and eventually inexcitability (Schaffer *et al.*, 1994). That addition of the antioxidant catalase (100 IU/ml) to the extracellular solution delayed the onset of these effects suggests that reactive oxygen species were the cause of these effects. Previously, experiments on frog atrial myocytes bathed in Rose Bengal-containing medium, exposed to excitation light (a combination that produces photosensitiser-generated reactive oxygen species) revealed suppression of sodium, calcium and potassium currents as well as enhancing a time-independent outward current designated I_{leak} (Tarr & Valenzeno, 1991; Tarr *et al.*, 1994). Similarly, I_{Kr} function in canine myocytes and hERG current expressed in HEK 293 cells have also been shown to be impaired by reactive oxygen species (Wang *et al.*, 2004).

However, since the advent of fast voltage-sensitive dyes, a large number have been developed and they do not all display the same characteristics. For example, analysis of three voltage-sensitive dyes in brain slices showed differences in phototoxicity and pharmacological actions (Chang & Jackson, 2003); the dye RH414 was found to have phototoxic effects, RH155 was found to have pharmacological effects at relatively high staining levels, whilst no adverse effects were detected using the dye RH482. The large number of fast voltage-sensitive dyes that are available is illustrated by the fact that, in 1981, already more than 1000 of these dyes had been screened for signal-to-noise ratio in the squid giant axon (Cohen *et al.*, 1974; Gupta *et al.*, 1981; Ross *et al.*, 1977). More recently, dyes have been developed that allow for uses in combination with other well characterised dyes. For example, the dye RH237 has spectral characteristics which allow optical recordings to be made of the membrane potential, whilst simultaneously monitoring intracellular calcium concentration using analogues of Rhod-2 or Fluo-3 calcium sensitive dyes (Fast, 2005). Owing to the importance of both membrane potential and intracellular calcium transients in the onset of a number of cardiac dysfunctions, this combination is extremely beneficial to cardiac physiologists. Additionally, a number of styryl dyes have been developed which are excited by near infrared wavelengths (>700 nm) and emit above 900 nm. Whilst in multicellular and whole heart preparations these dyes may be advantageous with regards depth penetration, owing to lower levels of light scattering exhibited by light of wavelengths 600-1000 nm, they may provide other advantages also. As they are untested in isolated heart cells, it is not possible to say whether they might exhibit fewer phototoxic or pharmacological effects.

There have also been a number of advances in the techniques used to record changes in membrane potential optically. In the introduction I have briefly surmised the basic classes of voltage-sensitive dyes; however this was limited to basic epifluorescent applications. Further examples of techniques to optically record membrane potential include the use of

Förster Resonance Energy Transfer (FRET). This system uses two fluorescent components. The first is a hydrophobic ion that binds to the plasma membrane and rapidly redistributes itself on opposite side of the membrane following changes in potential. The second binds specifically to one face of the membrane and functions as a FRET partner to the membrane bound fluorophore. For example, González & Tsien, show that, by fixing coumarin-labelled phospholipids into the membrane, they can act as a donor to oxonol (DiSBAC_n(3)) dyes. Using DiSBAC₆(5), the response time constant is 400 μs and the change in fluorescence ratio is <20% per mV (Gonzalez & Tsien, 1997; Gonzalez & Maher, 2002).

I have demonstrated that it is possible to record cardiac APs using di-4-ANEPPS and di-8-ANEPPS and have successfully recorded drug-induced changes in APD. The limitations that were imposed on these measurements by pharmacological and phototoxic effects may be removed with more extensive dye screening. Whilst ideally, assessing the suitability of new dyes in cardiac preparations would be performed in native tissue, the large quantity of available dyes and low throughput nature of the assays, such as sharp electrode recordings from M cells or Purkinje fibres, may make this non-feasible. It is currently possible to screen compounds commercially for activity at a range of ion channels. For example, by using medium throughput planar patch clamp technologies to screen compounds against a panel of cardiac ion channels expressed in cloned cells, a process which is currently available commercially (see the webpage, Chantest, 2007), it is possible to obtain a profile of which ionic currents a compound or dye may inhibit. Currently the ion channels that can be screened in this way include: HERG, Kv1.5, Kv4.3, KvLQT1/mink, Nav1.5, Cav1.2 and NCX1.

The ideal dye would fluoresce only when bound in the membrane and have a linear ratiometric response with membrane potential; properties that both di-4-ANEPPS and di-8-ANEPPS exhibit. However, additional benefits would include: a larger signal-to-noise ratio, reduced production of free radicals and photobleaching, as well as a complete absence of pharmacological effects. Owing to the large number of fast voltage-sensitive dyes that have been synthesised, it is highly probable that some that are as yet untested in cardiac tissue may yield advantages over di-4-ANEPPS and di-8-ANEPPS.

6.1.5. The immediate future for an optical assay determining cardiac action potential duration in safety pharmacology screening.

The studies used in this project to detect drug-induced alterations in AP morphology have largely focused on the use of guinea pig ventricular myocytes, which, although they do demonstrate a number of advantages in screening for drug-induced arrhythmia and are used in

a number of screening assays, also possess a number of differences to the human cardiac AP. Owing to the well characterised AP of canine ventricular muscle and similarities in ion channel expression and heterogeneity, the canine M cell represents a preferable cell type for use as a substitute to human tissue. Clearly, the efforts in chapter 4 to screen for a more suitable dye for this assay, in which calcium current measurements were performed upon the canine M cell, were intended for future use in this cell type. However, as is seen in chapter 3, original efforts to transfer the assay from guinea pig cells into canine cells did not meet with great success; the same loading conditions used for di-4-ANEPPS in guinea pig myocytes resulted in substantial phototoxicity in canine M cells.

Thus the immediate future is to address the conditions required for use of optical dyes in canine M cells. Such work is continuing at present and has thus far produced some promising results. In particular, by substantially lowering the concentration of di-4-ANEPPS, such that the M cells are not preloaded, but instead are continually perfused with a 100 nM maintenance dose, and using a limited time of exposure of 5 seconds in every 4 minutes, has produced some satisfactory results. These include alterations in APD in response to a number of previously well-characterised compounds. At present this work is in its early stages, however it does seem likely that the assay has the potential to be successfully transferred into the canine M cell (see Appendix B).

6.1.6. Possible long-term developments for an optical assay determining cardiac action potential duration in safety pharmacology screening.

Currently, the use of an optical assay in the configuration used throughout these studies does provide benefit in terms of throughput. In part this arises from the ease of use of the system, which also provides the benefit that it does not require a skilled electrophysiologist as an operator, as well as the ease and speed with which recordings may be made. However, the throughput is still limited to a single cell per experiment, which wholly underestimates the potential of the use of cardiac myocytes as a medium (as compared to the Purkinje fibre). Thus, if the assay provides continued success in a pharmaceutical environment, investment to increase the throughput would be astute.

There are a number of different approaches that may be made to modifying the system. The simplest methods, which require less effort to validate and obtain the correct conditions, are to use the same software and hardware for acquisition, but to increase the number of cells that may be monitored during a single experiment. One option would be to provide an automated programmable mount for the tissue bath; as the design of the assay for

recording dose-response relations incorporates finite periods of time during which a cell is exposed to excitation light, it would be possible for a tissue bath to move so the objective focuses on one (previously selected) cell to another at times when recordings are made. This is particularly feasible, because there are generally a number of cells that are present in the tissue bath during each experiment. Another option could be to provide a number of tissue baths, all being simultaneously perfused and each with its own set of photomultiplier tubes and objectives for data acquisition.

Other options may involve changing the hardware for acquisition of the light signal. Modern CCD camera technology allows for faster rates of image acquisition. For example, cooled CCD cameras have been reported to achieve up to 2000 frames per second (Djurisic *et al.*, 2003) and fast rate cameras have previously been used for the mapping of cardiac APs in whole hearts. For example, the assessment of new long wavelength dyes included the use of a 100x100 pixel camera at 1000 frames per second to record APs from whole frog hearts (Salama & Choi, 2000). The use of a camera to increase throughput is possible because the output of a camera provides a field of view, thus allowing for multiple regions (cells) to be selected for analysis. These cameras may be very well suited to this type of assay; although faster rates of acquisition have the drawback that spatial resolution is less well defined, this is less important in an assay where quantitative light collection is paramount. In my experiments recording emitted fluorescence from a single cell with photomultiplier tubes (PMTs), resolution was unimportant because the field of view was determined with the use of a separate infrared camera. During experiments where a CCD camera may be used to record from multiple cells, resolution would only need to be sufficient to obtain an outline of the myocytes being studied.

The ideal method for increasing throughput, would be to develop a multiple-well format. However, the use of the cardiac myocyte as a medium presents difficulties in using this type of assay. Isolation of cardiac myocytes never provides a 100% yield of healthy cells. My experience is that an isolation of cardiac myocytes very rarely yields greater than 90% living cells. Dead ventricular cardiac myocytes loaded with either di-4-ANEPPS or di-8-ANEPPS fluoresced very brightly (in some instances enough to saturate the PMTs). In a multi-well format it would therefore be necessary to remove all of the dead cells to avoid interference from the light they would emit. Klauke *et al.*, (2005) have developed an open architecture microarray in which isolated myocytes have been micropipetted and stimulated. Furthermore, using a PMT and di-8-ANEPPS they also successfully recorded cardiac APs and using a CCD camera, calcium transients from intact cells. Such a system may allow for increased throughput using faster frame rate cameras for acquisition of changes in membrane potential with a voltage-sensitive dye. This system may be particularly suitable for screening

candidate compounds in a pharmaceutical environment as the architecture of such an array allows for pipetting of drugs without cross-talk between microwells.

6.1.7. Summary.

In this thesis I have demonstrated the feasibility of recording drug-induced cardiac AP prolongation and triangulation from isolated cardiac myocytes using fast voltage-sensitive dyes. This is a technique that may be of particular benefit for safety-pharmacology screens because it provides higher throughput than standard microelectrode techniques currently used, for example when compared to Purkinje fibre assays (Gintant *et al.*, 2001), whilst still providing an indication of the effects of test compounds in native tissue.

I have also demonstrated that some voltage sensitive dyes have both pharmacological and phototoxic effects. These include di-4-ANEPPS, which was determined to be the optimum dye assessed in the current study. Additionally, there was a differential response between myocytes isolated from different species when using voltage-sensitive dyes. Using the conditions that were successful for recording APs from guinea pig ventricular myocytes showed pronounced phototoxicity when applied to canine M cells.

Further work may include: optimisation of the conditions required for recording APs from canine myocytes, which may be more suitable for use within the pharmaceutical industry; testing of alternate fast voltage-sensitive dyes for increased signal-to-noise ratio and fewer side-effects; and optimisation of the technique for higher throughput use.

APPENDIX A.

In Chapter 5 action potential durations were calculated using a Microsoft Excel based spreadsheet. To accomplish this, the raw data was processed in two ways. Firstly, traces were smoothed using a 10-point moving average. This did not reduce the number of data points but removed some of the noise. Additionally, sampling at 10 kHz provided 10 data points per millisecond; thus averaging the data in this manner did not alter the timescale of the AP enough to effect measurements of APDs. Figure A-1 shows an average of 5 APs recorded from a guinea pig myocyte, in the absence of test compounds, and a screen shot of a 10-point moving average of the same data. Separately, the raw data was also reduced tenfold by averaging samples recorded over 1 ms. This provided two averaged APs from which calculations could be made. Both used a 10-point average to smooth the data, but whilst one used a moving average at 10 kHz, the second was filtered to 1 kHz.

The baseline was calculated from smoothed 10 kHz data as an average of the last 200ms of a 1 s recording (the AP stimulus occurred 15 ms from the beginning of the recording). This value was then used to determine the beginning of the AP: when three consecutive data-points exceeded the baseline value plus three standard deviations, this was considered the beginning of the AP. The start of an AP was calculated as the first value within three standard deviations of the baseline that immediately preceded these values. Maximum depolarisation was determined as the first point, following the start of an AP, when a 1 ms average exceeded the average of the following 5 ms.

$$APD_x = [0\%repolariation] - \frac{x([0\%repolariation] - [100\%repolariation])}{100}$$

Equation A-1. Calculation for determining the amplitude at which repolarisation should be measured.

Where x is the percentage of repolarisation, $[0\%repolariation]$ is the maximum depolarisation and $[100\%repolariation]$ is the resting membrane potential.

APDs determined for repolarisation values of 40, 50 and 70% were then determined from 10 kHz-smoothed data. These were defined as the first time points when the corresponding value was less than the value calculated using equation A-1 and fell between an average of the previous 20 ms and the following 20 ms. Values of APD_{90} were determined in a similar manner. However, defining the time at 90% repolarisation required detection of a value closer to the RMP, during which noise was more inhibitive because the change in fluorescent signal was small (i.e. the signal to noise ratio had decreased). Therefore, values for APD_{90} were calculated as the time points from data that was less than the calculated value

for 90% repolarisation, but that lay between averages of the previous and following 5 ms using data filtered to 1 kHz.

Figure A- 2 compares values for APD calculated from APs recorded optically from guinea pig myocytes loaded with 5 μ M di-4-ANEPPS and a maintenance dose of 200 nM dye using either the Excel based-spreadsheet or manually. Similar to calculations performed using the spreadsheet, manual calculations used an average of the last 200 ms to calculate 100% repolarisation, whilst all other values were measured by hand. Both analysis techniques produced almost identical results, demonstrating the accuracy of the Excel-based spreadsheet. Values manually obtained for APD₉₀ were 220 \pm 14 ms compared with 230 \pm 12 ms ($p = 0.16$, paired Student's t test, $n = 6$).

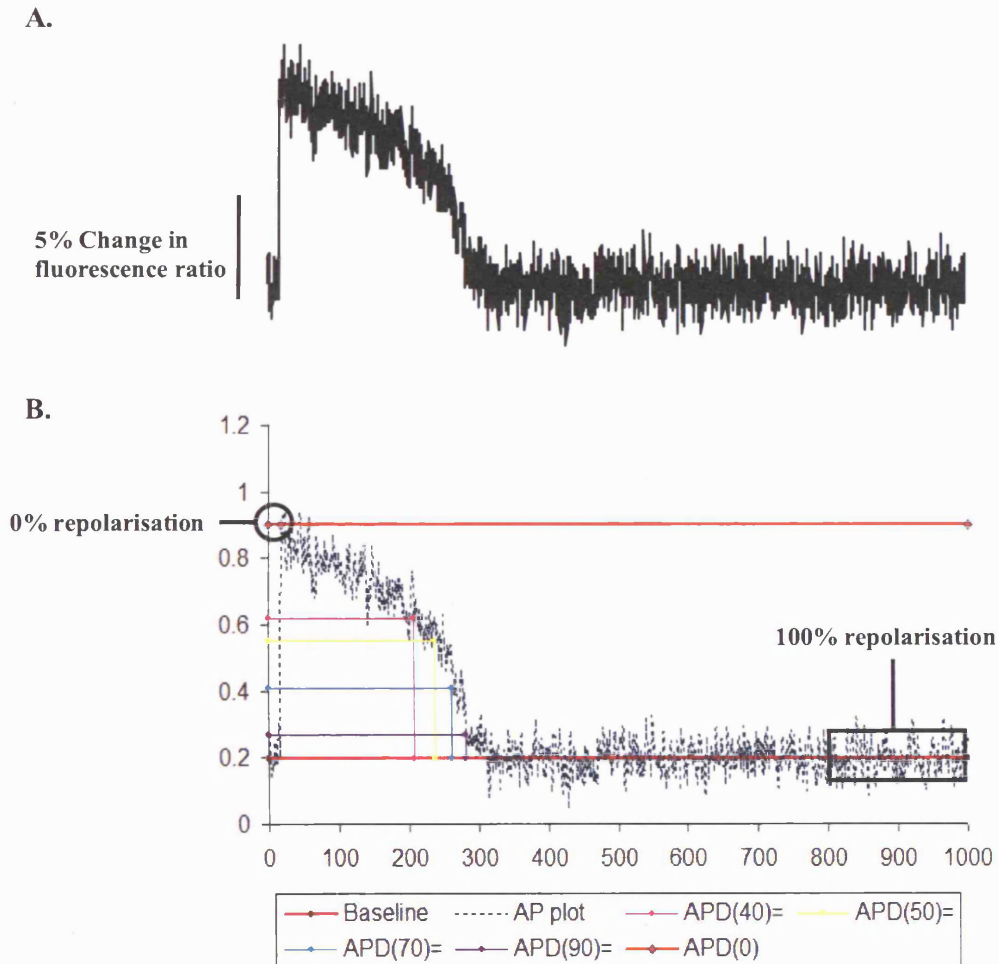


Figure A- 1. Computer assisted analysis of action potential durations.

(A) An average of 5 APs recorded from a guinea pig myocyte, in the absence of test compounds. (B) A screen shot of a 10-point moving average of the same data, with the positions of calculated APDs and 0 and 100% repolarisation values inset.

APPENDIX B.

In Chapter 6 I briefly referred to work that is ongoing using di-4-ANEPPS to monitor action potential durations (APDs) from isolated canine midmyocardial cells (M cell). Because this work was not done throughout the duration of the current study, it has not been included in great detail. However, I would be remiss if I did not provide an example of this ongoing work as it directly followed on from groundwork made in the current study.

The reason this is needed is because the conditions that proved to be successful for recording APDs from isolated guinea pig cardiac myocytes caused pronounced phototoxic effects when applied to the canine M cell. Guinea pig myocytes were incubated with 5 μ M di-4-ANEPPS for 20 min as well as being perfused with a 200 nM maintenance dose of the dye. To avoid phototoxic effects arising from prolonged exposure to excitation light, cells were only exposed for time periods of 5 s once in every 4 min. Using this technique it was possible to record action potentials (APs) for a minimum of six 5 s exposures. However, (refer to Chapter 3, Figure 3.5) the same protocol caused APD prolongation in canine M cells upon the first exposure and loss of stimulus on following exposures.

Recent work has demonstrated that using the same protocol for exposing cells to excitation light, 5 s in every 4 min, but by reducing the concentration of di-4-ANEPPS, it is still possible to record drug-induced changes in APD. This has been shown to be feasible by using 100 nM di-4-ANEPPS in the perfusate without preloading the cells prior to their placement in the tissue bath (where they were left to adhere to the surface for between 5 and 15 min). Figure-B1A shows averages of 5 APs recorded from an isolated canine M cell during perfusion with Tyrode containing either 0.1% DMSO, 1 μ M cisapride, which causes the AP to prolong, or 10 μ M cisapride, which causes the AP to shorten. Similarly, the graph in Figure B-1 compares the biphasic response from optical recordings from canine M cells to those recorded with a sharp electrode demonstrating an identical response between the two different techniques. Compared to values recorded in DMSO, the presence of 1 μ M cisapride caused a $16 \pm 10\%$ increase in optical measurements versus $12 \pm 8\%$ using a sharp electrode ($n = 5$ in both cases).

Although this work has not yet reached its conclusion it demonstrates that it is possible to record drug-induced changes in APD from canine M cells using the fluorescence emission of di-4-ANEPPS. However, reasons for the requirement for a different concentration of di-4-ANEPPS in canine cells compared to guinea pig cells remain to be determined. These may arise from species dependent differences or differences arising from the different cell isolation procedures (see Chapter 2 for details).

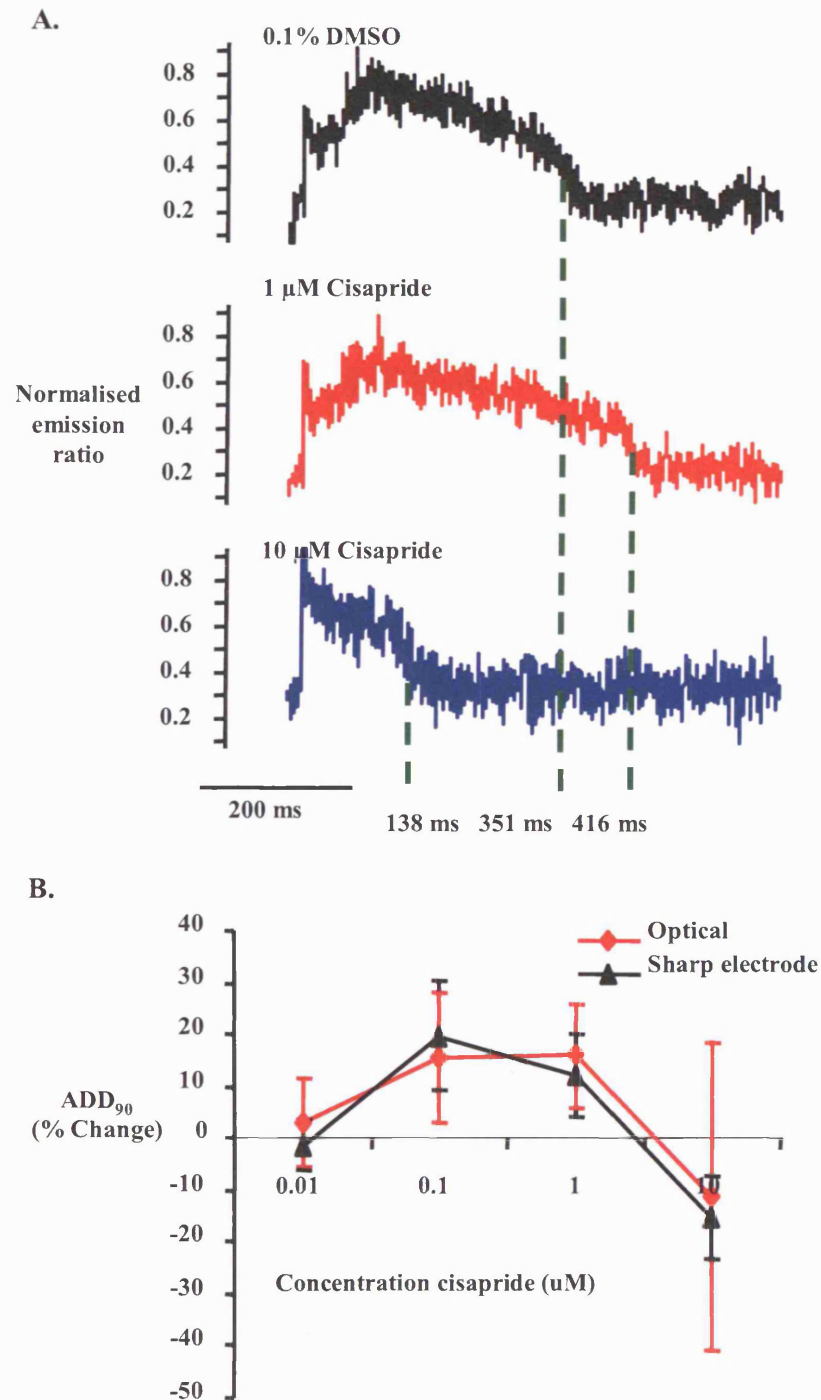


Figure B-1. Changes in APD in response to cisapride recorded from canine M cells using di-4-ANEPPS.

(A) Averages of 5 action potentials recorded from an isolated canine M cell loaded with 100 nM di-4-ANEPPS during perfusion with normal Tyrode containing 0.1% DMSO (black), 1 μ M cisapride (red) or 10 μ M cisapride (blue). (B) Graph showing changes in action potential duration as a percentage of the value recorded in 0.1% DMSO in response to increases in concentration of cisapride recorded from canine M cells with a sharp electrode (black) or optically with di-4-ANEPPS (red) ($n = 5$ in both cases).

Bibliography.

Abbott, G. W., Sesti, F., Splawski, I., Buck, M. E., Lehmann, M. H., Timothy, K. W., Keating, M. T., & Goldstein, S. A. (1999). MiRP1 forms I_{Kr} potassium channels with HERG and is associated with cardiac arrhythmia. *Cell* **97**, 175-87.

Abi-Gerges, N., Small, B. G., Lawrence, C. L., Hammond, T. G., Valentin, J. P., & Pollard, C. E. (2004). Evidence for gender differences in electrophysiological properties of canine Purkinje fibres. *Br J Pharmacol* **142**, 1255-64.

Abi-Gerges, N., Small, B. G., Lawrence, C. L., Hammond, T. G., Valentin, J. P., & Pollard, C. E. (2006). Gender differences in the slow delayed (I_{Ks}) but not in inward (I_{K1}) rectifier K^+ currents of canine Purkinje fibre cardiac action potential: key roles for I_{Ks} , beta-adrenoceptor stimulation, pacing rate and gender. *Br J Pharmacol* **147**, 653-60.

Advani, S. V. & Singh, B. N. (1995). Pharmacodynamic, pharmacokinetic and antiarrhythmic properties of d-sotalol, the dextro-isomer of sotalol. *Drugs* **49**, 664-79.

Ahmad, S. & Wolfe, S. (1995). Cisapride and torsades de pointes. *Lancet* **345**: 508. 1995.

Akar, F. G., Yan, G. X., Antzelevitch, C., & Rosenbaum, D. S. (2002). Unique topographical distribution of M cells underlies reentrant mechanism of torsade de pointes in the long-QT syndrome. *Circulation* **105**, 1247-53.

Anderson, M. E., Braun, A. P., Schulman, H., & Premack, B. A. (1994). Multifunctional Ca^{2+} /calmodulin-dependent protein kinase mediates Ca^{2+} -induced enhancement of the L-type Ca^{2+} current in rabbit ventricular myocytes. *Circ Res* **75**, 854-61.

Antzelevitch, C. (2001). Basic mechanisms of reentrant arrhythmias. *Curr Opin Cardiol* **16**, 1-7.

Antzelevitch, C. (2005). Role of transmural dispersion of repolarization in the genesis of drug-induced torsades de pointes. *Heart Rhythm* **2**, 9-15.

Armstrong, C. M. & Bezanilla, F. (1977). Inactivation of the sodium channel. II. Gating current experiments. *J Gen Physiol* **70**, 567-90.

- Armstrong, C. M. & Hille, B. (1998). Voltage-gated ion channels and electrical excitability. *Neuron* **20**, 371-80.
- Aronov, A. M. & Goldman, B. B. (2004). A model for identifying HERG K⁺ channel blockers. *Bioorg Med Chem* **12**, 2307-15.
- Backx, P. H. & Marban, E. (1993). Background potassium current active during the plateau of the action potential in guinea pig ventricular myocytes. *Circ Res* **72**, 890-900.
- Baker, L. C., London, B., Choi, B. R., Koren, G., & Salama, G. (2000). Enhanced dispersion of repolarization and refractoriness in transgenic mouse hearts promotes reentrant ventricular tachycardia. *Circ Res* **86**, 396-407.
- Balser, J. R. (2001). The cardiac sodium channel: gating function and molecular pharmacology. *J Mol Cell Cardiol* **33**, 599-613.
- Balser, J. R., Bennett, P. B., Hondeghem, L. M., & Roden, D. M. (1991). Suppression of time-dependent outward current in guinea pig ventricular myocytes. Actions of quinidine and amiodarone. *Circ Res* **69**, 519-29.
- Bardy, G. H., Ungerleider, R. M., Smith, W. M., & Ideker, R. E. (1983). A mechanism of torsades de pointes in a canine model. *Circulation* **67**, 52-9.
- Barry, W. H. (2006). Na⁺ "Fuzzy space": does it exist, and is it important in ischemic injury? *J Cardiovasc Electrophysiol* **17 Suppl 1**, S43-S46.
- Beach, J. M., McGahren, E. D., Xia, J., & Duling, B. R. (1996). Ratiometric measurement of endothelial depolarization in arterioles with a potential-sensitive dye. *Am J Physiol* **270**, H2216-H2227.
- Belus, A. & White, E. (2001). Effects of antibiotics on the contractility and Ca²⁺ transients of rat cardiac myocytes. *Eur J Pharmacol* **412**, 121-6.
- Belus, A. & White, E. (2002). Effects of streptomycin sulphate on I(CaL), I(Kr) and I(Ks) in guinea-pig ventricular myocytes. *Eur J Pharmacol* **445**, 171-8.

Ben-Oren, I., Peleg, G., Lewis, A., Minke, B., & Loew, L. (1996). Infrared nonlinear optical measurements of membrane potential in photoreceptor cells. *Biophys J* **71**, 1616-20.

Bennett, P. B., Yazawa, K., Makita, N., & George, A. L. (1995). Molecular mechanism for an inherited cardiac arrhythmia. *Nature* **376**, 683-5.

Bers, D. M. (2001). *Excitation Contraction Coupling and Cardiac Contractile Force*, 2nd Edition. ed. Kluwer Academic Publishers.

Bian, J., Cui, J., & McDonald, T. V. (2001). HERG K(+) channel activity is regulated by changes in phosphatidyl inositol 4,5-bisphosphate. *Circ Res* **89**, 1168-76.

Brachmann, J., Scherlag, B. J., Rosenshtraukh, L. V., & Lazzara, R. (1983). Bradycardia-dependent triggered activity: relevance to drug-induced multiform ventricular tachycardia. *Circulation* **68**, 846-56.

Brette, F., Komukai, K., & Orchard, C. H. (2002). Validation of formamide as a detubulation agent in isolated rat cardiac cells. *Am J Physiol Heart Circ Physiol* **283**, 1720-8.

Bridgland-Taylor, M. H., Hargreaves, A. C., Easter, A., Orme, A., Henthorn, D. C., Ding, M., Davis, A. M., Small, B. G., Heapy, C. G., Abi-Gerges, N., Persson, F., Jacobson, I., Sullivan, M., Albertson, N., Hammond, T. G., Sullivan, E., Valentin, J. P., & Pollard, C. E. (2006). Optimisation and validation of a medium-throughput electrophysiology-based hERG assay using IonWorkstrade mark HT. *J Pharmacol Toxicol Methods*.

Brunner, M., Kodirov, S. A., Mitchell, G. F., Buckett, P. D., Shibata, K., Folco, E. J., Baker, L., Salama, G., Chan, D. P., Zhou, J., & Koren, G. (2003). In vivo gene transfer of Kv1.5 normalizes action potential duration and shortens QT interval in mice with long QT phenotype. *Am J Physiol Heart Circ Physiol* **285**, 194-203.

Bullen, A. & Saggau, P. (1999). High-speed, random-access fluorescence microscopy: II. Fast quantitative measurements with voltage-sensitive dyes. *Biophys J* **76**, 2272-87.

Burashnikov, A. & Antzelevitch, C. (2000). Block of I(Ks) does not induce early afterdepolarization activity but promotes beta-adrenergic agonist-induced delayed afterdepolarization activity. *J Cardiovasc Electrophysiol* **11**, 458-65.

Burle Industries. Photomultiplier Handbook.

Cannon, S. C. (1996). Slow inactivation of sodium channels: more than just a laboratory curiosity. *Biophys J* **71**, 5-7.

Cantiello, H. F., Stow, J. L., Prat, A. G., & Ausiello, D. A. (1991). Actin filaments regulate epithelial Na⁺ channel activity. *Am J Physiol* **261**, 882-8.

Carlsson, L., Almgren, O., & Duker, G. (1990). QTU-prolongation and torsades de pointes induced by putative class III antiarrhythmic agents in the rabbit: etiology and interventions. *J Cardiovasc Pharmacol* **16**, 276-85.

Catterall, W. A., Goldin, A. L., & Waxman, S. G. (2005a). International Union of Pharmacology. XLVII. Nomenclature and structure-function relationships of voltage-gated sodium channels. *Pharmacol Rev* **57**, 397-409.

Catterall, W. A., Perez-Reyes, E., Snutch, T. P., & Striessnig, J. (2005b). International Union of Pharmacology. XLVIII. Nomenclature and structure-function relationships of voltage-gated calcium channels. *Pharmacol Rev* **57**, 411-25.

Cavalli, A., Poluzzi, E., De Ponti, F., & Recanatini, M. (2002). Toward a pharmacophore for drugs inducing the long QT syndrome: insights from a CoMFA study of HERG K(+) channel blockers. *J Med Chem* **45**, 3844-53.

Champeroux, P., Viaud, K., El Amrani, A. I., Fowler, J. S., Martel, E., Le Guennec, J. Y., & Richard, S. (2005). Prediction of the risk of Torsade de Pointes using the model of isolated canine Purkinje fibres. *Br J Pharmacol* **144**, 376-85.

Chang, P. Y. & Jackson, M. B. (2003). Interpretation and optimization of absorbance and fluorescence signals from voltage-sensitive dyes. *J Membr Biol* **196**, 105-16.

Chantest. <http://www.chantest.com/Flyers/Channelpanel.pdf>. 2007.

Chaudhary, K. W., O'Neal, J. M., Mo, Z. L., Fermini, B., Gallavan, R. H., & Bahinski, A. (2006). Evaluation of the rubidium efflux assay for preclinical identification of HERG blockade. *Assay Drug Dev Technol* **4**, 73-82.

Cheng, Y. & Prusoff, W. H. (1973). Relationship between the inhibition constant (K_1) and the concentration of inhibitor which causes 50 per cent inhibition (I_{50}) of an enzymatic reaction. *Biochem Pharmacol* **22**, 3099-108.

Chiang, C. E., Wang, T. M., & Luk, H. N. (2004). Inhibition of L-type Ca^{2+} current in Guinea pig ventricular myocytes by cisapride. *J Biomed Sci* **11**, 303-14.

Cho, H., Hwang, J. Y., Kim, D., Shin, H. S., Kim, Y., Earm, Y. E., & Ho, W. K. (2002). Acetylcholine-induced phosphatidylinositol 4,5-bisphosphate depletion does not cause short-term desensitization of G protein-gated inwardly rectifying K^+ current in mouse atrial myocytes. *J Biol Chem* **277**, 27742-7.

Choi, B. R., Burton, F., & Salama, G. (2002). Cytosolic Ca^{2+} triggers early afterdepolarizations and Torsade de Pointes in rabbit hearts with type 2 long QT syndrome. *J Physiol* **543**, 615-31.

Cohen, L. B., Salzberg, B. M., Davila, H. V., Ross, W. N., Landowne, D., Waggoner, A. S., & Wang, C. H. (1974). Changes in axon fluorescence during activity: molecular probes of membrane potential. *J Membr Biol* **19**, 1-36.

Committee for Proprietary Medicinal Products. (1997). Points to consider. The assessment of QT interval prolongation by non-cardiovascular medicinal products. CPMP/986/96 1997.

Cordeiro, J. M., Greene, L., Heilmann, C., Antzelevitch, D., & Antzelevitch, C. (2004). Transmural heterogeneity of calcium activity and mechanical function in the canine left ventricle. *Am J Physiol Heart Circ Physiol* **286**, 1471-9.

Cornfield, D. N., Stevens, T., McMurtry, I. F., Abman, S. H., & Rodman, D. M. (1994). Acute hypoxia causes membrane depolarization and calcium influx in fetal pulmonary artery smooth muscle cells. *Am J Physiol* **266**, 469-75.

Cukierman, S. (1996). Regulation of voltage-dependent sodium channels. *J Membr Biol* **151**, 203-14.

Curran, M. E., Splawski, I., Timothy, K. W., Vincent, G. M., Green, E. D., & Keating, M. T. (1995). A molecular basis for cardiac arrhythmia: HERG mutations cause long QT syndrome. *Cell* **80**, 795-803.

- Dainty, J. C. E. (1984). *Laser speckle and related phenomena*. Springer-Verlag, New York..
- del Camino, D., Holmgren, M., Liu, Y., & Yellen, G. (2000). Blocker protection in the pore of a voltage-gated K⁺ channel and its structural implications. *Nature* **403**, 321-5.
- Delgado, C., Artiles, A., Gomez, A. M., & Vassort, G. (1999). Frequency-dependent increase in cardiac Ca²⁺ current is due to reduced Ca²⁺ release by the sarcoplasmic reticulum. *J Mol Cell Cardiol* 1783-1793.
- Dessertenne, F. (1966). [Ventricular tachycardia with 2 variable opposing foci]. *Arch Mal Coeur Vaiss* **59**, 263-72.
- Diaz, G. J., Daniell, K., Leitza, S. T., Martin, R. L., Su, Z., McDermott, J. S., Cox, B. F., & Gintant, G. A. (2004). The [³H]dofetilide binding assay is a predictive screening tool for hERG blockade and proarrhythmia: Comparison of intact cell and membrane preparations and effects of altering [K⁺]_o. *J Pharmacol Toxicol Methods* **50**, 187-99.
- Djurisic, M., Zochowski, M., Wachowiak, M., Falk, C. X., Cohen, L. B., & Zecevic, D. (2003). Optical monitoring of neural activity using voltage-sensitive dyes. *Methods Enzymol* **361**, 423-51.
- Dong, M., Sun, X., Prinz, A. A., & Wang, H. S. (2006). Effect of simulated I(to) on guinea pig and canine ventricular action potential morphology. *Am J Physiol Heart Circ Physiol* **291**, 631-7.
- Dorn, A., Hermann, F., Ebneith, A., Bothmann, H., Trube, G., Christensen, K., & Apfel, C. (2005). Evaluation of a high-throughput fluorescence assay method for HERG potassium channel inhibition. *J Biomol Screen* **10**, 339-47.
- Drolet, B., Khalifa, M., Daleau, P., Hamelin, B. A., & Turgeon, J. (1998). Block of the rapid component of the delayed rectifier potassium current by the prokinetic agent cisapride underlies drug-related lengthening of the QT interval. *Circulation* **97**, 204-10.
- Dumaine, R. & Cordeiro, J. M. (2007). Comparison of K(+) currents in cardiac Purkinje cells isolated from rabbit and dog. *J Mol Cell Cardiol* **42**, 378-89.

Durell, S. R., Hao, Y., & Guy, H. R. (1998). Structural models of the transmembrane region of voltage-gated and other K⁺ channels in open, closed, and inactivated conformations. *J Struct Biol* **121**, 263-84.

Durrer, D., Formijne, P., van, D. A. M., van, Buller, J., & Meyler, F. L. (1961). The electrocardiogram in normal and some abnormal conditions; in revived human fetal heart and in acute and chronic coronary occlusion. *Am Heart J* **61**, 303-16.

Durrer, D. & Roos, J. P. (1967). Epicardial excitation of the ventricles in a patient with wolff-Parkinson-White syndrome (type B). *Circulation* **35**, 15-21.

Eckardt, L., Haverkamp, W., Mertens, H., Johna, R., Clague, J. R., Borggrefe, M., & Breithardt, G. (1998). Drug-related torsades de pointes in the isolated rabbit heart: comparison of clofilium, d,l-sotalol, and erythromycin. *J Cardiovasc Pharmacol* **32**, 425-34.

Einthoven, W. (1901). Un nouveau galvanometre. *Arch Neerl Sc Ex Nat* **6**, 625.

Eisner, D. A., Choi, H. S., Diaz, M. E., O'Neill, S. C., & Trafford, A. W. (2000). Integrative analysis of calcium cycling in cardiac muscle. *Circ Res* **87**, 1087-94.

Ekins, S., Crumb, W. J., Sarazan, R. D., Wikel, J. H., & Wrighton, S. A. (2002). Three-dimensional quantitative structure-activity relationship for inhibition of human ether-a-go-go-related gene potassium channel. *J Pharmacol Exp Ther* **301**, 427-34.

Endoh, M. & Blinks, J. R. (1988). Actions of sympathomimetic amines on the Ca²⁺ transients and contractions of rabbit myocardium: reciprocal changes in myofibrillar responsiveness to Ca²⁺ mediated through alpha- and beta-adrenoceptors. *Circ Res* **62**, 247-65.

Entcheva, E., Kostov, Y., Tchernev, E., & Tung, L. (2004). Fluorescence imaging of electrical activity in cardiac cells using an all-solid-state system. *IEEE Trans Biomed Eng* **51**, 333-41.

Fast, V. G. (2005). Simultaneous optical imaging of membrane potential and intracellular calcium. *J Electrocardiol* **38**, 107-12.

Fedida, D., Wible, B., Wang, Z., Fermini, B., Faust, F., Nattel, S., & Brown, A. M. (1993). Identity of a novel delayed rectifier current from human heart with a cloned K⁺ channel current. *Circ Res* **73**, 210-6.

Ficker, E., Taglialatela, M., Wible, B. A., Henley, C. M., & Brown, A. M. (1994). Spermine and spermidine as gating molecules for inward rectifier K⁺ channels. *Science* **266**, 1068-72.

Findlay, I. (2003). Is there an A-type K⁺ current in guinea pig ventricular myocytes? *Am J Physiol Heart Circ Physiol* **284**, 598-604.

Fish, J. M. & Antzelevitch, C. (2004). Role of sodium and calcium channel block in unmasking the Brugada syndrome. *Heart Rhythm* **1**, 210-7.

Flewellling, R. F. & Hubbell, W. L. (1986). The membrane dipole potential in a total membrane potential model. Applications to hydrophobic ion interactions with membranes. *Biophys J* **49**, 541-52.

Gima, K. & Rudy, Y. (2002). Ionic current basis of electrocardiographic waveforms: A model study. *Circulation Research* **90**, 889-896.

Gintant, G. A., Limberis, J. T., McDermott, J. S., Wegner, C. D., & Cox, B. F. (2001). The canine Purkinje fiber: an in vitro model system for acquired long QT syndrome and drug-induced arrhythmogenesis. *J Cardiovasc Pharmacol* **37**, 607-18.

Girouard, S. D., Laurita, K. R., & Rosenbaum, D. S. (1996). Unique properties of cardiac action potentials recorded with voltage-sensitive dyes. *J Cardiovasc Electrophysiol* **7**, 1024-38.

Gonzalez, J. E. & Maher, M. P. (2002). Cellular fluorescent indicators and voltage/ion probe reader (VIPR) tools for ion channel and receptor drug discovery. *Receptors Channels* **8**, 283-95.

Gonzalez, J. E. & Tsien, R. Y. (1997). Improved indicators of cell membrane potential that use fluorescence resonance energy transfer. *Chem Biol* **4**, 269-77.

Grant, A. O., Starmer, C. F., & Strauss, H. C. (1983). Unitary sodium channels in isolated cardiac myocytes of rabbit. *Circ Res* **53**, 823-9.

Guo, D., Zhao, X., Wu, Y., Liu, T., Kowey, P. R., & Yan, G. X. (2007). L-type calcium current reactivation contributes to arrhythmogenesis associated with action potential triangulation. *J Cardiovasc Electrophysiol* **18**, 196-203.

Gupta, R. K., Salzberg, B. M., Grinvald, A., Cohen, L. B., Kamino, K., Leshner, S., Boyle, M. B., Waggoner, A. S., & Wang, C. H. (1981). Improvements in optical methods for measuring rapid changes in membrane potential. *J Membr Biol* **58**, 123-37.

Guthrie, H., Livingston, F. S., Gubler, U., & Garippa, R. (2005). A place for high-throughput electrophysiology in cardiac safety: screening hERG cell lines and novel compounds with the ion works HTTM system. *J Biomol Screen* **10**, 832-40.

Hamlin, R. L. (2007). The guinea pig in cardiac safety pharmacology. *J Pharmacol Toxicol Methods* **55**, 1-2.

Haughland, R. P. & Johnson, I. D. (1999). Intracellular ion indicators.

Haverkamp, W., Breithardt, G., Camm, A. J., Janse, M. J., Rosen, M. R., Antzelevitch, C., Escande, D., Franz, M., Malik, M., Moss, A., & Shah, R. (2000). The potential for QT prolongation and proarrhythmia by non-antiarrhythmic drugs: clinical and regulatory implications. Report on a policy conference of the European Society of Cardiology. *Eur Heart J* **21**, 1216-31.

Haws, C. M., Winegar, B. D., & Lansman, J. B. (1996). Block of single L-type Ca^{2+} channels in skeletal muscle fibers by aminoglycoside antibiotics. *J Gen Physiol* **107**, 421-32.

Hermesmeyer, K. (1988). Ion channel effects of pinacidil in vascular muscle. *Drugs* **36 Suppl 7**, 29-32.

Hess, P. (1988). Elementary properties of cardiac calcium channels: a brief review. *Can J Physiol Pharmacol* **66**, 1218-23.

Hille, B. (2001). *Ion Channels of Excitable Membranes* Sinauer Associates Inc., U.S.; 3rd Ed edition.

Hirai, S., Kotake, H., Kurata, Y., Hisatome, I., Hasegawa, J., & Mashiba, H. (1990). Effect of pinacidil on the electrophysiological properties in guinea-pig papillary muscle and rabbit sinoatrial node. *J Pharm Pharmacol* **42**, 339-43.

Hodgkin, A. L. & Huxley, A. F. (1952). Currents carried by sodium and potassium ions through the membrane of the giant axon of *Loligo*. *J Physiol* **116**, 449-72.

Holley, L. K. & Knisley, S. B. (1997). Transmembrane potentials during high voltage shocks in ischemic cardiac tissue. *Pacing Clin Electrophysiol* **20**, 146-52.

Hondeghem, L. M. (2005). TRIad: foundation for proarrhythmia (triangulation, reverse use dependence and instability). *Novartis Found Symp* **266**, 235-44.

Hondeghem, L. M., Carlsson, L., & Duker, G. (2001). Instability and triangulation of the action potential predict serious proarrhythmia, but action potential duration prolongation is antiarrhythmic. *Circulation* **103**, 2004-13.

Hondeghem, L. M. & Hoffmann, P. (2003). Blinded test in isolated female rabbit heart reliably identifies action potential duration prolongation and proarrhythmic drugs: importance of triangulation, reverse use dependence, and instability. *J Cardiovasc Pharmacol* **41**, 14-24.

Hondeghem, L. M., Lu, H. R., van Rossem, K., & De Clerck, F. (2003). Detection of proarrhythmia in the female rabbit heart: blinded validation. *J Cardiovasc Electrophysiol* **14**, 287-94.

Honig, P. K., Wortham, D. C., Zamani, K., Conner, D. P., Mullin, J. C., & Cantilena, L. R. (1993). Terfenadine-ketoconazole interaction. Pharmacokinetic and electrocardiographic consequences. *JAMA* **269**, 1513-8.

Hoshi, T., Zagotta, W. N., & Aldrich, R. W. (1990). Biophysical and molecular mechanisms of Shaker potassium channel inactivation. *Science* **250**, 533-8.

Hoshi, T., Zagotta, W. N., & Aldrich, R. W. (1991). Two types of inactivation in Shaker K⁺ channels: effects of alterations in the carboxy-terminal region. *Neuron* **7**, 547-56.

Hryshko, L. V. & Bers, D. M. (1990). Ca current facilitation during postrest recovery depends on Ca entry. *Am J Physiol* **259**, 951-61.

Huser, J., Lipp, P., & Niggli, E. (1996). Confocal microscopic detection of potential-sensitive dyes used to reveal loss of voltage control during patch-clamp experiments. *Pflugers Arch*. **433**, 194-199.

Hutter, O. F. & Noble, D. (1961). Anion conductance of cardiac muscle. *J Physiol* **157**, 335-50.

Inoue, S. (1986). *Video Microscopy* Plenum Press, New York.

Isacoff, E. Y., Jan, Y. N., & Jan, L. Y. (1991). Putative receptor for the cytoplasmic inactivation gate in the Shaker K⁺ channel. *Nature* **353**, 86-90.

Janse, M. J. & Wit, A. L. (1989). Electrophysiological mechanisms of ventricular arrhythmias resulting from myocardial ischemia and infarction. *Physiol Rev* **69**, 1049-169.

Jervell, A. & Lange-Nielsen, F. (1957). Congenital deaf-mutism, functional heart disease with prolongation of the Q-T interval and sudden death. *Am Heart J* **54**, 59-68.

Johnson, E. A. & Tille, J. (1961). Investigations of the electrical properties of cardiac muscle fibres with the aid of intracellular double-barrelled electrodes. *J Gen Physiol* **44**, 443-67.

Josephson, I. R., Sanchez-Chapula, J., & Brown, A. M. (1984). A comparison of calcium currents in rat and guinea pig single ventricular cells. *Circ Res* **54**, 144-56.

Josephson, M. E. (2001). Foreword. pp. 33-46.

Kaplan, W. D. & Trout W.E. (1969). The behaviour of four neurological mutants of drosophila. *Genetics* 399-409.

Kass, R. S. & Sanguinetti, M. C. (1984). Inactivation of calcium channel current in the calf cardiac Purkinje fiber. Evidence for voltage- and calcium-mediated mechanisms. *J Gen Physiol* **84**, 705-26.

Keating, M. T. & Sanguinetti, M. C. (2001). Molecular and cellular mechanisms of cardiac arrhythmias. *Cell* **104**, 569-80.

Kiehn, J., Lacerda, A. E., Wible, B., & Brown, A. M. (1996). Molecular physiology and pharmacology of HERG. Single-channel currents and block by dofetilide. *Circulation* **94**, 2572-9.

Kii, Y. & Ito, T. (2002). Drug-induced ventricular tachyarrhythmia in isolated rabbit hearts with atrioventricular block. *Pharmacol Toxicol* **90**, 246-53.

Klauke, N., Smith, G. L., & Cooper, J. M. (2005). Stimulation of isolated ventricular myocytes within an open architecture microarray. *IEEE Trans Biomed Eng* **52**, 531-8.

Klausner, R. D., Kleinfeld, A. M., Hoover, R. L., & Karnovsky, M. J. (1980). Lipid domains in membranes. Evidence derived from structural perturbations induced by free fatty acids and lifetime heterogeneity analysis. *J Biol Chem* **255**, 1286-95.

Knisley, S. B., Justice, R. K., Kong, W., & Johnson, P. L. (2000). Ratiometry of transmembrane voltage-sensitive fluorescent dye emission in hearts. *Am J Physiol Heart Circ Physiol* **279**, 1421-33.

Kolliker, A. & Muller, H. (1856). Nachweis der negativen Schwankung des Muskelstromes am natürlich sich contrahirenden Muskel". *Verh Phys Med Ges* **6**, 528-33.

Kongsamut, S., Kang, J., Chen, X.L., Roehr, J., & Rampe D. (2002). A comparison of the receptor binding and HERG channel affinities for a series of antipsychotic drugs. *Eur J Pharmacol* **16;450(1)**, 37-41.

Kubo, Y., Baldwin, T. J., Jan, Y. N., & Jan, L. Y. (1993). Primary structure and functional expression of a mouse inward rectifier potassium channel. *Nature* **362**, 127-33.

Lawrence, C. & Rodrigo, G. C. (1999). A Na⁺-activated K⁺ current (I_{K,Na}) is present in guinea-pig but not rat ventricular myocytes. *Pflugers Arch* **437**, 831-8.

Lawrence, C. L., Bridgland-Taylor, M. H., Pollard, C. E., Hammond, T. G., & Valentin, J. P. (2006). A rabbit Langendorff heart proarrhythmia model: predictive value for clinical identification of Torsades de Pointes. *Br J Pharmacol* **149**, 845-60.

Lawrence, C. L., Pollard, C. E., Hammond, T. G., & Valentin, J. P. (2005). Nonclinical proarrhythmia models: predicting Torsades de Pointes. *J Pharmacol Toxicol Methods* **52**, 46-59.

Lazzara, R. (1997). Twisting of the points. *J Am Coll Cardiol* **29**, 843-5.

Leaf, A. & Xiao, Y. F. (2001). The modulation of ionic currents in excitable tissues by n-3 polyunsaturated fatty acids. *J Membr Biol* **184**, 263-71.

Leaf, A., Xiao, Y. F., Kang, J. X., & Billman, G. E. (2003). Prevention of sudden cardiac death by n-3 polyunsaturated fatty acids. *Pharmacol Ther* **98**, 355-77.

Leblanc, N. & Hume, J. R. (1990). Sodium current-induced release of calcium from cardiac sarcoplasmic reticulum. *Science* **248**, 372-6.

Lederer, W. J., Niggli, E., & Hadley, R. W. (1990). Sodium-calcium exchange in excitable cells: fuzzy space. *Science* **248**, 283.

Leifert, W. R., McMurchie, E. J., & Saint, D. A. (1999). Inhibition of cardiac sodium currents in adult rat myocytes by n-3 polyunsaturated fatty acids. *J Physiol* **520 Pt 3**, 671-9.

Lemaire, S., Piot, C., Leclercq, F., Leuranguer, V., Nargeot, J., & Richard, S. (1998). Heart rate as a determinant of L-type Ca^{2+} channel activity: mechanisms and implication in force-frequency relation. *Basic Res Cardiol* **93 Suppl 1**, 51-9.

Lewis, G., Feil, S., & Stroud, W. D. The nature of auricular flutter. *Heart* **7**, 131-346. 1920.

Li, X. W., Niu, S. C., Zhang, X. P., Lu, J. Y., Bai, F., Zhang, L., & Wu, B. W. (2006). Differences of promethazine and terfenadine on ion channels in guinea pig ventricular myocytes. *Chin Med J (Engl)* **119**, 944-7.

Liu, D. W., Gintant, G. A., & Antzelevitch, C. (1993). Ionic bases for electrophysiological distinctions among epicardial, midmyocardial, and endocardial myocytes from the free wall of the canine left ventricle. *Circ Res* **72**, 671-87.

Liu, D.-W. & Antzelevitch, C. (1995). Characteristics of the Delayed Rectifier Current (I_{Kr} and I_{Ks}) in Canine Ventricular Epicardial, Midmyocardial, and Endocardial Myocytes : A Weaker I_{Ks} Contributes to the Longer Action Potential of the M Cell. *Circ Res* **76**, 351-365.

Liu, S., Melchert, R. B., & Kennedy, R. H. (1997). Inhibition of L-type Ca^{2+} channel current in rat ventricular myocytes by terfenadine. *Circ Res* **81**, 202-10.

Loew, L. M. (1999). Potentiometric Membrane Dyes and Imaging Membrane Potential in Single Cells. From Fluorescent and Luminescent Probes for Biological Activity. Ed. by Mason W. T.

Loew, L. M. (2001). Mechanisms and Principles of Voltage-Sensitive Fluorescence. pp. 33-46. From Fluorescent and Luminescent Probes for Biological Activity. Ed. by Mason W. T.

Lopatin, A. N., Makhina, E. N., & Nichols, C. G. (1994). Potassium channel block by cytoplasmic polyamines as the mechanism of intrinsic rectification. *Nature* **372**, 366-9.

Lopez-Lopez, J. R., Shacklock, P. S., Balke, C. W., & Wier, W. G. (1995). Local calcium transients triggered by single L-type calcium channel currents in cardiac cells. *Science* **268**, 1042-5.

Lu, H. R., Vlamincx, E., Van Ammel, K., & De Clerck, F. (2002). Drug-induced long QT in isolated rabbit Purkinje fibers: importance of action potential duration, triangulation and early afterdepolarizations. *Eur J Pharmacol* **452**, 183-92.

Luo, C. H. & Rudy, Y. (1994). A dynamic model of the cardiac ventricular action potential. II. Afterdepolarizations, triggered activity, and potentiation. *Circ Res* **74**, 1097-113.

Mackiewicz, U. & Lewartowski, B. (2006). Temperature dependent contribution of Ca^{2+} transporters to relaxation in cardiac myocytes: important role of sarcolemmal Ca^{2+} -ATPase. *J Physiol Pharmacol* **57**, 3-15.

MacKinnon, R., Aldrich, R. W., & Lee, A. W. (1993). Functional stoichiometry of Shaker potassium channel inactivation. *Science* **262**, 757-9.

MacNeil, D. J. (1997). The side effect profile of class III antiarrhythmic drugs: focus on d,l-sotalol. *Am J Cardiol* **80**, 90G-98G.

MacNeil, D. J., Davies, R. O., & Deitchman, D. (1993). Clinical safety profile of sotalol in the treatment of arrhythmias. *Am J Cardiol* **72**, 44A-50A.

Mannuzzu, L. M., Moronne, M. M., & Isacoff, E. Y. (1996). Direct physical measure of conformational rearrangement underlying potassium channel gating. *Science* **271**, 213-6.

Mayer, A. G. Rhythmical pulsations in scyphomedusae. I. *Carnegie Inst.* **47**, 64. 1906.

McAllister, R. E. & Noble, D. (1967). The effect of subthreshold potentials on the membrane current in cardiac Purkinje fibres. *J Physiol* **190**, 381-7.

- McDermott, J. S., Salmen, H. J., Cox, B. F., & Gintant, G. A. (2002). Importance of species selection in arrhythmogenic models of Q-T interval prolongation. *Antimicrob Agents Chemother* **46**, 938-9.
- Mechmann, S. & Pott, L. (1986). Identification of Na-Ca exchange current in single cardiac myocytes. *Nature* **319**, 597-9.
- Miller, A. L. & Langton, P. D. (1998). Streptomycin inhibition of myogenic tone, K⁺-induced force and block of L-type calcium current in rat cerebral arteries. *J Physiol* **508** (Pt 3), 793-800.
- Milnes, J.T., Witchel, H.J., Leaney, J.L., Leishman, D.J., & Hancox, J.C. (2006). hERG K⁺ channel blockade by the antipsychotic drug thioradizine: An obligatory role for the S6 helix residue F656. *Biochem Biophys Res Commun* **351**, 273-80.
- Mines, G. R. (1913). On dynamic equilibrium in the heart. *J Physiol* **46**, 349-83.
- Ming, Z. & Nordin, C. (1995). Terfenadine blocks time-dependent Ca²⁺, Na⁺, and K⁺ channels in guinea pig ventricular myocytes. *J Cardiovasc Pharmacol* **26**, 761-9.
- Mitcheson, J. S., Chen, J., Lin, M., Culberson, C., & Sanguinetti, M. C. (2000a). A structural basis for drug-induced long QT syndrome. *Proc Natl Acad Sci U S A* **97**, 12329-33.
- Mitcheson, J. S., Chen, J., & Sanguinetti, M. C. (2000b). Trapping of a methanesulfonanilide by closure of the HERG potassium channel activation gate. *J Gen Physiol* **115**, 229-40.
- Mitra, R. & Morad, M. (1985). A uniform enzymatic method for dissociation of myocytes from hearts and stomachs of vertebrates. *Am J Physiol* **249**, 1056-60.
- Morad, M. & Salama, G. (1979). Optical probes of membrane potential in heart muscle. *J Physiol* **292**, 267-95.
- Morales, M. J., Castellino, R. C., Crews, A. L., Rasmusson, R. L., & Strauss, H. C. (1995). A novel beta subunit increases rate of inactivation of specific voltage-gated potassium channel alpha subunits. *J Biol Chem* **270**, 6272-7.

Morgan, T. K. & Sullivan, M. E. (1992). An overview of class III electrophysiological agents: a new generation of antiarrhythmic therapy. *Prog Med Chem* **29**, 65-108.

Neher, E. & Sakmann, B. (1976). Single-channel currents recorded from membrane of denervated frog muscle fibres. *Nature* **260**, 799-802.

Neher, E., Sakmann, B., & Steinbach, J. H. (1978). The extracellular patch clamp: a method for resolving currents through individual open channels in biological membranes. *Pflugers Arch* **375**, 219-28.

Nerbonne, J. M. (2000). Molecular basis of functional voltage-gated K⁺ channel diversity in the mammalian myocardium. *J Physiol* **525 Pt 2**, 285-98.

Nichols, C. G., Ripoll, C., & Lederer, W. J. (1991). ATP-sensitive potassium channel modulation of the guinea pig ventricular action potential and contraction. *Circ Res* **68**, 280-7.

Nygren, A., Lomax, A. E., & Giles, W. R. (1922). Heterogeneity of Action Potential Durations in Isolated Mouse Left and Right Atria Recorded Using Voltage-Sensitive Dye Mapping. *Am J Physiol Heart Circ Physiol*.

Obaid, A. L., Loew, L. M., Wuskell, J. P., & Salzberg, B. M. (2004). Novel naphthylstyryl-pyridium potentiometric dyes offer advantages for neural network analysis. *J Neurosci Methods* **134**, 179-90.

Ogden, D. (1994). Microelectrode electronics. From Microelectrode Techniques: The Plymouth Workshop Handbook. 2nd Edition. Ed. by Ogden, D.

Ohtani, H., Taninaka, C., Hanada, E., Kotaki, H., Sato, H., Sawada, Y., & Iga, T. (2000). Comparative pharmacodynamic analysis of Q-T interval prolongation induced by the macrolides clarithromycin, roxithromycin, and azithromycin in rats. *Antimicrob Agents Chemother* **44**, 2630-7.

Persson, F., Carlsson, L., Duker, G., & Jacobson, I. (2005). Blocking characteristics of hERG, hNav1.5, and hKvLQT1/hminK after administration of the novel anti-arrhythmic compound AZD7009. *J Cardiovasc Electrophysiol* **16**, 329-41.

Pfizer Inc. U.S. Prescribing information (69-5549-002). Tikosyn (dofetilide capsules). 2004. New York: Pfizer, Inc..

Poelzing, S., Roth, B. J., & Rosenbaum, D. S. (1929). Optical Measurements Reveal Nature of Intercellular Coupling Across the Ventricular Wall. *Am J Physiol Heart Circ Physiol*.

Pratt, C. M., Ruberg, S., Morganroth, J., McNutt, B., Woodward, J., Harris, S., Ruskin, J., & Moye, L. (1996). Dose-response relation between terfenadine (Seldane) and the QTc interval on the scalar electrocardiogram: distinguishing a drug effect from spontaneous variability. *Am Heart J* **131**, 472-80.

Pruvot, E. J., Katra, R. P., Rosenbaum, D. S., & Laurita, K. R. (2004). Role of calcium cycling versus restitution in the mechanism of repolarization alternans. *Circ Res* **94**, 1083-90.

Puglisi, J. L., Yuan, W., Bassani, J. W., & Bers, D. M. (1999). Ca²⁺ influx through Ca²⁺ channels in rabbit ventricular myocytes during action potential clamp: influence of temperature. *Circ Res* **85**, e7-e16.

Rampe, D., Roy, M.L., Dennis, A., & Brown, A.M. (1997). A mechanism for the proarrhythmic effects of cisapride (Propulsid): high affinity blockade of the human cardiac potassium channel HERG. *FEBS Lett.* **417**(1), 28-32.

Ravens, U. & Wettwer, E. (1998). Electrophysiological aspects of changes in heart rate. *Basic Res Cardiol* **93 Suppl 1**, 60-5.

Redfern, W. S., Carlsson, L., Davis, A. S., Lynch, W. G., MacKenzie, I., Palethorpe, S., Siegl, P. K., Strang, I., Sullivan, A. T., Wallis, R., Camm, A. J., & Hammond, T. G. (2003). Relationships between preclinical cardiac electrophysiology, clinical QT interval prolongation and torsade de pointes for a broad range of drugs: evidence for a provisional safety margin in drug development. *Cardiovasc Res* **58**, 32-45.

Redfern, W. S., Wakefield, I. D., Prior, H., Pollard, C. E., Hammond, T. G., & Valentin, J. P. (2002). Safety pharmacology--a progressive approach. *Fundam Clin Pharmacol* **16**, 161-73.

Reuveny, E., Slesinger, P. A., Inglese, J., Morales, J. M., Iniguez-Lluhi, J. A., Lefkowitz, R. J., Bourne, H. R., Jan, Y. N., & Jan, L. Y. (1994). Activation of the cloned muscarinic potassium channel by G protein beta gamma subunits. *Nature* **370**, 143-6.

Rezazadeh, S., Hesketh, J. C., & Fedida, D. (2004). Rb⁺ flux through hERG channels affects the potency of channel blocking drugs: correlation with data obtained using a high-throughput Rb⁺ efflux assay. *J Biomol Screen* **9**, 588-97.

Ridley, J.M., Milnes, J.T., Witchel, H.J., & Hancox, J.C. (2004). High affinity HERG K⁺ channel blockade by the antiarrhythmic agent dronedarone: resistance to mutations of the S6 residues Y652 and F656. *Biochem Biophys Res Commun* **325**, 883-91.

Ridley, J.M., Milnes, J.T., Duncan, R.S., McPate, M.J., James, A.F., Witchel, H.J., & Hancox, J.C. (2006). Inhibition of the HERG K⁺ channel by the antifungal drug ketoconazole depends on channel gating and involves the S6 residue F656. *FEBS letters* **580**, 1999-2005.

Roden, D. M. & George, A. L. (1997). Structure and function of cardiac sodium and potassium channels. *Am J Physiol* **273**, 511-25.

Rodrigo, G. C. & Chapman, R. A. (1990). A sodium-activated potassium current in intact ventricular myocytes isolated from the guinea-pig heart. *Exp Physiol* **75**, 839-42.

Rodrigo, G. C. & Chapman, R. A. (1991). The calcium paradox in isolated guinea-pig ventricular myocytes: effects of membrane potential and intracellular sodium. *J Physiol* **434**, 627-45.

Rodrigo, G. C., Dhanapala, S., & Macknight, A. D. (1999). Effects of eicosapentaenoic acid on the contraction of intact, and spontaneous contraction of chemically permeabilized mammalian ventricular myocytes. *J Mol Cell Cardiol* **31**, 733-43.

Rogart, R. B., Cribbs, L. L., Muglia, L. K., Kephart, D. D., & Kaiser, M. W. (1989). Molecular cloning of a putative tetrodotoxin-resistant rat heart Na⁺ channel isoform. *Proc Natl Acad Sci USA* **86**, 8170-4.

Rohr, S. & Salzberg, B. M. (1994). Multiple site optical recording of transmembrane voltage (MSORTV) in patterned growth heart cell cultures: assessing electrical behavior, with microsecond resolution, on a cellular and subcellular scale. *Biophys J* **67**, 1301-15.

Ross, W. N., Salzberg, B. M., Cohen, L. B., Grinvald, A., Davila, H. V., Waggoner, A. S., & Wang, C. H. (1977). Changes in absorption, fluorescence, dichroism, and Birefringence in stained giant axons: optical measurement of membrane potential. *J Membr Biol* **33**, 141-83.

Russel, W. M. S. & Burch, R. L. (1959). *The Principles of Humane Experimental Technique*. reprinted by Universityies Federation for Animal Welfare, Potters Bar, UK, 1992, Methuen, London (1959).

Saint, D. A., Ju, Y. K., & Gage, P. W. (1992). A persistent sodium current in rat ventricular myocytes. *J Physiol* **453**, 219-31.

Sakmann, B. & Neher, E. (1984). Patch clamp techniques for studying ionic channels in excitable membranes. *Annu Rev Physiol* **46**, 455-72.

Salama, G. & Choi, B. R. (2000). Images of Action Potential Propagation in Heart. *News Physiol Sci* **15**, 33-41.

Sanguinetti, M. C., Curran, M. E., Spector, P. S., & Keating, M. T. (1996a). Spectrum of HERG K⁺-channel dysfunction in an inherited cardiac arrhythmia. *Proc Natl Acad Sci U S A* **93**, 2208-12.

Sanguinetti, M. C., Curran, M. E., Zou, A., Shen, J., Spector, P. S., Atkinson, D. L., & Keating, M. T. (1996b). Coassembly of K(V)LQT1 and minK (IsK) proteins to form cardiac I(Ks) potassium channel. *Nature* **384**, 80-3.

Sanguinetti, M. C., Jiang, C., Curran, M. E., & Keating, M. T. (1995). A mechanistic link between an inherited and an acquired cardiac arrhythmia: HERG encodes the I_{Kr} potassium channel. *Cell* **81**, 299-307.

Satoh, H. (1993). Comparative electrophysiological and mechanical actions of ATP-sensitive potassium channel openers in canine Purkinje fibers. *Gen Pharmacol* **24**, 565-75.

Schaffer, P., Ahammer, H., Muller, W., Koidl, B., & Windisch, H. (1994). Di-4-ANEPPS causes photodynamic damage to isolated cardiomyocytes. *Pflugers Arch* **426**, 548-51.

Schlotthauer, K. & Bers, D. M. (2000). Sarcoplasmic reticulum Ca(2+) release causes myocyte depolarization. Underlying mechanism and threshold for triggered action potentials. *Circ Res* **87**, 774-80.

Schroeder, K., Neagle, B., Trezise, D. J., & Worley, J. (2003). Ionworks HT: a new high-throughput electrophysiology measurement platform. *J Biomol Screen* **8**, 50-64.

Sharma, V., Lu, S. N., & Tung, L. (2002). Decomposition of field-induced transmembrane potential responses of single cardiac cells. *IEEE Trans Biomed Eng* **49**, 1031-7.

Sharma, V., Susil, R. C., & Tung, L. (2005). Paradoxical loss of excitation with high intensity pulses during electric field stimulation of single cardiac cells. *Biophys J* **88**, 3038-49.

Sharma, V. & Tung, L. (2002). Spatial heterogeneity of transmembrane potential responses of single guinea-pig cardiac cells during electric field stimulation. *J Physiol* **542**, 477-92.

Shimizu, W. & Antzelevitch, C. (1999). Cellular and ionic basis for T-wave alternans under long-QT conditions. *Circulation* **99**, 1499-507.

Sicouri, S. & Antzelevitch, C. (1993). Drug-induced afterdepolarizations and triggered activity occur in a discrete subpopulation of ventricular muscle cells (M cells) in the canine heart: quinidine and digitalis. *J Cardiovasc Electrophysiol* **4**, 48-58.

Sipido, K. R., Callewaert, G., & Carmeliet, E. (1995). Inhibition and rapid recovery of Ca^{2+} current during Ca^{2+} release from sarcoplasmic reticulum in guinea pig ventricular myocytes. *Circ Res* **76**, 102-9.

Snyders, D. J. (1999). Structure and function of cardiac potassium channels. *Cardiovasc Res* **42**, 377-90.

Sorota, S., Zhang, X. S., Margulis, M., Tucker, K., & Priestley, T. (2005). Characterization of a hERG screen using the IonWorks HT: comparison to a hERG rubidium efflux screen. *Assay Drug Dev Technol* **3**, 47-57.

Staub, C., De Schutter, E., & Knopfel, T. (1994). Voltage-imaging and simulation of effects of voltage- and agonist-activated conductances on soma-dendritic voltage coupling in cerebellar Purkinje cells. *J Comput. Neurosci.* **1**, 301-311.

Stevens, T., Cornfield, D. N., McMurtry, I. F., & Rodman, D. M. (1994). Acute reductions in PO₂ depolarize pulmonary artery endothelial cells and decrease. *Am J Physiol* **266**, 1416-21.

Sugden, J. K. (2004). Photochemistry of dyes and fluorochromes used in biology and medicine: some physicochemical background and current applications. *Biotech Histochem* **79**, 71-90.

Sun, X. & Wang, H. S. (2005). Role of the transient outward current (I_{to}) in shaping canine ventricular action potential--a dynamic clamp study. *J Physiol* **564**, 411-9.

Szabo, G., Szentandrassy, N., Biro, T., Toth, B. I., Czifra, G., Magyar, J., Banyasz, T., Varro, A., Kovacs, L., & Nanasi, P. P. (2005). Asymmetrical distribution of ion channels in canine and human left-ventricular wall: epicardium versus midmyocardium. *Pflugers Arch* **450**, 307-16.

Takacs, J., Iost, N., Lengyel, C., Virag, L., Nestic, M., Varro, A., & Papp, J. G. (2003). Multiple cellular electrophysiological effects of azimilide in canine cardiac preparations. *Eur J Pharmacol* **470**, 163-70.

Tamargo, J., Caballero, R., Gomez, R., Valenzuela, C., & Delpon, E. (2004). Pharmacology of cardiac potassium channels. *Cardiovasc Res* **62**, 9-33.

Tarr, M., Arriaga, E., Goertz, K. K., & Valenzano, D. P. (1994). Properties of cardiac I_{leak} induced by photosensitizer-generated reactive oxygen. *Free Radic Biol Med* **16**, 477-84.

Tarr, M. & Valenzano, D. P. (1991). Modification of cardiac ionic currents by photosensitizer-generated reactive oxygen. *J Mol Cell Cardiol* **23**, 639-49.

Terrar, D. A., Wilson, C. M., Graham, S. G., Bryant, S. M., & Heath, B. M. (2007). Comparison of guinea-pig ventricular myocytes and dog Purkinje fibres for in vitro assessment of drug-induced delayed repolarization. *J Pharmacol Toxicol Methods*.

Thomsen, M. B., Verduyn, S. C., Stengl, M., Beekman, J. D., de Pater, G., van Opstal, J., Volders, P. G., & Vos, M. A. (2004). Increased short-term variability of repolarization predicts d-sotalol-induced torsades de pointes in dogs. *Circulation* **110**, 2453-9.

Thomsen, M. B., Volders, P. G., Beekman, J. D., Matz, J., & Vos, M. A. (2006). Beat-to-Beat variability of repolarization determines proarrhythmic outcome in dogs susceptible to drug-induced torsades de pointes. *J Am Coll Cardiol* **48**, 1268-76.

Trube, G. & Hescheler, J. (1984). Inward-rectifying channels in isolated patches of the heart cell membrane: ATP-dependence and comparison with cell-attached patches. *Pflugers Arch* **401**, 178-84.

Tsau, Y., Wenner, P., O'Donovan, M. J., Cohen, L. B., Loew, L. M., & Wuskell, J. P. (1996). Dye screening and signal-to-noise ratio for retrogradely transported voltage-sensitive dyes. *J Neurosci Methods* **70**, 121-9.

Tseng, G. N. (1998). Calcium current restitution in mammalian ventricular myocytes is modulated by intracellular calcium. *Circ Res* **63**, 482.

U.S. Department of Health and Human Services. (2005). Guidance for industry. S7B nonclinical evaluation of the potential for delayed ventricular repolarisation (QT interval prolongation) by human pharmaceuticals. Food and Drug Administration, Centre for Drug evaluation and Research, Centre for Biologies Evaluation and Research.

Vandenberg, C. A. (1987). Inward rectification of a potassium channel in cardiac ventricular cells depends on internal magnesium ions. *Proc Natl Acad Sci USA* **84**, 2560-4.

Viswanathan, P. C., Shaw, R. M., & Rudy, Y. (1999). Effects of I_{Kr} and I_{Ks} heterogeneity on action potential duration and its rate dependence: A simulation study. *Circulation* **99**, 2466-2474.

Vohra, J. (2003). Drug-induced Prolonged Repolarisation (Acquired Long QT Syndrome) Arrhythmias. *Heart, Lung and Circulation* **12**, supplement.

Volders, P. G., Sipido, K. R., Vos, M. A., Spatjens, R. L., Leunissen, J. D., Carmeliet, E., & Wellens, H. J. (1999). Downregulation of delayed rectifier K(+) currents in dogs with chronic complete atrioventricular block and acquired torsades de pointes. *Circulation* **100**, 2455-61.

Vos, M. A., Verduyn, S. C., Gorgels, A. P., Lipcsei, G. C., & Wellens, H. J. (1995). Reproducible induction of early afterdepolarizations and torsade de pointes arrhythmias by d-sotalol and pacing in dogs with chronic atrioventricular block. *Circulation* **91**, 864-72.

Waggoner, A. S., Wang, C. H., & Tolles, R. L. (1977). Mechanism of potential-dependent light absorption changes of lipid bilayer membranes in the presence of cyanine and oxonol dyes. *J Membr Biol* **33**, 109-40.

Wakefield, I. D., Pollard, C., Redfern, W. S., Hammond, T. G., & Valentin, J. P. (2002). The application of in vitro methods to safety pharmacology. *Fundam Clin Pharmacol* **16**, 209-18.

- Waller, A. D. (1887). A demonstration on man of electromotive changes accompanying the heart's beat. *J Physiol* **8**, 229–34.
- Walsh, K. B. & Kass, R. S. (1988). Regulation of a heart potassium channel by protein kinase A and C. *Science* **242**, 67-9.
- Walsh, K. B. & Kass, R. S. (1991). Distinct voltage-dependent regulation of a heart-delayed IK by protein kinases A and C. *Am J Physiol* **261**, 1081-90.
- Wang, J., Wang, H., Zhang, Y., Gao, H., Nattel, S., & Wang, Z. (2004). Impairment of HERG K(+) channel function by tumor necrosis factor-alpha: role of reactive oxygen species as a mediator. *J Biol Chem* **279**, 13289-92.
- Wang, Q., Curran, M. E., Splawski, I., Burn, T. C., Millholland, J. M., VanRaay, T. J., Shen, J., Timothy, K. W., Vincent, G. M., de Jager, T., Schwartz, P. J., Toubin, J. A., Moss, A. J., Atkinson, D. L., Landes, G. M., Connors, T. D., & Keating, M. T. (1996). Positional cloning of a novel potassium channel gene: KVLQT1 mutations cause cardiac arrhythmias. *Nat Genet* **12**, 17-23.
- Wang, T., Bergstrand, R. H., Thompson, K. A., Siddoway, L. A., Duff, H. J., Woosley, R. L., & Roden, D. M. (1986). Concentration-dependent pharmacologic properties of sotalol. *Am J Cardiol* **57**, 1160-5.
- Wang, Z., Fermini, B., & Nattel, S. (1993). Sustained depolarization-induced outward current in human atrial myocytes. Evidence for a novel delayed rectifier K⁺ current similar to Kv1.5 cloned channel currents. *Circ Res* **73**, 1061-76.
- Ward, O. C. (1964). A new familial cardiac syndrome in children. *J Ir Med Assoc* **54**, 103-6.
- Weerapura, M., Nattel, S., Chartier, D., Caballero, R., & Hebert, T. E. (2002). A comparison of currents carried by HERG, with and without coexpression of MiRP1, and the native rapid delayed rectifier current. Is MiRP1 the missing link? *J Physiol* **540**, 15-27.
- Weiss, J. N., Venkatesh, N., & Lamp, S. T. (1992). ATP-sensitive K⁺ channels and cellular K⁺ loss in hypoxic and ischaemic mammalian ventricle. *J Physiol* **447**, 649-73.

- Windisch, H., Ahammer, H., Schaffer, P., Muller, W., & Platzer, D. (1995). Optical multisite monitoring of cell excitation phenomena in isolated cardiomyocytes. *Pflugers Arch* **430**, 508-18.
- Wolff, C., Fuks, B., & Chatelain, P. (2003). Comparative study of membrane potential-sensitive fluorescent probes and their use in ion channel screening assays. *J Biomol Screen* **8**, 533-43.
- Woosley, R. L., Chen, Y., Freiman, J. P., & Gillis, R. A. (1993). Mechanism of the cardiotoxic actions of terfenadine. *JAMA* **269**, 1532-6.
- Wright, A. G. Light sensors and detection methods for TLD. *Article from Electron Tubes Ltd.*
- Wymore, R. S., Gintant, G. A., Wymore, R. T., Dixon, J. E., McKinnon, D., & Cohen, I. S. (1997). Tissue and species distribution of mRNA for the I_{Kr} -like K^+ channel, *erg*. *Circ Res* **80**, 261-8.
- Wysowski, D. K. & Bacsanyi, J. (1996). Cisapride and fatal arrhythmia. *N Engl J Med* **335**, 290-1.
- Xiao, R. P., Cheng, H., Lederer, W. J., Suzuki, T., & Lakatta, E. G. (1994). Dual regulation of Ca^{2+} /calmodulin-dependent kinase II activity by membrane voltage and by calcium influx. *Proc Natl Acad Sci U S A* **91**, 9659-63.
- Xiao, Y. F., Gomez, A. M., Morgan, J. P., Lederer, W. J., & Leaf, A. (1997). Suppression of voltage-gated L-type Ca^{2+} currents by polyunsaturated fatty acids in adult and neonatal rat ventricular myocytes. *Proc Natl Acad Sci U S A* **94**, 4182-7.
- Xiao, Y. F., Kang, J. X., Morgan, J. P., & Leaf, A. (1995). Blocking effects of polyunsaturated fatty acids on Na^+ channels of neonatal rat ventricular myocytes. *Proc Natl Acad Sci U S A* **92**, 11000-4.
- Xu, H., Guo, W., & Nerbonne, J. M. (1999). Four kinetically distinct depolarization-activated K^+ currents in adult mouse ventricular myocytes. *J Gen Physiol* **113**, 661-78.
- Yan, G. X., Shimizu, W., & Antzelevitch, C. (1998). Characteristics and distribution of M cells in arterially perfused canine left ventricular wedge preparations. *Circulation* **98**, 1921-7.

Yang, N., George, A. L., & Horn, R. (1996). Molecular basis of charge movement in voltage-gated sodium channels. *Neuron* **16**, 113-22.

Yellen, G. (1998). The moving parts of voltage-gated ion channels. *Q Rev Biophys* **31**, 239-95.

Yuan, W. & Bers, D. M. (1994). Ca-dependent facilitation of cardiac Ca current is due to Ca-calmodulin-dependent protein kinase. *Am J Physiol* **267**, 982-93.

Zagotta, W. N., Hoshi, T., & Aldrich, R. W. (1990). Restoration of inactivation in mutants of Shaker potassium channels by a peptide derived from ShB. *Science* **250**, 568-71.

Zhang, J., Davidson, R. M., Wei, M. D., & Loew, L. M. (1998). Membrane electric properties by combined patch clamp and fluorescence ratio imaging in single neurons. *Biophys J* **74**, 48-53.

Zhou, Z. & Bers, D. M. (2000). Ca²⁺ influx via the L-type Ca²⁺ channel during tail current and above current reversal potential in ferret ventricular myocytes. *J Physiol* **523 Pt 1**, 57-66.

Zygmunt, A. C., Goodrow, R. J., & Antzelevitch, C. (2000). I(NaCa) contributes to electrical heterogeneity within the canine ventricle. *Am J Physiol Heart Circ Physiol* **278**, 1671-8.